



HAL
open science

**Conception and fabrication of reusable microfluidic tools
to study the dynamics of biological phenomena :
application to antibiotic influx/efflux in bacteria and to
cell migration during mouse development**

Xuan Zhao

► **To cite this version:**

Xuan Zhao. Conception and fabrication of reusable microfluidic tools to study the dynamics of biological phenomena : application to antibiotic influx/efflux in bacteria and to cell migration during mouse development. Micro and nanotechnologies/Microelectronics. Université Paris Saclay (COmUE), 2017. English. NNT : 2017SACLS226 . tel-01591980

HAL Id: tel-01591980

<https://theses.hal.science/tel-01591980>

Submitted on 22 Sep 2017

HAL is a multi-disciplinary open access archive for the deposit and dissemination of scientific research documents, whether they are published or not. The documents may come from teaching and research institutions in France or abroad, or from public or private research centers.

L'archive ouverte pluridisciplinaire **HAL**, est destinée au dépôt et à la diffusion de documents scientifiques de niveau recherche, publiés ou non, émanant des établissements d'enseignement et de recherche français ou étrangers, des laboratoires publics ou privés.

NNT : 2017SACLS226

THESE DE DOCTORAT
DE
L'UNIVERSITE PARIS-SACLAY
PREPAREE A
L'UNIVERSITE PARIS-SUD

ECOLE DOCTORALE N° 575
Electrical, optical, bio-physics and engineering

Spécialité de doctorat : Electronique et Optoélectronique, Nano- et Microtechnologies

Par

Xuan ZHAO

Conception and fabrication of reusable microfluidic tools to study the dynamics of biological phenomena: application to antibiotic influx/efflux in bacteria and to cell migration during mouse development

Thèse présentée et soutenue au C2N Orsay, le 7 Septembre 2017 :

Composition du Jury :

M. Bruno LE PIOUFLE	Professeur ENS Cachan, Laboratoire SATIE	Président
M. Vincent STUDER	DR CNRS, Institut Interdisciplinaire de Neurosciences	Rapporteur
Mme Marie-Caroline JULLIEN	DR CNRS, Laboratoire Gulliver ESPCI	Rapporteur
M. Pierre-Henri PUECH	CR INSERM, Laboratoire Adhésion et Inflammation	Examineur
M. Charlie GOSSE	CR CNRS, Centre de Nanosciences et de Nanotechnologies	Directeur de thèse

Université Paris-Saclay

Espace Technologique / Immeuble Discovery

Route de l'Orme aux Merisiers RD 128 / 91190 Saint-Aubin, France



Acknowledgements

My first thanks will be given to Bruno Le Pioufle, Vincent Studer, Marie-Caroline Jullien, and Pierre-Henri Puech, members of the committee who have accepted to read my PhD manuscript and judge my work.

Secondly, I would like to express my sincere gratitude to my thesis advisor, Charlie Gosse (C2N Marcoussis, CNRS), for his kind encouragement, clear guidance, great patience, and continuous support throughout the whole research project. His comprehension and knowledge of microfluidics, microfabrication, and numerical simulations were extremely valuable for improving the quality of my thesis and of the publications that have been written. His insightful comments and suggestions helped me to make progresses in my microfluidic studies, in the redaction of the dissertation as well as in the capture of my future career.

I am also extremely grateful to Matthieu Réfrégiers (DISCO beamline, SOLEIL Synchrotron) for his invitation and for the permission to conduct my research on the TELECOM microscope. My integration in the beamline team and the financial support I have benefited for my work were much valuable. I also appreciated all the members of the Biology Laboratory and of the Chemistry Laboratory of the SOLEIL Synchrotron for their help and assistance during my experimentals.

I am grateful to my collaborators, Aitana Perea-Gomez, Isabelle Migeotte, Diana Suárez-Boomgaard, Joni Frederick, Julia Vergalli, and Anne-Marie Tran, for their help and for the harmonious cooperation during my thesis period.

I want to express my deep appreciation to my friends and colleagues for their support: Elsa Mazari, Anne-Claire Loüer, Hugo Salmon, Antoine Barbot, and Qiongdi Zhang, who were Ph.D students in the same laboratory than me. All the members of the C2N clean room are also deeply acknowledged for their kind guidance on the use of the machines and for the constructive exchanges and discussions we had all these years.

Finally, I would like to express my great respect to my family for their warmly encouragement and continuous support.

Table of content

Part I. A reusable microdevice for dynamic studies of antibiotics uptake in immobilized individual bacterium

Chapter I. Various view points on antibiotherapy	11
I. Historical perspective on drug discovery and development	11
I.1. Early findings	11
I.2. The discovery of antagonism between microorganisms	12
I.3. The discovery of penicillin	12
I.4. The golden era	14
I.4.1. Natural compounds in the 1940s-1950s	14
I.4.2. Semi-synthetic drugs in the 1960s	14
I.4.3. Synthetic quinolones in the 1980s	15
I.5. The discovery void	15
II. Public health issues related to drug resistance	16
II.1. Emergence of the phenomena and anticipated consequences	16
II.2. Reported causes	17
II.2.1. Endopathic factors	17
II.2.2. Exopathic factors	19
II.3. Possible solutions	20
II.3.1. Rational use of antibiotics by doctors and patients	20
II.3.2. Increase supervision and support by policy makers	20
III. Cellular and molecular aspects	21
III.1. Classification of bacteria according to their structure	21
III.1.1. Appearance and shape	21
III.1.2. Result of Gram staining	22
III.2. Classification of antibiotics according to their target	23
III.2.1. Inhibition of cell wall synthesis	24
III.2.2. Disruption of the cytoplasmic membrane	25

III.2.3. Inhibition of folate synthesis	25
III.2.4. Inhibition of protein synthesis	26
III.2.5. Inhibition of nucleic acids synthesis	27
III.3. Classification of resistances according to their mechanism	28
III.3.1. Drug inactivation by an enzyme	29
III.3.2. Alteration of the target site	29
III.3.3. Changes of membrane permeability	30
III.3.4. Active expulsion of the drug from the bacteria	30
III.4. Description of the biomolecules involved in drug influx/efflux	30
III.4.1. The cell wall of the Gram-negative bacteria	30
III.4.2. The OmpC and OmpF porins	31
III.4.3. The multi drug efflux pumps	32
Chapter II Strategies used for influx/efflux measurements	35
I. A review of the literature	35
I.1. Bulk studies	36
I.1.1 Natural systems	36
I.1.2 Artificial systems	37
I.2. Single cell studies	38
I.2.1. Natural systems	38
I.2.2 Artificial systems	39
I.3 Single protein studies	40
II. Our biological system	41
II.1. <i>Escherichia coli</i> , a typical Gram-negative bacteria	42
II.1.1. Main characteristics	42
II.1.2. Relevance for public health	43
II.1.3. Use as a model organism	43
II.2. Quinolones, a family of fluorescent antibiotics	44
II.2.1. Structural properties	44
II.2.2. Mechanism of action	45
II.2.3. Relevance for public health	46
II.2.4. Spectroscopic properties	47
III. The experiments performed at SOLEIL	47
III.1. Intrinsic fluorescence imaging of antibiotic concentration	48
III.1.1. Necessity of a real-time label-free technique	48
III.1.2. Description of the Telemos epifluorescence microscope	49
III.1.3. Specific issues related to UV fluorescence observation	51

III.2. Previous protocol _____	52
III.2.1. Description _____	52
III.2.2. Limitations _____	54
III.3. Proposed protocol _____	54
Chapter III. Design and fabrication of the microdevice _____	55
I. Criteria to be fulfilled _____	55
I.1. Complete cell immobilization _____	55
I.2. Parallel monitoring of individual bacteria _____	56
I.3. Quick change of the chemical environment _____	56
I.4. Practicity _____	57
II. Existing technologies _____	57
II.1. Electromagnetic trapping _____	57
II.1.1. Dielectrophoresis _____	57
II.1.2. Optical tweezers _____	59
II.2. Physico-chemical traps _____	61
II.2.1. Surface coating _____	61
II.2.2. Gel matrix _____	61
II.3. Steric traps _____	63
II.3.1. Microfluidic growth chamber and growth track _____	63
II.3.2. Elastomeric ring valve _____	66
II.3.3. Semi-permeable membrane onto a growth chamber _____	67
II.4. Comparison and conclusion _____	67
III. Tentative implementations _____	68
III.1. Dielectrophoresis _____	69
III.2. Elastomeric button valve _____	69
IV. Final solution _____	71
IV.1. Reflection around the static chamber _____	71
IV.2. Design of the flow device _____	72
IV.3. Compliance with the requirements _____	73
IV.4. Fabrication protocols _____	74
Chapter IV. Description of an experiment step by step _____	77
I. Bacteria culture _____	77
I.1. Experiments on the BL21 (DE3) strain _____	77
I.2. Experiments on the AG100/AG100A/AG102 strains _____	77

II. Reagent preparation	78
II.1. NaPi Buffer	78
II.2. Antibiotic solution	78
III. Microfluidic actuation	79
III.1. Immobilization of the bacteria	79
III.2. Installation of the fluidic system	79
III.3. Selection of an appropriate field of view	80
III.4. Modulation of the antibiotic concentration	81
IV. Image acquisition and data analysis	83
IV.1. Optical set up	83
IV.2. Experiments on the BL21 (DE3) strain	84
IV.3. Experiments on the AG100/AG100A/AG102 strains	86
Chapter V. Microdevice characterization	87
I. Finite element method simulations	87
I.1. Generalities	87
I.2. Hydrodynamics	87
I.3. Solute transport	89
II. Numerical and experimental results	90
II.1. Hydrodynamics	91
II.2. Solute transport	92
III. Discussion	95
III.1. Selection of the field of view	95
III.2. Variability and stability	97
IV. Comparison of our microdevice with the existing solutions	98
IV.1. Steric immobilization in microfluidic growth chambers	98
IV.2. Physico-chemical trapping at the surface of a microfluidic channel	101
Chapter VI. Experiments on bacteria	103
I. Influx/efflux studies	103
I.1. Device validation on the uptake of ciprofloxacin by the BL21 (DE3) strain	103
I.2. Preliminary results on the uptake of fleroxacin by the AG100/AG100A/AG102 strains	105
I.3. Perspectives on the use of efflux modulators and/or other bacterial species	105
II. Cell growth studies	106

Part II. Reusable microdevices to study the dynamics of cell migration during mouse development

Chapter I. Technical context	111
I. Electroporation for transgenesis	111
I.1. Pore opening upon electric field application	112
I.2. Entry of nucleic acids into the cytoplasm	115
II. Electroporation in embryology	116
II.1 Goal of the transfection experiments	116
II.1.1. Cell fate mapping	116
II.1.2. Gene function study	116
II.2. Localization strategies	117
II.2.1. Orientation of the embryo	117
II.2.2. Containment of the nucleic acids solution	117
II.2.3. Generation of an electric field gradient	118
II.2.4. Combination of both molecular localization and electric field focusing	119
III. Electroporation and microsystems	119
III.1 Microelectrodes	119
III.2 Dielectric guides	120
IV. Electroporation at the LPN	121
IV.1. Biological insights	121
IV.2. The project and the collaboration	122
IV.3. The dielectric guide devices	123
IV.3.1. General architecture	123
IV.3.2 List of the various demonstrators and prototypes	124
Chapter II. Microdevice design and processing	129
I. Choice of materials and microfabrication technologies	129
I.1 The laboratory demonstrators so far realized	130
I.1.1 Soft lithography (EM5)	130
I.1.2 Mix “craft” technologies (EM6)	131
I.1.3. Achievements and limitations	131
I.2. The industrial prototypes	132

I.2.1 Thermoplastic manufacturing	132
I.2.2 MEMS-type manufacturing	134
I.2.3 Strategy selection	134
II. Overview of the different processes available to make a glass micro chip	135
II.1. Etching	135
II.1.1 Dry etching	135
II.1.2 Wet etching	137
II.2. Electrochemical discharged machining	138
II.3. Sand blasting	140
II.4. Femtosecond laser ablation	141
II.5. Selective laser-induced Etching (SLE)	143
II.6 Bonding	144
II.6.1. Direct bonding	145
II.6.2. Anodic bonding	145
II.6.3. Adhesive bonding	147
II.6.4. Eutectic bonding	147
II.6.5. Sol-gel bonding	148
II.7. Summary of the possibilities offered by the various techniques	149
III. Comparative experiments on individual technological steps	150
III.1 Through hole manufacturing	150
III.2 Wafer bonding	151
IV. Validation of the two protocols selected to produce an all-in-glass device	152
IV.1 Design update between the EM6 and EM7 devices	152
IV.2 Workflow selection and evaluation	154
IV.2.1. Microfabrication process by wet etching, laser ablation and bonding	154
IV.2.2. Microfabrication process by SLE	156
Chapter III. Microfabrication protocols	159
I. The SU-8/parafilm single-use device (EM6)	159
II. The reusable all-in-glass device series (EM7)	161
II.1. EM7-01	161
II.2. EM7-02 and EM7-11	163
III. The use of protection layers during glass micromachining	164
III.1. Wet etching	164
III.2. Laser ablation	166
Chapter IV Results and discussion	167

I. Simulations	167
I.1 Description of the models	167
I.2 Determination of the permeation threshold	169
II. Electroporation experiments	170
Chapter V. Perspectives	173
I. Post-electroporation culture	173
II. Measurement of temperature and pH jumps	174
References	177

Part I. A reusable microdevice for dynamic studies of antibiotics uptake in immobilized individual bacterium

Chapter I. Various view points on antibiotherapy

I. Historical perspective on drug discovery and development

Antibiotics are one of the greatest achievements in the history of medicine, without which many diseases could not have been fought. We do not need to emphasize on how many lives have been saved and how significantly these drugs contributed to the control of infectious diseases. The history of antibiotic development is also instructive. Similarly to what can be observed for many other inventions, after accumulation of many years of experience, phenomena have been interpreted along with the progresses made in other basic sciences, and finally fundamental studies have been transformed into industrial production, so as to better serve mankind.

One of the contributions of the founder of microbiology, Louis Pasteur, was to point out that many diseases were caused by microbial infection. Several microorganisms can induce human diseases: bacteria (such as *Escherichia coli*), viruses (such as coronaviruses), fungi (such as lichen planus), and protozoa (such as plasmodia). Among them, bacteria, fungi, and protozoa can effectively be killed by antibiotics.

I.1. Early findings

In many ancient cultural records, people around the world have been known to utilize fungi, molds as well as some plants to treat infections. Moldy bread and soil have been employed to treat ulcers, intestinal infections, and wounds. So the use of bacterial products in the treatment of disease is very old, but people did not know terms like “bacteria” and “antibiotic”. Indeed, it was not until the second half of the 19th century that the development of antibiotics was really initiated.

I.2. The discovery of antagonism between microorganisms

With the development of microbiology, from the 1870s onwards, the essence of the concept of antibiosis was discovered and reported by various scholars. John Burdon Sanderson and William Roberts independently observed that fungi were capable of inhibiting bacterial growth in certain culture media. In 1874 the latter scientist named this phenomenon “antagonism” (Roberts 1874). In 1876, John Tyndall did a similar observation, concluding that fungi consumed the oxygen necessary to bacteria multiplication and pointing out that, in the competition for survival between molds and bacteria, molds were usually the winner (Tyndall 1876). In 1877, Louis Pasteur and Jules François Joubert evidenced the antagonistic role of microorganisms present in the air while trying to culture *Bacillus anthracis* in urine. They even sometimes succeeded in preventing the anthrax infection of an animal by inoculating these aerial microorganisms at the same time than *Bacillus anthracis* (Pasteur and Vallery-Radot 1933). In 1899 Rudolph Emmerich and Oscar Löw isolated germs from the infected bandages that caused green infections in open wounds. This microorganism was *Pseudomonas aeruginosa*. They noticed that this bacterium, as well as the extracts from its cultures, was active against a number of other pathogenic bacteria, like *Vibrio cholerae*, *Corynebacterium diphtheriae*, and *Bacillus anthracis* (Hays, Wells et al. 1945) (Aminov 2010).

Thus, by the beginning of the 20th century, antagonistic phenomena involving microorganisms had been discovered and proved to be numerous. Various strains of *Penicillium* and *Pseudomonas* had been studied, and their potential for the treatment of diseases had been evaluated.

I.3. The discovery of penicillin

In the first decades of the 20th century, antibiotic research was only a continuation of the one of the former century, without any new development. In 1910, the German doctor Paul Ehrlich synthesized arsphenamine (salvarsan, Figure I - 1), which was effective to treat syphilis without being too harmful to the human body. The 1920s were characterized by the sole isolation of kojic acid (in 1912, from *Aspergillus oryzae* colonies growing on rice) and penicillic acid (in 1913, from a mold growing on maize). From 1920 to 1929, the only discovered molecules were actinomycin (isolated from a soil actinomycete by Gratia and Dath (Hogg 2013) and pyocyanin (chemically synthesized by Wrede and Strack (MacDonald 1967)). However, the effects of the two latter substances were not high or the drugs were toxic: without great practical value, these findings did not have much impact.

In 1928 Fleming fortuitously discovered penicillin (Figure I - 1). While studying the morphology of colonies of *Staphylococcus aureus*, a colony of *Penicillium notatum* accidentally contaminated his Petri dish. Under a magnifying glass he found that the colonies of *Staphylococci* around the *Penicillium* colony were apparently dissolved. It was later confirmed that *Penicillium* had

a lytic effect on *Staphylococcus*. In 1929, Fleming named the anti-bacterial substance found in the cultures of this fungus “penicillin” (Fleming 1929). It was a pity that this discovery was not taken seriously, and that no further exploration was undertaken.

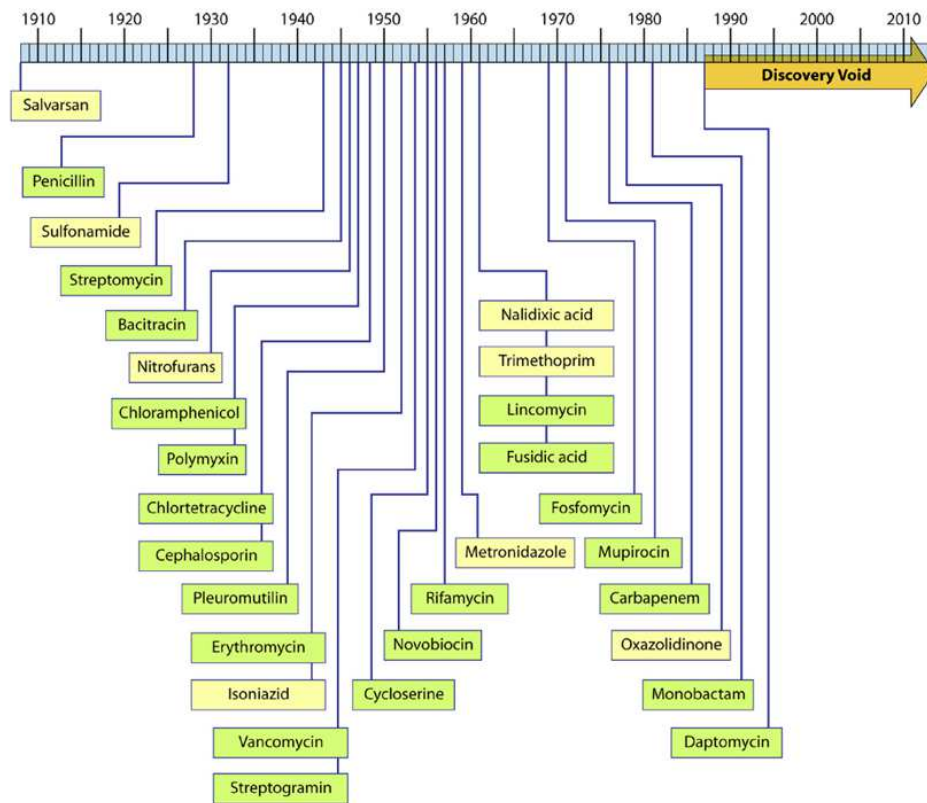


Figure I - 1. Timeline for the discovery of various antibiotics (in yellow) and of the distinct classes of antibacterials (in green). The indicated dates are those reported for the initial discoveries or patents. Image taken from (Silver 2011).

In 1932 a German chemist at Bayer Laboratory accidentally synthesized a red compound later named “Prontosil”. Next, the chemist Gerhard Domagk proved the effectiveness of this substance to treat some streptococcal infections. The discovery and development of this first sulfonamide drug opened a new era in medicine (Lesch 2007) (Figure I - 1) .

In the meantime, the discovery of penicillin still got unappreciated. In fact, the molecule has not been put into clinical application until 1944. It was Howard Florey, professor of pathology at Oxford University, who helped to further promote the development of penicillin as a drug. In 1938-1939 he conducted a systematic study of the known antimicrobial molecules produced by microorganisms. Fleming's penicillin was one of the substances the most noticeable to him. Luckily, Florey got help from the chemist Ernest Chain and soon after they were able to extract and purify the active substance from *Penicillium spp.* cultures. By 1940, the product was pure enough to meet the

requirements for human intramuscular injection. In the first clinical trial, the therapeutic effect was obvious, even with a little amount of drug (Macfarlane and Taylor 1979). From these days, the treatment of infectious diseases hugely changed. During the Second World War, mass production of penicillin saved thousands of death-threatened lives.

I.4. The golden era

In the 1940s, the history of antibiotics turned a new page. With the development of new concept in microbiology, biochemistry, and organic chemistry, as well as with the advancement of molecular biology, the method for discovering new antibiotics has gradually improved and become more rational.

I.4.1. Natural compounds in the 1940s-1950s

Selman Waksman is another important figure in the history of antibiotics. He and his colleagues screened consciously and purposefully thousands different soil microbes before they isolated streptomycin in 1943 (Figure I - 1), which could cure tuberculosis (Schatz and Waksman 1944).

The works of Waksman inspired other researchers in the world, a large-scale screening of antibiotics produced by soil microorganisms began. Aureomycin (1945), chloramphenicol (1947), oxytetracycline (1950), nystatin (1950), erythromycin (1952), and kanamycin (1957) were all discovered in the following two decades. While researches for antibiotics have entered in a purposeful, planned and systematic stage, production methods were industrialized with the establishment of large antibiotic pharmaceutical companies. In 1956, Eli Lilly and Company isolated *Amycolatopsis orientalis* from soil collected in Indonesia. After purification, a compound was found to kill various *Staphylococci* and most Gram-positive bacteria: vancomycin was born (Levine 2006).

I.4.2. Semi-synthetic drugs in the 1960s

However, the discovery of new antibiotics from microbes significantly slowed down at the end of the 1950s and semi-synthetic antibiotics were developed. Semi-synthesis uses compounds isolated from natural sources (e.g. plant material or bacterial or cell cultures) as starting materials, the chosen raw materials usually have the basic skeleton of the final product and most of its functional groups, and even have the desired configuration for the final product.

In 1958 John C. Sheehan opened up the road to semi-synthetic penicillins through the synthesis of 6-aminopenicillanic acid (Sheehan 1967). In the next few years, scientists developed this big family of semi-synthetic drugs with, for instance, phenoxymethylpenicillin (Penicillin V), methicillin, and ampicillin. In 1961, Edward Abraham found cephalosporin C in the metabolites of *Cephalosporium* (Loder, Newton et al. 1961) (Figure I - 1). It is an important antibiotic in the

cephalosporin family, from which the other semi-synthetic cephalosporins could be derived (Eykyn 1971).

1.4.3. Synthetic quinolones in the 1980s

In 1962 Lesher et al. reported the nalidixic acid (Figure I - 1). In fact, this molecule appeared as an impurity during the manufacture of quinine (Lesher, Froelich et al. 1962). Although this compound had only shown a weak activity against several Gram-negative bacteria *in vitro*, its discovery facilitated the design and synthesis of new analogues: it can be called the ancestor of the quinolone family. The synthetic quinolones obtained in the 1980s were developed very rapidly because of their considerable clinical and scientific interest. These antibiotics, which are widely used in contemporary anti-infective therapy, are broad spectrum and highly effective.

1.5. The discovery void

At this point, the history of antibiotics can be drawn a comma. In recent years, antibiotics have become less effective and resistance has suddenly increased (Figure I - 2 a).

It is also important to note that since the 1980s the annual number of novel antibiotics being introduced on the market has declined steadily (Figure I - 2 b). From 1996 to 2000, only six new antibiotics were developed up to clinic. This trend became more obvious while entering the new century. In 2003 only a single new product - daptomycin was on the list of the approved drugs and 2004 was even blank. Over the past decade, only tenth of drugs have been developed and approved. What is even more worrying is that there have been no successful discoveries of novel agents since 1987, and the drugs that are entered on the market of recent years are issued from the old discoveries.

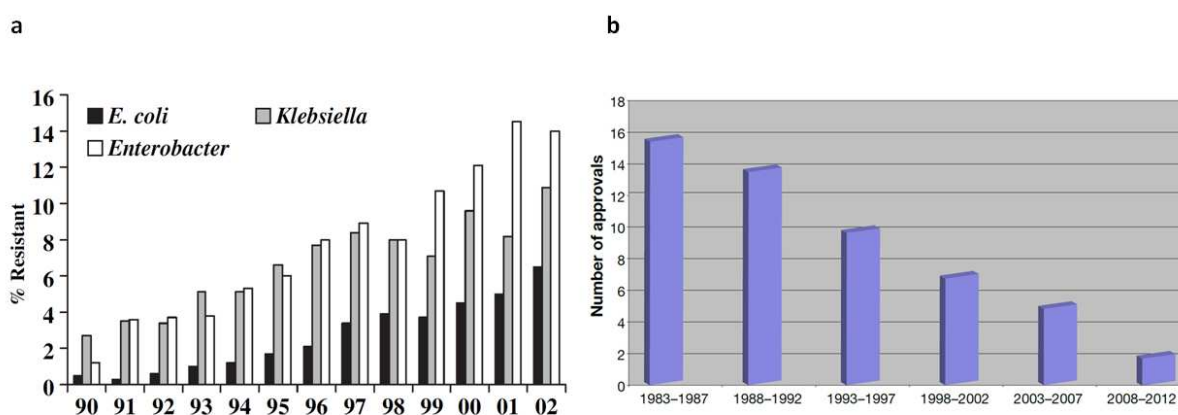


Figure I - 2. (a) Increase in antibiotic resistant strains of *E. coli*, *Enterobacter spp.*, and *Klebsiella spp.* from 1990 to 2002. (b) Number of novel antibiotics approved and entering clinic use from 1983 to 2012. Image taken from (Livermore 2004) and (Cain 2012).

II. Public health issues related to drug resistance

In order to win the fight against bacteria, microbiologists and pharmaceutical chemists have been constantly moving forward on the road of searching new antibiotics. However, bacteria are evolving and mutant strains resistant to commonly used antibiotics have appeared. More problematically, today the pace of development of new antibiotics is falling far behind the speed of bacterial resistance.

II.1. Emergence of the phenomena and anticipated consequences

Antimicrobial resistance is said to occur when the targeted microorganisms change in ways that render the medication used to cure the infections they cause ineffective (WHO Drug Resistance).

On the World Health Day of 2011, the World Health Organization devised the slogan “Antimicrobial resistance: No action today, no cure tomorrow”, thus calling for the halt of drug abuse. (WHO World Health Day 2011). The first report on antibiotic resistance based on global data collected from 114 countries was published in April 2014 (Organization 2014).

In the early 20th century, one third of all deaths of the world were due to infectious diseases like pneumonia, tuberculosis, enteritis, and diarrhea. Today, heart diseases and cancer are the leading killers, with fewer than 4.5 % of deaths by pneumonia and influenza. This important result was achieved through the use of antibiotics (CDC 1999). However, humans have now reached another extreme: abuse of antibiotics leads to the rapid emergence of drug resistant bacteria.

Drug resistance is a serious problem in modern medicine. Once dozens of units of penicillin were able to save lives, which is not the case anymore. In 2014, there were about 480 000 new drug resistance tuberculosis cases, and the current extensively drug resistance tuberculosis has been reported in 92 countries and regions. These patients have to endure longer courses and worse treatment effects (WHO Antimicrobial Resistance 2014). A world-wide metagenomic study has shown that drug resistant microorganisms are now ubiquitous in nature (Nesme, Cecillon et al. 2014). This means that humans are about to return to an era without antibiotics. A large number of infectious diseases, which had once been conquered or totally eradicated, become again incurable diseases, with which minor bacterial infection could result in fatal consequences. More dramatically, bacteria that we have to face are enhanced versions of those of hundred years ago.

It is of urgent need to develop new targets, or even new mechanisms, as countermeasures. Some bacteria are even listed as “crucial priority” for which new antibiotics are urgently needed (e.g.

Acinetobacter baumannii carbapenem-resistant, *Pseudomonas aeruginosa* carbapenem-resistant, and *Enterobacteriaceae* carbapenem-resistant) (WHO 2017 FEB media). The additional cost associated with resistant pathogen infections was estimated at 5 billion USD in 2004 (America 2004) and they cost trillions USD to address in 2016 (UN 2016 SEP media). The development of new drugs, after all, is a giant project. It is difficult to catch the speed of bacterial mutation. Meanwhile, mankind, who are already heavily dependent on antibiotics, are now more in need of new drugs than ever. If we cannot control the drug resistance, the economic burden will be heavy of the whole society.

II.2. Reported causes

Basically, antibiotic resistance is a consequence of evolution via natural selection. Bacterial resistance needs to be considered from two aspects, endopathically and exopathically. More precisely, endopathic causes are the genetic factors that provide of bacteria almost innumerable possibilities of evolutionary directions whereas exopathic causes include the misuse of antibiotics in the medical process and the abuse of antibiotics in livestock, both providing an environmental selective pressure giving selection an orientation (Figure 1 - 3).

II.2.1. Endopathic factors

Intrinsic resistance. It is the innate ability of a bacterial species to resist a particular drug through its inherent structural or functional characteristics, which allow tolerance to a particular drug or a class of antibiotics. For example, many Gram-negative bacteria (e.g. *Pseudomonas aeruginosa*) are insensitive to penicillins and vancomycin because they lack the main target of the drug, i.e. a thick cell wall composed of peptidoglycans.

Acquired resistance. It occurs when a bacterium becomes resistant to a particular drug to which it was initially susceptible. Two mechanisms may be involved: either the mutation of a given gene that helps the bacterium to survive or the acquisition of genetic material from a bacterium that is already resistant, mainly through the transfer of genetic elements such as plasmids, transposons, or integrons.

Genetic mutation is the fundamental cause of drug-resistance in bacteria. Bacteria can be traced back to three billion years ago. Therefore, uninterrupted evolution conferred them an extraordinary ability to adapt to the environment. Spontaneous random mutations occur accidentally in all bacterial populations, at every moment. Most of mutations are harmful or useless; only a few are both harmless and useful, for instance because they provide a weak drug resistance. However, it is almost impossible to confer a bacterium a perfect resistance through only one single mutation. In

the reality, there is no sudden emergence of drug-resistance, this phenomena is a consequence of gradually accumulated mutations.

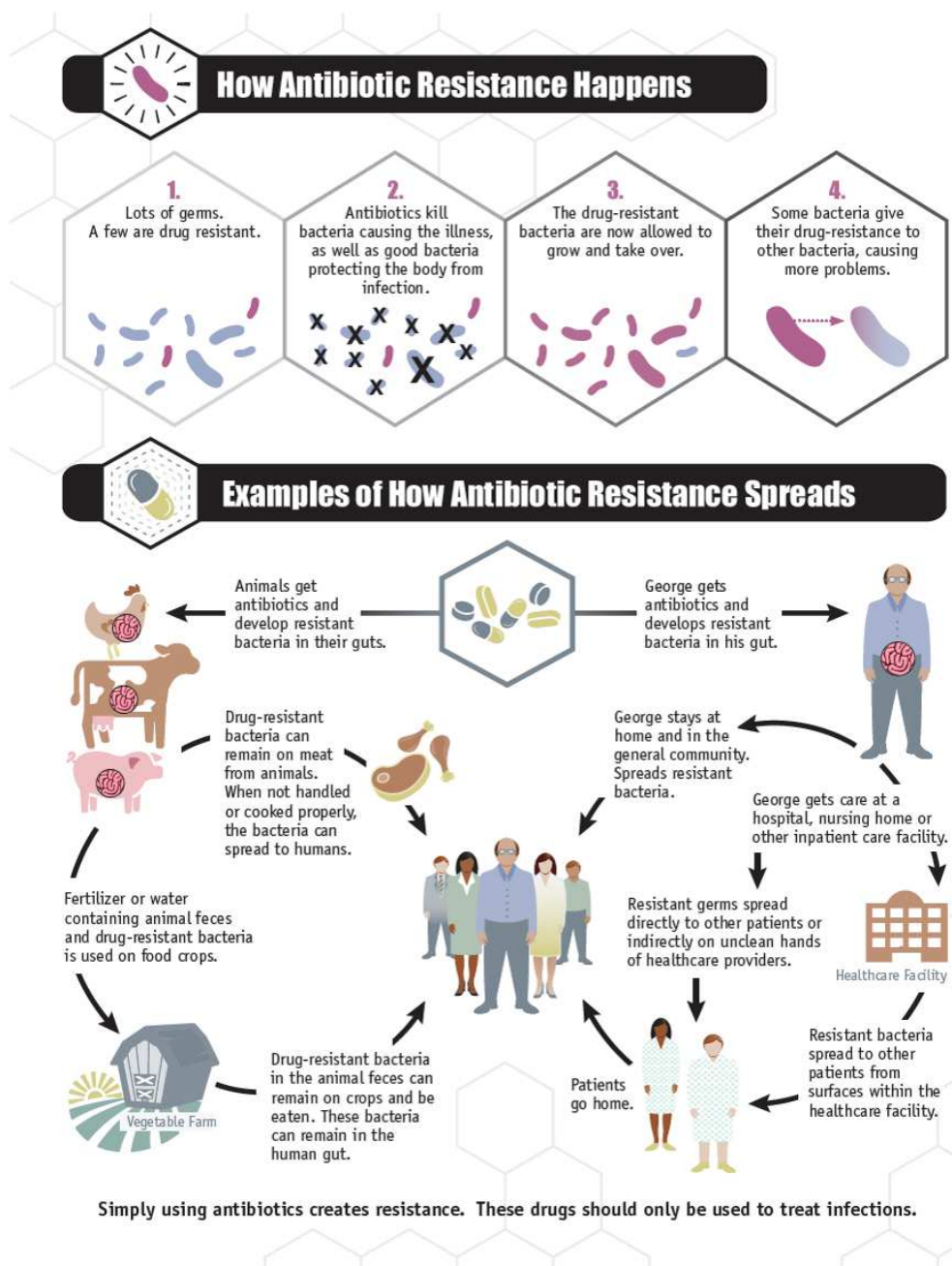


Figure 1 - 3. Diagram illustrating the reason why antibiotic resistance happens and how it spreads (Prevention 2013)

Besides spontaneous mutations, resistance can be due to a gene that is coming from some other bacteria. For instance, plasmids are circular extra chromosome that can be transferred from one bacterium to another by conjugation, i.e. through cell-cell contact. Natural isolates of *E. coli* typically harbor some plasmids in various sizes: one to five small plasmids and one to two large

plasmids (Hartl, Medhora et al. 1986) (Selander, Caugant et al. 1987). The small plasmids are usually smaller than 7.5 kb, and the large ones range from 40 to 200 kb. A given plasmid can carry several drug-resistant genes. The R plasmid, also known as the resistance plasmid, is commonly found in clinical studies. It is also known that plasmids can encode a variety of enzymes, in order to passivate antibiotics by biochemical modification (Bennett 2008) (Hawkey 1998).

Another process involved in horizontal gene transfer relies on transposon. They are DNA sequences that can change their positions within the genome, sometimes creating or reversing mutations. In bacteria, transposons can also jump from chromosomal DNA to plasmid DNA and back, allowing for the transfer and/or permanent addition or removal of genes (Pray 2008).

Finally, integrons are mobile genetic elements with the ability to capture and mobilize genes that are contained in mobile elements called gene cassette. Notably they can work on the gene encoding antibiotic resistance by site-specific recombination. An integron provides a promoter for an expression of the genes of the cassette, and thus acts both as a natural cloning system and as expression vector (Hall and Collis 1995).

II.2.2. Exopathic factors

Misuse of antibiotics in human medicine. The fact that bacteria develop resistance to a drug enters in the framework of the theory of the evolution. However, the way drugs are used, or we could say misuse, affects how quickly and how widely drug resistance occurs.

A study published at 2003 reported that 30 % of the antibiotics received by hospitalized adult patients were unnecessary (Hecker, Aron et al. 2003). Ten years after, the Center for Disease Control and Prevention of USA (CDC) estimated that up to 50 % of antibiotics were unnecessary or inappropriately prescribed (Health and Services 2013).

We have discussed above that, even before antibiotics were applied in the medicine on a large scale, there was already a very small quantity of bacteria with accidentally acquired resistance genes. Nevertheless, it was almost of no significance for the bacterial population since the resistance could not spread because of the lack of selective pressure. Later antibiotics appeared, bacteria without this gene (i.e. sensitive strains) were killed one after another, whereas those having this gene were able to survive and benefited from the available space to reproduce. Thus, the resistance is not triggered by the application of antibiotics, the evolution of resistant strains is a natural phenomenon associated with the survival of the fittest. Certainly, genetic mutations and transfers are happening in nature at all times, but to make those low occurrence phenomena to become meaningful and influential, it needs a strong fecundity. Of course, for simple organisms like bacteria, it is not too difficult.

Use of antibiotics in agriculture. The amount of antibiotics used for human is negligible compared with the one used for livestock. According to the CDC, more than 70 % of the antibiotics sold in the US market in 2013 are used in agriculture (Kennedy 2013). In most other countries, this figure is also more than 50 %. The use of antibiotics in agriculture is primarily intended to prevent the infection of animals, but another aim, more controversial, is to accelerate growth in order to make more profits. The British economist Jim O'Neill, commissioned by the British government, estimated the global annual consumption of antibiotics to be between 63 000 and 240 000 tonnes. By 2030 global agricultural consumption of antibiotics is expected to increase by 67 % with respect to its 2010 level (O'Neill 2015).

II.3. Possible solutions

II.3.1. Rational use of antibiotics by doctors and patients

When normally used, antibiotics can kill almost all of the targeted bacteria – even if some survive they are usually eliminated by the immune system. However, if the correct dose of antibiotics is not respected, bacteria are not killed completely at once. The less-sensitive strains survive to establish new populations or continue to mutate on this resistance basis. Therefore, the effects of the prescription are compromised by inappropriate drug choices, inadequate doses, uncompleted treatments, and/or too frequent change of antibiotics. Consequently, acute infection turns into chronic one, giving resistant bacteria a chance. Those bacteria that have escaped from antibiotherapy not only have grown with a tenacious survivability but are now also able to transfer resistance gene to other bacteria.

Besides, at any time, we should not forget the basic good way to eliminate bacteria: disinfection and isolation.

II.3.2. Increase supervision and support by policy makers

In the area of public health there is a need to ensure strong national or even supra-national actions, to address antibiotic resistance. For instance, one must improve surveillance of drug resistant infections, strengthen programs dedicated to the prevention and control of diseases, and finally regulate and promote the appropriate use of medicines. In addition, the development of new antibiotics, vaccines, and diagnostic methods should be supported at the government level. To be more precise, societies can hardly rely on big pharmaceutical companies to face the emergence of drug-resistant bacteria. Indeed, the latter actors have turned attention to the treatments of chronic diseases, a more lucrative activity than the painstaking development of new antibiotics.

III. Cellular and molecular aspects

Macroscopic phenomena are always related to the microscopic ones, so in this part we will briefly review and explain the interaction between bacteria and antibiotics at small scale.

III.1. Classification of bacteria according to their structure

Bacteria can be classified in many ways, according to their appearance, to their nutritional type (autotrophic or heterotrophic), to their oxygen requirement during growth (obligate aerobe, facultative anaerobe, microaerophile, aerotolerant, or obligate anaerobe), to their temperature preference (psychrophiles, psychrotrophs, mesophiles, thermophiles, or hyperthermophiles), or to their cell structure. We will introduce two examples of classification methods which we have found meaningful for guiding the present doctoral studies.

III.1.1. Appearance and shape

Typical appearances of bacteria are shown in Figure I - 4. Most bacteria have sizes in the range of 1 to 5 μm . They can be organized in between cocci, bacilli, and spirillar bacteria.

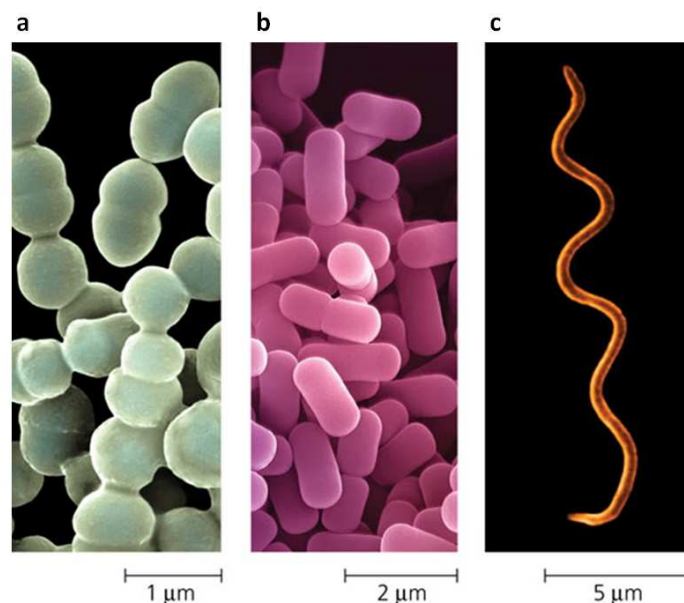


Figure I - 4. Different shapes of bacteria. (a) Cocci (spherical bacteria). (b) Bacilli (rod-shaped) bacteria. (c) Spiral bacteria. Images taken from <http://www.ppdictionary.com/gnbac.htm>.

Cocci. This is a kind of bacterium that generally has a round shape (spherical or ovoid) and which average diameter is 0.5 - 2.0 μm . Some stay as single cell after division, but others adhere to each other. They can then be classified into several categories, according to their arrangement:

diplococci are paired; tetrads are in clusters of four arranged in the same plane; sarcina are in cube of eight; streptococci are organized in chains; and staphylococci are organized like grapes.

Bacilli. They are rods of various size, length, curvature, and thickness. The majority of them are straight rods of medium length 2 - 5 μm and width 1 μm . For most bacilli both ends of the cell are round. However, a few have flattened ends (such as *Bacillus anthracis*), tapered ends (such as *Fusobacterium*), or expanded rod-shaped ends (such as *Corynebacterium diphtheria*). Generally, bacilli are found as single cells, but sometimes they are in pairs or in chains.

Spiral bacteria. They are rods displaying a significant bending. *Vibrio* presents only one curve, like a comma, whereas spirillum is larger, elongate, and spiral shaped.

In this doctoral thesis, studies on a typical bacillus will be performed at the single cell scale. Fortunately, *E. coli* stays in a dispersed state after reproduction. The immobilization method will be relatively simpler than what would have been necessary for bacteria that stay aggregated like streptococci or for those that present a complex three dimensional structure like spiral bacteria.

III.1.2. Result of Gram staining

The Gram test enables to classify bacteria into two large groups, based on the structure of the cell wall (Figure I - 5). The process includes staining by crystal violet, mordant incubation with Gram's iodine, decoloring with alcohol, and counterstaining with safranin. Gram-positive bacteria appear dark violet and Gram-negative ones red. We will concentrate on the Gram-negative bacteria, since this category is the one that includes most of the resistant strain – the structure of these microorganisms will be described in more details in Chapter I, Section III.4.1.

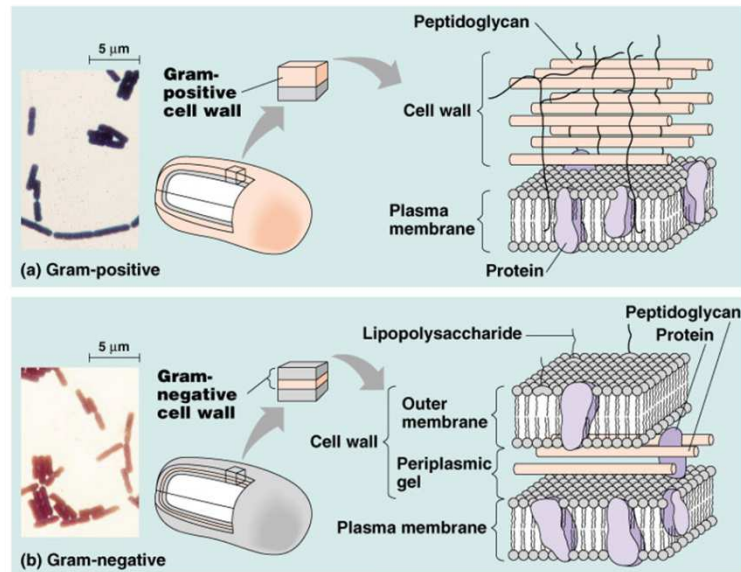


Figure I - 5. Diagrams illustrating the difference between Gram-positive and Gram-negative bacteria. (a) Gram-positive bacteria have a thick peptidoglycan layer that protects a single membrane. (b) Gram-negative bacteria have two membranes, an outer one and an inner one, that enclose a thin peptidoglycan matrix and that delineate the periplasmic space. Image taken from (Campbell and Reece 2002).

The distinction of pathogens between Gram-positive and Gram-negative is of important significance for the choice of antibiotics. For example, the mechanism of action of penicillin is to interfere with the synthesis of peptidoglycans. On one hand, the cell wall of Gram-positive bacteria is a thick layer of peptidoglycans and penicillin will weaken its structure, thereby inducing the death of the cells. On the other hand, the outmost layer of Gram-negative bacteria is mainly composed of lipopolysaccharides, the proportion of peptidoglycans is small, and the effect of penicillin is thus greatly reduced.

III.2. Classification of antibiotics according to their target

The term "antibiotic" was introduced by Selman Waksman in 1942. It describes an antibacterial substance which is produced by a microbe and which is antagonistic to the growth of some other microorganisms (Kresge, Simoni et al. 2004).

Nowadays, an antibiotic can be natural or synthetic. A commonly used distinction is made between "bactericidal" and "bacteriostatic" molecules. Bactericidal agents are able to destroy bacteria. It includes drugs that primarily compromise the integrity of some cell structures like the cell wall (e.g. β -lactams), the cell membrane (e.g. daptomycin and polymyxins), or the bacterial DNA (e.g. fluoroquinolones). On the contrary, bacteriostatic medicines block bacterial division without killing the organism. Most bacteriostatic agents act by inhibiting protein synthesis (e.g. sulfonamides,

tetracyclines, and macrolides). The distinction is not absolute: an antibiotic can be both bacteriostatic and bactericidal; it depends on the applied dose and on the targeted microorganisms (Leekha, Terrell et al. 2011).

Antibiotics are classified by their specific mechanisms of action. The mechanisms against Gram-positive and Gram-negative bacteria can be quite similar, but, as we have seen above with the penicillin example, their outcome may vary significantly depending on the considered category. So far, five main targets that have been exploited (Figure I - 6): the cell wall synthesis, the cell membrane integrity, the folate synthesis, the protein synthesis, and the nucleic acid synthesis (Gallo, Lancini et al. 2013).

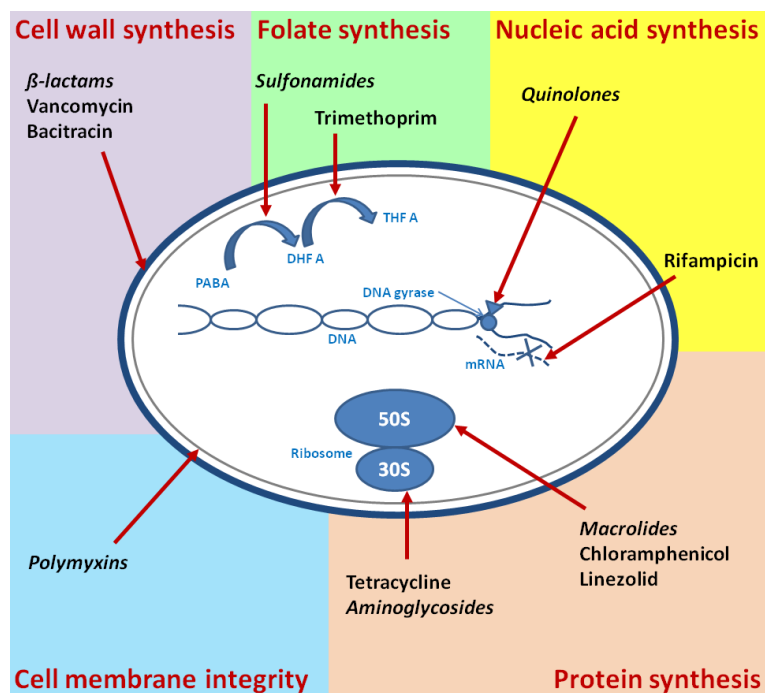


Figure I - 6. The five main molecular targets of antibiotics – drug families are denoted with italics. See Figure I - 7, Figure I - 8, Figure I - 10, and Figure I - 9 for molecular structures.

III.2.1. Inhibition of cell wall synthesis

Antibiotics that interfere with cell wall synthesis do it by blocking peptidoglycan synthesis. More precisely, bacteria exposed to a hypoosmotic environment will die because their weakened cell wall cannot stand the turgor pressure anymore. These drugs are active against growing bacteria, and they are bactericidal. Typically, they include β -lactams (e.g. penicillins, cephalosporins, carbapenems), vancomycin, and bacitracin (Figure I - 7).

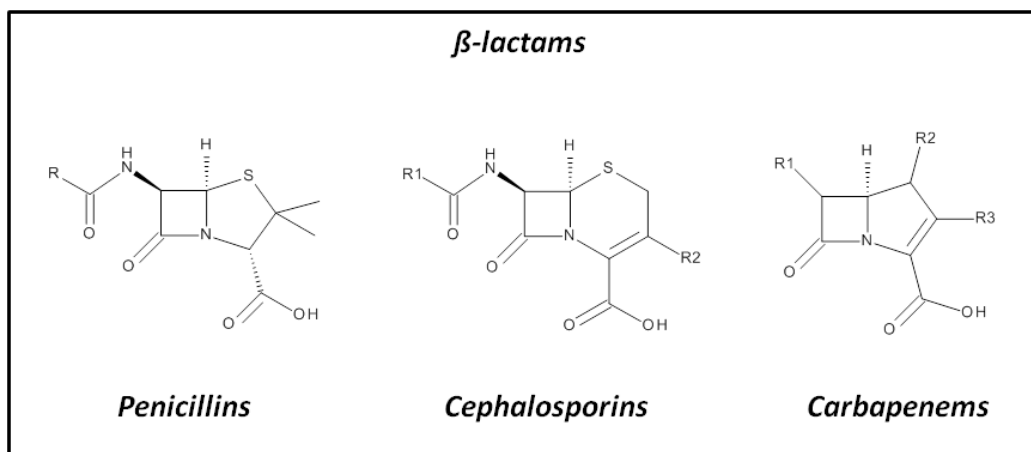


Figure I - 7. Molecular structures of drugs that inhibit cell wall synthesis – all molecules belong to the β -lactam family.

For Gram-positive bacteria, which lack an outer membrane, the β -lactams diffuse directly through the cell wall and bind to the penicillin-binding proteins (PBPs), which results in cell lysis. For Gram-negative bacteria, β -lactams enter the cell through porin channels located on the outer membrane and bind to PBPs on the surface of the cytoplasmic membrane. It blocks the function of PBPs, weakens cell wall, and leads to cell lysis.

III.2.2. Disruption of the cytoplasmic membrane

Polymyxin molecules diffuse through the outer membrane and through the cell wall of susceptible cells. They can then bind to the cytoplasmic membrane and destabilize it. This causes the cytoplasm to leak out of the cell, resulting in cell death.

III.2.3. Inhibition of folate synthesis

For many organisms, para-aminobenzoic acid (PABA) is an essential metabolite which is involved in the synthesis of folic acid, an important precursor in the synthesis of nucleic acids. Sulfonamides are structural analogues of PABA and compete with it for the dihydropteroate synthetase binding pocket. On the other hand, trimethoprim acts on the folic acid synthesis pathway a step further, inhibiting the dihydrofolate reductase. Both sulfonamides and trimethoprim are bacteriostatic. When they are used together they produce a sequential blockade of the folic acid synthesis pathway and have a synergistic effect (Figure I - 8).

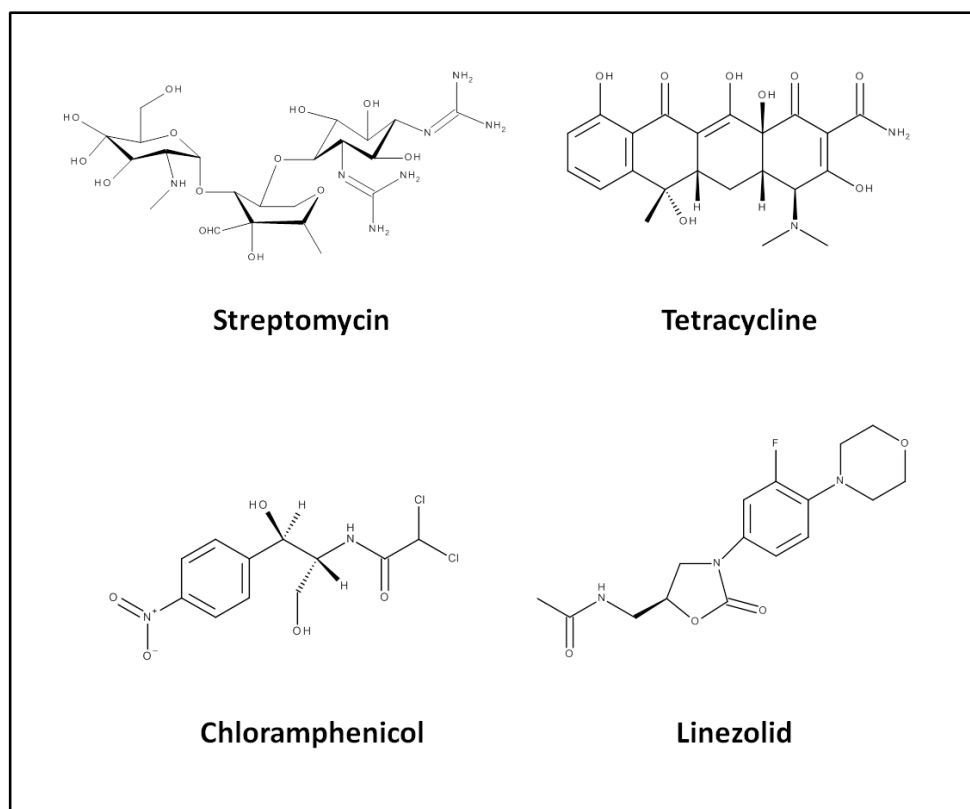


Figure I - 9. Molecular structures of drugs that inhibit protein synthesis.

III.2.5. Inhibition of nucleic acids synthesis

Fluoroquinolones interfere with DNA synthesis by blocking enzymes called DNA topoisomerase. These enzymes first bind to DNA and introduce double-stranded breaks that allow the DNA to unwind, and thus maintain a normal topological state during chromosome replication. Fluoroquinolones trap these enzymes at the DNA cleavage stage so that the DNA strands are prevented to rejoin and be repaired, resulting in cell death. This family of drug will be described extensively later in Chapter II, Section II.2 (Figure I - 10).

Rifampicin binds to the DNA-dependent RNA polymerase, it thus blocks the synthesis of RNA and yields cell death (Calvori, Frontali et al. 1965).

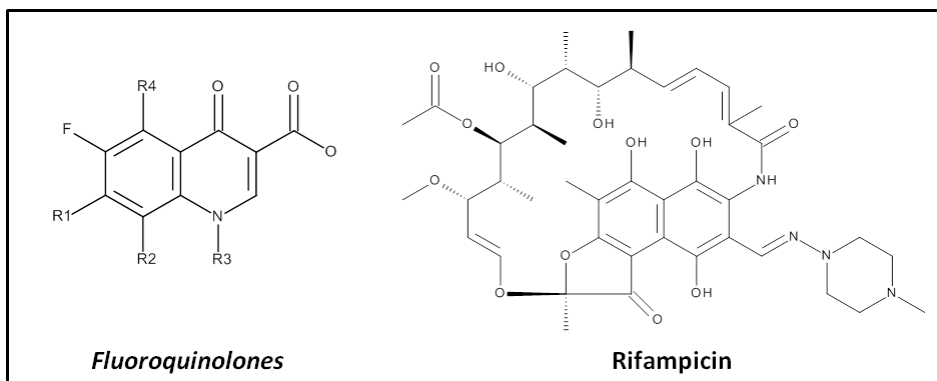


Figure I - 10. Molecular structures of drugs that inhibit nucleic acids synthesis.

III.3. Classification of resistances according to their mechanism

We have described the different mechanisms of action of antibiotics, based on their different target sites. However, for an antibiotic to be effective, it must also satisfy another condition: its concentration close to the target site must be high enough to favor reaction. Thus, it implies that the drug penetrates the surface of bacterium, reaches the surroundings of the target site, and accumulates there. Additionally, the molecules should not be inactivated nor expelled from bacteria before binding.

In general, bacterial resistance consists in countermeasures against the conditions mentioned above. The most common scenarios are summarized in the following picture (Figure I - 11) and some details are provided in the text.

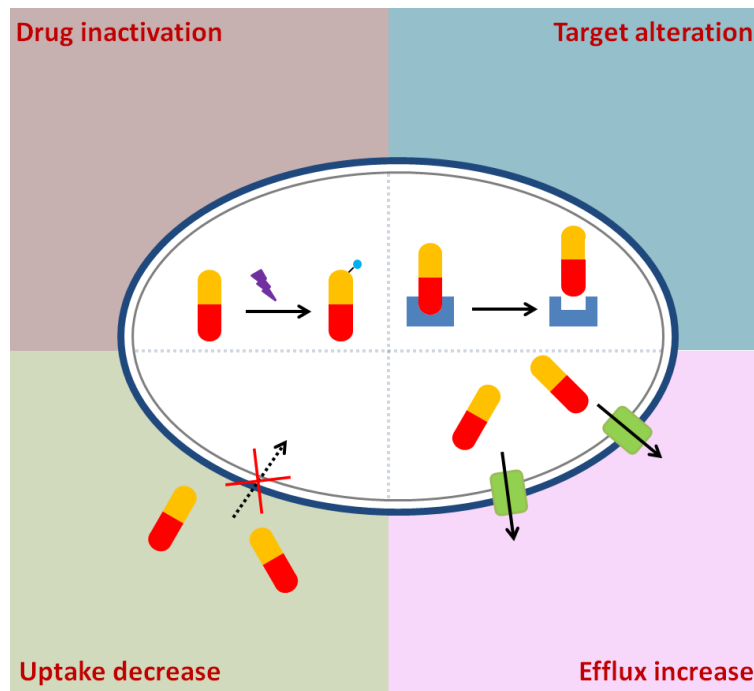


Figure I - 11. The four main mechanisms of antibiotic resistance.

III.3.1. Drug inactivation by an enzyme

β -lactamases are enzymes that hydrolyse β -lactam drugs, and more precisely the four-atom ring common to all the antibiotics of this group (Figure I - 7). In Gram-negative bacteria, the drug enters the cell through the porin channels and encounters β -lactamases in the periplasmic space. This results in a hydrolysis before the molecule reaches its target, i.e. PBPs. In Gram-positive bacteria, β -lactamases are secreted in the extracellular medium and destroy drugs before they encounter the cell.

Aminoglycoside modifying enzymes represent another class of countermeasure, which are produced by some Gram-negative bacteria. These enzymes catalyze the modification at $-OH$ or $-NH_2$ groups of the 2-deoxystreptamine nucleus or of the sugar moieties of these drugs. Such enzymes include, for example, aminoglycoside O-phosphotransferases (APHs), aminoglycoside O-adenyltransferases (ANTs), and aminoglycoside N-acetyltransferases (AACs).

Resistance can finally be conferred by an enzyme called chloramphenicol acetyltransferase which attaches covalently one or two acetyl groups to the hydroxyl groups of chloramphenicol (Figure I - 9), preventing its binding to the ribosome.

III.3.2. Alteration of the target site

Subtle changes in the structure of the target sites are likely to produce strong resistance. For instance, shape of PBPs in Gram-positive and Gram-negative bacteria may be altered through

mutations, so that β -lactams can no longer recognize them. Methylation of ribosomal RNA confers bacteria some resistance against macrolides, lincosamides, and streptograms. Mutations in the genes of topoisomerase II – also called DNA gyrase – and topoisomerase IV bring quinolone resistance (Willmott and Maxwell 1993).

III.3.3. Changes of membrane permeability

Outer membrane proteins like OmpC and OmpF form non-specific transmembrane channels called porins, that allow drugs to enter the cell. When bacteria are put into contact with antibiotics too many times, the strain mutates, resulting in the inactivation of the translocation through OmpC/OmpF. As a result, the entrance of molecules like β -lactams or quinolones is reduced (see Chapter I, Section III.4.2 for more details). In most cases, the loss of translocation through porins is not the sole mechanism of resistance at play, but it can work synergistically with other mechanisms to significantly increase resistance.

III.3.4. Active expulsion of the drug from the bacteria

A wide variety of efflux pumps are related to antibiotic resistance in both Gram-positive and Gram-negative bacteria. These transmembrane proteins form channels that actively expel an antibiotic out of the cell, nearly as fast as it enters (see Chapter I, Section III.4.3 of for more details).

III.4. Description of the biomolecules involved in drug influx/efflux

Among the resistance mechanisms discussed above, we are more interested in the influx / efflux ones. The movement of ions, or molecules, between the intracellular space and the extracellular one is achieved through specific channels. We will here describe in detail the structure of the envelope of Gram-negative bacteria, *E. coli* being taken as a representative example.

III.4.1. The cell wall of the Gram-negative bacteria

The structure of the cell wall of Gram-negative bacteria is presented in Figure I - 12. It is characterized by the presence of two membranes, which constitute two hydrophobic barriers that a molecule must cross to enter the cytoplasm. The outer membrane is an asymmetric bilayer located outmost of the bacteria. It contains phospholipids on its inner leaflet and lipopolysaccharides (LPS) on its outer one (Delcour 2009). Moreover, the outer membrane includes integral proteins which serve as entry ports for various molecules, the porins. The inner membrane is a phospholipid bilayer which also contains various integral membrane proteins.

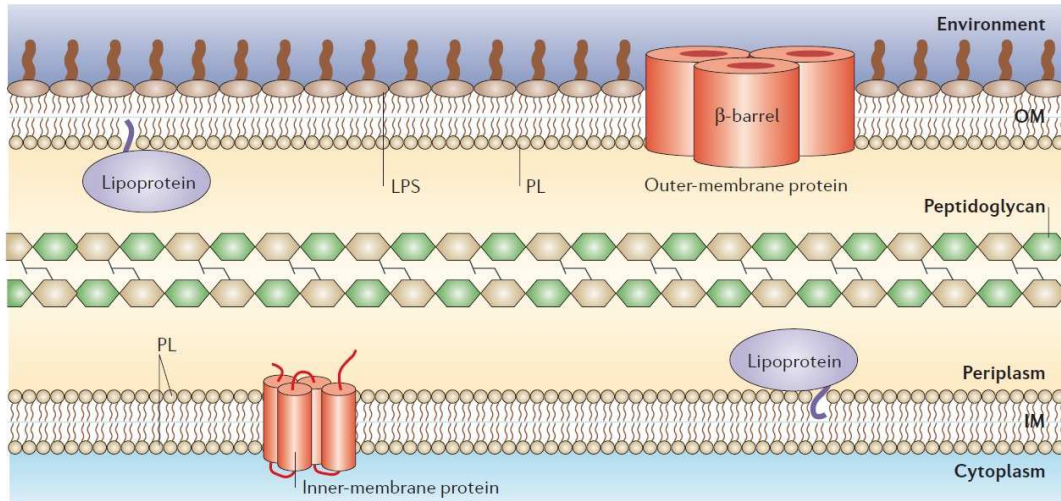


Figure I - 12. Diagram of the cell envelope of Gram-negative bacteria – LPS, PL, OM, and IM stand for lipopolysaccharides, phospholipids, outer membrane, and inner membrane, respectively. Image taken from (Ruiz, Kahne et al. 2006).

The periplasm is an aqueous compartment between the outer membrane and the inner one. It contains the cell wall, which is made of peptidoglycans. The amount of peptidoglycans in Gram-negative bacteria is much smaller than in Gram-positive ones.

III.4.2. The OmpC and OmpF porins

A large number of different types of proteins exist on the outer membrane. Some of them are extremely abundant, for instance, general diffusion porins can be present at more than 10^5 copies per cell, taking 1 % to 2 % of its total geometric surface (Delcour 2009).

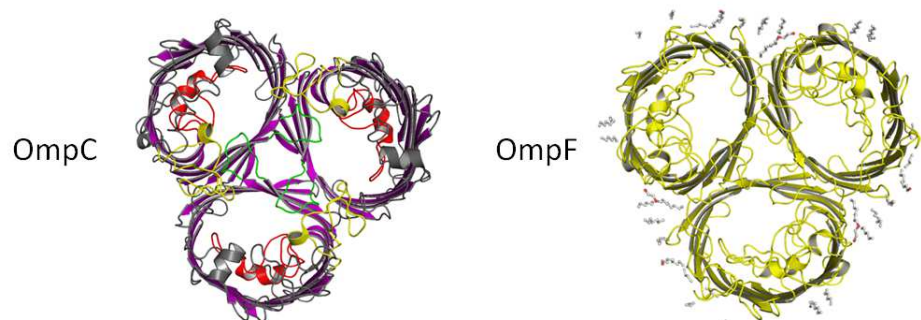


Figure I - 13. Top view of the trimeric structure of the OmpC and OmpF porins. Image adapted by T. Schirmer from (Cowan, Schirmer et al. 1992) (Basle, Rummel et al. 2006).

Escherichia coli mainly contain three kinds of outer membrane proteins: the porins OmpF, OmpC, and PhoE. The two first ones are highly similar in sequence, they are also the two main channels related to antibiotic resistance. Therefore, we will only discuss about them in the following.

(Cowan, Schirmer et al. 1992) (Basle, Rummel et al. 2006). These proteins are passive diffusion channels. Besides nutrient molecules uptake, small drugs like β -lactam, quinolones, tetracycline, and chloramphenicol can enter the cell by diffusion through them. These proteins are generally water filled channel, folded in β -barrel conformations. The narrowest constriction in these porins determines the maximum size of a solute that can pass through them (Hancock 1987) (Nikaido and Rosenberg 1981). The size cut-off is around 600 Da. OmpC is one of the earliest known porins, the diameter of its pore is 1.08 nm (Figure I - 13) (Nikaido and Rosenberg 1983). On the other hand, the pore of OmpF is larger, with a 1.16 nm diameter (Figure I - 13) (Nikaido and Rosenberg 1983). Because of this size difference, OmpC is less permeable than OmpF, it can only allow the passage of very small molecules (Koebnik, Locher et al. 2000) (Schirmer 1998) .

Bacterial resistance mechanisms are complex. As seen above, one of them is closely related to change in the outer membrane permeability. More specifically, resistance occurs through changes in the respective amount of the various outer membrane proteins (Nikaido 1989). Different porins have different permeabilities to different substances, down-regulation of high permeability porins and up-regulation of the low permeability porins can restrict the entry of antibiotics, thereby enhancing resistance. The expression of OmpC and OmpF is reciprocally regulated by the two-component systems EnvZ / OmpR and CpxA-CpxR. The expression of OmpC is enhanced and the expression of OmpF is decreased under unfavorable environment, e.g. high temperature, hyper-osmosis, and antibiotic stress (Batchelor, Walther et al. 2005) (Yoshida, Qin et al. 2006) (Raja, Murali et al. 2008). In the *E.coli* resistant strains, it is often found that the expression of OmpC increases so that this channel will replace the larger OmpF (Pagès, James et al. 2008).

III.4.3. The multi drug efflux pumps

It is a prerequisite for a drug to be effective that a sufficient quantity of it can reside in the bacteria, close to the target. The active efflux system consists in proteins located on the bacterial cell membrane, it can selectively or non-selectively expel the antibiotics from bacteria. The mechanism of drug resistance caused by efflux pumps was first reported in the early 1970s, in relation to the study of resistance to tetracycline. Since, various drug efflux systems have been discovered. At present, they are divided into five super families, according to amino acid sequence homologies. More specifically, one has the ATP binding cassettes (ABC) transporters family, the major facilitator superfamily (MFS), the small multidrug resistance (SMR) family, the multidrug and toxic compound extrusion (MATE) family, and the resistance-nodulation-division (RND) family. ABC transporters use ATP as a source of energy, whereas the other pumps are powered by protons. In the latter process, the protons enter the cell and the drug is expelled outside.

Efflux pumps can comprise either a single or multiple components. Examples of efflux pumps from each family are shown in Figure I - 14. For instance, efflux pumps of the RND family, which are expressed by Gram-negative bacteria, include three parts: an efflux transporter located in the cytoplasmic membrane of the bacterium (e.g. AcrB); an accessory protein, also known as membrane-fusion protein, located in the periplasmic space (e.g. AcrA); and an outer-membrane channel located in the outer membrane of the bacterium (e.g. TolC) (Koronakis, Eswaran et al. 2004). AcrAB-TolC is one of the most important systems that produces multi-drug resistance in *E. coli*. It can simultaneously produce high-level multi-drug resistance against many kinds of antibiotics (e.g. tetracycline, chloramphenicol, fluoroquinolones, β -lactams, neomycin, and erythromycin) (Nikaido and Takatsuka 2009). Additionally, it transports dyes, detergents, biocides, and even some organic solvents.

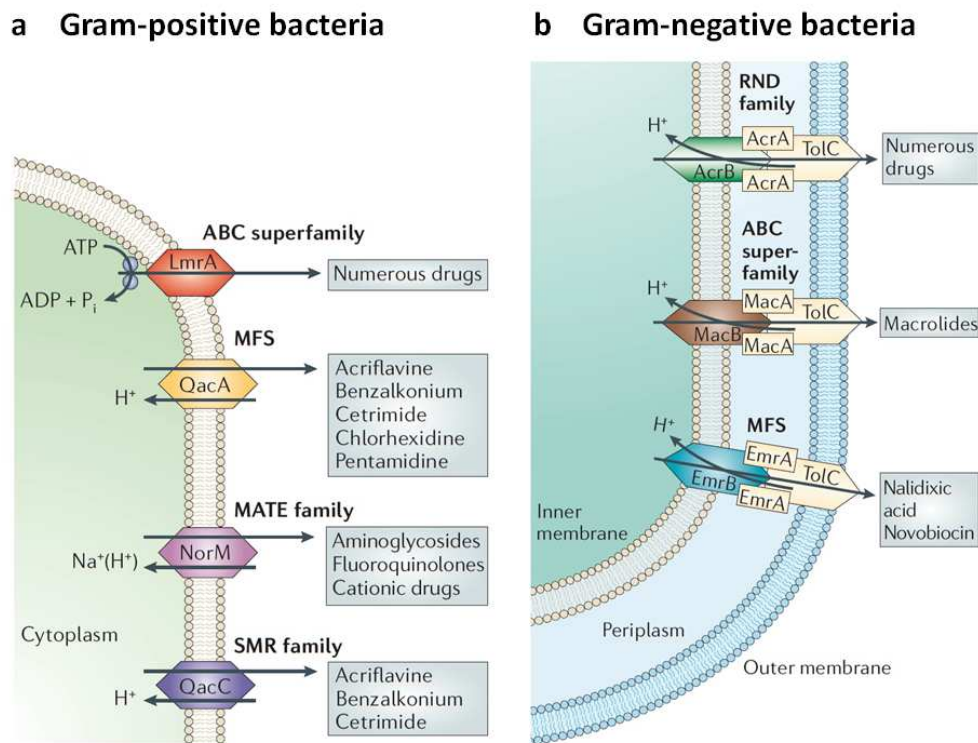


Figure I - 14. Diagram displaying the efflux pumps associated with multidrug-resistance. Boxes contain the name of the transported drugs in Gram-positive and Gram-negative bacteria. Image taken from (Pidcock 2006).

Chapter II Strategies used for influx/efflux measurements

I. A review of the literature

Among the many mechanisms leading to drug resistance, we are more specifically interested by the ones related to influx and efflux (see Chapter I, Section III.4). We will here provide a few examples of methods that have been developed by previous researchers. They will be first presented according to the scale at which studies were performed (Figure I - 15). Secondly, this classification will be subdivided according to the scrutinized biological objects, i.e. to their either natural or artificial nature.

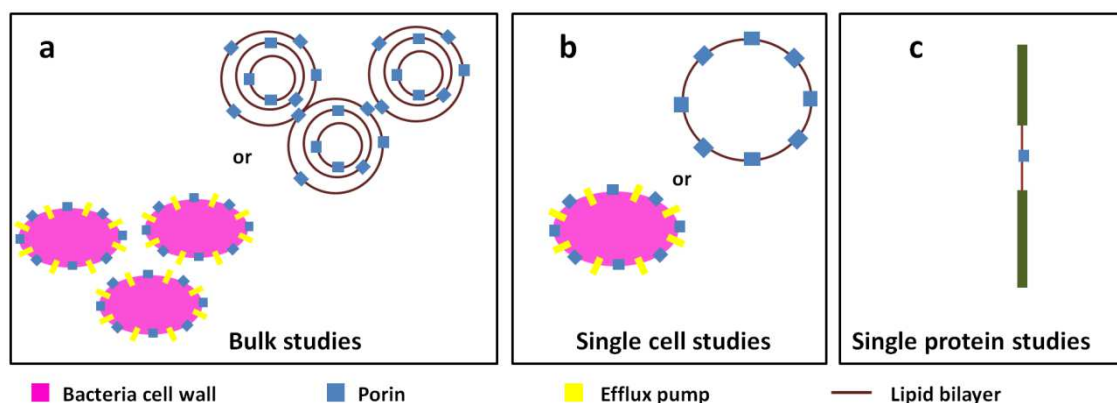


Figure I - 15. The different scales at which influx/efflux is studied systems. (a) Bulk studies emphasize on the collective studies of a group of objects (bacteria or liposomes). (b) Single cell studies emphasize on the behavior of a single cell or a single liposome. (c) Single protein studies focus on a single protein.

When using real bacteria, it is difficult to decouple the influx from the efflux, except through the use of mutants with altered properties (like the ones of the AG100 series, see Chapter IV, Section IV.3). Therefore artificial systems including a single molecular species (either a porin or an efflux pump) may be beneficial. However, efflux is an active process requiring energy and the artificially obtained systems may have problems to precisely reflect a complex reality. For instance, it seems unrealistic to reconstruct a respiratory chain in a liposome to test the CCCP adjuvant (see Chapter VI, Section I.3), which is a proton gradient disruptor.

I.1. Bulk studies

These methods are the first that have been developed.

I.1.1 Natural systems

Bacteria are grown in a nutrient solution until a satisfactory optical density. They are then harvested by centrifugation, washed with buffer, and re-suspended. Antibiotic is next added and during incubation and at appropriate time intervals, a certain volume of suspension is collected and washed with buffer. Microorganisms are then centrifuged and separated from the supernatant (Figure I - 16) (Chapman and Georgopapadakou 1988) (Chapman and Georgopapadakou 1989). Finally, after an optional lysis step, the drug contained in the microorganisms is quantified using various techniques: measurement of the radioactivity of isotopically labeled drugs (Bedard, Wong et al. 1987) (Mortimer and Piddock 1991), colorimetries of the β -lactam that have degraded in the periplasm by β -lactamases (Lim and Nikaido 2010) (Zimmermann and Rosselet 1977), measurement fluorescence spectroscopy of the intrinsic signature of quinolones or tetracycline (Mortimer and Piddock 1991) (Chapman and Georgopapadakou 1989) (Phetsang, Blaskovich et al. 2014) (Ammor, Flórez et al. 2006), mass spectrometry (Phetsang, Pelingon et al. 2016) (Cai, Rose et al. 2009), or evaluation of the biological effect of the lysate on bacteria colonies (Mortimer and Piddock 1991) (Bedard, Wong et al. 1987).

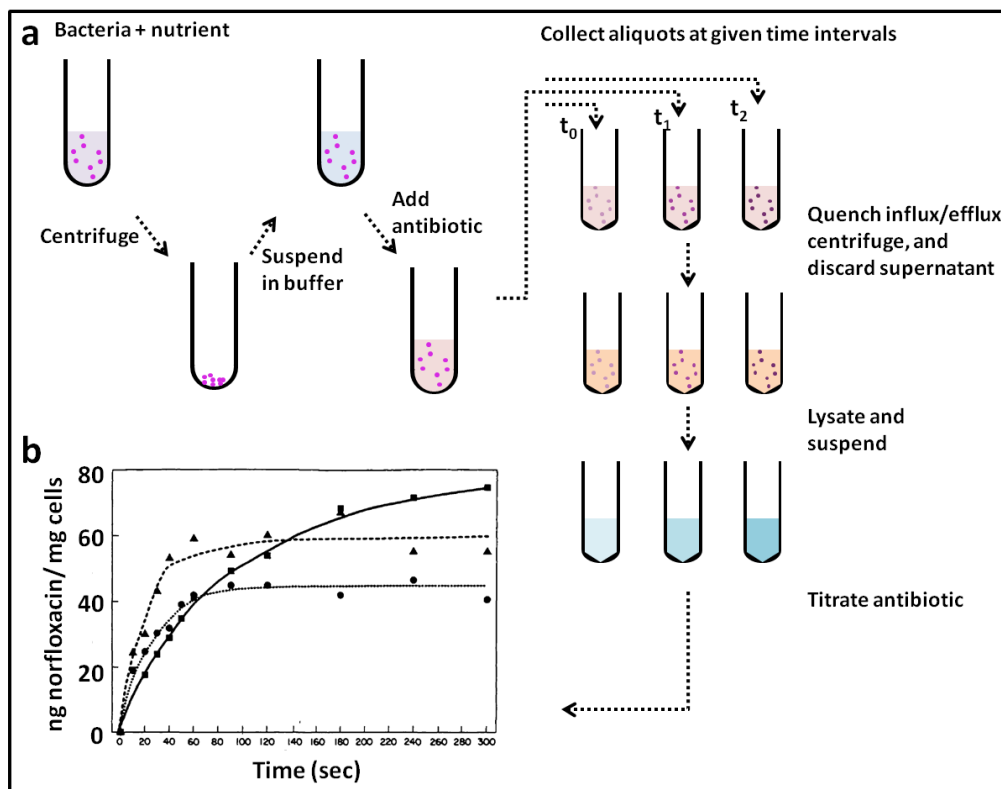


Figure I - 16. Schematic representation of a typical influx / efflux bulk study performed on living bacteria. (a) Microorganisms are incubated with the antibiotic and the amount of drug present inside them is determined as a function of time by aliquot collection, separation and titration quantification. (b) Example of uptake curve measured using UV fluorescence spectroscopy to evaluate the drug titer of the lysate supernatant. Image (b) take from (Mortimer and Piddock 1991).

1.1.2 Artificial systems

Liposome swelling assays are performed using pure porins embedded into multilamellar vesicles that also encapsulate some molecules unable to cross the membrane. This suspension is mixed with an isoosmotic solution containing the antibiotic and the optical density (OD) is monitored. If the solute cannot permeate the multilamellar liposomes, the OD remains unchanged. However, if the solute is permeable, this will lead to an osmotic gradient and induce an influx of water towards the inside of the liposomes, thereby swelling them (Figure I - 17). One intrinsic problem with this method is that porin integration is not controllable, and that the flux per porin cannot be estimated accurately. So alternative technologies for porin studies were sought (Yoshimura and Nikaido 1985) (Nikaido and Rosenberg 1983).

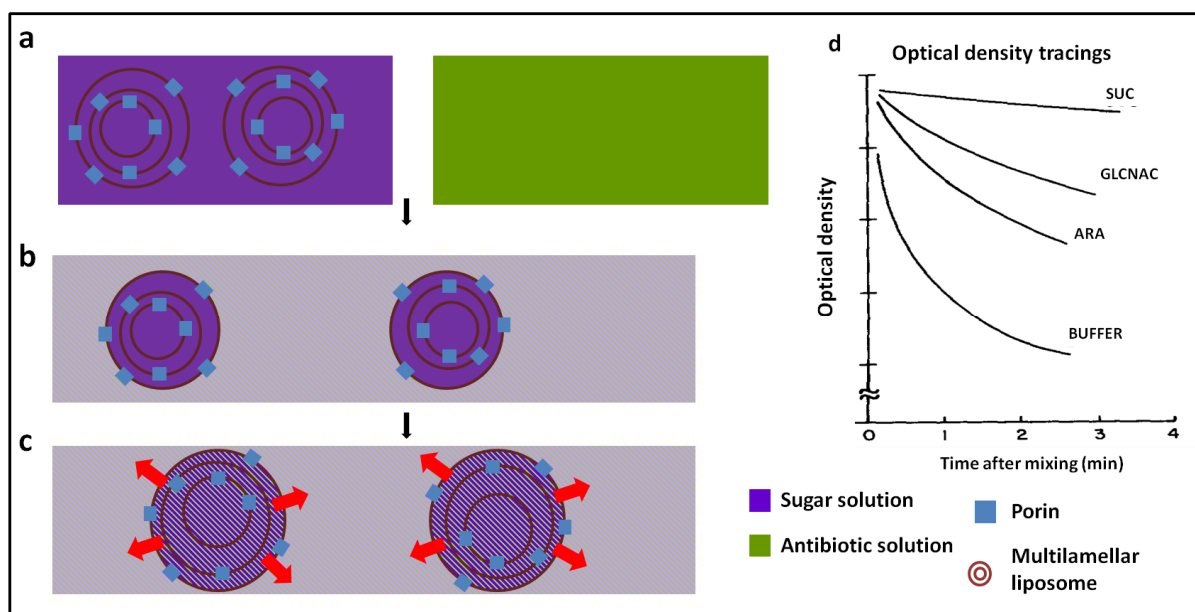


Figure I - 17. Schematic representation of the swelling assay dedicated to the measurement of influx on proteoliposomes including porins. (a-c) Multilamellar liposomes are prepared in a solution of a non interacting and non permeable solute, and mixed with an isoosmotic antibiotic solution. Eventually, the entry of the antibiotics into the liposomes leads to their swelling. (b) Time trace of the OD obtained in a study on small molecule permeation (SUC: sucrose, GLCNAC: N-acetyl-D-glucosamine, ARA: L-arabinose). Image (d) taken from (Nikaido and Rosenberg 1981).

In addition to the above method of relying on OD measurement, fluorescence changes can be used to characterize the molecular transport through the membrane of vesicle. In this case the experiments must of course track solutes that are fluorescent or use reporters which emission is modulated when the concentration of the translocated molecular varies. Such systems have been harnessed to study porins as well as efflux pumps (Nikaido and Takatsuka 2009) (Ghale, Lanctôt et al. 2014) (Verchère, Dezi et al. 2015).

1.2. Single cell studies

In addition to bulk studies there are methods that no longer deal with object assemblies but rather focus on single bacteria or single liposome. When living cells are scrutinized, this approach becomes especially pertinent to emphasize on genetic variations in a given population.

1.2.1. Natural systems

In the report of Pu et al., the efflux process of Bocillin FL, a fluorescent conjugate of a β -lactam (Figure I - 24), is followed in *E. coli* relying on epifluorescence microscopy. Bacteria are first incubated with the drug and then trapped onto a coverslip coated with poly-L-lysine. The images are taken as soon as the antibiotic solution is flushed away and replaced by fresh medium, the microfluidic washing process being very quickly thanks to the advective flow (Figure I - 18). The efflux

rate is then extracted for individual cells from the decrease of the fluorescent signal over time. It is found that a single exponential function can be used for fitting (Pu, Zhao et al. 2016).

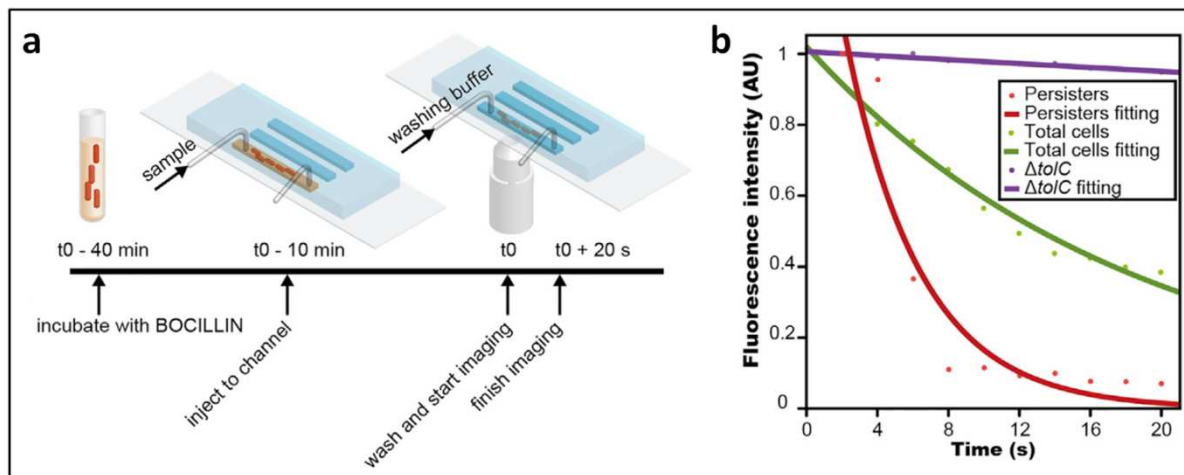


Figure I - 18. Schematic representation of efflux rate measurements performed in epifluorescence microscopy on bacteria immobilized in a fluidic channel. (a) *E. coli* that have been incubated with the fluorescent antibiotic Bocillin FL are injected into a PDMS microfluidic channel coated with poly - L- lysine, so that they will attach to the coverslip. The imaging by total internal reflection fluorescence (TIRF) microscopy starts as soon as the medium containing the antibiotic is washed away and replaced by fresh M9 minimal medium. (b) Intracellular fluorescent intensity decays after antibiotic removal is well fitted by a single exponential function. Results are presented for 3 different cells: persisters, which resist the antibiotic; susceptibles, which do not resist; and $\Delta TolC$ mutants, which have a reduced ability to expel drug molecules. Image taken from (Pu, Zhao et al. 2016).

My PhD has been performed according to a similar approach and the work of my predecessors will be introduced below (Chapter II, Section III.2).

1.2.2 Artificial systems

The reports of Cama et al. (Cama, Chimere et al. 2014) (Cama, Bajaj et al. 2015) (Cama, Schaich et al. 2016) propose a microfluidic chip to monitor the influx process. Porins are embedded into giant unilamellar vesicles at an estimated density of 1700 to 1800 molecules per μm^2 (Cama, Bajaj et al. 2015). The suspension of vesicles is mixed with a solution of quinolone in a T-shaped channel and the flow is kept running over long trajectories. Knowing the distance between two given positions in the channel, it is possible to calculate the time difference for the same vesicle to pass through these two points. By analyzing the fluorescence intensity increment between the two images, the number of antibiotic molecules that have entered into the vesicle can be determined (Figure I - 19).

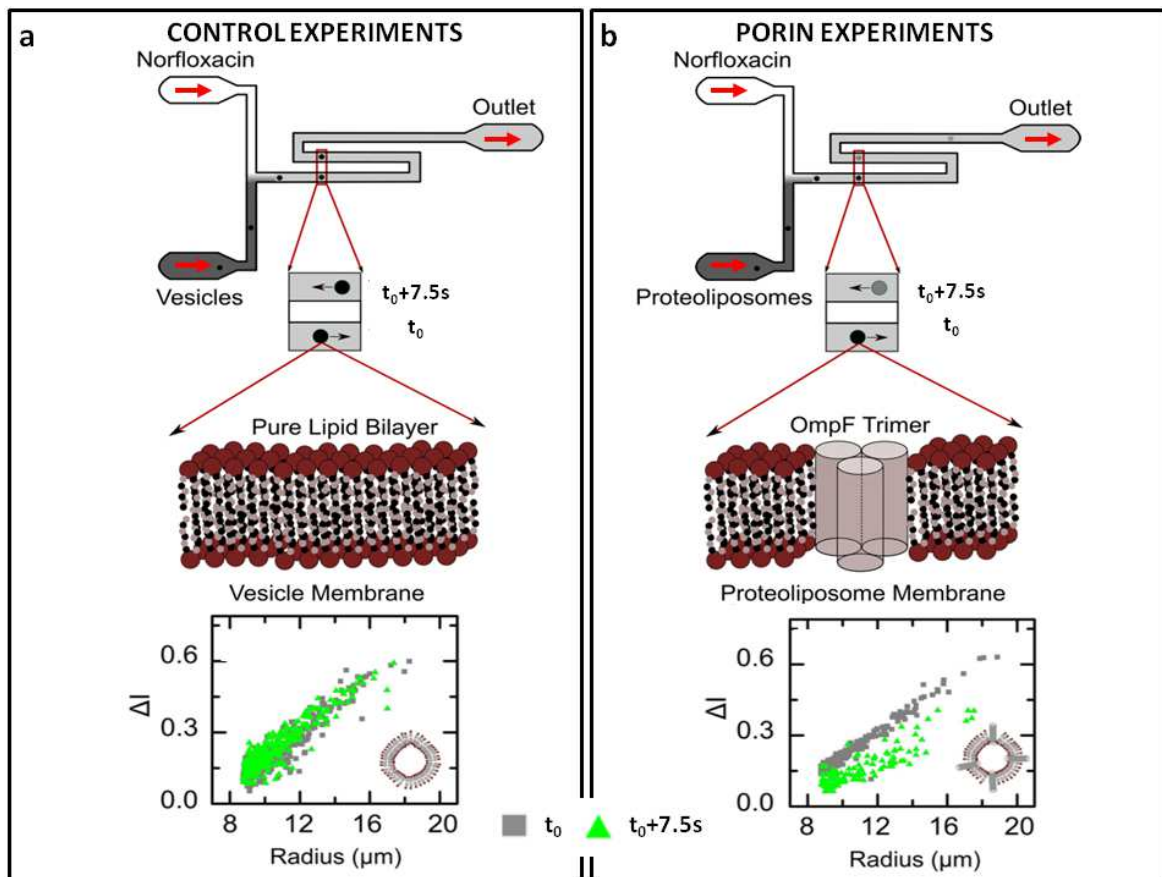


Figure I - 19. Schematic representation of the lipid vesicle assay. Liposomes or proteoliposomes are mixed with a fluoroquinolone solution (norfloxacin at 1mM) in a T-junction microfluidic chip and the drug autofluorescence is measured on an UV epifluorescence microscope. The vesicles are detected at an initial time t_0 immediately after mixing and 7.5 s later, which corresponds to a distance of 7.4 mm downstream. Detection of the autofluorescence intensities within the vesicles at both points enables the calculation of the drug permeability coefficient for each vesicle. (a) Control experiments, i.e. pure lipid bilayer vesicle with no porin. (b) Proteoliposome experiments, i.e. vesicle with embedded OmpF. Image adapted from (Cama, Bajaj et al. 2015).

I.3 Single protein studies

Single channel electrophysiology is another approach to study porins. It provides single channel resolution and it is able to provide information on the interaction of pore with the translocated molecules (e.g. the antibiotic).

Patch-clamp is a useful method to achieve single channel ion current measurement. However, the size of the bacteria is too small: an *E. coli* is about 3 μm length and 1 μm width, while a micro pipette used in patch-clamp technology has a diameter of 1-3 μm (Fertig, Blick et al. 2002) (Goodman and Lockery 2000). The shape and size constraints of micro pipette aperture result in the following artificial system instead of using natural system.

The experimental setup typically includes a teflon wall with a circular aperture (60 to 80 μm in diameter) that separates two symmetrical compartments (cuvettes). An artificial lipid bilayer is

stretched on this aperture and a stock solution of porin is added to one of the chambers. Additionally, electrolyte fills the two cuvettes, and a transmembrane voltage is applied. The insertion of a porin into the lipid bilayer results in a well characterized jump of the ionic current. Single channel monitoring can be achieved by choosing the appropriate protein concentration. The addition of antibiotic to one chamber and their subsequent diffusion through the porin yields ion current blockades. Thus, high resolution analysis of these ion current fluctuations permits a detailed tracking of the transport of single solute molecule, on a millisecond time-scale (Figure I - 20) (Delcour 1997) (Delcour 2009).

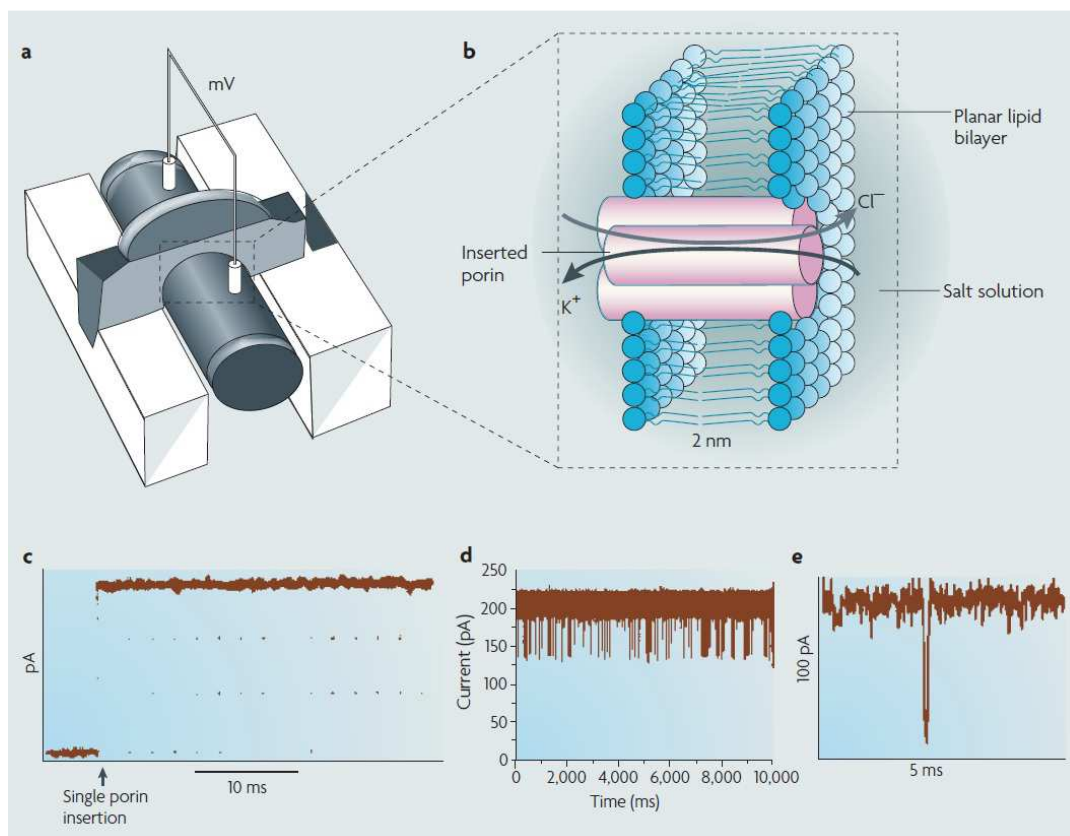


Figure I - 20. Schematic representation of electrophysiology measurements of antibiotic translocation through porins inserted in suspended membrane, i.e. black lipid membrane. (a) Experimental set up with the artificial phospholipid membrane separating the two chambers filled with an electrolyte solution and with the electrical apparatus used to both apply a fixed voltage across the membrane and detect the resulting ionic current. (b) Schematic view of a porin trimer inserted in the lipid bilayer. (c) Increased in conductance observed following the insertion of a single porin into the membrane. (d) Current blockades observed after addition of antibiotic in one of the chambers (here 5 mM ampicillin). (e) Zoom on a single event. Experimental conditions were 1 M KCl; 50 mV of transmembrane potential. Image taken from (Pages, James et al. 2008).

II. Our biological system

Unlike in the previous examples, in which artificial physico-chemical models are used to decipher the workings of the influx / efflux machinery, we decided to deal with live bacteria. More

precisely, we chose to study the interaction between *E. coli* and ciprofloxacin, which are respectively a representative Gram-negative bacteria and a representative fluoroquinolone molecule. This choice is in the line with the previous research conducted by the DISCO beamline of SOLEIL synchrotron, in collaboration with the UMR-MD1 team in Marseille.

II.1. *Escherichia coli*, a typical Gram-negative bacteria

In addition to the proteins related to drug resistance that have been introduced in the previous section, we here present *E. coli*'s main characteristics, the relationship of this microorganism with human being and the associated public health issues, as well as the reasons why it has been chosen as a model organism.

II.1.1. Main characteristics

The *Enterobacteriaceae* are a large family of Gram-negative bacteria that includes, along with many harmless symbionts, some familiar pathogens such as *Salmonella*, *Escherichia*, *Klebsiella*, *Serratia*, and *Shigella*.

Escherichia coli was described for the first time in 1885 by the German pediatrician Theodore Escherich, who found this microbe associated with infant enteritis (Nomenclature 1958). *E. coli* is the representative species of the genus *Escherichia*. DNA-DNA hybridization studies have led to the identification of five other species within this genus: *E. hermannii*, *E. vulneris*, *E. fergusonii*, *E. albertii*, and the recently described *E. marmotae* (Brenner, Davis et al. 1982) (Brenner, McWhorter et al. 1982) (Farmer III, Fanning et al. 1985) (Huys, Cnockaert et al. 2003) (Liu, Jin et al. 2015). All these species are generally related to human pathology and each has its own biochemical characteristics — that make it possible to identify them.

E. coli are rod-shape bacilli measuring 0.3 to 1 μm in diameter and 1 to 3 μm in length. These dimensions can vary considerably depending on the strain and on the growth conditions. *E. coli* has flagella throughout its body, used for movement around its environment. Its type of metabolism is chemo-heterotrophic. Nonsporulating, facultative anaerobes, *E. coli* possess both a respiratory chain and a fermentative metabolism. More precisely, it is able to produce ATP by aerobic respiration if oxygen is present or to switch to sugar fermentation to produce lactic acid and gas if oxygen is absent. *E. coli* cannot grow at extreme temperatures or pH, nor can it perform photosynthesis. It is a prokaryote, containing only a simple organelle ribosome, no nucleus, but a nuclear region. Its genome is a circular molecule of about 4 700 kbp, coding for more than 4 200 proteins. *E. coli* cytoplasm can also harbor multiple circular plasmids DNA (Chapter I, Section II. 2.1).

II.1.2. Relevance for public health

Escherichia coli is a bacterium that is commonly found in the gut of humans, and of some other warm-blooded animals (mammals and birds) (Kaper, Nataro et al. 2004) (Greatorex and Thorne 1994). It colonizes the human digestive tract asymptotically in the first few hours after birth and it is therefore the dominant bacterial species of the facultative anaerobic flora of the human colon (Freter, Brickner et al. 1983) (Berg 1996). Its ecological niche is located in the layer of mucus secreted by the epithelium of the colon; along with the other components of the microflora. This bacteria thus provides a protective barrier for the mucosa (Poulsen, Lan et al. 1994). The concentration of *E. coli* per gram of faeces varies from individual to individual but is around 10^7 to 10^9 colony forming units (CFU), which is higher than in other mammals (Tenaillon, Skurnik et al. 2010).

For a very long period of time, *E. coli* has been regarded as a non-pathogenic bacterium, being part of the normal intestinal flora. However, some strains can cause severe foodborne diseases. By the middle of 20th century some serotypes were already known to be pathogenic to humans and animals. The infection is usually transmitted through consumption of contaminated water or food, such as undercooked meat products and raw milk. The Foodborne Disease Burden Epidemiology Reference Group (FERG) of the WHO estimated that, from 2010 to 2015, there were ~ 582 million cases of foodborne enteric diseases and 351 000 associated deaths, of which 37 000 were due to the enteropathogenic *E. coli* (WHO World Health Day 2015). For example, the O157: H7 serotype, which was first discovered in 1982 in the United States, is enterohaemorrhagic. An infection with this type of pathogenic bacteria may lead to hemorrhagic diarrhea, sepsis, and sometimes kidney failure. Therefore, such pathogen is particularly dangerous, especially for children and elderly (Karch, Tarr et al. 2005). As pointed out in a report of 2002, this serotype caused 73 000 illnesses in the United States annually in the few years preceding the study and 52 % of the transmission routes were foodborne.

II.1.3. Use as a model organism

A model organism is a non-human species that is widely studied, usually due to its short generation cycle, simple nutritional requirements, well established genetic background, and also ease of breeding and reproducing in laboratory conditions. It additionally has particular experimental values so that research results can help to understand a representative phenomenon, also found in other species.

E. coli has many attributes that make it an ideal candidate for being a model organism (Watson 1992) (Blount 2015):

- It is able to grow and reproduce very rapidly. Its population can double in about 20 minutes, facilitating the experiments on evolution thanks to its adaptative faculties.

- *E. coli* can survive in variable growth conditions. Culture media containing simple and inexpensive ingredients and nutrients can successfully support its growth.
- Most of the naturally occurring strains of *E. coli* are harmless to humans and to the environment.
- *E. coli* can easily be genetically manipulated. It is a simple prokaryotic organism, the genome of many strains of *E. coli* has been sequenced and the genetic characters of this microorganism are well investigated.
- Finally, plasmids, which are additional and separated DNA components, are useful tool for scientists to study cell physiology or to produce some products. *E. coli* has served as a host organism to express exogenous genes through the so-called recombinant DNA technology. Thus, the most important advantage contributing to the use of *E. coli* as a model organism is also that it plays an important role in the field of biotechnology.

II.2. Quinolones, a family of fluorescent antibiotics

These molecules are broad-spectrum antibiotics. This term qualifies an antibiotic that acts against a wide range of disease-causing bacteria, Gram-positive as well as Gram-negative ones.

II.2.1. Structural properties

Quinolones displays a common 4-quinolone skeleton. The first quinolone, the nalidixic acid, was introduced clinically in 1962 to treat urinary tract infections (Figure I - 1), as it showed antibacterial activities against certain Gram-negative pathogens (Hooper and Rubinstein 2003). This molecule is now rarely used because of its poor oral absorption and its side effects (Rubinstein 2001). Today, the currently prescribed quinolones are mostly fluoroquinolones, which have a fluorine atom attached to the central ring system (Figure I - 21).

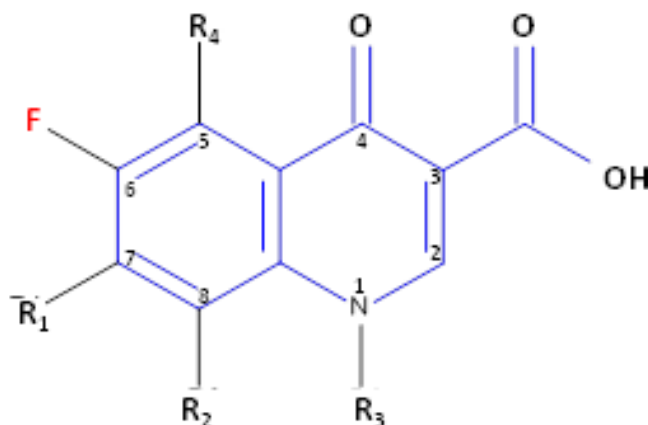


Figure I - 21. Generic molecular structure of fluoroquinolones. The 4-quinolone skeleton is in blue and the characteristic fluorine atom in position 6 is in red. The R1 group is often a piperazine one.

Quinolones are divided into generations. The nonfluorinated drugs always enter into the first-generation category. For the other generations no commonly accepted classification applies except that, in general, the spectrum of the earlier generations is narrower than the one of the later generations (Ball 2000) (King, Malone et al. 2000). During the evolution between generations, modifications have been brought onto the basic molecular structure, for instance, replacing hydrogen by fluorine at position 6, substituting a diamine residue at position 7, or adding new residues at position 1 (Figure I - 21). Those changes have led to enhanced antibacterial efficacy or reduced side effects. Upon medical prescription the effective concentrations of fluoroquinolones in human tissues is often around 1 - 30 nmol/mL (Matchette, Agrawal et al. 2007). Currently, quinolone products have reached their fourth generation.

II.2.2. Mechanism of action

The target of fluoroquinolones is bacterial DNA, which implies that the drug molecules must enter the bacteria to be effective. The viability of a cell depends on the supercoiling of its genome, a parameter that is controlled by enzyme such as the topoisomerase II (also known as DNA gyrase) or the topoisomerase IV. More precisely, these two proteins are able to relax the additional twist that is generated by the added during replication. Quinolones can disrupt the function of these enzymes and cause irreversible damage to chromosomes, thus inhibiting bacterial cell division (Figure I - 22) (Hooper 2000, Hooper 2001) (Drlica and Zhao 1997). It is generally accepted that the activity of quinolones is to inhibit topoisomerase IV in the Gram-positive bacteria and topoisomerase II in the Gram-negative ones (Kohanski, Dwyer et al. 2010).

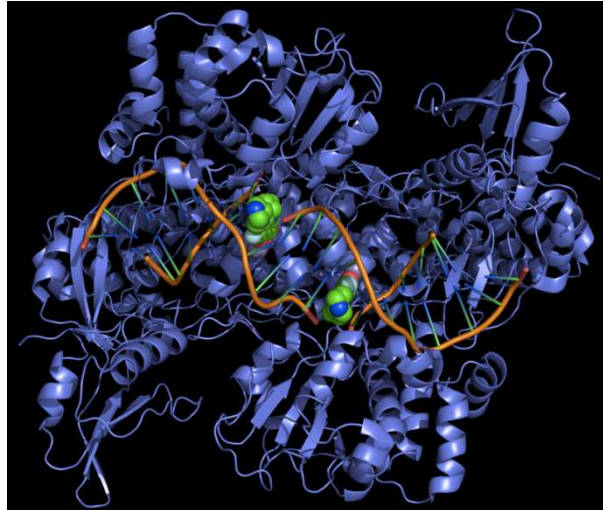


Figure I - 22. Structure of the bacterial topoisomerase II (in blue) with DNA (in orange) and two complexed ciprofloxacin molecules (in green). Image taken from (Wikipedia quionolone).

II.2.3. Relevance for public health

Fluoroquinolones are broad-spectrum antibiotics. The most frequently prescribed molecules today are Avelox (moxifloxacin), Cipro (ciprofloxacin), and Levaquin (levofloxacin). They represent several tenth of the global antibiotic prescription. Their coverage is indeed wide, from genitourinary infections, respiratory infections, and intestinal infections to typhoid. However, extensive and broad uses bring many hazards on the long term:

- The extensive application of broad-spectrum antibiotics favors the emergence of a large number of resistant strains, at the patient level as well as at the population one.
- Long-term prescription increases the occurrence of adverse effects. For instance, gastrointestinal reactions (e.g. nausea, dyspepsia, vomiting), central nervous system reactions (e.g. dizziness, insomnia, headache), as well as hepatotoxicity have been reported.
- During the long-term and high-dose application of broad spectrum antibiotic, pathological, neutral, as well as beneficial bacteria are indiscriminately attacked. Resistant strains can not only survive, but also gain some opportunity to multiply because of the loss of the normal flora and of the related disappearance of antagonists. Flora imbalance can finally lead to a secondary infection.

II.2.4. Spectroscopic properties

In our studies, fleroxacin and ciprofloxacin are chosen as models for the fluoroquinolones family. Their chemical structure and their fluorescence excitation/emission spectra are shown in Figure I - 23. These drugs have generally 2 excitation peaks, a main one with a maximum in the 250 - 275 nm range, and a broader weaker secondary one located around 330 nm. The emission peak is located around 420 nm (Albini and Monti 2003).

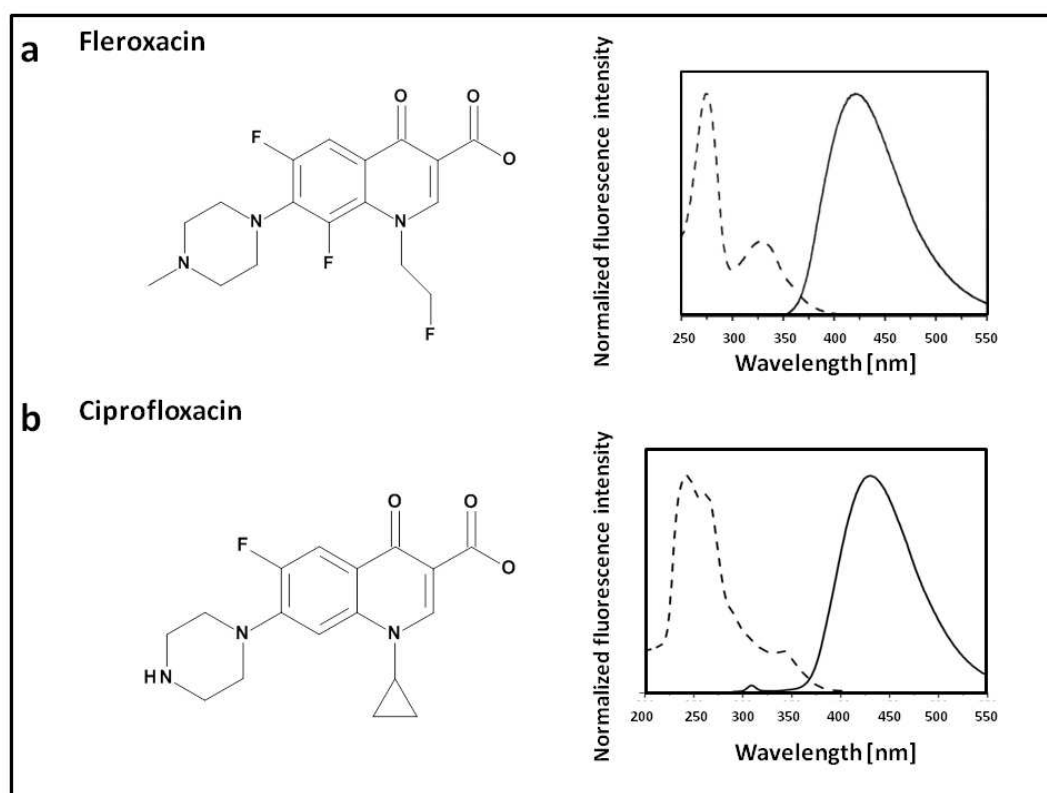


Figure I - 23. Chemical structures and fluorescence spectra of two fluoroquinolones – (a) Fleroxacin and (b) Ciprofloxacin. Excitation (---) and emission (—) spectra of the drugs dissolved at 750 ng/mL in PBS pH=7. Data provided by the DISCO beamline.

III. The experiments performed at SOLEIL

This research was initiated in 2013 as a part of an Innovative Medicines Initiative called TRANSLOCATION. More precisely, our sub project was led by the UMR-MD1 in Marseille and by the SOLEIL synchrotron. Its goal was to develop a label-free measurement under an UV microscope, in order to obtain real-time for obtaining knowledge of the transport of antibiotics across the bacteria cell wall. Understanding the mechanisms that bacteria use to expel out certain molecules would surely help to decipher some of the inner working of drug resistance. Concretely, with this thesis my

task was to conceive and fabricate a microfluidic device with the help of which the temporal and spatial resolution of the influx/efflux measurements could be improved.

III.1. Intrinsic fluorescence imaging of antibiotic concentration

III.1.1. Necessity of a real-time label-free technique

Studying the dynamics of transport of molecules or atoms in biological systems, or the dynamics of chemical reactions, often require to label the compound of interest. Generally, this can be achieved by isotopic labelling or by conjugation to a fluorophore.

At the atomic level, isotopic labelling was developed by George de Hevesy (George de Hevesy, 1943). Specific atoms in the reactant are substituted by their isotope. Then, the molecule is allowed to be transported in the living object and to enter the metabolic pathway. Through the tracking of the spatial position of the isotope, as well as through the determination of the molecular species it now belongs to, the fate of the original reactant can be hypothesized. In this technique, the physical and chemical properties of the labelled compounds are not very different from the one of the unlabelled one, which prevents artifacts. However, the labelling process is not an easy nor a cheap one, and the detection has a poor temporal and spatial resolution. Nevertheless, the influx/efflux of many antibiotics has been studied in this way. For instance, reports exist on quinolones (Diver, Piddock et al. 1990), tetracycline (Shales, Chopra et al. 1980), and chloramphenicol (Mortimer and Piddock 1993).

Conjugating the compound of interest to a fluorescent dye is an alternative strategy. Small fluorophores such as fluorescein, bodipy, and rhodamine have molecular weights that vary from several hundreds to a thousand Daltons. Although small, those fluorescent groups thus have a size similar or larger than the molecule to be marked (Figure I - 24). As a consequence, it likely changes its transport properties and reactivity. However, compared with isotopic labelling, this method is less expensive and more convenient. In addition, the spatial and temporal resolutions are better: single cell and sub-second of observations are possible (Pu, Zhao et al. 2016).

As an example of transition between the two previously described labelling techniques, we can cite studies on the binding mechanism of β -lactams (Figure I - 7) onto Penicillin Binding Proteins (PBP). First, isotope labelling was used in 1972 by Suginaka et al. who reported the structure and function of PBP as a necessary element for bacteria to maintain normal morphology (Suginaka, Blumberg et al. 1972) (Spratt 1977) (Noguchi, Matsuhashi et al. 1979). They could indeed detect the presence of this protein on the surface of the bacteria relying on radioactive penicillin. Then, in a subsequent study, a fluorescent derivative of penicillin V was synthesized, called Bocillin FL (Zhao, Meier et al. 1999). More precisely, a bodipy group was grafted on the R position of the general β -

lactam structure (Figure I - 24). This molecule could be tracked, with an excitation set at 488 nm and an emission band pass filter 530 ± 15 nm are used (Pu, Zhao et al. 2016).

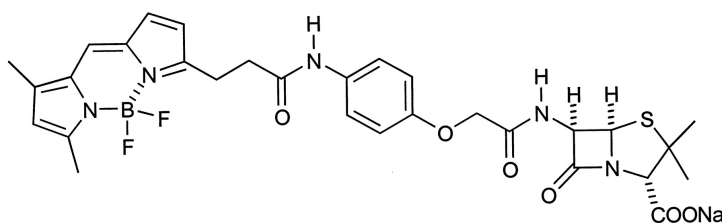


Figure I - 24. Structure of Bocillin FL. Image taken from (Pu, Zhao et al. 2016).

Fortunately, labelling is not always necessary. Drugs like quinolones and tetracyclines (Figure I - 10, Figure I - 9) present conjugated structures that can indeed be excited and emit fluorescence in the UV range (Albini and Monti 2003) (Jamme, Villette et al. 2010) (Ammor, Flórez et al. 2006). This fluorescence is intrinsic to the antibiotic, and the drug now can be detected without necessitating the introduction of a foreign label that could modify its biolocalization or any of its properties. Hence, besides mass spectrometry (Phetsang, Pelingon et al. 2016) (Cai, Rose et al. 2009), fluorescence spectrometry can also be a label-free technique. However, until very recently it was not able to provide real-time monitoring — compare the methods in Section I.1.1 to the ones in Section I.2.1 and I.2.2 of current chapter.

III.1.2. Description of the Telemos epifluorescence microscope

Synchrotron SOLEIL is a third generation machine. The work carried out during my PhD was performed on the Telemos imaging endstation of the DISCO beamline (see Chapter IV, Section IV.1 for details).

Synchrotron radiation. It is an electromagnetic radiation emitted when charged particles are accelerated radially, that is, when they are subjected to an acceleration perpendicular to their velocity vector. The acceleration can be produced by bending magnets, undulators, and/or wigglers. Such technology usually provides a broad continuous spectrum from far infrared to hard X-rays. These photons can then be used directly or filtered at a desired wavelength through an optical element, such as a grating or a crystal monochromator. In general, the following characteristics are found:

- Synchrotron radiation light is generated in ultra-high vacuum, no pollution is caused by impurities.
- A synchrotron is a high intensity light source, with high radiated power density. X-rays issued from a third-generation machine are 10^8 to 10^{10} times brighter than the ones coming from a conventional X-ray machine.
- Light drawn from the bending magnet is almost completely linearly polarized on the electron orbital plane. In addition, any polarization state can be obtained from a specially designed element. Such a light source can thus be used to study the orientation of particular parameters in a sample.
- Synchrotron radiation light is concentrated in a very narrow cone centered around the direction of the electron movement. It is almost as parallel as in a laser. With such collimation it is possible to undertake studies on trace elements in very small samples.
- Synchrotron radiation is pulsed. The pulse duration is narrow, being tunable between 10^{-11} and 10^{-8} s with a spacing between 10^{-5} and 10^{-3} s. Such a feature is very useful to study the dynamics of physical, chemical, or biological phenomena.
- The electron beam inside the storage ring can live up to about 10 h, leading to a stable beam position and a good reproducibility.

UV fluorescence microscopy. UV microscopes were first developed by August Köhler and Moritz von Rohr (Swingle and Briggs 1907). It is known that the resolution of optics is inversely proportional to the wavelength of light, so when short wavelengths UV are used, the resolution is improved. As for standard epifluorescence microscope, the light source is generally a mercury-vapor lamp and the optical path makes use of an excitation filter, a dichroic mirror, and an emission filter. An important issue encountered in UV microscopy is the transparency of the optical components (e.g. coverslips and lenses). Most of ordinary glasses absorb a large amount of light under 340 nm, so we have to use materials such as quartz, which can transmit UV down to 190 nm.

The DISCO beamline uses light ranging from the Vacuum Ultra Violet (VUV) range to the visible one, i.e. from 180 nm to 700 nm. It performs researches in biochemistry, chemistry, and cell biology (Jamme, Villette et al. 2010) (Jamme, Kascakova et al. 2013).

When using synchrotron radiation coupled with an epifluorescence microscope, the excitation wavelength is precisely selected by the line monochromator; therefore, no excitation filter is required and the wavelength of the excitation photons is very accurately defined. Additionally, the greatest benefit that we have is the high photon flux. For instance, at the wavelength of 280 nm, the

photon flux reaches $1.6 \times 10^{12} \text{ s}^{-1}$, this corresponds to 10^{-5} W power (Data provided by DISCO beamline).

III.1.3. Specific issues related to UV fluorescence observation

Label-free fluorescence microscopy is a powerful tool; however, when applied to our project two issues have to be discussed.

Autofluorescence. The objects that we are studying all display natural fluorescence under UV illumination. On one hand, bacteria include autofluorescent proteins having tryptophan and tyrosine residues, as well as small molecules such as nicotinamide adenine dinucleotide (NADH), and flavin adenine dinucleotide (FAD); on the other hand, the antibiotic molecules are also fluorescent. The problem is that there are considerable overlaps of the excitation and emission peaks (Figure I - 25), suggesting that the autofluorescence signal issued from the bacteria will perturb the quantitative determination of the fluoroquinolone concentration in the 420 – 480 nm collection channel.

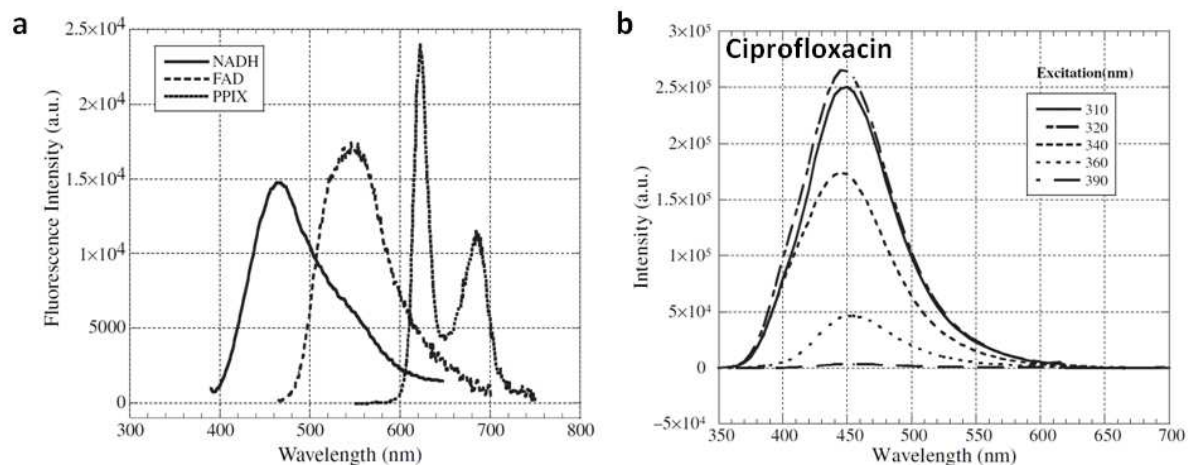


Figure I - 25. (a) Fluorescence emission spectra of autofluorescent molecules that can be found in bacteria. Fluorescence emission spectra of NADH excited at 340 nm, FAD at 450 nm, and protoporphyrin IX at 408 nm. (b) Fluorescence emission spectra of ciprofloxacin recorded in phosphate-buffered saline using different excitation wavelengths, from 310 to 390 nm. Images taken from (Matchette, Agrawal et al. 2007).

Toxicity. In the 260 to 320 nm range, some biological substances show a strong specific absorption. For instance, nucleic bases display strong absorption peaks in the 260 to 280 nm region (Cantor and Schimmel 1981). This property can be used for detection as well as for specific destruction of the chromosome and thus alteration of the genetic transcription: this is the principle of UV sterilization. (Meulemans 1987).

Moreover, generation of reactive oxygen species (ROS) by UV irradiation has been documented (He and Häder 2002) (Heck, Vetrano et al. 2003). These ROS can react with cellular constituents, resulting in protein damage and lipid peroxidation. As a consequence, it may lead to the alteration of the permeability of the bacterial membrane and/or disruption of transmembrane ion gradients. These phenomena can eventually cause cell death (Pattison and Davies 2006) (Santos, Moreirinha et al. 2013).

In our case, the intensity deposited on the sample is around 0.4 μW per pixel, since 1 pixel = $0.5 \times 0.5 \mu\text{m}^2$, it corresponds to 1.6 W/mm^2 (Jamme, Villette et al. 2010). Depending on the brightness of the sample, damage can be limited by using low integration times or lower resolution images. Furthermore, we want to make clear that our research topic is not the growth cycle nor the study of bacteria lineage, but the influence of the number of efflux pumps on drug accumulation. We focus on physiological processes taking place on a dozen of minutes time-scale so we assume not to be concerned too much by the deleterious effects of UV illumination.

III.2. Previous protocol

Before the beginning of my PhD work, experiments on the DISCO beamline were performed in the “static chamber” (Kascakova, Maigre et al. 2012) (Cinquin, Maigre et al. 2015), a set up that did not involve any fluidic actuation.

III.2.1. Description

The excitation wavelength was set at 290 nm, a wavelength still located in the excitation peak of fluoroquinolones, but, at the same time, a position that minimizes the contribution of bacterial autofluorescence (Figure I - 23, Figure I - 25) (Wagnières, Star et al. 1998). Therefore, enough photons could be obtained while not being too much polluted by unmeaningful signal.

Bacteria were centrifuged after culture. The next steps were then carried out rapidly. First, some drops of antibiotic solution were added to the bacteria pellet and the suspension was stirred. Then, half a microliter of the mixture was deposited on a quartz coverslip, and another identical coverslip was superimposed. These two disks were subsequently clamped in a cell holder, and mounted onto the microscope stage (Figure I - 26).

After focusing, interlaced UV fluorescence and transmission video acquisition was undertaken. More precisely, three channels were defined: a transmission one to monitor the bacteria position (acquisition during 100 ms); a 327 - 353 nm fluorescence emission one to record the

autofluorescence (acquisition during 30 s); and a 420 - 480 nm fluorescence emission one to record the antibiotic uptake (acquisition during 30 s).

When analyzing the data, separation the bacterial autofluorescence signal from the drug fluorescence signal is an important operation. Two spectral channels were to enable this deconvolution, thanks to crosstalk coefficient that had previously been measured with a spectrofluorometry. Importantly, these coefficients have been found to vary during acquisition because of the induced photochemical reactions. Therefore, data acquired in cuvette were of limited use and one had to rely on calibration performed by microfluorospectrometry on the microscope itself. As a conclusion, one can say that crosstalk and bleaching correction was not an easy process.

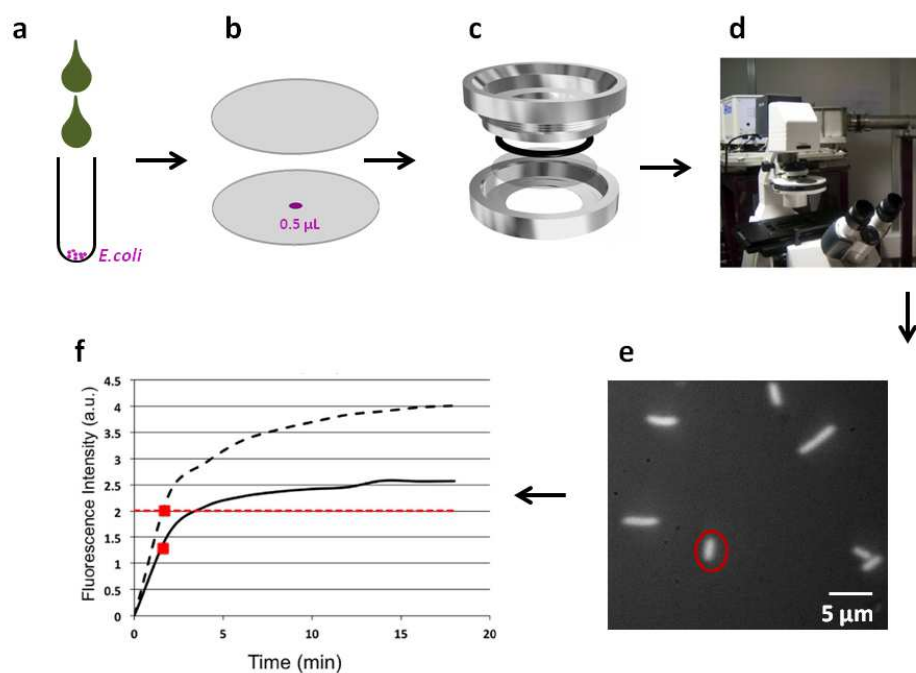


Figure I - 26. Schematic representation of the previous protocol used at SOLEIL to record UV fluorescence time-lapse movies of influx/efflux. (a) Antibiotic solution is added to the centrifuged bacteria after culture. (b) A drop of bacteria mixed with the antibiotic is mounted between two coverslips. (c) The two disks are clamped in the holder, resulting in the so-called “static chamber”. (d) The holder is mounted onto the epifluorescence microscope for monitoring. (e) Images of bacteria are acquired in fluorescence. (f) Images of bacteria are acquired in UV fluorescence and analyzed to yield antibiotic uptake curves. Image taken from (Cinquin, Maigre et al. 2015).

III.2.2. Limitations

We found that, although this protocol gave access to some information on antibiotic uptake, it presented several drawbacks:

- The first minutes of the phenomena were missed because of sample preparation and focus adjustment. Therefore, the curve reporting on fluorescence intensity versus time was not complete;
- Bacteria were completely isolated from the external environment, i.e. the one accessible to the experimentalist. There was no possibility to supply a different antibiotic solution nor to replace it by buffer. Besides, if the imaging process ran for too long the observation chamber could eventually dry;
- It was difficult to acquire the background signal, i.e. without antibiotic, because the first image was taken after uptake had already begun and because the chamber was already filled with antibiotic. Therefore, if this information was needed another sample had to be prepared. However, even though bacteria were from the same culture batch, their autofluorescence could vary because of uncertainties on dilution or on cell mounting.
- The leakage of the bacteria autofluorescence signal into the drug channel, as well as the different bleaching time between the proteins and the drug, complicated a lot the extraction of quantitative data.

III.3. Proposed protocol

As a result, we thought of using a microfluidic device, by which the above issues could be solved one by one:

- Bacteria suspended in buffer are first immobilized in the chamber and the experimentalist can wait until all parameters are well adjusted before starting the introduction of the antibiotic;
- Fluid actuation brings the possibility of connecting the observation chamber with the environment. In such a way, we can control the onset of drug injection but also change the type of injected solution during the course of an experiment. It thus opens opportunities to test the response of the same bacteria to different antibiotic concentrations or different drug/adjuvant mixtures;
- Enough time to get the background information is available between bacteria immobilization and antibiotic injection;
- Bacteria can be irradiated before the antibiotic solution is introduced, so as to photobleach their autofluorescence. The latter signal is then no longer mixed into the one of the drug.

Chapter III. Design and fabrication of the microdevice

I. Criteria to be fulfilled

An important prerequisite that has to be satisfied before implementing a microfluidic technology is a clear understanding of the user's needs, in order to be able to devise microdevices with the appropriate properties. More specifically, we will address below four technical criteria: complete cell immobilization, parallel monitoring, quick change of the chemical environment, and practicality.

I.1. Complete cell immobilization

Even though they can be collectively called "trapping", motion restriction and complete immobilization refer to two different notions. More precisely, motion restriction emphasizes on the fact that bacteria are identifiable and traceable. For instance, when nDEP force is used, one bacterium is held at the center of an electrode cage, but it can still move and tumble (Fritzsche, Rosenthal et al. 2013). This trapping method allows bacteria to be identified, to be distinguished from another one, but the remaining degrees of freedom result in different orientations on each captured image, or worst in a halo when long-exposure time are used. The first strategy to analyze data is then to choose a ROI larger than the microorganism, so that automatic analysis of the fluorescent intensity can be performed. However, too much background signal will be included, which will degrade the signal-to-noise ratio. The second strategy is to manually select the outlines of the bacteria on every image to obtain the fluorescence intensity corresponding to this sole in this

region. However, the size of the selected ROI will vary. Both methods result in imprecise analysis, so that complete immobilization is the only acceptable way of working for us.

I.2. Parallel monitoring of individual bacteria

We would like to have enough number cells in the same image so that it can permit to collect as much information as possible. We have adopted time-lapse video acquisition, so it is possible to analyze independently region-of-interest for each cell by defining appropriate ROI (see Chapter IV, Section IV.2). However, for this strategy to be effective, we need a microdevice that guarantees an arrangement of bacteria in monolayer in order to have positioned in the same focal plane.

We must also provide to each cell a similar environment in term of exposure to antibiotics. Fortunately, *E.coli* cells are generally well dispersed, especially after stirring, and the NaPi buffer is in which the cells stay alive, halt the growth and division: those two features prevent bacteria from gathering into clusters.

I.3. Quick change of the chemical environment

We want to rapidly apply, in series, different compounds (e.g. antibiotics, adjuvants, efflux pump inhibitors) to bacteria. Thus, we need a clear understanding of the mass transfer regimes.

There are two ways by which a solute can reach bacteria: diffusion and advection. Diffusion is always present, it is associated with thermal motion. On the contrary, advection can be present or absent, depending on the experimental conditions. Indeed it is associated with the transport of matter on a large-scale, for instance by a flowing fluid, it is not always present.

If the characteristic length of the system is denoted l and the diffusion coefficient of the solute D , the characteristic time associated with diffusion is $\tau_D = l^2/D$. If the characteristic flow velocity is denoted u , the characteristic time of advection is $\tau_u = l/u$. The ratio of these two times forms the Péclet number: $Pe = \tau_D/\tau_u = lu/D$. If $Pe < 1$, diffusive effects are predominant; conversely, if $Pe > 1$, advective transport takes a higher importance.

Our goal is to design a device and the corresponding experimental protocol. By playing on the different geometrical structures we can manipulate the flow rates and the hydrodynamic resistances for each compartment. Similarly, we have a direct control on the overall applied flow rate. Therefore, we can define the respective importance of advection and diffusion, with the limitation that thermal motion is always the ultimate phenomenon ensuring mixing.

I.4. Practicity

Most microfluidic chips are usually disposable because they are fabricated by bonding a PDMS stamp with a SiO₂ substrate, which makes them difficult to clean and recycle. We mentioned that all optical components for UV microscope are in quartz to minimize absorption, one of the limitations faced while conceiving the device was that the fragile 170 μm thick quartz coverslips are ordered from a supplier located in the USA, and that the delivery cycle is very long (2 months for 200 pieces). In addition, the cost of quartz is high. As a consequence, these two constrains are hardly compatible with the daily consumption of the laboratory, and requirements for a reusable device were strong.

Reusability infers that the production of this device should be easy to assemble and disassemble. Indeed, microbiology laboratories lack clean room facilities.

II. Existing technologies

Microfluidic chips have become an attractive tool for biology over the past 20 years, for reviews on early developments, see (Tabeling 2006), (Whitesides 2006), (Janasek, Franzke et al. 2006), (Psaltis, Quake et al. 2006), (Craighead 2006), (deMello 2006), (El-Ali, Sorger et al. 2006), and (Yager, Edwards et al. 2006). With the help of advanced microfabrication techniques (Xia and Whitesides 1998), (Voldman, Gray et al. 1999), researchers have developed many platforms and devices to capture, manipulate, monitor, and analyze different types of cells. Depending on the object being studied, devices are designed at different scales. More precisely, for eukaryotic cells, which are from ten to several tens of microns large, channels and chambers have a size ranging from a few microns to hundreds of microns. Conversely, the development of chips is a considerable challenge for smaller cells such as bacteria, which are motile and difficult to trap. In the following part, I will analyze the articles that have been published on the latter topic and analyze the features of the reported techniques with respect to the criteria introduced in the preceding section.

II.1. Electromagnetic trapping

II.1.1. Dielectrophoresis

Dielectrophoresis (DEP) is a phenomenon in which a force is exerted on a dielectric particle when it is subjected to a non-uniform electric field (Pohl 1978). This force does not require the particle to be charged, it just needs to have a dielectric constant different from the one of the

surrounding medium. The strength of this force depends largely on this discrepancy but also on the particle shape and size, as well as on the frequency of the electric field.

When a polarizable object is located in a non-uniform electric field, a DEP force, F_{DEP} , appears due to the heterogeneity between the external field and the induced dipole of the object. One has

$$F_{DEP} = 2\pi R^3 \varepsilon_m \operatorname{Re}[K_{CM}] \nabla |\overrightarrow{E_{rms}}|^2$$

R is the particle radius, K_{CM} the Clausius-Mossotti factor, $\operatorname{Re}[K_{CM}]$, the real part of the latter parameter, ε_m the medium permittivity, and $\nabla |\overrightarrow{E_{rms}}|^2$ the square of the electric field gradient. More precisely, the K_{CM} factor can be expressed as

$$K_{CM} = \frac{\varepsilon_p^* - \varepsilon_m^*}{\varepsilon_p^* + 2\varepsilon_m^*}$$

where ε^* is the complex permittivity, of either the medium (m) or the particle (p). They are similarly written as

$$\varepsilon^* = \varepsilon - i \frac{\sigma}{\omega}$$

with σ the electrical conductivity and ω the angular frequency of electric field.

At certain frequencies, the polarizability of the particle is greater than the one of the medium, $\operatorname{Re}[K_{CM}] > 0$ and DEP is positive (pDEP): the particle is directed towards the regions of important electric fields; at other frequencies, the polarizability of particle is lower than the one of medium, $\operatorname{Re}[K_{CM}] < 0$ and DEP is negative (nDEP): the particle is repelled towards the regions of weak electric fields. This principle serves as theoretical basis to achieve on chip separation and manipulation; i.e. trapping of specific biological objects (cells, bacteria) according to their dielectrical properties.

Examples of application of DEP to life sciences include the pairing of cells in pDEP traps to position them before electrofusion (Hamdi, Français et al. 2013); the exploration of the electrical parameters characterizing viable or dead yeasts (Markx, Talary et al. 1994); the continuous separation of yeasts with a mix of hydrodynamic and DEP effects (Doh and Cho 2005); the augmentation of the adherence of bacteria onto a substrate by pDEP or nDEP in order to increase the efficiency of immuno-capture (Yang, Banada et al. 2008, Yang 2009); and the observation of the growth of single bacteria held by pDEP for dozen of hours (Peitz and van Leeuwen 2010).

Kortmann et al. (Kortmann, Chasanis et al. 2009) and Fritzsche et al. (Fritzsche, Rosenthal et al. 2013) (Figure I - 27) have proposed a device enabling contactless levitation of selected bacterial cells by nDEP. The electromagnetic force is generated by eight electrodes arranged as a cage, four on the substrate above and four on the one below. Quick periodic switching of the current immobilizes the cell at the center of the cage, where it experiences the lowest field intensity. Since DEP forces are strong enough to hold bacterium even if a flow is applied, and since the channel is thick enough to enable significant flow rates, sudden changes of the chemical environment are possible thanks to solute advection. Moreover, this device is reusable, because no cell adheres to surfaces. If it is necessary to change the studied cell, one just has to release the current cell and trap another one.

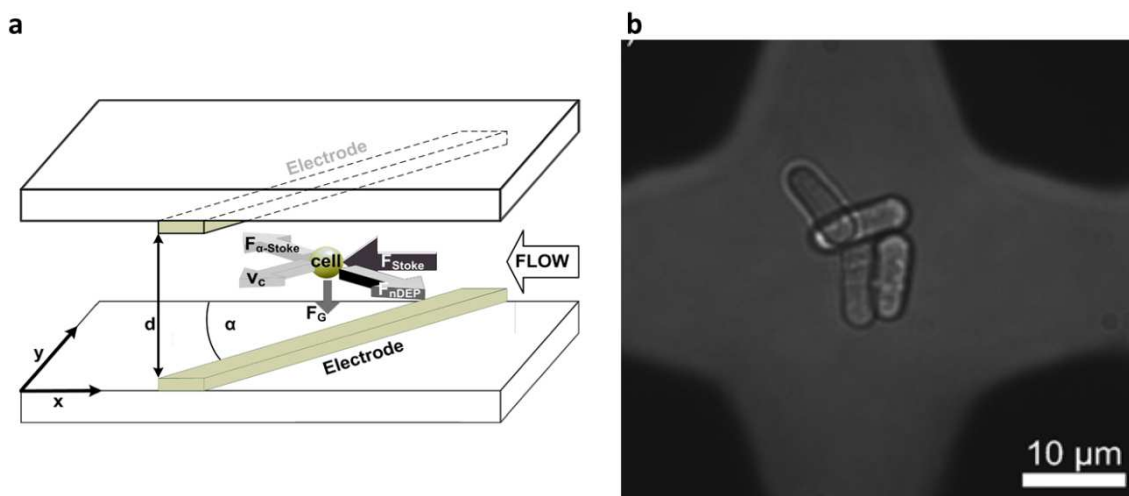


Figure I - 27. Devices to trap cells by DEP. (a) Diagram indicating the main forces that apply to a cell during DEP manipulation in a hydrodynamic flow. Only two of the eight electrodes that make the cage are represented. Image taken from (Fritzsche, Rosenthal et al. 2013). (b) Picture of bacteria hold by nDEP in a steady flow. Image taken from (Kortmann, Chasanis et al. 2009).

Although this technique may be appropriate for many applications, it is not in our case. First, a limited number of cells are held in place. The arrangement of eight electrodes fills most of the field of view (the cage center is about $20 \mu\text{m} \times 20 \mu\text{m}$) whereas only a single $1 \mu\text{m} \times 3 \mu\text{m}$ bacterium is observed. Second, only identification can be achieved but not immobilization: bacteria still display Brownian motion at the bottom of the potential well. Third, despite growth upon long-term retention is a good indication that DEP does not damage bacteria, the influence of the applied electric field on the influx/efflux system, which is powered by an electric gradient, is unknown.

II.1.2. Optical tweezers

Optical tweezers are a physical instrument based on the mechanical effects of lasers, which capture particles by using an optical potential well formed by the interaction between a strongly

convergent light field and particles having a refractive index different than the one of the surrounding medium. Arthur Ashkin achieved the laser-driven manipulation of micron-sized particles for the first time in 1969 (Ashkin 1970). Based on the study of this phenomenon, he proposed manipulating the particles by optical potential and realized the first capture of glass balls in water by using two laser beams propagating in opposite directions. In 1986, Ashkin et al. found that a single beam of an intense focused laser was sufficient to form a three-dimensional stable optical trap that could attract particles and confine them near the focal point: the first optical tweezers were born (Ashkin, Dziedzic et al. 1986) (Ashkin 1997).

Handling samples by optical tweezers can avoid mechanical contact, and the associated damages, and pollutions, showing outstanding advantages in the field of biology, especially for microbiology and biophysics. Optical tweezers are often used to study single cell or single molecule. Importantly in the latter case the manipulated object is attached to a bead that is employed as a handle (Ishii and Yanagida 2000) (Kitamura, Tokunaga et al. 1999) (Visscher, Schnitzer et al. 1999) (Okada and Hirokawa 1999).

As far as trapping of motile bacteria is concerned, some effective optical devices have been proposed, such as silicon photonic crystals (van Leest and Caro 2013) and tapered optical fibers (Xin, Xu et al. 2012) (Xin, Liu et al. 2014). As with the previously described DEP method, bacteria can be repeatedly trapped and released, and the liquid environment can be renewed quickly. In studies by Probst et al. (Probst, Grunberger et al. 2013) (Figure I - 28) and Wakamoto et al. (Wakamoto, Ramsden et al. 2005) optical tweezers are used in another way. They are not applied directly to hold the bacteria in place, but to capture and to move them from one spot to another, for example between a supply channel and a culture chamber.

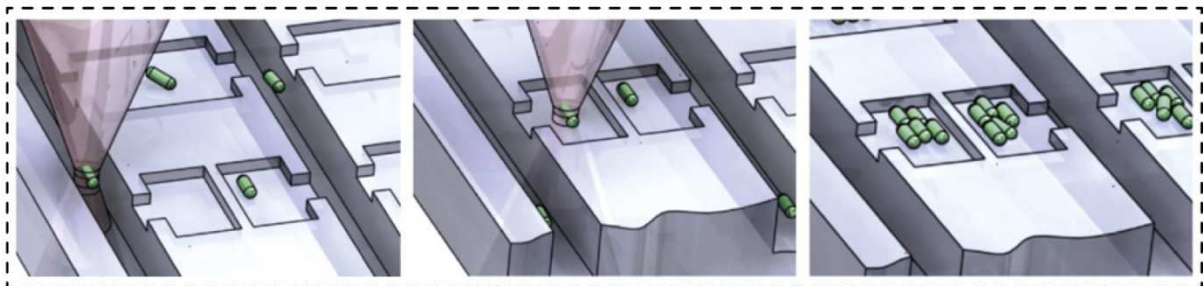


Figure I - 28. Filling of a culture chamber by micromanipulation of individual bacterium with optical tweezers. Image taken from (Probst, Grunberger et al. 2013).

Despite many advantages, optical trapping is not applicable in our case. Firstly, a limited number of bacteria cannot be trapped at the same time in the same field of view, because of the difficulty to multiplex optical wells. Secondly, as for DEP, only identification can be achieved, not

immobilization. Thirdly, we need to trap bacteria for 20-30 minutes, whereas control of bacterium by optical tweezers often lasts much less. Consequently, risks of losing microorganisms or of frying them are present.

II.2. Physico-chemical traps

II.2.1. Surface coating

Another way to enhance cell adhesion is to rely on a coating layer. More specifically, it consists in making use of the interaction between a positively charged polymer and the negatively charged cells. The adhesive layer is first deposited at the surface of the microfluidic channel. It can consist in poly-L-lysine (Pu, Zhao et al. 2016) or poly-ethylenimine (Si, Li et al. 2015), for instance. A cell suspension is subsequently loaded and microorganisms are allowed to sediment for a while. The advantage of this technique is that liquid actuation can be rapid thanks to the large channel thickness and the resistance of bacteria to shear stress. Molecular transport essentially takes place by advection, allowing the experimentalist to switch the chemical landscape within a second or less.

In fact, even without coating layer, cells can attach to the surface of materials because of impurities. Bacteria will be stuck on the bottom surface of the chip (Elfving, LeMarc et al. 2004). However, the number of trapped bacteria is low and the stability of adhesion is not good. All these methods to trap cells are very popular but not suitable to us. The main reason is that the bacterium is held by one point and continues to pivot around it (Figure I - 29).

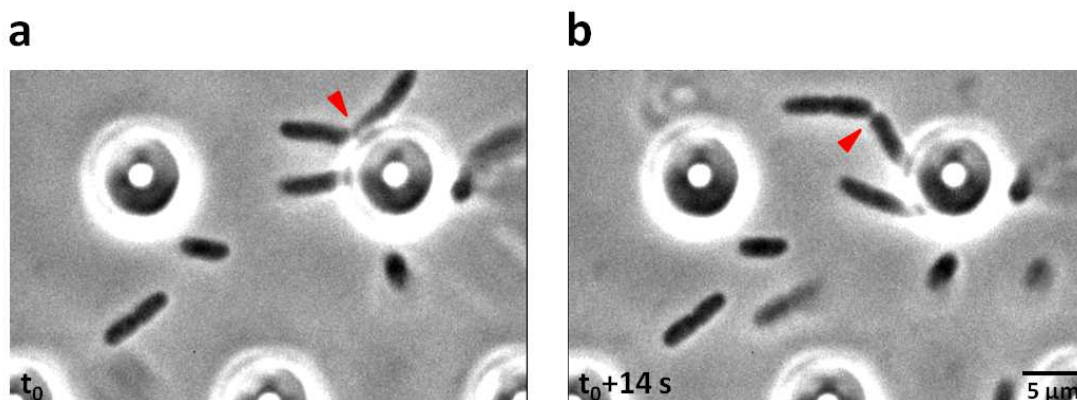


Figure I - 29. Snapshots at two different time points of bacteria adhering to a layer of poly-ethylenimine. Arrow heads indicate clearly pivoting bacteria (Si, Li et al. 2015).

II.2.2. Gel matrix

Agarose is a commonly used bio-friendly and biocompatible jelly-like material. For instance, agarose plates are traditionally employed to culture microbes, such as bacteria and fungi. They

provide a growth support and welcome a liquid medium that contains the necessary nutrients. In the report of Dusny et al. (Dusny, Grunberger et al. 2015) bacteria are inoculated onto the surface of a low melt agarose pad. Then, this pad is inverted and placed onto a coverslip to carry on growth observations (Figure I - 30). In a different approach developed by Choi et al. (Choi, Jung et al. 2013, Choi, Yoo et al. 2016), or by the Ibidi company (Ibidi Chemotaxis), melted agarose is mixed with the bacteria and injected into the microfluidic channels in which solidification occurs (Figure I - 31). Dusny's goal is to follow growth cycle and morphology changes whereas Choi's one is to determine the minimal inhibitory concentration for antibiotics.

The utilization of agarose provides dual function, it is the immobilization agent as well as the medium in which diffusion occurs. Although this method is quite convenient and common, the slow diffusion across large agarose pads does not meet our expectations.

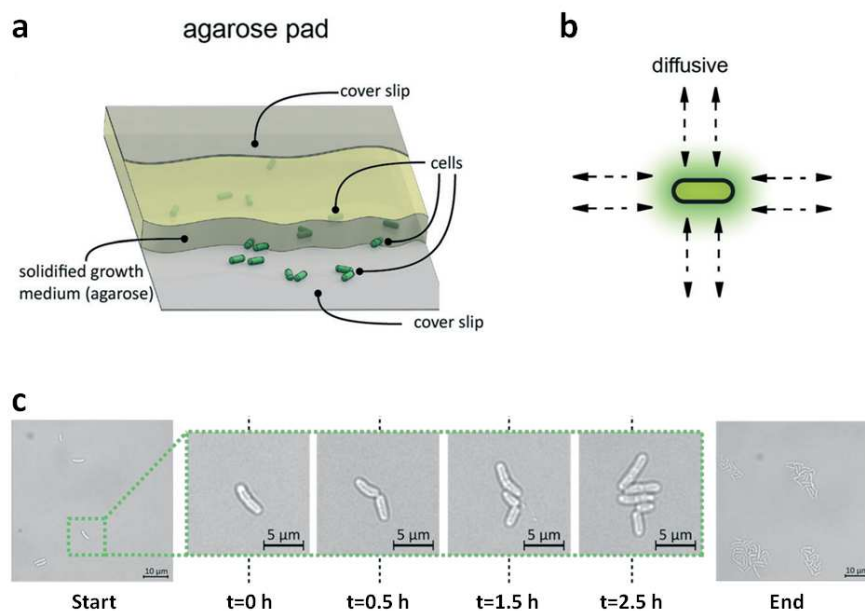


Figure I - 30. Bacteria growth under an agarose pad. (a) Microorganisms are sandwiched between a coverslip and an agarose pad, itself covered with another coverslip. **(b)** Nutrients diffuse through the agarose matrix to reach the bacteria. **(c)** Time-lapse bright field movie of cell division. Images taken from (Dusny, Grunberger et al. 2015).

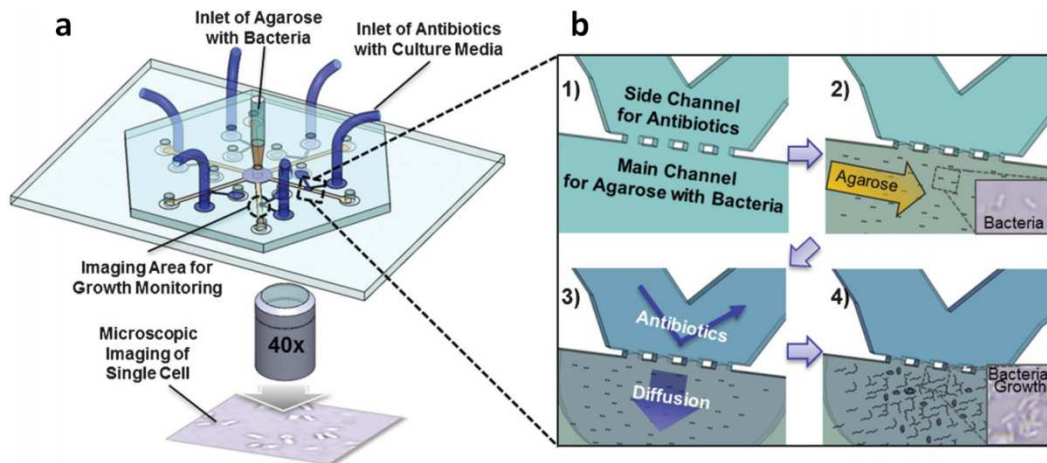


Figure I - 31. Bacteria growth and minimal inhibitory concentration (MIC) determination in an agarose gel. (a) Diagram of the whole fluidic setup. (b1-b2) Bacteria mixed with unsolidified agarose solution are injected into a microfluidic channel. Once agarose solidification has occurred, microorganisms are immobilized in the gel matrix. (b3) An antibiotic solution is loaded and drug molecules diffuse through the gel. (b4) Growth is observed using bright field microscopy. Image taken from (Choi, Jung et al. 2013).

II.3. Steric traps

II.3.1. Microfluidic growth chamber and growth track

Figure I - 32 shows several microdevices that have been employed to study bacteria in different situations and at different scales. A large and thick chamber is necessary if the emphasis is put on group behavior. However, if a lineage study is performed, the bacterium and its progeny need to be confined in a relatively small area: either a 2D chamber or a 1D track. The most extreme situation is when bacteria are completely separated and trapped in a femtoliter point-like chamber.

The microfluidic growth chamber approach uses flat chambers, around 1 μm deep, with one or two sides open into supply channels around 10 μm deep (Mather, Mondragon-Palomino et al. 2010). These glass-PDMS devices allow a two dimensional, monolayered growth of colonies over many generations. The first individual bacterium is seeded into the chamber and fed by nutrient molecules that diffuse from the port connecting the supply channels (Grunberger, Paczia et al. 2012) (Grünberger, Probst et al. 2015) (Wang, Ran et al. 2015) (Mustafi, Grunberger et al. 2014) (Probst, Grünberger et al. 2015) (Kramer, Singh et al. 2015) (Ullman, Wallden et al. 2013). Once cells overflow the chamber, they are continuously washed out by the flow in the supply channels (Figure I - 33).

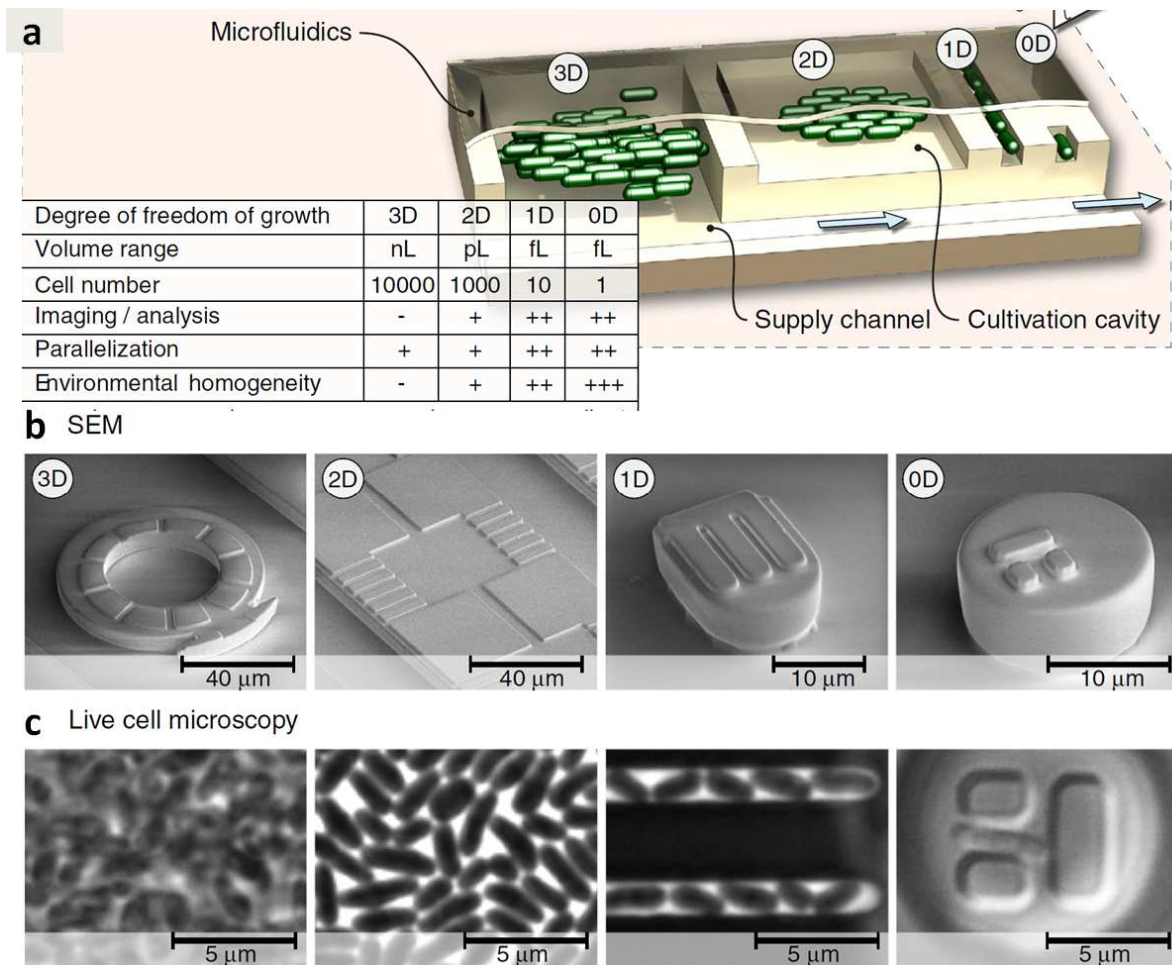


Figure I - 32. Microfluidic tools for microbial cell analysis at different scales. (a) Various possible geometries including nanoliter cavities for 3D cell microcolonies, picoliter chambers for 2D cell monolayers, femtoliter channels for 1D cell rows, and ultimately femtoliter single-cell traps. (b) Corresponding scanning electron microscope images of the cell culture devices. (c) Corresponding optical microscopic images of bacteria in place. Images taken from (Grunberger, Wiechert et al. 2014).

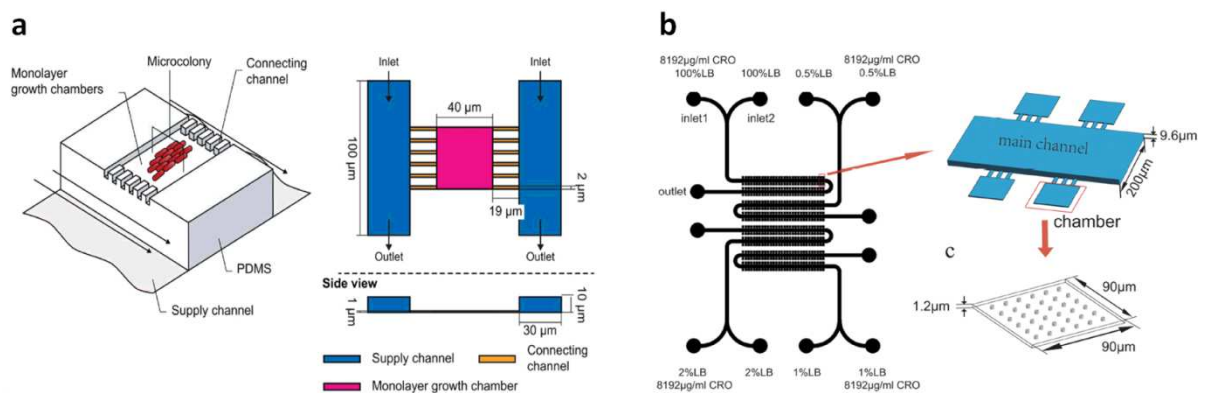


Figure I - 33. Microfluidic growth chambers, according to two different designs (a) chamber allowing diffusion of the small molecules from both sides. Image taken from (Grünberger, Probst et al. 2015). (b) Chamber allowing diffusion of the small molecules from only one side. Images taken from (Wang, Ran et al. 2015).

First, the fabrication of shallow chambers is hard to guarantee. Second, such microsystems are not reusable. We mentioned that in our experiment the photon energy range imposes to employ quartz as substrate. However, using the conventional method of plasma bonding would lead to a large consumption of expensive wafers.

II.3.2. Elastomeric ring valve

The elastomeric ring valve is derived from the elastomeric valve proposed by Stephen Quake (Unger 2000) (Chou, Unger et al. 2000). Its main application is for switching on/off the flow running in a microfluidic channel. The air injected in the control channel deforms the “ceiling” of the flow channel and the liquid cannot pass any more in this underneath pipe. Many studies make use of the tool, for instance to control the entry and exit of reagents in and out from microchemstat or microreactor (Galas, Haghiri-Gosnet et al. 2013) (Park, Wu et al. 2013) (Balagaddé, You et al. 2005).

In several papers a Swiss research group (Eyer, Kuhn et al. 2012) (Eyer, Stratz et al. 2013) (Stratz, Eyer et al. 2014) has proposed a method to study isolated single-cell. First, fluid carries bacteria and one of them will be stopped by a barrier (Figure I - 35 a). Then, an air-controlled elastomeric ring valve is actuated and an isolated chamber is thus defined around the barrier (Figure I - 35 b). On the subsequent steps cell lysis and immunoassay based on fluorescence can be performed.

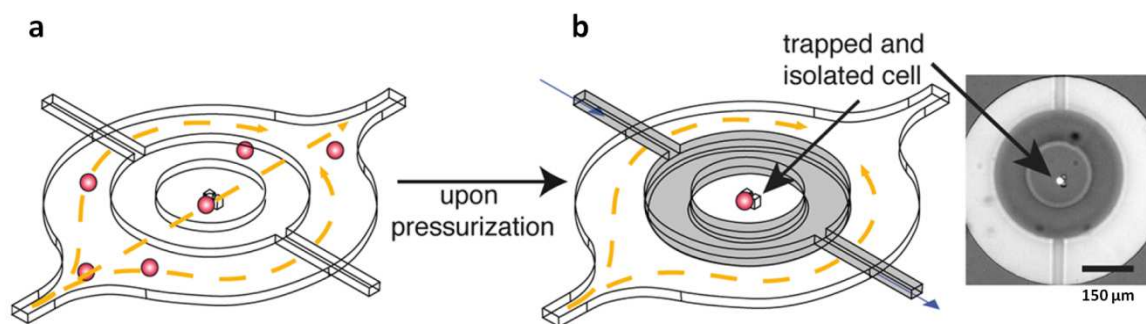


Figure I - 35. Elastomeric ring valve to isolate single cell. (a) Cells flow in the channel and one of them is arrested by the barrier. (b) The valve is actuated, thus separating the chamber from the surrounding media. Image taken from (Eyer, Stratz et al. 2013).

This technology displays a single-cell resolution but is not suitable for imaging. The chambers for bacteria (*E. coli*) are 10 μm high, which is too large for complete immobilization. Unless the chamber height becomes similar to the bacteria diameter, the microorganism cannot be stopped to a

given position in the focal plane. In addition, no entrance is reserved for fluidic coupling to an external molecular source: changing solute is thus not possible.

II.3.3. Semi-permeable membrane onto a growth chamber

This microsystem is composed of three layers (Figure I - 36). For its assembly, a drop of bacteria suspension is firstly placed on a coverslip including the pattern of the culture chamber, then it is covered by a semi-permeable membrane, and finally the microfluidic channel is stacked on the top. These three layers are sandwiched in a custom-made PMMA holder. When used, the microfluidic channel is filled with drug molecules which diffuse through the semi-permeable membrane from above towards the culture chamber. Interestingly, these devices are reminiscent of the one proposed for experiments on eukaryotic cells (Morel, Galas et al. 2012).

These culture chambers can be formed by etching in a glass (Inoue, Wakamoto et al. 2001) (Wakamoto, Ramsden et al. 2005) or patterned in a negative photoresist (Delince, Bureau et al. 2016). The size of the individual chamber is not less than 20 μm in diameter (Inoue, Wakamoto et al. 2001). In such a wide area complete immobilization is not possible. Therefore it is not appropriate method for us.

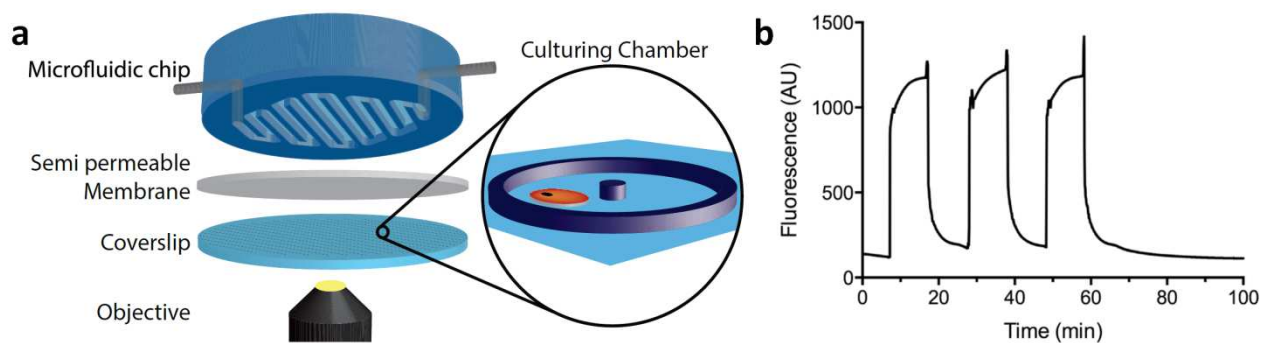


Figure I - 36. Layout and properties of a growth chamber with a semi-permeable membrane. (a) The device is composed of 3 layers, they are respectively, a coverslip patterned matrix of culture chambers, semi-permeable membrane, and a microfluidic channel. (b) Time-trace of the total fluorescence intensity in one chamber when the medium in the microfluidic channel is repeatedly switched between buffer containing FITC or not. Images taken from (Delince, Bureau et al. 2016).

II.4. Comparison and conclusion

The advantages and drawbacks of the approaches discussed above are summarized in Table I - 1. We have classified the various techniques according to the four requirements detailed in Chapter

III, Section I. We found it difficult to fulfill all our needs but the microfluidic growth chamber was the closest to our expectations, despite its non-reusability.

Technology	Immobilization	Parallel monitoring	Change of environment		Practicity		Ref.
					Easy manipulation	Reusability	
DEP	no	no	yes	advection	no	yes	Kortmann et al. 2009 Fritzsch et al. 2013
Optical Tweezers	no	no	yes	advection	no	yes	Xin et al. 2014
Surface Coating	no	yes	yes	advection	yes	no	Pu et al. 2015 Si et al. 2015
Gel matrix	yes	yes	no		yes	no	Dusny et al. 2015 Choi et al. 2013
Microfluidic growth chambers & tracks	yes	yes	yes	diffusion	yes	no	Grünberger et al. 2015 Wang et al. 2015 Wang et al. 2010 Long et al. 2013
Elastomeric ring valve	no	no	no		no	yes	Eyer et al. 2013 Stratz et al. 2014
2D diffusion semi-permeable membrane	no	no	no		no	yes	Delincé et al. 2016
Static chamber	yes	yes	no		yes	yes	Cinquin et al. 2015 Kascakova et al 2012

Table I - 1. Features summarized for mentioned methods.

III. Tentative implementations

In an exploratory stage, I first tried two technologies inspired from works reported on DEP and on the elastomeric valve (see Chapter III, II.1.1 and II.3.3). However, these studies were not finalized because their principle did not prove effective as quickly as expected.

I first designed and fabricated an interdigitated network of electrodes in order to use nDEP (see Chapter III, Section II.1.1) to concentrate bacteria, which can push the bacteria into the center of inter-electrode space or above the electrodes. But since the bacteria above the electrodes cannot be observed by inverted microscopes, we aimed to be able to observe the former ones (Figure I - 37 a). In this trial both the conductivity and the permittivity of the liquid medium, as well as the bacteria concentration were not well adjusted. As a consequence, we only observed a biofilm floating in the

channel but not at all the nDEP phenomenon (Figure I - 37 b). A deeper search in the literature evidenced that this technology requires a careful adjustment of the various parameters, among which not only the electric field amplitude and frequency but also the buffer conductivity and permittivity. The poor outcome of the preliminary experiments, added to a more fundamental incompatibility with the use of the NaPi buffer (see Chapter IV, Section II.1) pruned us to abandon this method without trying further investigations.

III.1. Dielectrophoresis

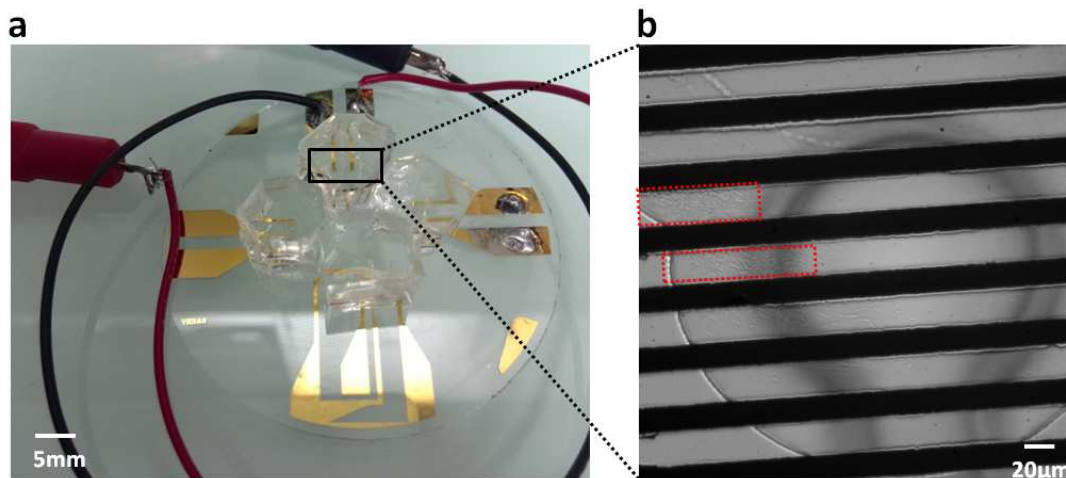


Figure I - 37. Attempt of DEP manipulation. (a) Glass chip including 4 gold microelectrodes arrays and the corresponding PDMS chambers. (b) Zoom on the electrodes, bacteria arranged in biofilm are highlighted with red rectangles.

III.2. Elastomeric button valve

The use of a bilayer PDMS technology has been introduced in Section II.3.3. The discussed elastomeric ring valve is very similar to the elastomeric button one that has been proposed in order to protect an area of a coverslip during liquid renewal (Maerkl and Quake 2007) (Bates and Quake 2009) (Geertz, Shore et al. 2012) (Gerber, Maerkl et al. 2009). In our work we planned to trap bacteria under this button (Figure I - 38).

From the technology point of view, two layers of PDMS are bonded thanks to the interdiffusion of two preparations having different PDMS base and initiator mass ratios, this phenomena occurring during the solidification process. More precisely, the 5:1 ratio used for the control channel layer is poured onto a mold whereas the 20:1 ratio used for the flow channel layer is often spun-coated onto another mold. When solidification is not entirely finished, the control channel layer is peeled from its mold and aligned over the flow channel layer. Then, the assembled

chip is cured in an oven to complete solidification. At the end, the double layered PDMS assembly can be bonded to the suitable substrate (Figure I - 39).

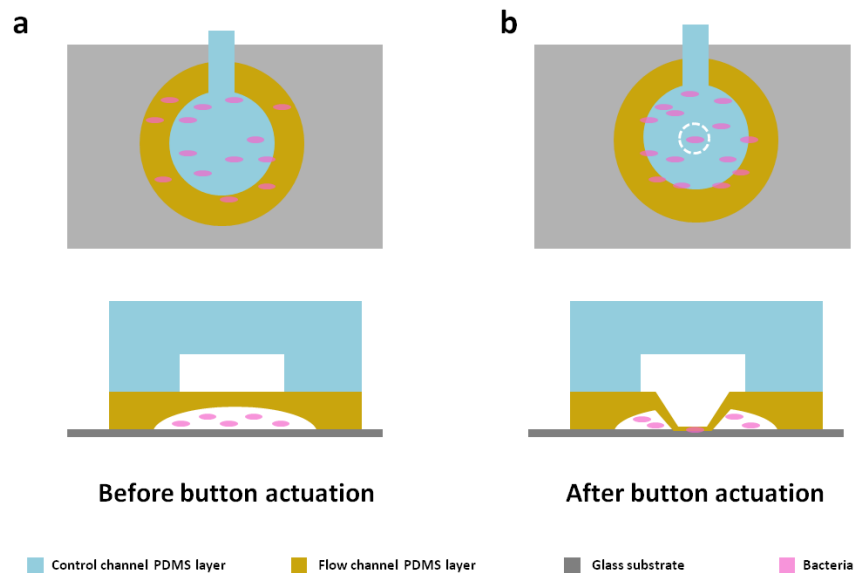


Figure I - 38. Anticipated mechanism for the elastomeric button valve dedicated to bacteria immobilization. (a) Actuation off, bacteria float in the flow channel; (b) Actuation on, bacteria are pressed under the button. The dashed line delineates the zone under the button.

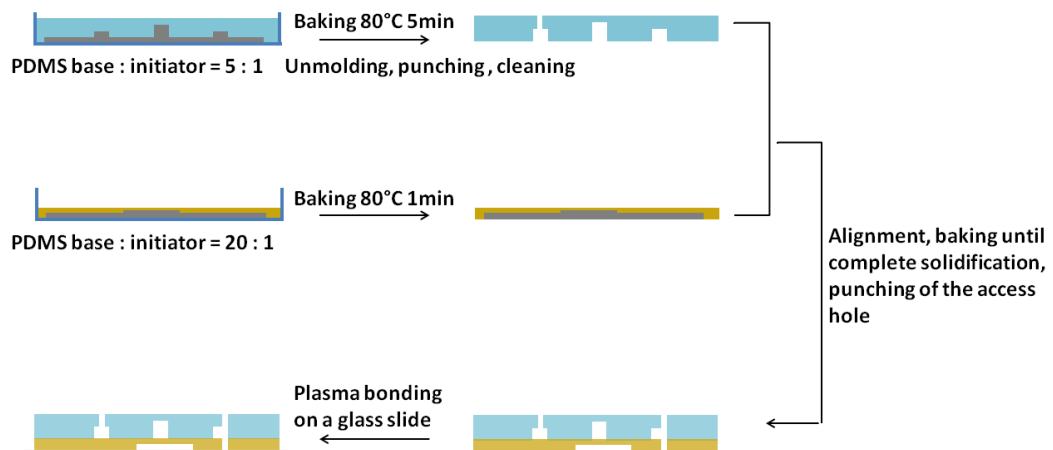


Figure I - 39. Fabrication process for the elastomeric button valve.

In our study, we expected that bacteria would be squeezed under a button, which could have been patterned with grooves in order to allow small molecules to diffuse to their target.

Unfortunately, we found that the valve pushed bacteria away instead of pressing them onto the glass substrate (Figure I - 40).

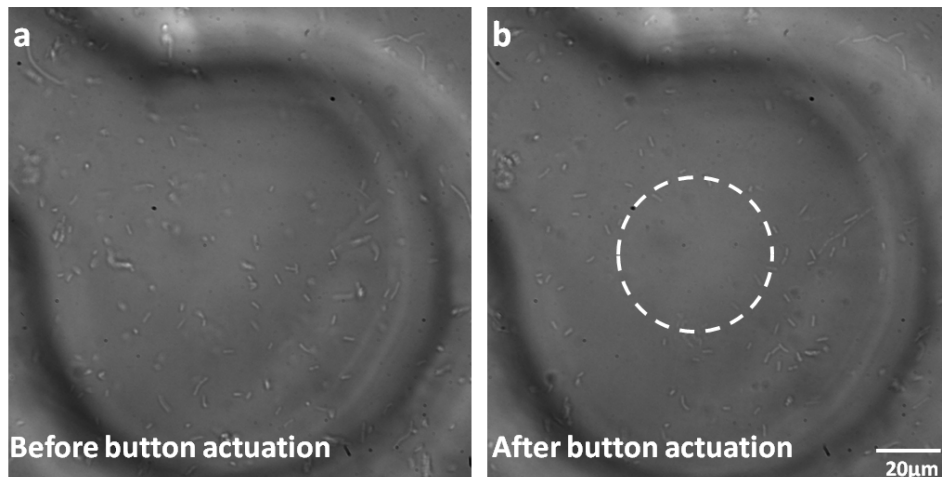


Figure I - 40. Application of the elastomeric button valve strategy for bacteria immobilization. (a) Actuation off, bacteria float in the flow channel. (b) Actuation on, bacteria are pushed away and not immobilized between the membrane and the substrate. The dashed line delineates the zone under the button.

IV. Final solution

Having realized that the above technologies were not feasible, I turned to techniques similar to the microfluidic growth chambers, and thus efforts were made to render it reusable.

IV.1. Reflection around the static chamber

As stated above, immobilization in the static chamber was quite good (Figure I - 26 d). Moreover, the set up was dismountable. Nevertheless it lacked a mean to communicate with the environment. It then came to my mind that we could introduce some modifications on the coverslip to provide some access to the chamber content. More precisely, we included a central hole to be used as an entry port for antibiotic or wash buffer, as well as an exit groove devised to collect waste. The drop of bacteria suspension is positioned at the center on the substrate and the assembly of the set up is performed thanks to an Attofluor holder (Figure I - 41). Some bacteria are hence gently immobilized at the center of the cover slip. When we want to change the solute, the appropriate solution is added through the access hole with a micro pipette, impregnating the zone where bacteria are located, and the excess of fluid falls into the trash groove.

We put our ideas into practice but noticed some problems: the flow is “alive” but not enough. Only a few droplets of antibiotic are not sufficient to renew efficiently the environment of bacteria; the injection volume is indeed limited by the size of the groove trash — too much injected liquid

injection results in backflow. In addition, the solution change has to be done with a pipette and touching the setup might cause one to lose focus.

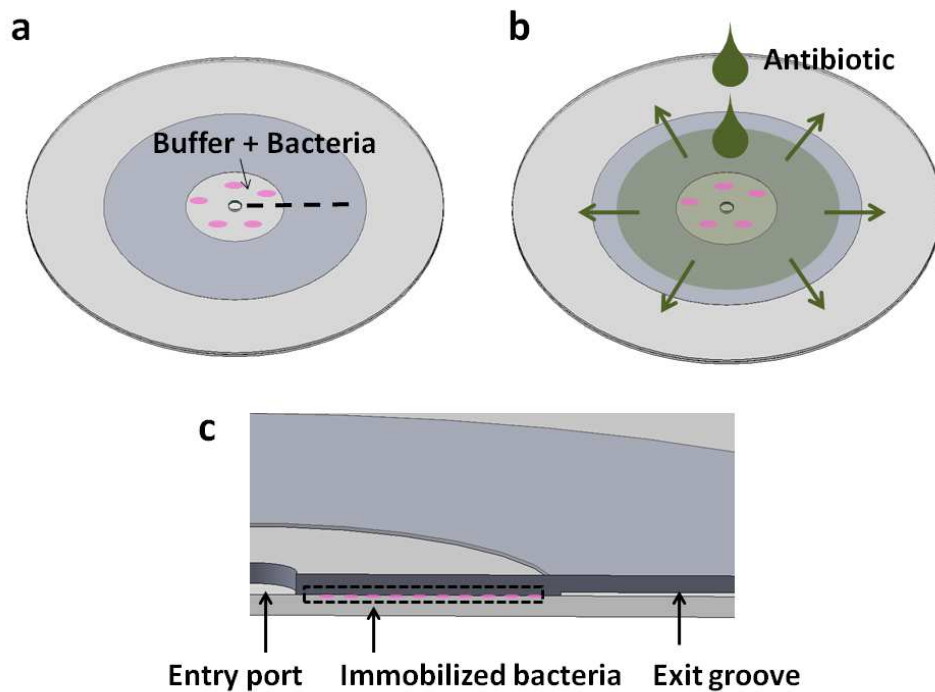


Figure I - 41. Diagram for the “improved static chamber”. (a) Immobilization of bacteria at the center of the substrate. (b) Addition of the antibiotic solution through the entry port. (c) Zoomed cross-section along the dashed line in (a).

IV.2. Design of the flow device

Inspired from the former attempt, I have designed a new microsystem. The concept of this flow device is consistent with the one of the microfluidic growth chamber (see Chapter III, Section II.3.1): imposing a constant external concentration source in thick supply channels and maintaining the bacteria trapped in a thin observation chamber, both component being connected to each other (Figure I - 42 a, b)(Westerwalbesloh, Grünberger et al. 2015). However, in our case, the chamber height is not defined by features in the PDMS stamp, but by the bacteria that act as spacers (Figure I - 42 a, b). The immobilization process is thus similar to the one used in the previous static chamber.

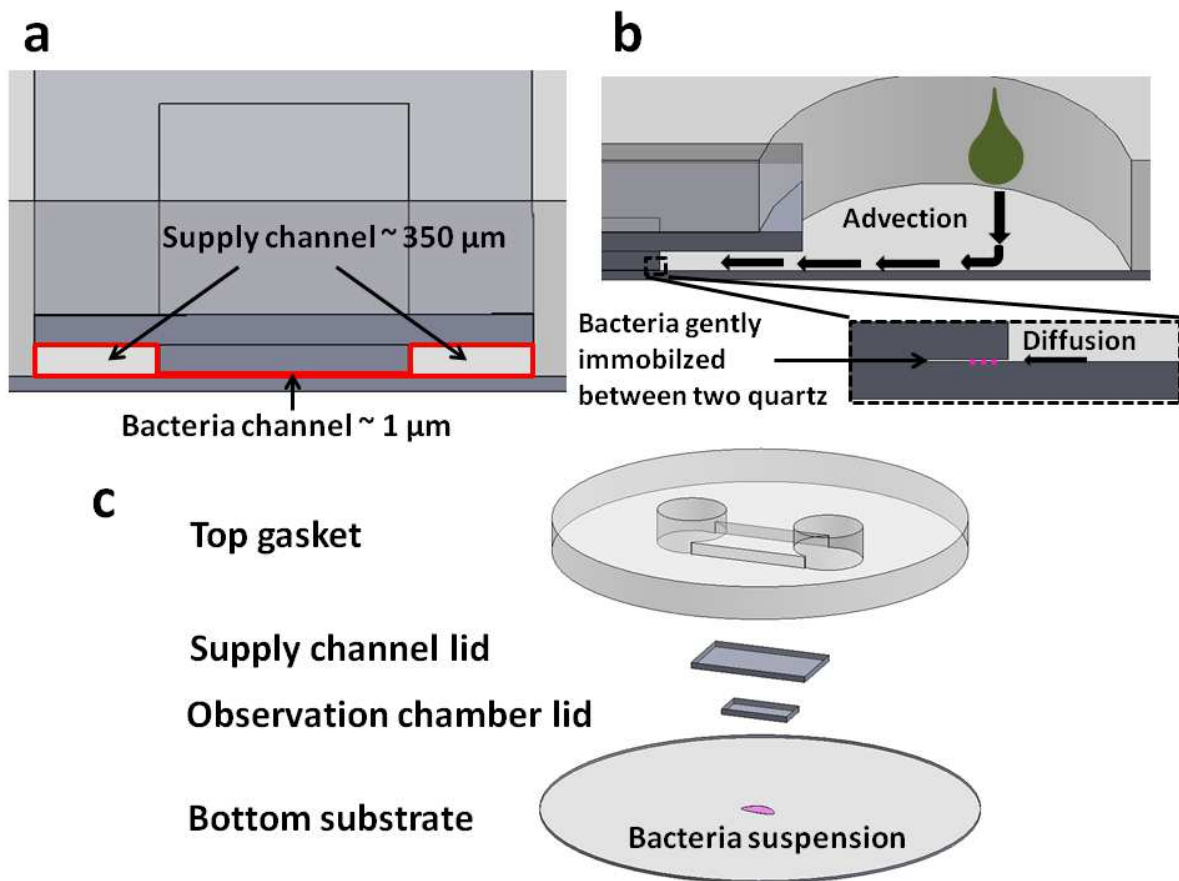


Figure I - 42. Diagrams for the flow device. (a) Cross-section emphasizing on the contrast between the thickness of the supply channels and the one of the bacteria chamber. (b) Once the liquid enters the supply channels, it quickly renews their contents, providing an external concentration source for diffusion into the bacteria chamber. (c) The four parts of this device, i.e. the gasket, the supply channel lid, the observation chamber lid, and the bottom substrate. The buffer droplet containing the bacteria is also represented: it has to be deposited on the bottom substrate before assembling.

There are 4 parts in the device (Figure I - 42 c): conventional 1 inch quartz wafer of thickness $170 \mu\text{m}$ called the “bottom substrate”; a little $3 \text{ mm} \times 2 \text{ mm}$ piece of $350 \mu\text{m}$ thick quartz called the “observation chamber lid”; another $7 \text{ mm} \times 4 \text{ mm}$ piece of $350 \mu\text{m}$ thick quartz that serves as “supply channel lid”, and finally a piece of PDMS with a cavity of $7 \text{ mm} \times 4 \text{ mm} \times 0.68 \text{ mm}$ that serves as a watertight “top gasket”.

IV.3. Compliance with the requirements

The flow device, i.e. the final solution we propose, can meet the 4 aforementioned requirements:

- Immobilization: In the static chamber, the equivalents of the “bottom substrate” and “observation chamber lid” were two 1 inch quartz wafers. We know that, the larger the

surface of the coverslip is, the more likely we have to face incomplete planarity matching due to stress and curvature, resulting in an interspace which height is superior to 1 μm (Figure I - 43). As a consequence bacteria are not well immobilized. Conversely, if the surface of one of the coverslips is reduced, there is more possibility to form a thin chamber with a homogeneous height in which bacteria are immobilized tightly. Here the size of the present observation chamber lid is reduced to 3 mm \times 2 mm. Of course it could be still smaller, but in that case it would also be more difficult to fabricate and manipulate.

- Parallel monitoring: As stated before, the distribution of cells in the previous static chamber was satisfactory (Figure I - 26 d). With the use of an appropriate density, isolation of individual bacteria to achieve parallel monitoring is thus feasible. Our strategy is more controlled than flow seeding (Grünberger, Probst et al. 2015) and simpler than optical tweezers seeding (Probst, Grünberger et al. 2013) (Wakamoto, Ramsden et al. 2005); we obtain easily cells that are well dispersed and isolated when the observation chamber lid is positioned.

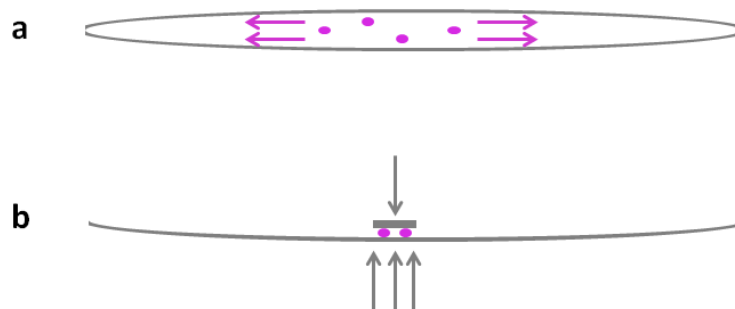


Figure I - 43. Influence of the quartz pieces curvature on the immobilization. (a) Previous static chamber. (b) Bacteria chamber used in the flow device.

- Change of the solute in the chamber: Quartz is used for the supply channels. This material is easily wetted by water and thus fluid filling and exchange is achieved without observing any bubble.
- Practicality: No complicated pattern design nor tedious fabrication process (see Section IV.4) is involved. The assembly of the different parts is realized by screwing of the POCmini-2 holder, without any bonding. Hence, a convenient and reusable device has been developed.

IV.4. Fabrication protocols

Figure I - 44 introduces all the parts needed to produce the flow device.

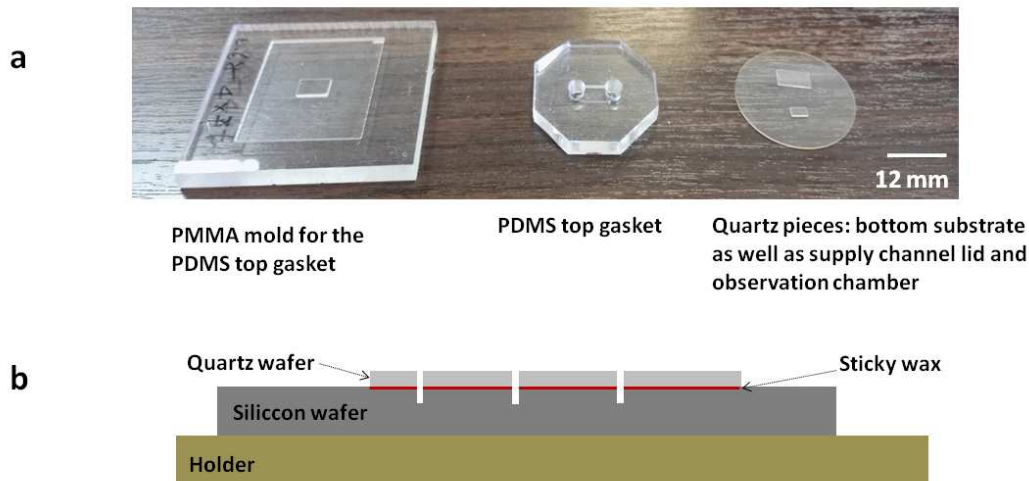


Figure I - 44. Device micromachining. (a) Picture of the PMMA mold used to fabricate the top gasket by soft lithography and of the 4 different parts which assembly yields the final microsystem: the PDMS top gasket and the 3 quartz parts. (b) Temporary assembly used during quartz dicing. The blade must enter in the silicon wafer to ensure the total cutting of the quartz wafer.

Top gasket molding. The PDMS gasket is a simple rectangular cavity. It is large and deep, without any micro-size pattern. The corresponding mold is fabricated on a PMMA (poly-methyl methacrylate) sheet by a milling using a Mini-Mill/GX (Minitech Machinery Corporation, USA) and a 1 mm in diameter drill (Performance Micro Tool, USA). The machined PMMA mold is then cleaned in soap bath with ultra-sound.

PDMS base and initiator are mixed with a 10:1 mass ratio and poured onto the mold, degassed, put in oven of 70 °C, and incubated for 2 h. The access hole and exit hole, 4 mm in diameter, are manually punched at both ends of the cavity.

Supply channel and observation chamber lids dicing. Small dimension quartz pieces are sawn in a 350 μm thick substrate, which is of the same material than the bottom substrate. A dicing saw (model 8003; ESEC, Switzerland) is used, with a resin blade running at 25 000 rpm. It is noteworthy that, prior to sawing, the 350 μm quartz wafer is stuck onto a silicon one with sticky wax and not installed directly onto the holder which ensures a total vertical cut (Figure I - 44 b).

Cleaning. After dicing, the intermediate sticky wax layer is removed in a trichloroethylene bath at 90 °C. The quartz pieces released from the silicon wafer are then gathered and cleaned in an isopropanol bath with ultra-sound, and finally dried under a nitrogen gas flow.

All quartz parts are reusable. After use in a microbiology experiment, their surface is scrubbed in a 2 % Hellmanex™ III detergent solution and rinse with deionized water. The substrate and lids are next soaked in an ethanol bath, and finally dried with precision Kimtech Science wipes.

Chapter IV. Description of an experiment step by step

I. Bacteria culture

I.1. Experiments on the BL21 (DE3) strain

For the sake of accessibility and practicality, the commercial and non-pathogenic *E. coli* strain BL21 (DE3) (cat. C2527H, New England BioLabs, USA) is used to characterize the microfluidic device. As received 50 μ L tubes are stored at -80 °C. They correspond to competent cells but this detail is assumed to have no incidence on our results. The culture is initiated by inoculating 4 mL of Luria-Bertani broth (LB, Sigma-Aldrich, USA) contained in a plastic cultivation tube with 25 μ L of stock bacteria. Growth takes place at 37 °C for about 3 h on a rotary shaker at 180 rpm, until reaching an optical density of ~ 0.6 at 600 nm, which roughly corresponds to the mid-exponential phase. Then, this bacteria solution is centrifuged in 2 tubes at 3000 g, 20 °C, for 15 min and the supernatant is discarded. Both aliquots are then kept on ice.

I.2. Experiments on the AG100/AG100A/AG102 strains

The *E. coli* AG100, AG100A, and AG102 laboratory strain (Viveiros, Jesus et al. 2005) (Okusu, Ma et al. 1996) are provided by our collaborators from the UMR-MD1 laboratory in Marseille and the culture is performed using their protocol.

A pre-culture is initiated the night before the experiment: a colony being picked up from the agar pad with an oese and used to inoculate 2-3 mL of LB broth contained in a 15 mL culture tube. A rotary shaker keeps aerating the medium at 37°C, 160 rpm, overnight (about 8 h). The next day, 20 μ L of pre-culture are transferred in 20 mL of LB broth contained in a 100 mL Erlenmeyer flask, and

shaking is performed at 37°C, 160 rpm for about 3 h. When $OD_{600} \sim 0.6$ the culture is stopped and bacteria are centrifuged at 3000 g, 20 °C for 15 min. The supernatant is discarded and the microorganisms are re-suspended in 10 times less (i.e. usually 1.9 mL) NaPi buffer (see below). Subsequently, 100 μ L of the new mixture are diluted into 1 mL of buffer to measure the OD_{600} value, at this time, it should equal to 0.06. The remaining 1.8 mL is divided in 120 μ L aliquots which are centrifuged at 3000 g, 20 °C, for 15 min. After removal of the supernatant, these tubes are kept on ice until needed.

II. Reagent preparation

II.1. NaPi Buffer

NaPi is the buffer used to suspend bacteria, to dilute drug, and to wash bacteria from drug. It is actually a phosphate buffer supplemented with $MgCl_2$. In such buffer bacteria growth is halted but microorganisms remain alive. Furthermore, the components in this buffer are simple, under our imaging conditions these chemicals do not add fluorescence.

Preparing NaPi 50mM pH 7 necessitates to first prepare the following 3 solutions:

(A) NaH_2PO_4 (Sigma-Aldrich) dissolved at 50 mM (1.1998 g in 200 mL H_2O)

(B) $Na_2HPO_4 \cdot 12H_2O$ (Sigma-Aldrich) dissolved at 50 mM (3.58 g in 200 mL H_2O)

(C) $MgCl_2 \cdot 6H_2O$ (Sigma-Aldrich) dissolved at 2 mM (406.62 mg in 1 mL H_2O)

For 250 mL of NaPi, 110.5 mL of (A), 139.5 mL of (B), and 625 μ L of (C) are mixed. After pH have been adjusted to pH 7, the solution is sterilized by filtration on a membrane (0.22 μ m Millipore syringe filter, Millex-GP, Sigma-Aldrich) and it is stored at 4 °C in the refrigerator.

II.2. Antibiotic solution

Two fluoroquinolone molecules are used in the experiments: ciprofloxacin (Sigma-Aldrich) and fleroxacin (Sigma-Aldrich). The former drug is dissolved at 16 μ g/mL (48.3 μ M) in NaPi buffer. This concentration, relatively important with respect to clinical standards (Matchette, Agrawal et al. 2007), is selected in order to obtain a good signal-to-noise ratio when imaging the device during the fluidic characterization phase. The latter drug is dissolved at 1 μ g/mL (2.7 μ M) in NaPi buffer, which enables to acquire clinically relevant data, in continuity with the ongoing work of our Marseille collaborators.

III. Microfluidic actuation

III.1. Immobilization of the bacteria

Centrifuged bacteria are re-suspended in 0.03 mL of NaPi buffer, a volume that will ensure an optimal density of bacteria in the field of view. Next, 0.2 μ L of the suspension are deposited at center of the bottom substrate. Thereafter, the observation chamber lid is positioned and pressed onto the droplet gently, in order to yield a thin layer of liquid that sticks the two glass pieces together by capillarity. The exceeding liquid is simply squeezed out by pressing and left as it is. Then, the already integrated top gasket and supply channel lid are added, their positioning with respect to the observation chamber lid being achieved by hand. Therefore, the lateral dimensions of the supply channels may vary within a few percents. Nevertheless, the natural affinity between the clean quartz surfaces and the PDMS yields reversible seals so that further adjustment is always possible.

It is worth noting that the experimentalist should not let dry the extra volume of bacteria suspension which is located around the observation chamber lid. Indeed, the microorganisms may stick to the surface and act like an obstacle (Figure I - 47). In order to prevent this phenomenon, 10 μ L of buffer are injected by the access ports after the assembly of the top gasket, to prevent any drying and to facilitate the evacuation of the exceeding bacteria during the “control” phase (see Section III.4).

The parts making the device are finally screwed tightly in a POC mini-2 holder (PeCon GmbH, Germany) and the assembly is mounted onto the microscope.

III.2. Installation of the fluidic system

Since no permanent sealing is performed between the various parts of the microdevice, classical insertion of metal ports into a reduced-size punched hole cannot be employed. Consequently, tubing for fluidic actuation is installed using plasticine. Two bent needles (Venofix® 25G, 0.5×15 mm; B. Braun, Germany) for buffer and drug solutions are fixed above the input port. A larger diameter needle (18G, 1.5” 1.2×40 mm; Terumo, Japan) is fixed above the exit port and kept perpendicular to the bottom substrate to eliminate waste.

Three syringe pumps (Aladdin-1000; World Precision Instruments, USA) are used: one for the drug, one for the buffer, and one for the waste elimination. Liquid coming from the input port spreads and flows quickly in the supply channel thanks to the hydrophilicity of quartz. At the other side of the supply channels, liquid is eliminated by aspiration to prevent overflowing (Figure I - 45).

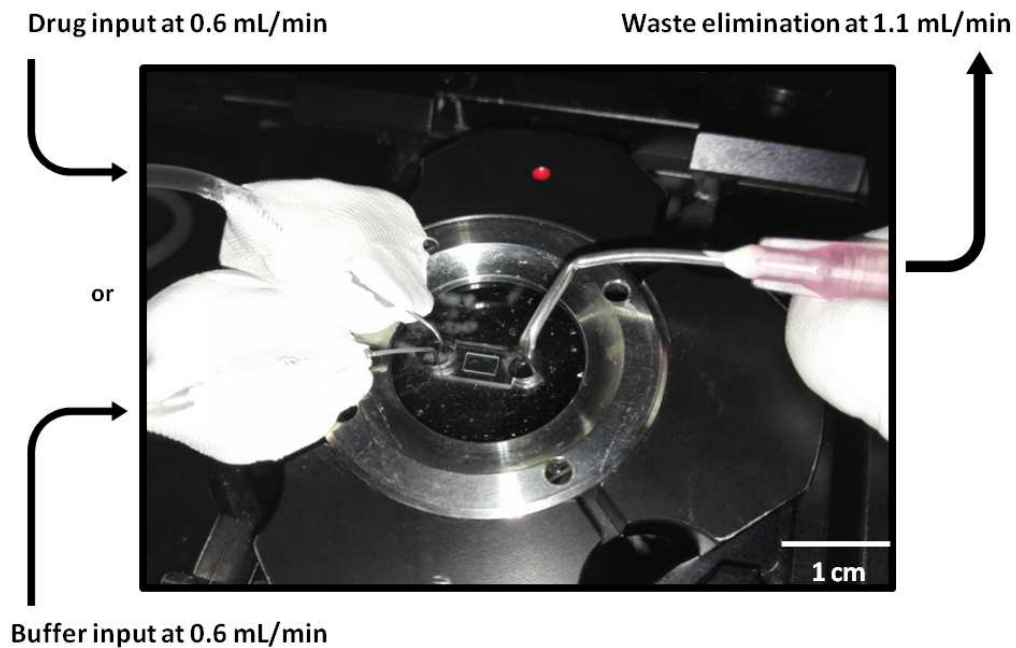


Figure I - 45. Picture of device mounted on the microscope stage and of the associated fluidic connections.

III.3. Selection of an appropriate field of view

Immobilization is not always perfect because of the curvature of the quartz substrate or because of the presence of dusts. Therefore, sometimes, bacteria are still moving in some parts of the observation chamber, meaning that the space is locally larger than $1\ \mu\text{m}$. Consequently, it is important to find a place where bacteria are just immobilized, without being crushed.

The field of view is also adjusted in order to collect information on bacteria located between 15 and $35\ \mu\text{m}$ inside the observation chamber, so that the portal edge of the observation chamber is surely included in the image (Figure I - 46). The scrutinized area is chosen not too close to the lid edge so that microorganisms can be trapped efficiently (some chips are formed during the dicing process); however, it is not too far so that the characteristic time for solute exchange remains satisfactory (see Chapter V). Furthermore, data are recorded 200 to $300\ \mu\text{m}$ apart from the device longitudinal symmetry axis in order to benefit from high enough flow velocities in the portal supply channel. Indeed, we found it much easier to flush bacteria that can be stuck around the observation chamber edge when working outside of the stagnation region (Figure I - 51).

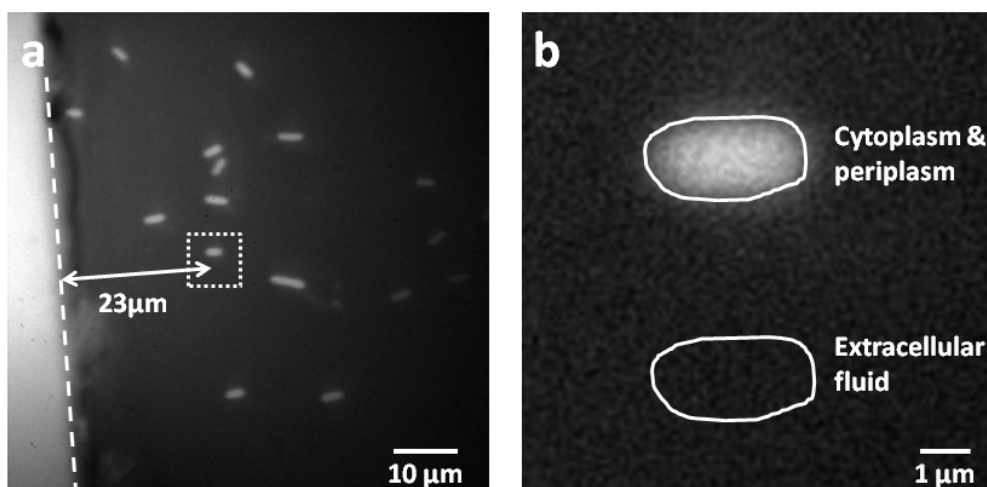


Figure I - 46. Selection of an appropriate field of view and of the region of interest. (a) Typical field of view roughly located 200 μm aside the device longitudinal symmetry axis. Between 10 and 20 *E. coli* BL21 (DE3) bacteria are trapped within this 70 μm \times 70 μm window. This image was acquired 165 s after the onset of antibiotic perfusion. A bacterium, 23 μm from the edge, is selected (dotted square). The dash line delineates the front edge of the observation chamber. (b) ROI selection for both the “cytoplasm and periplasm” and for the “extracellular fluid” areas. The ciprofloxacin solution dissolved at 48.3 μM in NaPi, and the pure NaPi buffer, their perfusion flow rate was 0.6 mL/min.

III.4. Modulation of the antibiotic concentration

In general, both drug and buffer injections are performed at 0.6 mL/min whereas aspiration run at 1.1 mL/min. Importantly, the access ports of our device are open so that flowrates do not need to be conserved. Furthermore, some air unavoidably enters the syringe connected to the outlet. In fact, liquid actuation inside the microdevice is more driven by a combination of gravity and capillary forces than by a clearly imposed pressure gradient (Figure I - 45).

An experiment consists in 4 successive steps, which are called: evacuation, control, flush-in, and flush-out.

Evacuation. Bacteria accumulated next to the edge of the observation chamber lid, and that blocks its entrance, are removed (Figure I - 47). This step lasts 3 min, the UV shutter is closed. If this special step is not added to remove the blocking bacteria, the diffusion process can be significantly slowed down.

Control. The shutter is opened and the chosen areas are irradiated by the synchrotron beam for 1 min 15 s. During this period background information are recorded. Photobleaching of the intrinsic fluorescence of molecules like tyrosine, tryptophan, and NADH is also achieved (Figure I - 48).

As a result, the acquired signal that will be subsequently collected is totally due to the antibiotic fluorescence. In other words, the autofluorescence signal and the drug fluorescence are now separated.

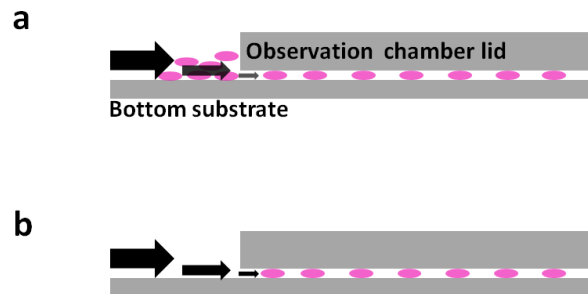


Figure I - 47. Diagram of the removal of bacteria from the edge of the observation chamber. (a) Before and (b) after the evacuation step.

Flush-in. The drug pump is switched on to perfuse the bacteria and the buffer pump is switched off. It lasts about 5 min so as to reach the maximum of antibiotic uptake.

Flush-out. The buffer pump is switched on to wash the bacteria and the drug pump is switched off. It lasts also 5 min to reach almost the starting fluorescence level inside bacteria.

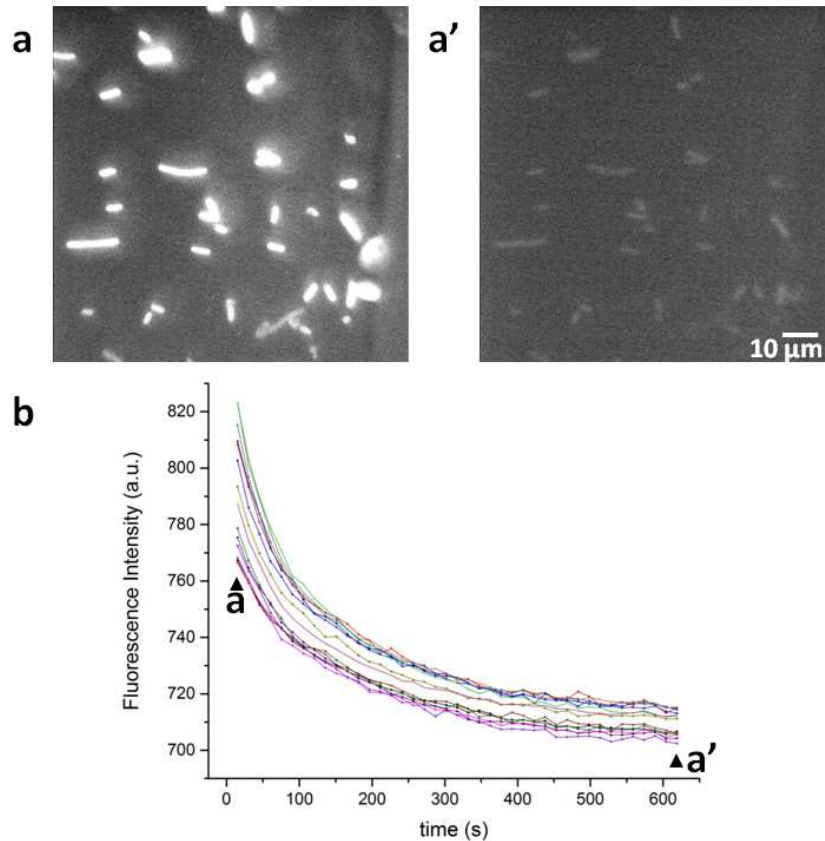


Figure I - 48. Example of bacteria intrinsic fluorescence photobleaching. (a) Before and (a') after a 10 min irradiation. (b) Fluorescence intensity data collected on the “cytoplasm and periplasm” ROI of several bacteria (see Section IV.2). Arrow heads correspond to the time points at which the two images have been recorded in (a-a'). Excitation: 290 nm; emission: 327-353 nm, 100× objective.

IV. Image acquisition and data analysis

IV.1. Optical set up

The full-field imaging system is built around an inverted Axio Observer Z1 microscope (Zeiss, Germany) (Figure I - 49). The white light beam (180 - 600 nm) of the DISCO beamline of the SOLEIL synchrotron (Jamme, Kascakova et al. 2013) (Jamme, Villette et al. 2010) (Giuliani, Jamme et al. 2009) is first monochromatized by an iHR320 monochromator (Horiba Jobin-Yvon, France) equipped with a 100 grooves per mm grating and exit slits fixed at 0.1 mm, corresponding to bandpass of 0.137 nm. The incident light at 290 nm is then reflected by a dichroic filter having an edge at 310 nm (FF310-Di01-25×36; Semrock, USA), towards an Ultrafluar 100 × glycerin objective having a numerical aperture of 1.25 (Zeiss). After sample epi-illumination, the emitted light is filtered between 420 and 480 nm through a band pass emission filter (QMAX/E 420-480; Omega Optical, USA) mounted on a

filter wheel and recorded on a CCD camera (PIXIS 1024 EUV; Princeton Instruments, USA). Importantly, quartz coverslip (ESCO Optics, USA) and glycerin (Immersol G; Zeiss, Germany) are used to mount the sample.

The whole setup is controlled thanks to Micro-Manager 1.4.21 (Edelstein, Amodaj et al. 2010). The exposure time associated with each spectral channel can be adjusted according to the drug concentration and to the fluorophore brightness. For specific parameter settings, see Sections IV.2 and IV.3.

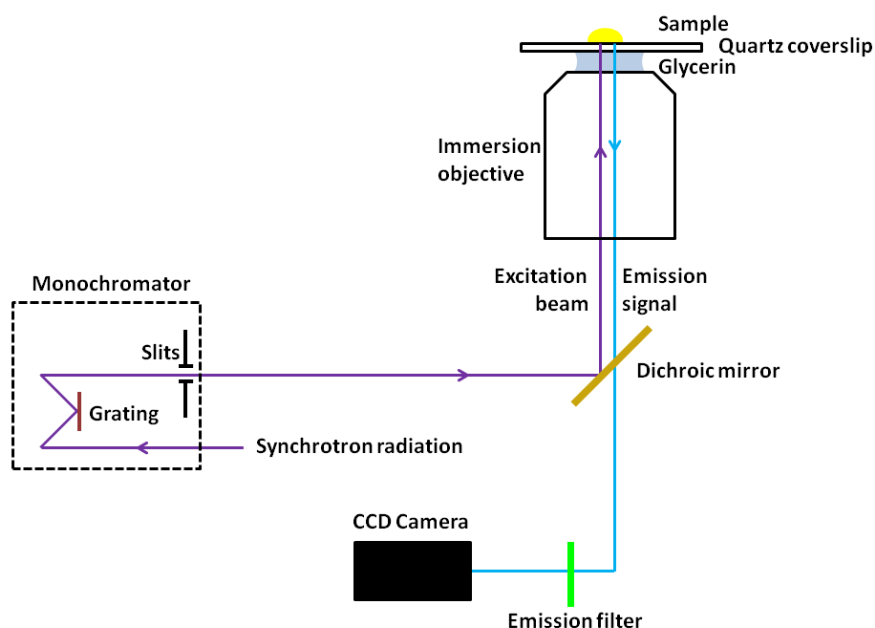


Figure I - 49. Diagram of the TELEMOS full-field epifluorescence microscope installed as an endstation on the DISCO beamline. Image adapted from (Bertrand, Réfrégiers et al. 2013).

IV.2. Experiments on the BL21 (DE3) strain

In order to best exploit the fluorescent character of antibiotics, the choice of the excitation wavelength should be the main excitation peak. However, we selected 290 nm as a compromise enabling to collect enough photons from the drug without collecting too much photons from the bacteria components (see Chapter II, Section III.1.3).

For the flow device characterization experiments, the drug is used at a quite high concentration in order to yield a very contrasted fluorescence signal (see Chapter IV, Section II.2). As a result the exposure time could be shortened. With a 48.3 μM (16 $\mu\text{g}/\text{mL}$) ciprofloxacin titer, the exposure time is set at 15 s in the drug fluorescence channel — 100 ms are used for the transmission channel and 10 ms intervals are inserted for changes.

Series of images are loaded as stacks in the FIJI software (Schindelin, Arganda-Carreras et al. 2012). A first region of interest (ROI), called “cytoplasm and periplasm”, is defined inside a selected bacterium (Figure I - 46 b); those approximately 650 pixels roughly correspond to the projected surface of the cell. A second ROI, denoted “extracellular fluid”, is next drawn 5 to 6 μm away, in a place where no bacterium is present; it has an identical area and shape than the previous one. For each ROI, the fluorescence signal is finally computed from the associated movie and plotted as a function of time (Figure I - 50).

More specifically, raw data are corrected from the background by subtraction of the average signal issued from the 5 last frames of the “control” step. Then, the signal corresponding to the drug concentration jump is normalized at 1 by dividing the “extracellular fluid” data by the maximum value obtained on the “flush-in” step (Figure I - 50). In summary, one has

$$I_{extra}^{corr}(n) = \frac{I_{extra}^{raw}(n) - \langle I_{extra}^{raw}(n) \rangle_{control}}{\max[I_{extra}^{raw}(n)]_{flush-in}}$$

The same normalization is also performed for the “cytoplasm and periplasm” data (Figure I - 50), which yields

$$I_{cyto-peri}^{corr}(n) = \frac{I_{cyto-peri}^{raw}(n) - \langle I_{cyto-peri}^{raw}(n) \rangle_{control}}{\max[I_{extra}^{raw}(n)]_{flush-in}}$$

n being the frame number.

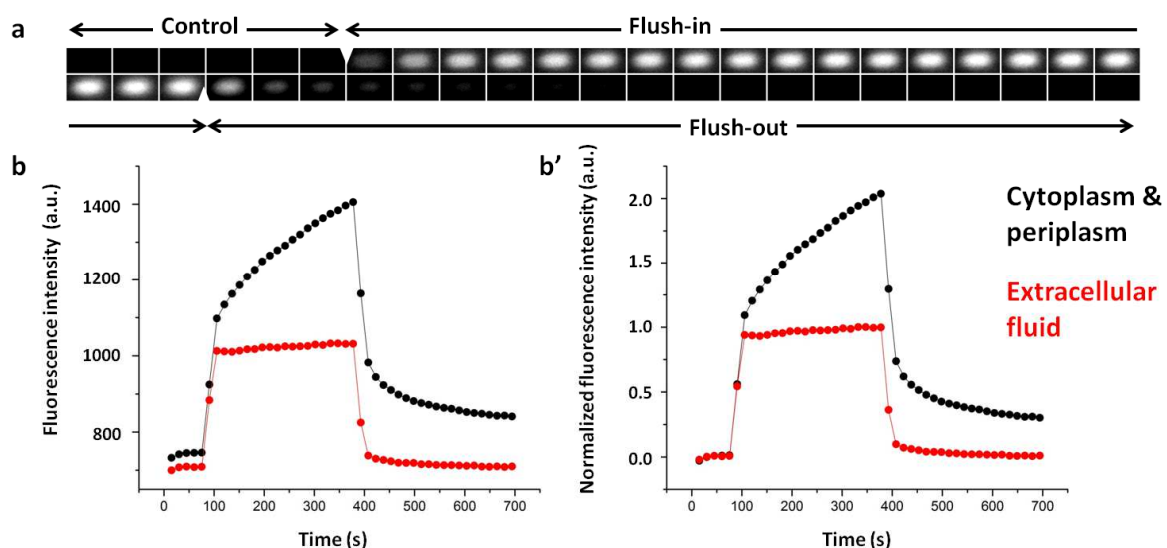


Figure I - 50. Procedures to collect and analyze influx/efflux data. (a) Time-lapse imaging of the immobilized bacterium of Figure I - 46. The frame interval was 15.11 s and the fluorescence exposure time 15 s. White triangles indicate changes in the perfused liquid. (b) Raw time traces for the associated signals. (b') Normalized time trace. Black and red markers are associated with the “cytoplasm and periplasm” and the “extracellular fluid” ROIs, respectively.

IV.3. Experiments on the AG100/AG100A/AG102 strains

For the AG 100 series of *E. coli*, the same excitation wavelength 290 nm is used. However, the choice of very important concentration of drug is not suitable any more, 2.7 μM (1 $\mu\text{g}/\text{mL}$) fleroxacin is thus used here. Because of the lowered concentration, the exposure time should be set longer to collect more efficient photons: 30 s exposure time in the drug fluorescence channel, 30 s pause without irradiation, and 0.1 s interval. The protocol concentrates first mainly on the “control” and “flush-in” periods, which are extended: control for 4 min and flush-in for 25 min. The disadvantage is that it results in losing the temporal resolution — the information during 30 sec is only summed up into one image.

The choice of the ROI is the same than in the experiments on BL21 (DE3), but MATLAB is used to treat and extract signals. As it is taken in charge specifically by another member in the team, the process is presented here in short. It is figured out that the darkfield of camera should be first subtracted from the raw data (average value equals to 700). Then the value of the 4th point of control phase is normalized to be 1, meaning that every signal has value 1 just before the flush-in process), then the values on the curve are proportionally reduced. The points on the curve correspond to the average intensity of the available *E.coli* in the field of view.

$$I_{\text{cyto-peri}}^{\text{corr}}(n) = \frac{I_{\text{cyto-peri}}^{\text{raw}}(n) - 700}{I_{\text{cyto-peri}}^{\text{raw}}(n = 4) - 700}$$

Chapter V. Microdevice characterization

The three first Sections of this Chapter are mainly issued from the text of an article in preparation (Zhao & Gosse 2017).

I. Finite element method simulations

I.1. Generalities

Both buffer flow and antibiotic transport were analyzed using the finite element method (FEM) software COMSOL Multiphysics 5.2 (R2015b release; COMSOL, USA). Computations were realized on a PowerEdge R720 workstation (Dell, USA) equipped with a 48 Go RAM and two E5-2650 0 processors running at 2.0 GHz. For those numerical evaluations we considered a single domain corresponding to the cavity in between the bottom substrate and the two lids, i.e. the cavity that includes the observation chamber and the four supply channels (Figure I - 51 a). Otherwise specified, the quality of the “physics-controlled mesh” was set at “fine”.

I.2. Hydrodynamics

The liquid flow was first computed as a “stationary” study with the “laminar flow” physics. The buffer was given the water properties, i.e. a density $\rho = 10^3 \text{ kg/m}^3$ and a dynamic viscosity $\mu = 10^{-3} \text{ Pa}\cdot\text{s}$, and the flow was considered as incompressible. Both inlet and outlet were characterized by constant pressures (the “normal flow” and “suppress backflow” settings being selected). More precisely, the value of the pressure difference, ΔP , was adjusted to 9.72 Pa in order to obtain a value of the flow rate, Q , equal to 0.6 mL/min. A “no slip” condition was enforced on all the other boundaries since they correspond to quartz or PDMS surfaces.

It is worth noting that, to increase resolution, the “finer” option of the “physics-controlled mesh” setting was selected for the calculation of the flow velocity map at the observation chamber entrance (Figure I - 51 b',c'). However, in that case the height mismatch between the supply channels and the observation chamber yielded a large number of elements and the simulated domain had to be restricted to a quarter of device. This size reduction was possible because (i) the considered geometry is clearly symmetric with respect to a mid-longitudinal cross-sectional plane; (ii) at low Reynolds number the flow before and after an obstacle is symmetric when the solid is symmetric with respect to a transverse cross-sectional plane. As far as boundary conditions were concerned, symmetry properties now applied on the mid-longitudinal cross-sectional plane and pressure at the mid-transverse cross-sectional plane was tuned such as $\Delta P = 4.86$ Pa.

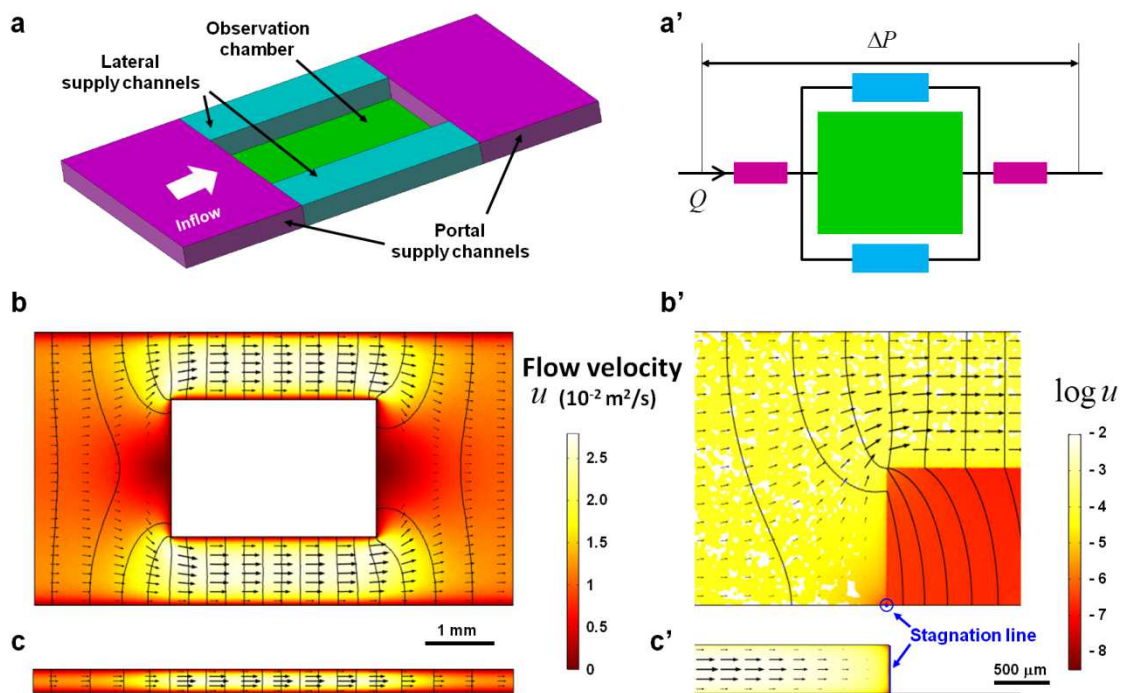


Figure I - 51. Analysis of the device hydrodynamics. (a) Three-dimensional view of the single domain that was considered for modeling. Coloring emphasizes on the compartments that have been delineated for hydrodynamic resistance computation (dimensions are given in Table I - 2). (a') Equivalent resistor model. (b,b') Flow velocity maps obtained by FEM simulations, data being plotted in the horizontal planes located 175 and 0.5 μm above the surface of the bottom substrate, respectively. A 9.72 Pa pressure difference was applied between the inlet and the outlet, in order to yield a 0.6 mL/min total flow rate. Black lines correspond to isobars, spaced by 0.5 Pa, and black arrows correspond to projections of the velocity vectors. (c,c') Corresponding flow velocity maps drawn in the longitudinal planes cutting the lateral supply channel and the whole device in their middle, respectively. White patches in b' are due to data extraction problems in COMSOL.

The inlet and the mid-transverse cross-sectional plane of the device were chosen for numerical evaluations of the flow rate. Because of boundary conditions or for symmetry reasons (see above), the velocity vector is normal to both surfaces. Consequently, integration of its norm, u , over the corresponding area simply yielded the associated flow rate, Q .

I.3. Solute transport

Once the hydrodynamic problem solved, the obtained velocity field was used as input to evaluate the antibiotic dispersion relying on the “transport of diluted species” physics. Of course molecular diffusion was also considered and, according to an evaluation found in the literature (Stewart 1996) the ciprofloxacin diffusion coefficient, D , had its value fixed at $6.9 \times 10^{-10} \text{ m}^2/\text{s}$. For each perfusion step we ran a “time dependent” study in which a constant “inflow” was imposed at the inlet. The associated concentration value was set at either 0 or 48.3 μM , depending if the pure buffer or the drug solution was used. The “outflow” boundary condition was set at the outlet and the “no flux” one on all the other surfaces. For each computation the concentration map obtained during the previous run was utilized as an initial condition. A time step of 0.1 s was used to investigate single perfusion cycle (Figure I - 52, Figure I - 53, Figure I - 54) whereas it was enlarged to 10 s for multicycle simulations (Figure I - 57, Figure I - 55 b''', Figure I - 56 b).

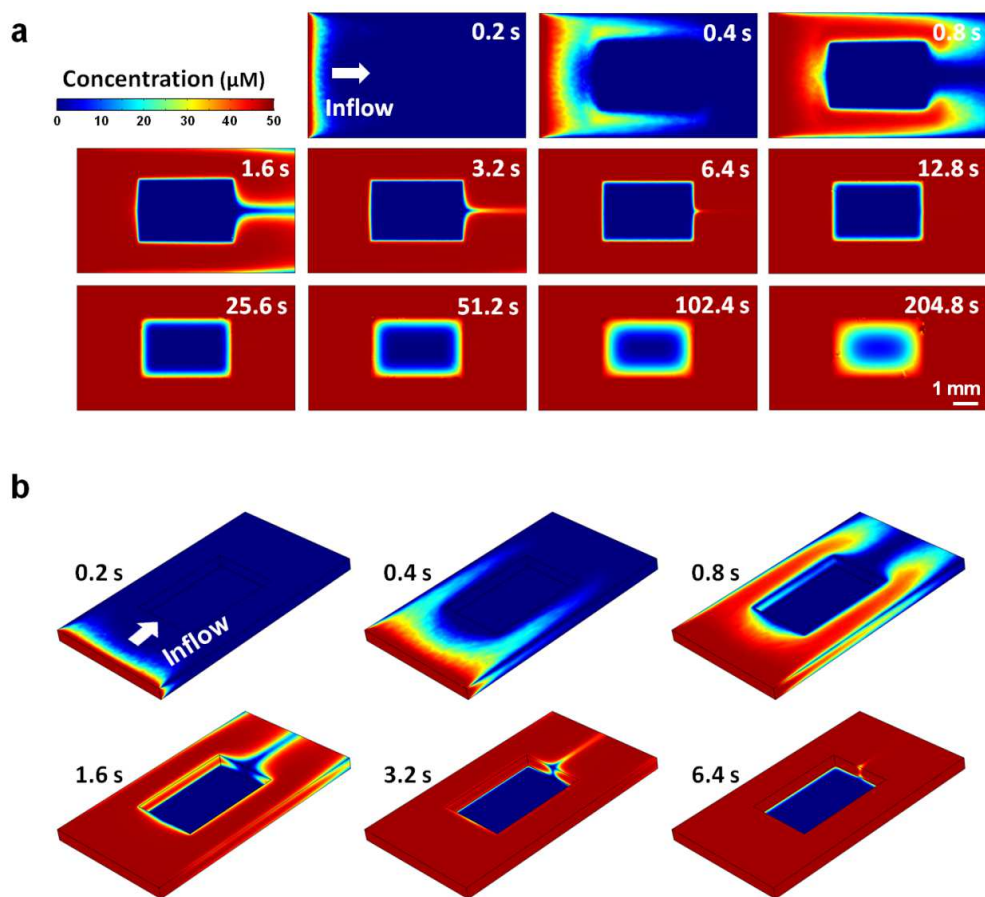


Figure I - 52. Antibiotic concentration maps obtained at various times after the onset of drug perfusion. A 9.72 Pa pressure difference was applied between the inlet and the outlet, in order to yield a 0.6 mL/min total flow rate. A $48.3\mu\text{M}$ ciprofloxacin concentration was imposed at the inlet. The displayed values correspond to FEM results collected at the surface of the simulation domain. (a) Vertical view emphasizing on the top surface. (b) Trimetric view including the top, front, and lateral surface.

Time traces of the antibiotic concentration were extracted by averaging this parameter over small surface elements that were parallel to the bottom substrate, located $0.5\ \mu\text{m}$ above it and having a few μm^2 area. Furthermore, the obtained data points were also averaged in time when numerical results had to be compared with experimental ones (Figure I - 54). In that case a 15 s window was selected in order to mimic at best video integration; however, the lack of synchronization between fluidic actuation and camera shutter operation prevented us to accurately define the origin of the movie with respect to solute exchange.

II. Numerical and experimental results

II.1. Hydrodynamics

Although our device consists in a single domain, for the sake of the analysis it is here divided in 5 compartments: 1 observation chamber plus 4 supply channels – 2 in portal positions, at both inlet and outlet, and 2 in lateral positions, running on both sides of the observation chamber (Figure I - 51). Each of these rectangular parallelepipeds has a width W , a height H , and a length L (Table I – 2). From an hydrodynamics view point the perfused liquid is water and thus, at such a small scale, the flow is assumed to be laminar (Stone, Stroock et al. 2004). This hypothesis was *a posteriori* validated by computation of the Reynolds number for each of the compartments: $Re = \rho u_{max} H / \mu$, with ρ the fluid density, μ its dynamic viscosity, and u_{max} its maximum velocity. Indeed, the data obtained both analytically and numerically (Table I – 2) yielded Re ranging from $\sim 10^{-7}$ in the observation chamber to 10 in the lateral supply channels.

First, estimates for the flow velocities u were calculated relying on a coarse-grain “resistor model” of the device (Figure I - 51 a’) (Tabeling 2006) (Bruus 2008). For each compartment, the pressure difference between its outlet and its inlet, ΔP , is related to the corresponding flow rate, Q , by an equivalent of the Ohm's law: $\Delta P = R Q$, with R the hydrodynamic resistance given by $R = [12\mu L / WH^3] \times [1 - 192H / \pi^5 W]^{-1}$ (Stone, Stroock et al. 2004) (Bruus 2008). Using composition rules similar to the ones found in electrokinetics (Tabeling 2006) (Bruus 2008) the whole microsystem resistance could be found, as well as the flow rate associated with each branch of the circuit when a total 0.6 mL/min value was imposed at the inlet of the portal supply channel (Table I – 2). Finally, flow velocities were roughly derived as $u = Q / S$, with $S = W \times H$ (Table I – 2). The observation chamber being 350 times thinner than the other compartments, its resistance is more than 7 orders of magnitude larger. This branch of the circuit nearly behaves like an open one since the flow rate running through it is negligible and since the fluid velocities are here $\sim 10^5$ smaller than in the other branches.

Next, FEM simulations were undertaken to gain more insights into the device hydrodynamics. Poiseuille flows with parabolic velocity profiles were obtained in most of the compartments (Figure I - 51 b, c, c’) except, of course, close to the front edge of the observation chamber lid (Figure I - 51 b). The main flow running through the portal supply channel here divides in two, towards the two lateral supply channels (Figure I - 51). As a consequence, a stagnation line can be evidenced along the intersection with the mid-longitudinal symmetry plane (Figure I - 51 b’, c’). Such feature surely explains the discrepancies observed between the preceding analytical evaluations and the numerical results. For instance, the whole device resistances differ by $\sim 15\%$ – despite the two computational techniques are in good agreement when applied to each individual compartments (Table I – 2). In addition, flow velocities in the supply channels vary by a factor 2 – although for both calculations the

total pressure drop was adjusted in order to achieve a same 0.6 mL/min flow rate at the inlet. Nevertheless, those discrepancies are within one order of magnitude and the conclusions drawn for the simple resistor model are still relevant. More specifically, the flow in the observation chamber remains weak. From a zoom calculated at higher spatial resolution, we can estimate $u < 10^{-6}$ m/s for the area over which influx/efflux measurements are realized (Figure I - 51b').

Compartment	(10^{-6} m)	(10^{-6} m)	(10^{-6} m)	Resistor model			FEM simulations		
				(Pa.s/m ³)	(m ³ /s)	(m/s)	(Pa.s/m ³)	(m ³ /s)	(m/s)
Portal supply channel	4000	350	2000	1.48×10^8 a	10^{-8}	7.14×10^{-3}	(1.50×10^8) b	10^{-8}	1.23×10^{-2} e
Lateral supply channel	1000	350	3000	1.08×10^9 a	5×10^{-9}	1.43×10^{-2}	(1.09×10^9) b	4.96×10^{-9}	2.64×10^{-2} f
Observation chamber	2000	1	3000	1.80×10^{16} a	2.99×10^{-16}	1.49×10^{-7}	(c) b	d	1.80×10^{-7} f
Whole device				8.34×10^8	10^{-8}		9.69×10^8	10^{-8}	

Table I - 2. Hydrodynamic parameters retrieved from analyzing the device behavior both analytically and numerically. W , H , and L are the width, height, and length of each compartment whereas $S = W \times H$ corresponds to its transverse cross-section and R to its hydrodynamic resistance. Q and u_{max} are the flow rate and maximum flow velocity obtained when a 0.6 mL/min flow rate is enforced at the device inlet. ^a Data evaluated according to Stone et al.,(Stone, Stroock et al. 2004) values are given with a ± 10 % precision. ^b Data collected using simulations on the sole considered compartment. ^c Non converging computations. ^d Numerical estimate differing from its expected value by more than several order of magnitude. ^e Data measured over the device inlet surface. ^f Data measured over the mid-transverse cross-sectional plane.

II.2. Solute transport

In order to determine the nature of the solute transport occurring in the various compartments, we computed the Peclet number, $Pe = lu/D$, using D the diffusion coefficient of the antibiotic, $u = Q/S$ the flow velocities determined with the resistor model, and l the characteristic distances associated with each part of the device. More precisely, for the portal supply channel we set $l_{PSC} = 2$ mm since it is the distance separating the observation chamber from the inlet and for the observation chamber we set $l_{OC} = 25$ μm since it is the distance separating the observed bacteria from the edge of the observation chamber lid. Thus, for the first compartment we have $Pe_{PSC} = 5.2 \times 10^5$ whereas for the second one we have $Pe_{OC} = 9 \times 10^{-3}$. As a consequence, molecular transport is achieved by advection in the portal supply channel and by diffusion in the observation chamber.

Orders of magnitude for transport times can further be derived: it takes $\tau_{PSC} = l_{PSC}/u_{PSC} \approx 0.1$ s for the drug to reach the lid edge and some additional $\tau_{OC} = l_{OC}^2/D \approx 1$ s to surround bacteria.

FEM simulations roughly confirm the preceding evaluations (Figure I - 52): the antibiotic is first transported by advection in the supply channels and then by diffusion in the observation chamber. One can for instance notice that, during the first seconds, vertical concentration profiles in the supply channels are parabolic, as expected for advection in a Poiseuille flow (Figure I - 52 b). However, the simulated concentration changes near the front edge of the observation chamber are ten times slower than the rough estimates issued from the resistor model. This discrepancy is in fact due to the hydrodynamic stagnation point present in the middle of the edge of the observation chamber lid, as evidenced on the concentration maps at 0.4 and 0.8 s (Figure I - 52).

To further emphasized on the two regimes characterizing molecular transport in the device, we compared the FEM results with a simple analytical model in which diffusion takes place in a semi-infinite medium, here the observation chamber, after application of a concentration step of height $C_0 = 48.3 \mu\text{M}$ (Figure I - 53). The response to this Heaviside stimulus is given by the complementary error function:

$$C(x, t) = C_0 \operatorname{erfc} \left[\frac{x}{2\sqrt{Dt}} \right]$$

with x the distance from the chamber edge (Carslaw and Jaeger 1959). For $t > 10$ s the two curves superimposed which means that apart from the delay induced by advection, especially in the stagnation region, molecular diffusion is the main phenomenon taking place in the observation chamber.

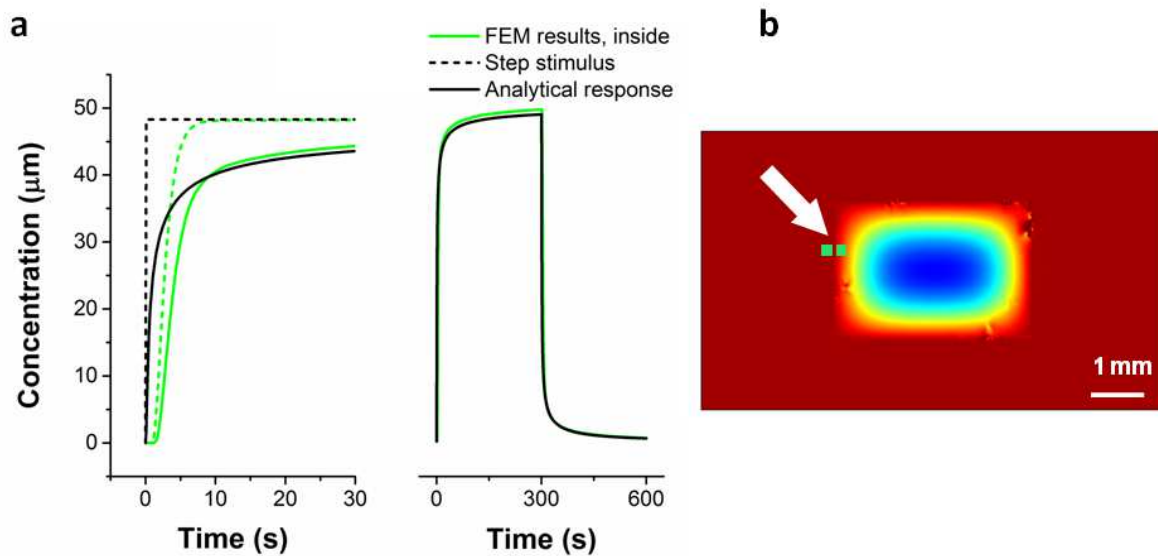


Figure I - 53. (a) Time traces of the antibiotic concentration obtained by averaging the results of the FEM simulations over a $4 \mu\text{m} \times 4 \mu\text{m}$ surface positioned $0.5 \mu\text{m}$ above the bottom substrate and located $25 \mu\text{m}$ outside or inside the observation chamber, $200 \mu\text{m}$ aside the device longitudinal symmetry axis. Those data are compared with an analytical evaluation of the diffusion process assuming step variations of the antibiotic concentration at the front edge of a semi-infinite observation chamber. (b) Horizontal cross-section plane indication the position of the 2 ROIs.

Finally, the results issued from the simulations were analyzed with respect to the experimental data. Since fluorescence was integrated for 15 s on the CDD sensor, FEM data were processed in a similar way (Figure I - 54 b). It resulted in sharper concentration variations that indeed reflected correctly what was observed under the microscope (Figure I - 54 a). Please note that to find a computed concentration time trace that agreed fairly with measurements we had to adjust by hand the origin of the numerical averaging procedure; indeed, in our experiment syringe pump actuation was not synchronized with video acquisition.

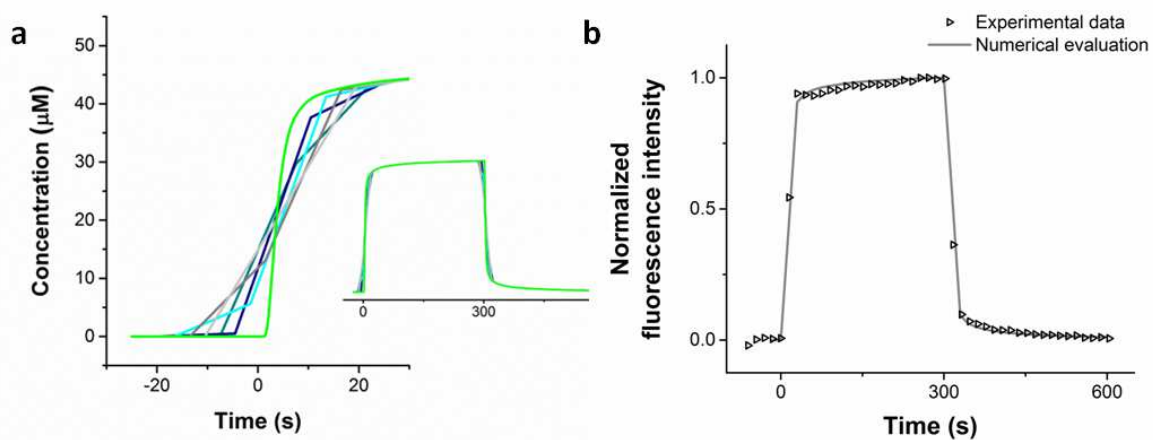


Figure I - 54. Computational approach to decipher the influence of the camera integration time on fluorescence intensity measurements. (a) First, the time trace of the antibiotic concentration, in green, was obtained by averaging the results of the FEM simulations over a $4 \mu\text{m} \times 4 \mu\text{m}$ ROI situated $25 \mu\text{m}$ inside the

observation chamber, 0.5 μm above the bottom substrate and 200 μm aside the device longitudinal symmetry axis. For both the drug solution and the pure buffer a 9.72 Pa pressure difference was applied between the inlet and the outlet, in order to yield a 0.6 mL/min total flow rate. The ciprofloxacin concentration imposed at the inlet was changed from 0 to 48.3 μM at $t = 0$ s, and switched back to 0 at $t = 300$ s. The time step for these simulations was 0.1 s. Next, data were averaged over 15 s windows: it resulted in the 5 blue-gray curves, which only differ by the origin of the latter integration process. More precisely, the various starting positions are separated by 3 s increments in order to account for several possible synchronization delays between the acquisition sequence and the fluid exchange one. (b) Comparison between the real signals extracted from the experiment shown in Figure I - 62 and the best fitting data obtained in (a).

III. Discussion

III.1. Selection of the field of view

Numerical simulations were further used to validate the choice of the scrutinized area. As evidenced in Figure I - 55, at the scale of the CDD camera integration time, solute exchange takes place with the same dynamics along both the front edge of the observation chamber and the lateral ones. However, when looking at the phenomena at a higher resolution we can notice that drug reaches more quickly the bacteria located close to the lateral supply channel than the ones in portal position. Once more this observation can simply be explained by the presence of the hydrodynamic stagnation point. Diffusion is indeed similar all around the edges of the chamber but this molecular step starts earlier where the lid edge is parallel to the main direction of the flow, although this place may be farther from the inlet.

We also try to set the region of interest at different locations inside the observation chamber (Figure I - 56). Without any surprise the larger the distance from the edge, the longer it takes to reach a given drug concentration. Additionally, on a larger time-scale, the response to a square-wave signal in antibiotic concentration displayed the damping in amplitude and the delay in phase that are associated with the propagation of diffusion waves in a semi-infinite medium. More precisely, for a cosine stimulus the response writes

$$C(x, t) = C_0 \exp \left[-x \sqrt{\frac{\omega}{2D}} \right] \cos \left[\omega t - x \sqrt{\frac{\omega}{2D}} \right] - \frac{2C_0}{\sqrt{\pi}} \int_0^{\frac{x}{2\sqrt{Dt}}} \cos \left[\omega \left(t - \frac{x^2}{4D\mu^2} \right) \right] e^{-\mu} d\mu$$

Where the second member of the equation corresponds to the transient (Carslaw and Jaeger 1959). One can thus evidence the characteristic length scale $L_D = \sqrt{2D/\omega}$ above which the initial signal will be significantly modified. Here $L_D \sim 350 \mu\text{m}$.

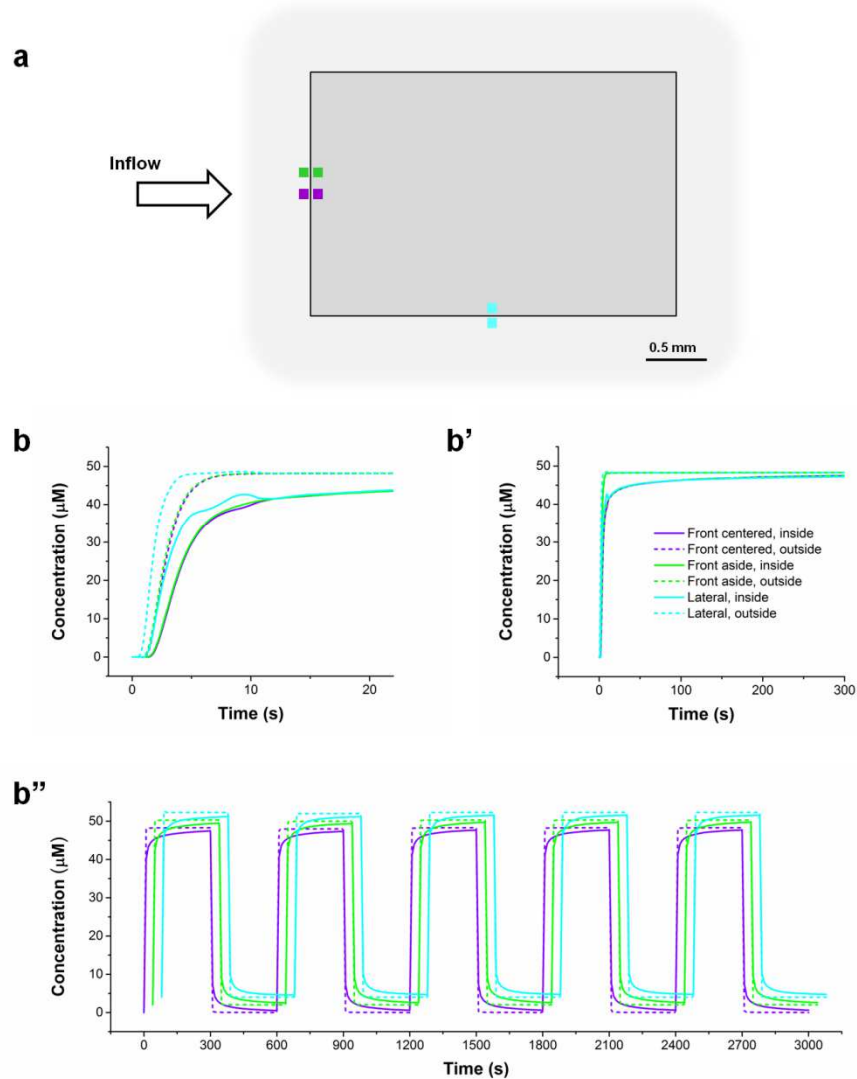


Figure I - 55. Variations of the antibiotic concentration as a function of the position around the observation chamber edge and of the number of injection/washing cycles. For both the drug solution and the pure buffer a 9.72 Pa pressure difference was applied between the inlet and the outlet, in order to yield a 0.6 mL/min total flow rate. The ciprofloxacin concentration imposed at the inlet was alternated between 48.3 and 0 μM every 300 s. (a) Location of the 6 ROIs over which data were collected. These 4 μm \times 4 μm surfaces, positioned 0.5 μm above the bottom substrate, were group in 3 couples, each of them including one ROI situated 25 μm inside the observation chamber and the other one 25 μm outside. Two of these couples were placed on the front edge, either aligned with the device longitudinal symmetry axis or 200 μm aside, whereas the last couple was centered on the lateral edge. (b-b'') Time traces of the antibiotic concentration obtained by averaging the results of the FEM simulations over each of the 6 ROIs. The wavelets present on the 'lateral, inside' curve in b are artefactual since their exact shape depends on the computation run and on the location, on the left or on the right side of the chamber. For the sake of clarity the data associated with each couple were shifted by 2 μM and 40 s in b''.

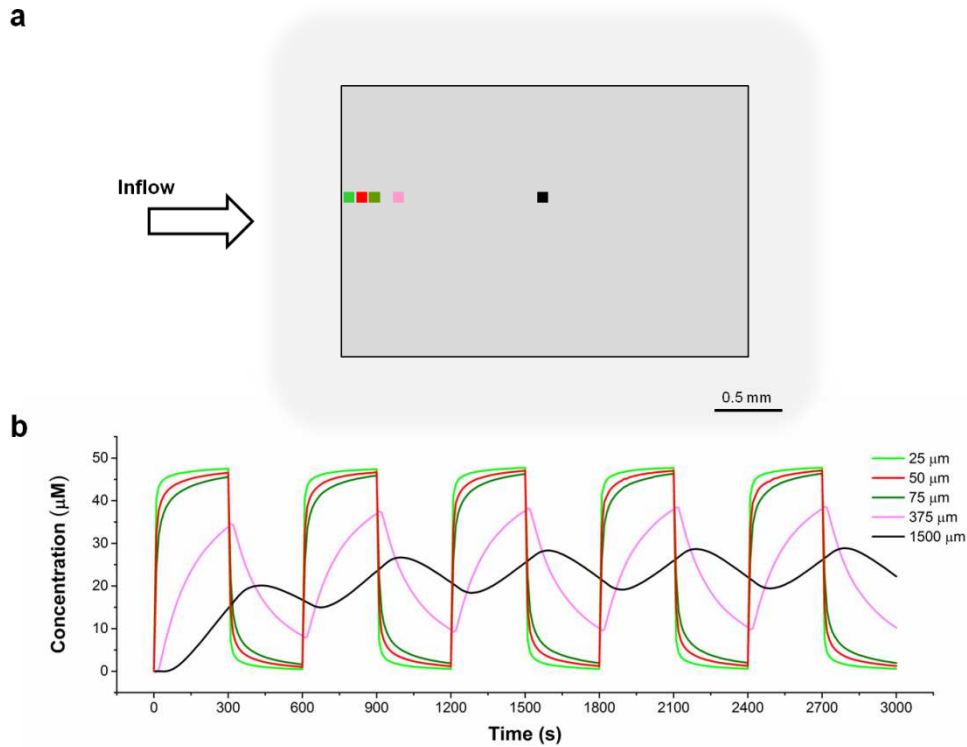


Figure I - 56. Variations of the antibiotic concentration as a function of the distance to the observation chamber edge and of the number of injection/washing cycles. For both the drug solution and the pure buffer a 9.72 Pa pressure difference was applied between the inlet and the outlet, in order to yield a 0.6 mL/min total flow rate. The ciprofloxacin concentration imposed at the inlet was alternated between 48.3 and 0 μM every 300 s. (a) Location of the 5 ROIs over which data were collected. The center of these 4 $\mu\text{m} \times 4 \mu\text{m}$ surfaces, positioned 0.5 μm above the bottom substrate, was situated 25, 50, 75, 375, or 1500 μm inside the observation chamber, 200 μm aside the device longitudinal symmetry axis. The light green and red ROIs are similar to the ones of Fig. 5, the position of former being similar to the usual position of the analyzed bacteria. The distance separating the pink ROI from the edge of the chamber roughly corresponds to the characteristic diffusion length associated with the present concentration modulation: $l_D = 363 \mu\text{m}$. (b) Time traces of the antibiotic concentration obtained by averaging the results of the FEM simulations over each of the 5 ROIs.

III.2. Variability and stability

Finally, we experimentally evaluated the robustness of the applied solute exchange (Figure I - 57). First, wherever bacteria are observed within 50 μm from the chamber edge, the dynamics of the concentration modulation is similar at the time-scale of the video exposure time. Second, discrepancies in signal intensity can be attributed to the Gaussian illumination profile, an issue that we straightforwardly solved by renormalizing our data (Chapter IV, Section IV.2).

On the other hand, multiple drug solution / washing buffer commutations are possible over several periods. Fluidic actuation displays a fairly good stability over more than 50 min.

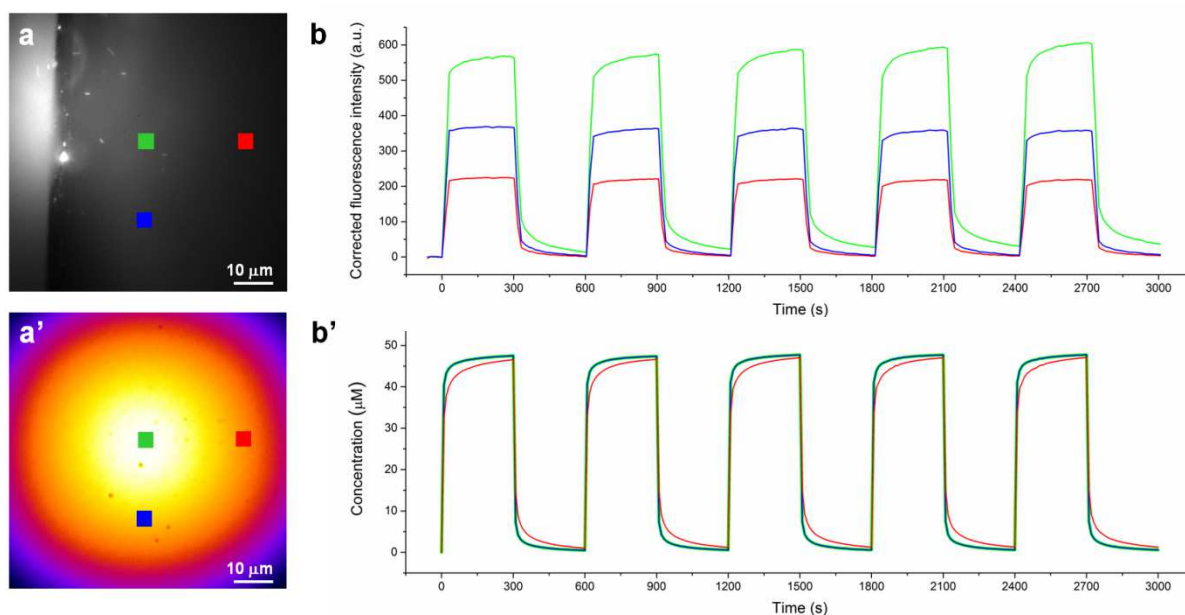


Figure I - 57. Variations of the fluorescence signal as a function of the position inside the observation chamber and of the number of injection/washing cycles. For both the drug solution and the pure buffer the perfusion flow rate was 0.6 mL/min. The ciprofloxacin concentration in the perfused liquid was alternated between 48.3 and 0 μM every 300 s. (a) Location of the 3 square ROIs which were analyzed. Each of them was 4 $\mu\text{m} \times 4 \mu\text{m}$ in size and was situated either 25 or 50 μm inside the observation chamber, roughly 200 μm aside the device longitudinal symmetry axis. The displayed image was acquired 150 s after the onset of antibiotic perfusion. (a') Intensity map obtained for the Gaussian illumination beam. (b) Time trace of the fluorescence intensity collected over each of the previous ROI and corrected by subtraction of the background (i.e. the signal averaged on the 5 images preceding drug injection). (b') Time trace of the antibiotic concentration obtained by averaging the results of the FEM simulations over each of the 3 ROIs.

IV. Comparison of our microdevice with the existing solutions

IV.1. Steric immobilization in microfluidic growth chambers

Three designs of bacteria chambers can be found in the literature, a set to which we have to have our own contribution (Grünberger, Probst et al. 2015) (Ullman, Wallden et al. 2013) (Wang, Ran et al. 2015), and (Zhao & Gosse 2017). Designs can be distinguished according to three points: the existence of connecting channels, the size of culture chamber, and the number of sides used to connect the supply channels (Table I - 3, Figure I - 58).

We have performed FEM simulations in order to evaluate the performances of these 4 devices with respect to the rapidity of solute transport. More specifically, a step concentration stimulus was imposed, at the border with the deep supply channel and different of the antibiotic was allowed to proceed by diffusion in the shallow chamber and concentrations were monitored at 3 different distances from the chamber edge: 10, 20, and 30 μm (Figure I - 58, Figure I - 59).

Bacteria chamber (μm)			Connecting channel (μm)				Type
Length	Width	Height	Length	Width	Height	Position	
40	40	1	19	2	1	Lateral, 2 sides	Grünberger et al. 2015
40	40	0.9	0	0	0	Lateral, 2 sides	Ullman et al. 2013a
90	90	1.2	40	10	1.2	Lateral, 1 side	Wang et al. 2015
3000	2000	1	0	0	0	Portal & lateral, 4 sides	Zhao & Gosse 2017

Table I - 3. Comparison of the parameters characterizing the designs of the existing microfluidic growth chambers.

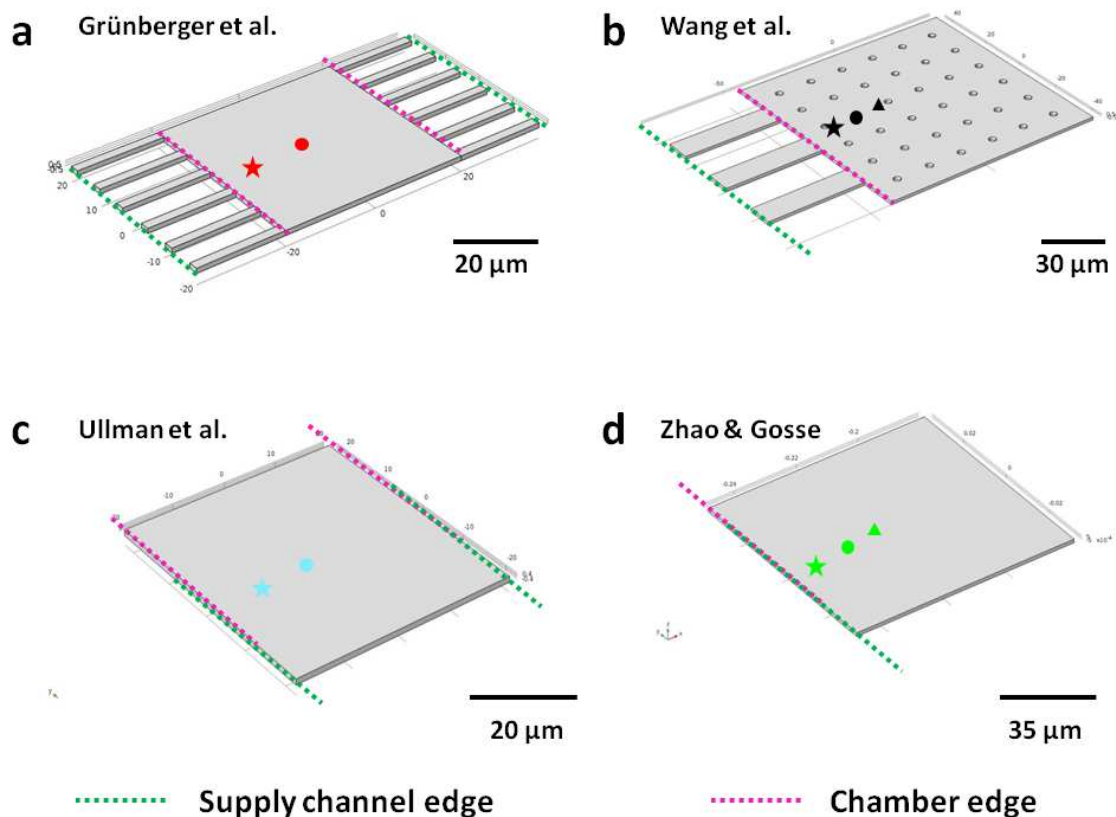


Figure I - 58. Model of the bacteria chambers used for the simulation studies. (a) Grünberger et al. (b) Wang et al. (c) Ullman et al. (d) Zhao & Gosse. Symbols represent the positions where concentration changes were observed (see Figure I - 59). The olive green lines are the supply channel borders and magenta lines delineate the chamber edge.

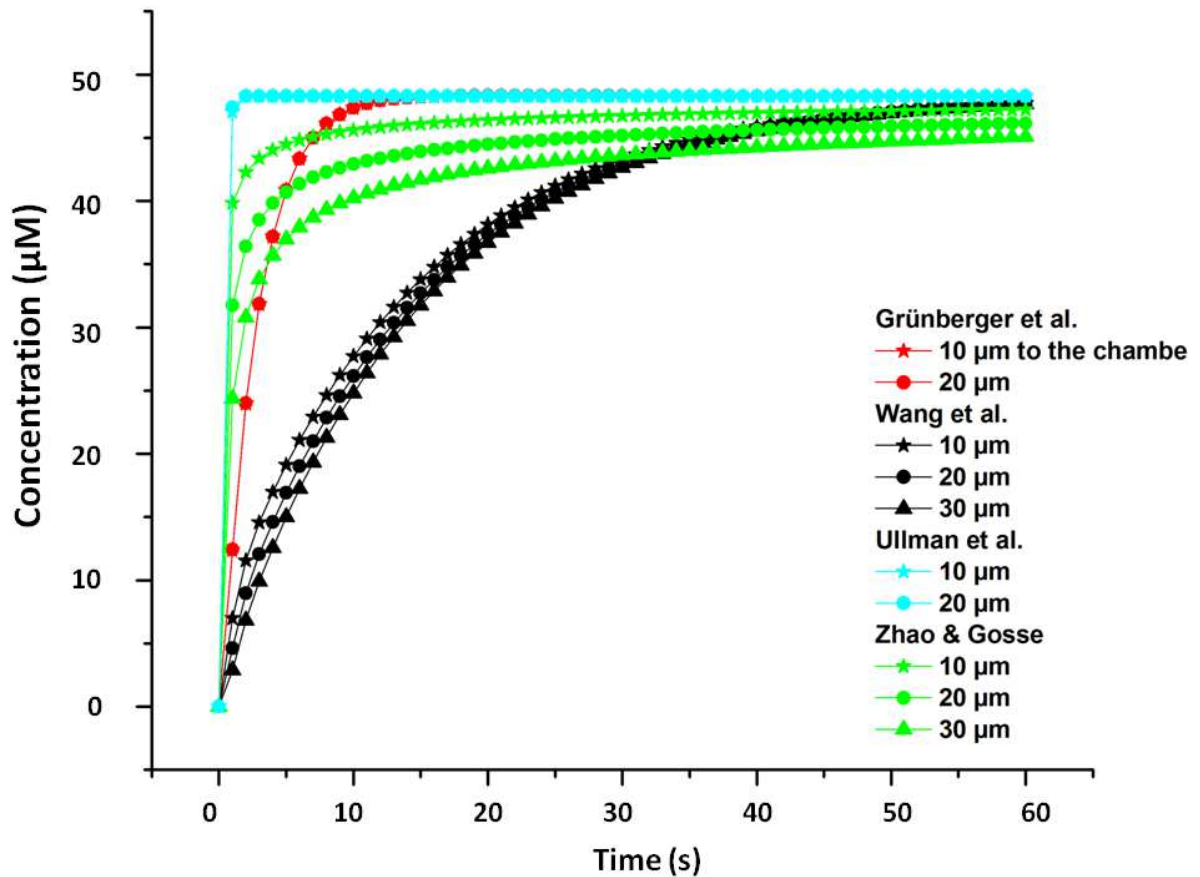


Figure I - 59. Concentration variations obtained by numerical simulations after applying a step stimulus of 48.3 μM at the supply channel of the Figure I - 58. Symbols correspond to the locations on Figure I - 58 (indications in micron, for the chamber edge.)

According to the above presentations and simulations, in Ullman's design, the molecular exchange is the fastest thanks to 2 reasons: 2 sides opening to the supply channel and no connecting channel exists. However, in Wang's design, the molecular exchange rate is the slowest because not only with 1 side of opening, but also diffusion begins from the connecting channel and the molecules need to cross them to reach the growth chamber. In the rest 2 designs, they can only meet one point: Grünberger's design has still the connecting channel, and Zhao's design expects molecules coming only from one side (in the field of view).

Another question that can be addressed is whether or not a 2-side entry spreads up solute exchange with respect to a single side one. Figure I - 60 displays simulations are based on Grünberger's design, with a small chamber surface ($40 \mu\text{m} \times 40 \mu\text{m}$). From the examination of the exact center of the chamber, it can be clearly seen that 2-side opening enables to reach concentration plateau faster.

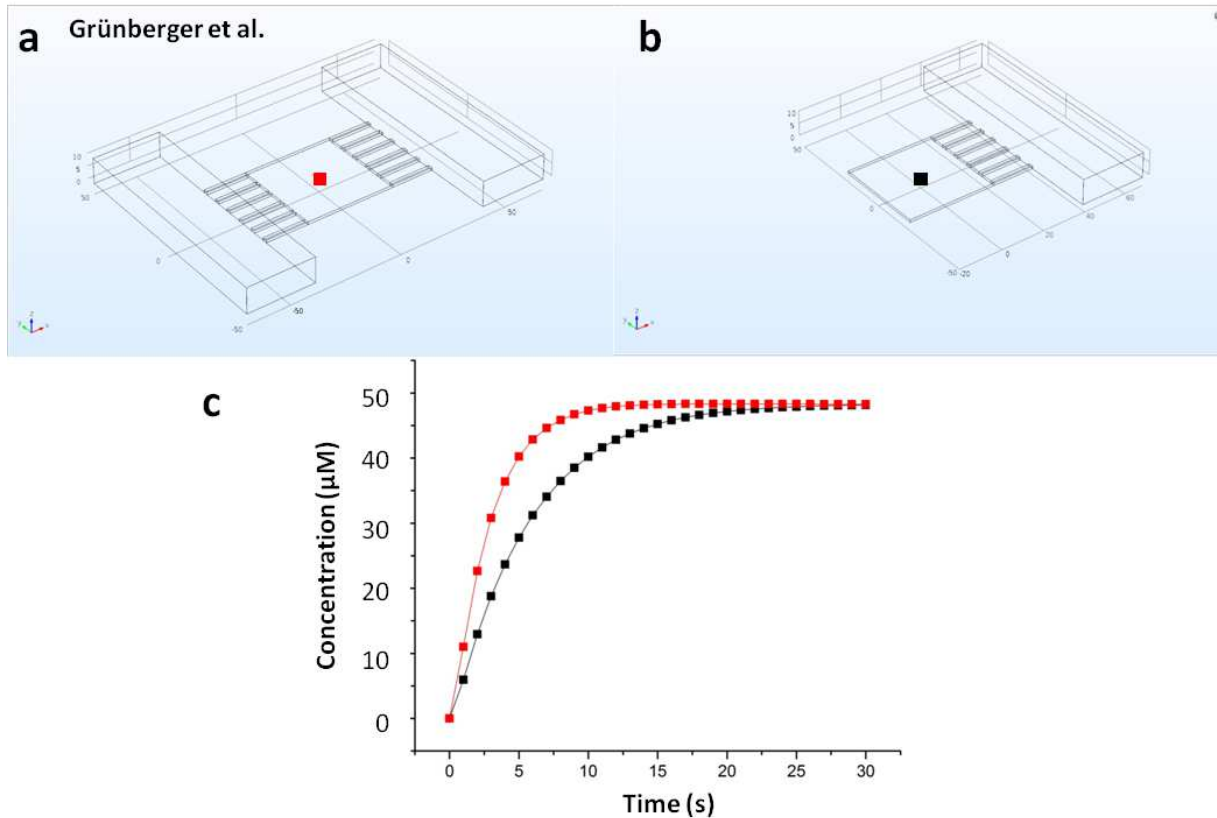


Figure I - 60 The difference of 1-side or 2-sides diffusion based on Grünberger’s design (Grünberger et al. 2015). (a) Reported chamber. (b) One supply channel of (a) is removed. (c) At the exact center, the concentration estimation as a function of time.

In conclusion we learnt that the relatively small size of individual chambers supplied by source of 2-side does help to reach the maximal concentration more quickly. Similarly, the shorter the connecting channels, the faster.

IV.2. Physico-chemical trapping at the surface of a microfluidic channel

In the aforementioned bacteria chambers (Grünberger, Probst et al. 2015) (Ullman, Wallden et al. 2013) (Wang, Ran et al. 2015), and (Zhao & Gosse 2017), solute exchange is achieved thanks to diffusion, because the small height of the compartment does not allow rapid flow and, consequently, $Pe < 1$. Yet, concentration variation would be faster if advection could also participate in solute transport. The optimal set up to fulfill such objective would be like the one of Figure I - 61. Bacteria are immobilized by natural impurities on the quartz surface, so there is no need of physico-chemical trapping or other assistant factor like electrical field. Liquid exchange is driven by simple advection, which is enabled by the thick channel height. Imaging is performed by total internal reflection

fluorescence microscopy, a thin region of a specimen (usually less than 200 nm) is acquired and the background fluorescence coming from molecules out of this layer is excluded.

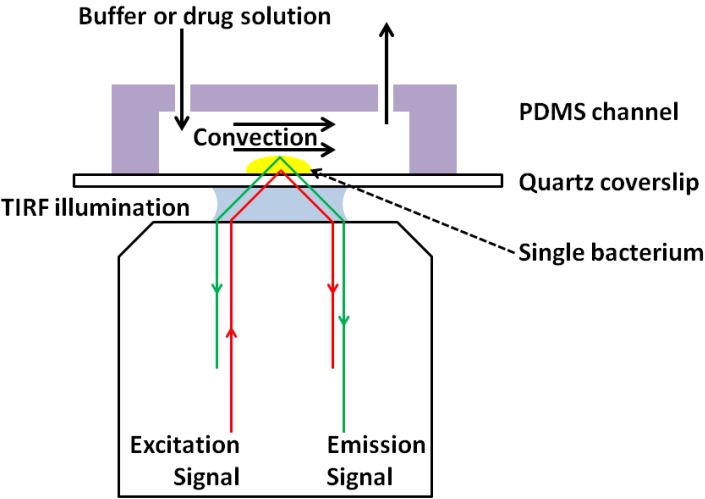


Figure I - 61. The simplest and optimal set up (not to scale).

Chapter VI. Experiments on bacteria

After the development of the flow device, we so far have made two application attempts: one concerned influx/efflux studies, in line with the main topic of this PhD work, and the other deals with microorganism culture.

I. Influx/efflux studies

I.1. Device validation on the uptake of ciprofloxacin by the BL21 (DE3) strain

During the device development, a commercial microbiological product, i.e. the BL21 (DE3) *E. coli* strain from New England Biolabs, was used for convenience. More precisely, this material was easily accessible, its quality was controlled and constant; thus, microdevice characterization was eased and freed from a number of experiment biases.

In order to have a general concept, we discuss from two ways the analysis.

As can be seen in the “extracellular fluid” time trace of Figure I - 62, the introduction of the antibiotic molecules is achieved within 2 video frames, i.e. 30 s. Indeed, the signal corresponding to the first point has not yet reached the highest value, but the one associated with the second point is on the plateau. After, the signal stays almost constant. Conversely, the fluorescence intensity inside bacteria keeps on increasing over the next 5 min. In the efflux phase, it is basically the reverse process that is observed. Therefore, one can conclude that solute exchange is fast enough to be employed with the present acquisition system, which is limited to a 15 s exposure time.

From the simulation point of view, it is confirmed by the concentration estimation. On one hand we can have a concept that each porin monomer can let pass about 10 - 100 fluoroquinolone molecules (e.g. norfloxacin) per second when the external concentration gradient equals to 1 mM

(Pagès, James et al. 2008) (Cama, Bajaj et al. 2015) (Cama, Schaich et al. 2016). Counting by 10^5 copies of porins per bacterium, so one bacterium can consumes 3×10^6 to 3×10^7 molecules per second; on the other hand, taking the position of “30 μm away from the edge at the 3rd sec” as example, that is 33.82 μM drug at place, which corresponds to 70% of the complete external concentration (48.3 μM), namely 2.04×10^{19} molecules/L, much more in excess than the consumption ability of bacteria. So we consider it to be an effective method to carry out such bacteria uptake experiment.

Until now, uptake data have only been considered qualitatively. A quantitative interpretation of these curves would require a more precise estimation of the necessity to deconvolute the influx/efflux signals from the device response. Additionally, we would have to refer to model of drug uptake in bacteria. Gram-negative bacteria have two cell membranes, which compartmentalize the cell into a periplasm and a cytoplasm. Antibiotics present in the extracellular environment cross the outer and inner membrane with different permeability coefficients and some transport equations have already been established (Zimmermann and Rosset 1977) (Nikaido and Rosenberg 1983).

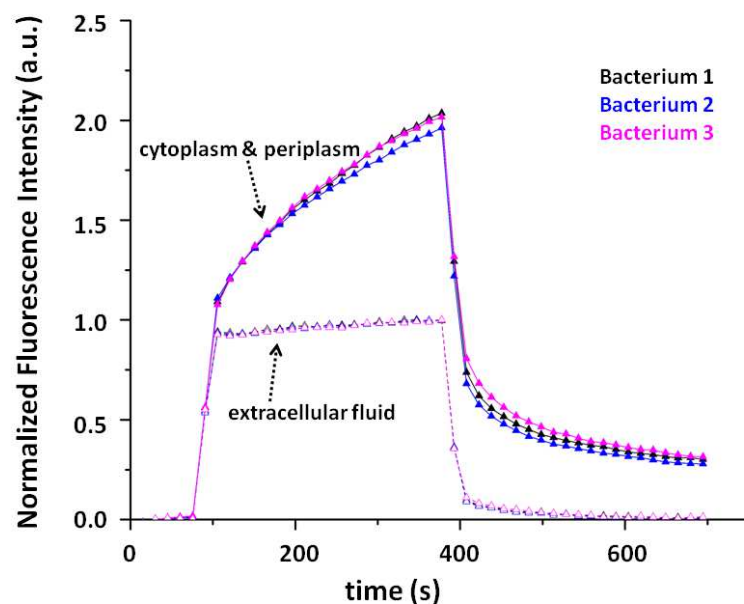


Figure I - 62. Time trace for the signals associated with 3 different bacteria, located 20 to 35 μm inside the observation chamber. Solid and open markers hold for the “cytoplasm and periplasm” and for the “extracellular fluid” ROIs, respectively.

I.2. Preliminary results on the uptake of fleroxacin by the AG100/AG100A/AG102 strains

Although protocol validation was performed on a commercial *E. coli*, strain without great interest, the goal of my PhD study was to collect biologically relevant data from bacteria issued from microbiology laboratories. In a first practical application of this device, we consequently try to evidence differences between strains in which the efflux system has been modified. Mutants of *E. coli* belonging to a well studied series were used: AG100 corresponds to the wild type, AG100A to a strain in which the AcrAB efflux pump is silenced, and AG102 to a strain in which the AcrAB efflux pump is overexpressed (Viveiros, Jesus et al. 2005) (Okusu, Ma et al. 1996). A lack of efflux pump removes any possibilities to clear the drug, whereas with more efflux pumps the ability to expel out antibiotic molecules increases. Due to time constraints, data collection is not totally achieved; nevertheless, some preliminary results are displayed in Figure I - 63. As expected, uptake in AG100A presents the plateau with the highest level of intensity, AG100 is in the middle, while AG102 is at the bottom.

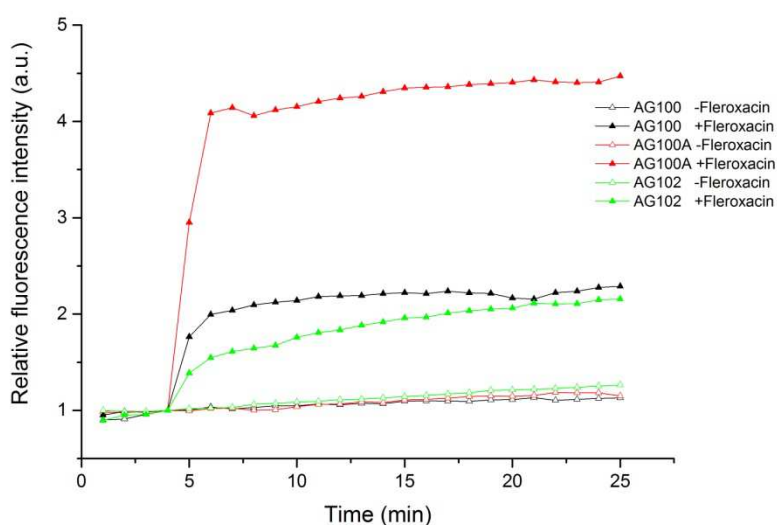


Figure I - 63. Preliminary results of mutant strains. Fleroxacin was dissolved at 1 $\mu\text{g}/\text{mL}$ in 50 mM NaPi buffer, pH=7, and flow at 0.6mL/min in the supply channel. Three bacteria, corresponding to the three strain of the series, i.e. AG 100, AG 100A, and AG 102, were first monitored when flushing with the sole buffer and then when flushing with the drug solution. Protocol for imaging is 30 s of acquisition in the 420 - 480 nm fluorescence channel, 30 s with the shutter closed, 0.1 s of interval in between each of the previous step.

I.3. Perspectives on the use of efflux modulators and/or other bacterial species

The discovery of molecules influencing efflux has contributed to restore some hope that the antimicrobials can become efficient again. Decoupling agents can dissipate the transmembrane gradient of protons and repress the operation of the pumps that use the proton motive force

(Pidcock 2006). For instance, these molecules include carbonyl cyanide 3-chlorophenyl hydrazone (CCCP) and dinitrophenol (DNP). Another family of compounds is capable of inhibiting RND pumps by competition with the substrate (Lomovskaya, Warren et al. 2001). A representant of this family is phenylalanine arginine- β -naphthylamide (PA β N), whose activity has been demonstrated on the AcrAB pump of Enterobacteriaceae (Pagès and Amaral 2009). However, the therapeutic use of PA β N in combination with an antibiotic is impossible because of its toxicity. More interestingly, efflux pump inhibitory properties have also been demonstrated for classes of drugs already used in humans. For instance, artesunate, a derivative of artemisinin (used against malaria) is able to potentiate β -lactam activities against *E. coli* and increased cell accumulation of daunorubicin, possibly through the inhibition of AcrAB-TolC expression (Li, Yao et al. 2011). Independently, quinoline and pyridoquinoline derivatives are investigated as inhibitors of AcrAB in *E. aerogenes* (Chevalier, Bredin et al. 2004) (Chevalier, Atifi et al. 2001).

The work planed on efflux modulators is still under design. To realize meaningful experiments, we will change the drug solution used the in flush-in phase into a drug plus adjuvant one (e.g. fleroxacin + CCCP) and then replace or not the buffer used in the flush-out phase by buffer supplemented with adjuvant. Doing so we expect to observe different levels of accumulation in cells and also to better understand the dynamics of inhibition.

In parallel, other bacterial species will be included in experiments, for example *Enterobacter aerogenes* and its mutants, which are of importance in medicine are studied by our collaborators from Marseille.

II. Cell growth studies

From the simulations we learn that mass transfer in the observation chamber is mainly driven by diffusion and that there is always a moment when the concentration there will equal the one of the external source. As long as the external supply flow is steady, the concentration in nutrients around bacteria can reach its maximum and remains stable.

Furthermore, even if the large upper wafer of the static chamber has been changed into a much smaller rectangular lid, in order to reduce the mismatch of curvature between the two pieces, eventual dust or particle may increase the interspace to a value larger than 1 μm . Therefore bacteria can gain space to grow and divide.

In one attempt, I tried to cultivate bacteria inside the device. An area 300 μm away from the edge was chosen, where several bacteria were isolated and almost trapped (according to the criteria,

they were not immobilized). Instead of drug, nutrients (i.e. LB medium) were perfused. The observation of growth lasted nearly 2 hours and cells divided twice. (Figure I - 64). Thus, this observation opens some perspectives with respect to the use of the flow device as a simple cultivation chamber in which lineage, genetic, or physiological studies could be performed.

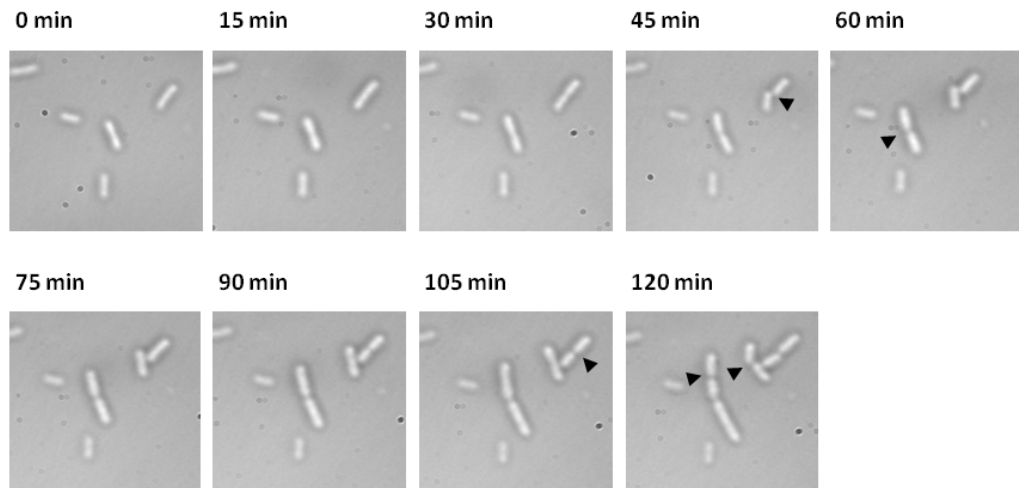


Figure I - 64. Trial of bacteria culture in the flow device. The bacteria position is 300 μm from the edge. Arrow heads indicate the dividing bacteria. LB medium is flowed at 0.1 mL/min in the supply channel.

Part II. Reusable microdevices to study the dynamics of cell migration during mouse development

Chapter I. Technical context

Transfection is a specialized technique for delivering exogenous genes into cells. With the development of research on gene and protein functions, it has become a basic laboratory method. Transfection protocols can be classified in three kinds: the physical, the chemical, and the biological ones. In the Section "2.4 *Competing transfection techniques*" of the handbook chapter reproduced below (Gosse et al. 2017, see the articles in Annexes), we introduced several of them. To make it short, an ideal transfection technique must be characterized by a high efficiency, a high reducibility, and a low cytotoxicity.

This thesis is part of the applied physics domain dealing with microdevices dedicated to biomedical applications, and more particularly we here focus on a transfection technique called electroporation. In this Chapter we will first recall the mechanisms of electroporation. Then, we will introduce the various implementations that have been performed in developmental biology. Finally, we will present some typical electroporation strategies that make use of the lab-on-a-chip concept.

I. Electroporation for transgenesis

Electroporation belongs to the category of the physical transfection method. It appeared in the 1980s (Neumann, Schaefer-Ridder et al. 1982). This technique can easily deliver DNA, RNA, proteins, or many other biologically active molecules into bacterial, yeast, animal, and plant cells. It is a convenient gene transfer method, which main advantages are the simplicity of implementation, the facility associated with the development of reproducible and efficient protocols, and the ease of adjustment and control of the electrical parameters. This is the reason why, for many researchers, electroporation is a promising technique. In order to understand its mechanism, we first discuss the effect of the electrical field on cells.

I.1. Pore opening upon electric field application

The first studies describing the *in vitro* effect of a pulsed field on a biological cell date from the late 1960s (Sale and Hamilton 1968) (Coster 1965). It was observed that, following the application of an electrical pulse, cell membranes were destroyed in a way similar to what happens during the dielectric break-down of a capacitor submitted to a too large voltage drop (Crowley 1973) (Zimmermann, Pilwat et al. 1974). A few years later, it was demonstrated that the perturbations resulting from the application of an intense electric field was not necessarily irreversible and that the pores formed in the membrane could allow some molecules to enter the cytoplasm (Mir, Banoun et al. 1988) (Rols, Delteil et al. 1998).

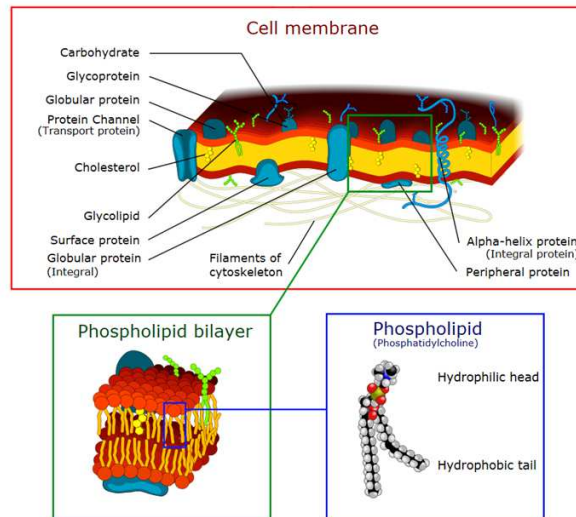


Figure II - 1. Composition of the plasma membrane of the eukaryotic cells. Image taken from (Wikipedia Cell membrane).

To understand the above phenomena, it is necessary to first discuss the anatomy of the cell membrane. The latter separation consists in a phospholipid bilayer into which proteins are inserted (Figure II - 1). The specific molecular structure of the phospholipids allows their spontaneous aggregation in a two-plane assembly, with the hydrophilic heads oriented towards the solution and the hydrophobic tails on the inside. The exchanges between the interior and the exterior of the cell are generally carried out through various proteins, or by diffusion through the phospholipids in the case of lipophilic molecules.

When a cell is placed between electrodes that are connected to a voltage generator, and when the applied electric field is sufficiently strong, the arising potential difference between the

inner and outer surfaces of the cell membrane can be sufficiently large to yield pores. More specifically, such phenomena occurs when the total transmembrane potential, TTV , exceed a given threshold voltage. For most bacteria, animal, and plant cells, TTV_{pore} threshold value is found between 200 mV and 250 mV (Neumann and Rosenheck 1972) (Teissie and Rols 1993) (Rols and Teissie 1990) (Weaver 1993) (Orlowski and Mir 1993). For erythrocytes this threshold value can reach up to 1 V (Kinosita and Tsong 1977). The resulting pores allow the passage of water and ions, thus making it possible to reduce the electrostatic energy accumulated on both sides of the membrane.

In fact, the total transmembrane potential TTV writes $TTV = RTV + ITV$, where RTV is the resting transmembrane voltage of the cell, known as its resting potential, and where ITV is the induced transmembrane voltage. The RTV value is constant all along the periphery of the cell: it is – 95 mV for skeletal muscle cells, – 50 mV for smooth muscle cells, – 70 mV for neurons, – 12 mV for erythrocytes (Wikilectures Resting Membrane Potential) (Sale and Hamilton 1968). Therefore, with the typical TTV_{pore} values given above one can easily see that the RTV can be neglected when estimating the ITV one has to apply to reach the electroporation threshold.

The key factor in electroporation is therefore the ITV , which results from the electric field application. The latter parameter can be expressed in a simple way assuming that the cell is spherical and behaves like a lossless dielectric, $ITV = 1.5 \times r \times E \times \cos \theta$, where E is the electric field far from the cell, r the radius of the cell, and θ the angle between the direction of the electric field and the normal of the surface of the cell at the point under study (Jordan, Neumann et al. 2013). The ITV is thus proportional to the size of the cell and to the intensity of the applied electric field. It is also not uniform on the surface of the same cell; actually, it is the greatest at the point of the cell facing the cathode and the lowest in front of the anode (Figure II - 2) (Escoffre, Portet et al. 2009).

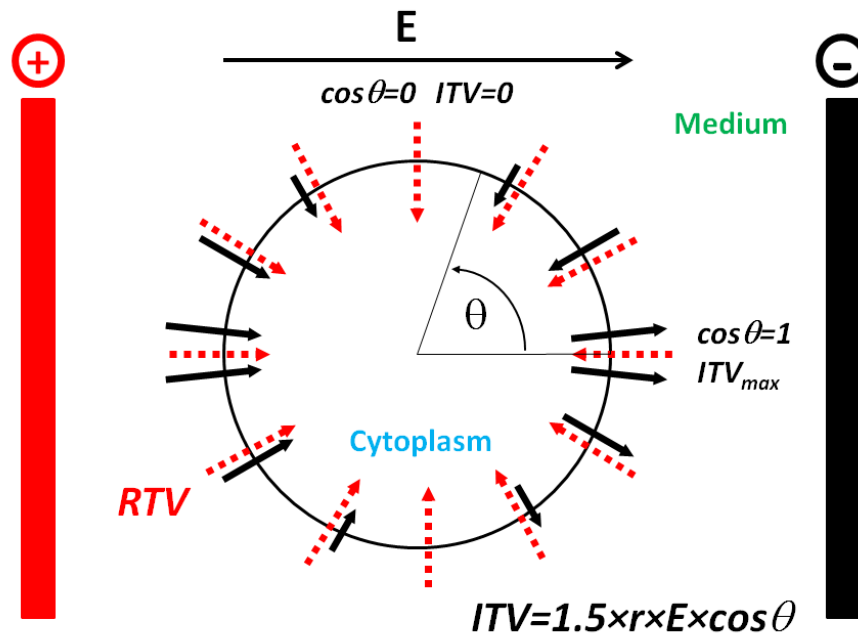


Figure II - 2. Diagram of the effect of an electrical field on a cell. r is the radius of the cell, E the intensity of the electric field, and θ the angle between the direction of the electric field and the normal at the cell membrane. The black arrows represent the transmembrane voltage induced by the electric field and the red arrows represent the resting transmembrane voltage. Image adapted from (Rols, Golzio et al. 2000).

As stated above, the permeabilization may be reversible. Although conventional electroporation pulses last a few tens of microseconds to a few tens milliseconds, the membrane takes several minutes before regaining its natural state and blocking again the diffusion of molecules (Pucihar, Kotnik et al. 2008). The figure below summarizes some effects and some application related to both pulse amplitude and duration (Figure II - 3). Sometimes the same level of pore formation can be achieved by combining different pulse duration and amplitude; nevertheless, in some situations, short pulses with high field strength are less effective than long pulses with lower field strength (Rols 2016).

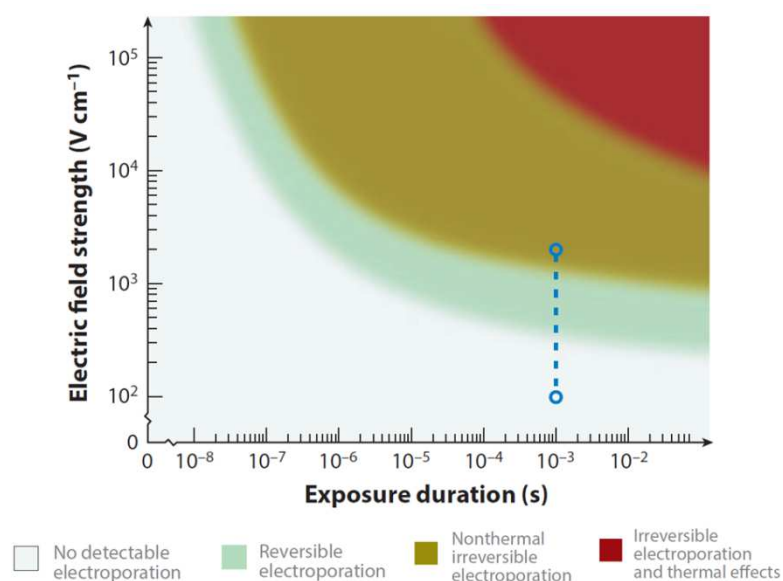


Figure II - 3. Diagram summarizing the different effects obtained by application of electrical pulses to cells. Image taken from (Yarmush, Golberg et al. 2014).

I.2. Entry of nucleic acids into the cytoplasm

The delivery of nucleic acids by electroporation is assumed to be a two-step process: the first phase is cell electroporation, as discussed in the previous Section, and the second phase is DNA electrophoresis. Said differently, the electrophoretic effect contributes to the entrance of the nucleic acids through the previously permeabilized plasma membrane.

Numerous studies have shown that for gene transfer to be effective, DNA must be added to the medium previous to the application of the electrical pulses (Sukharev, Klenchin et al. 1992) (Wolf, Rols et al. 1994) (Eynard, Rols et al. 1997) (Rols and Teissié 1998). Indeed, DNA is unable to cross the destabilized membrane by simple diffusion, but since it is negatively charged, it migrates towards the anode under the effect of the electric field and thus interacts with the cell membrane facing the cathode. The work of Golzio, Teissie et al. revealed that electrical pulses on the order of one millisecond are able to induce this interaction: accumulation of fluorescent plasmids was observed at the cell membrane, on the cathode side (Golzio, Teissié et al. 2002). Moreover, an effective gene expression is obtained only if the DNA molecules and the cell membrane yield stable complexes, which are not compromised by applying electrical pulses of inverse polarity for instance (Faurie, Rebersek et al. 2010).

This hypothesis of two-step process, i.e. permealization and electrophoresis, was further confirmed *in vivo* by studying combinations of pulses of high voltage and short duration (permeabilizing pulses) with low voltage and long duration pulses (nonpermeabilizing, electrophoretic pulses) (Bureau, Gehl et al. 2000).

II. Electroporation in embryology

In the developmental biology studies of the last century, two methods were employed to follow cell development and differentiation: transplantation and staining. Spemann made use of the naturally different color of two newt species to track the developmental fate of transplanted cells in a host embryo (1924); Le Douarin created quail-chicken chimera to visualize the differentiation and migration of embryonic cells (1969). On the other hand, Vogt, from the beginning of the 1920s, used dyes to track the fate of cells in embryo (1923). After decades of development, we can now use electroporation easily to mark cells of interest. This achievement is discussed in both the book of Nakamura (Nakamura 2009) and in our handbook chapter (Gosse et al. 2017, see the articles in Annexes).

II.1 Goal of the transfection experiments

This section is more detailed in Section "2. *Typical experiments*" of the handbook chapter. (Gosse et al. 2017, see the articles in Annexes).

II.1.1. Cell fate mapping

To understand developmental processes, the origin and the dynamics of given cell populations need to be precisely determined. Indeed, in the process of forming complex organisms, cells divide, die, migrate, and differentiate. Fate maps are then drawn by tracing the descendants of a particular cell population (cell lineage analysis) or even of a single cell (clonal analysis). Transfection can serve to mark cells, in order to be able to track their position. One can achieve cell labelling by modifying their gene expression to produce specific proteins like the enzyme β -galactosidase, which produces a colored compound that can be detected in fixed tissues, or fluorescent proteins, which allow live imaging experiments.

II.1.2. Gene function study

Modification of gene expression is commonly used to change the characteristics of the targeted cells, making them gaining or losing some functions. The activity of a protein of interest can be up- or down-regulated by modulating its synthesis or by interfering with its normal molecular behavior. Thus, in embryology, molecular signals can for instance be switched on and off to perturb regulatory pathways.

II.2. Localization strategies

Many researchers use some commercially available devices such as electroporation cuvettes to electroporate fertilized eggs (Buono and Linser 1991) (Zeller 2004). This method makes use of large electrodes and the molecules that need to be transfected are also present in great amount: neither the field nor the transgene is localized.

When electroporation is applied to a more complex biological structure like an embryo, it is often required to target precisely one given tissue or cell population. From an engineering point of view, we thus need some means to achieve the localization of the transfection. Since the implementation of electroporation needs two partners, an electric field to open pores and a DNA solution to obtain a biological effect, we can play on one or the other, or even both, to reach our objectives. Four corresponding strategies are summarized below; for more precise information please see the Section “3. *Strategies to spatially restrict transfection*” of the handbook chapter (Gosse et al. 2017, see the articles in Annexes).

II.2.1. Orientation of the embryo

The embryo is placed between parallel plates electrodes and the electroporation is achieved by controlling its orientation. Even if the molecules to be transfected are present everywhere, they will not cross the plasma membrane if pores are not opened, which will occur only for cells facing the electrodes. However, with this implementation localization is not very precise, especially when the targeted tissue is very flat.

II.2.2. Containment of the nucleic acids solution

This strategy also uses parallel plates as electrodes but it additionally relies on the microinjection of the DNA solution. Said differently, it involves disposing the transgene solution close to the targeted tissue by micro injection and applying a non-focalized electric field to transfect it. With such a technique the plasmid can be used in limited amount and its concentration can be quite well controlled (Figure II - 4).

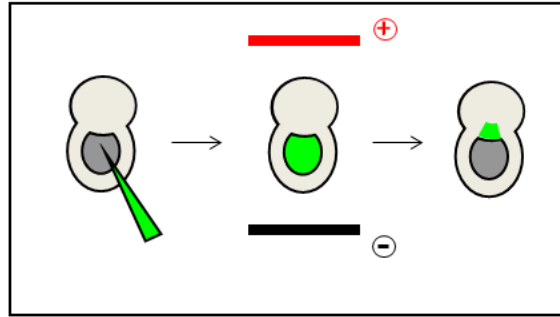


Figure II - 4. Electroporation strategy relying on both macroelectrodes and microinjection of the DNA solution.

II.2.3. Generation of an electric field gradient

Instead of controlling the place where nucleic acids are applied, this strategy chooses to restrain the area over which cells are porated. It can be achieved by a metal needle-type electrode pointing towards the targeted tissue (Figure II - 5). However, harmful chemical species are produced by electrolysis in the vicinity of the electrode, which by necessity must be very close to the embryo.

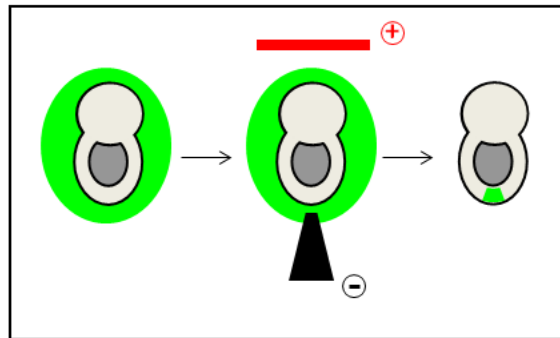


Figure II - 5. Electroporation strategy relying on a micro-needle electrode and a homogeneous DNA solution.

So there is another reported method which makes use of liquid electrode. A dielectric guide is filled with electrolyte, which allows shaping and focusing the electric field at the surface of the embryo (Figure II - 6). Metal electrodes are deported far from the biological object and, therefore, the generated harmful species cannot reach it.

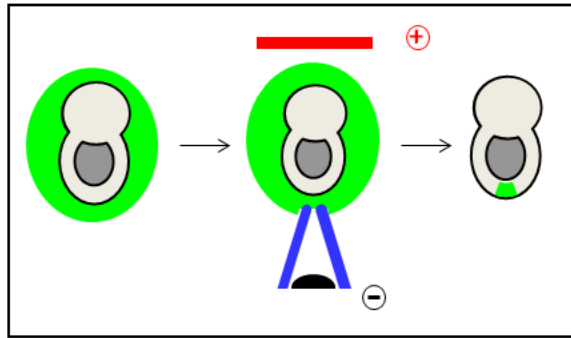


Figure II - 6. Electroporation strategy relying on a micropipette and on a homogeneous DNA solution.

II.2.4. Combination of both molecular localization and electric field focusing

In this strategy, microinjection and focalized electric field are used simultaneously, in order to further control the area over which of transfection is achieved.

III. Electroporation and microsystems

Here we will present some microdevices used for electroporation, which they make use of microelectrodes or dielectric guides. Although they deal with single cells, we can be inspired from their designs.

III.1 Microelectrodes

Such microdevices work sometimes as well as bulk strategies, but with some advantages related to fluidic systems. Indeed, they make it possible to treat a larger number of cells, as in cuvette, while allowing simultaneous observation and control of the movement of the suspended cells under a microscope. Basically, such chips can be composed of parallel plate electrodes on both the floor and ceiling of a straight microchannel (Lin, Jen et al. 2001); coplanar metal electrode pads metalized on a glass substrate (Adamo, Arione et al. 2013); or 3D electrodes fabricated by metallization and electroplating (Lu, Schmidt et al. 2005) (Figure II - 7). Miniaturization enables to decrease the interspace between electrodes, typically between 5 and 500 μm (Fox, Esveld et al. 2006), so in such chips it is possible to reach a high enough electric field with less important voltage.

It is important to note that the material used for the electrodes must be carefully chosen. Indeed, upon electric field application it is common to observe a release of metal ions or particles, at the interface between the electrodes and the solution (Tomov and Tsoneva 2000) (Stapulionis 1999). It is therefore necessary to avoid materials such as copper or aluminum because they produce Cu^{2+}

and Al^{3+} ions which have toxic effects on cells. Conversely, Au and Pt are materials which do not yield cellular toxicity but their cost is higher.

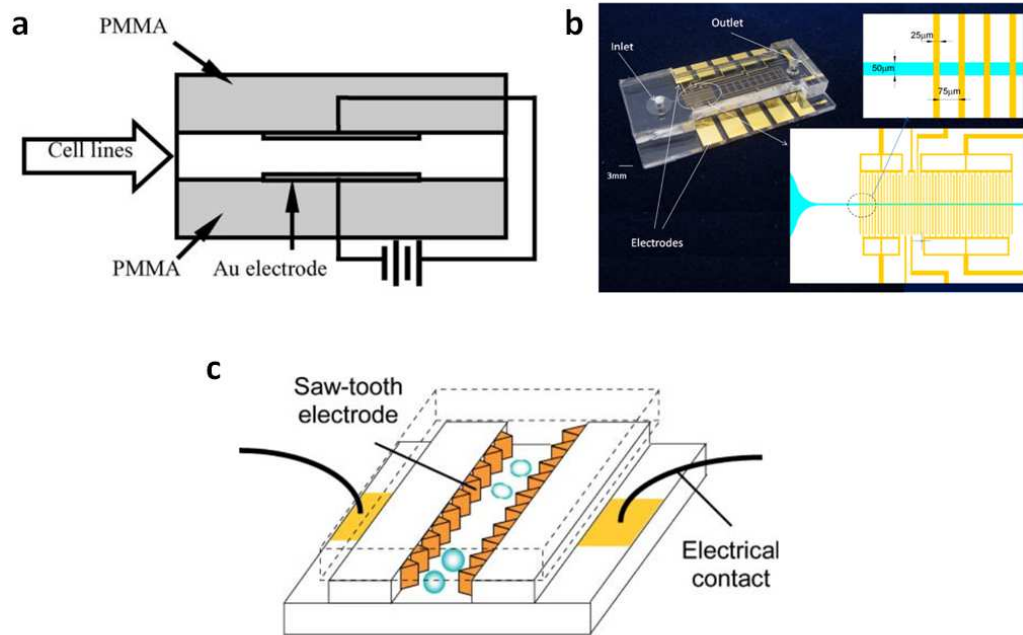


Figure II - 7. Examples of microelectrodes included into microfluidic chips for electroporation. Images taken from (Lin, Jen et al. 2001), (Adamo, Arione et al. 2013), and (Lu, Schmidt et al. 2005).

III.2 Dielectric guides

As stated above, with a dielectric guide the ions and toxic particles released at the electrodes are isolated by a large amount of buffer and cannot contact directly the organism. As their name implies it, dielectric guide are fabricated relying on dielectric materials (e.g. glass, photoresist, PDMS) and they form narrow channels, like pipes. The design and the operation principle published on devices working on cells will provide inspiration for our work.

In single cell electroporation using dielectric guides, cells are first immobilized and isolated, and then the electric pulse is applied. Cells, usually HeLa ones, are transported by the carrying fluid and sucked by a negative pressure in front of the dielectric guide. The tunnel generally presents an opening much smaller than the cell diameter (Khine, Lau et al. 2005) (Ionescu-Zanetti, Blatz et al. 2008). In another method implementation like optical tweezers were used to place cells (Figure II - 8) (Boukany, Morss et al. 2011).

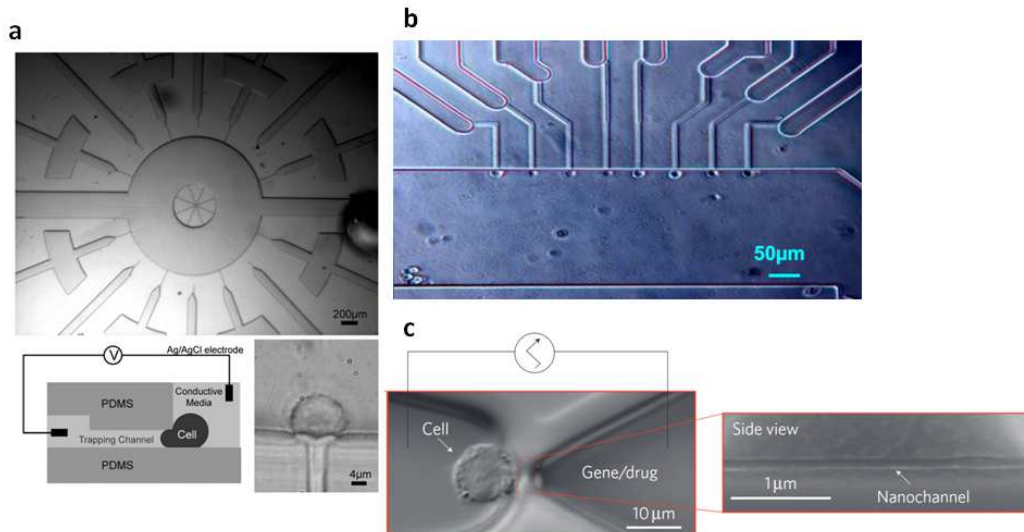


Figure II - 8. Examples of dielectric guides included into microfluidic chips dedicated to cell electroporation. Images taken from (Khine, Lau et al. 2005), (Ionescu-Zanetti, Blatz et al. 2008), (Boukany, Morss et al. 2011).

IV. Electroporation at the LPN

Our device will have to offer a focalized and efficient electroporation while ensuring embryo viability.

The research carried out during this PhD work focused on mouse embryos between 5.5 and 7.5 days post-coitum (E5.5 to E7.5), this post-implantation stage being a key period to study the specification of the antero-posterior axis. Understanding this event requires tools to precisely and reproducibly modify gene expression in a subpopulation of cells in order to monitor their behavior (see Section II.1). More precisely, we will develop a specific electroporation tool to transfect a group of cells that migrates from a distal position to an anterior one during this process.

IV.1. Biological insights

The gestation of mouse lasts 20 to 21 days and is divided into two periods. The first one, the pre-implantation stage, extends from fertilization to implantation of the blastocyst. The second one, the post-implantation stage, takes place between E4.5 and birth (Darribère 2003).

Shortly after implantation, at E5.5, the mouse embryo adopts the shape of an elongated cylinder, less than 200 μm long, and displays radial symmetry around the proximo-distal axis (Figure II - 9). The pluripotent epiblast (Epi) in the distal region is associated to two extra-embryonic tissues, the extraembryonic ectoderm (ExE) which abuts the epiblast proximally, and the visceral endoderm (VE), an absorptive epithelium essential for nutrient exchange that forms the outer layer of the conceptus (Figure II - 9). Dynamic reciprocal signaling between the epiblast and the extra-embryonic

tissues results in radial symmetry breaking, specification of the anterior-posterior (A-P) axis, gastrulation initiation, and formation of the definitive embryonic layers. Central to these processes is a VE subpopulation identified at E5.5 by a specific morphology and the expression of a distinct gene repertoire: the distal visceral endoderm (DVE) (Figure II - 9). These cells undergo a unidirectional movement towards one side of the embryo where they will define the future anterior pole. This movement is essential for correct positioning of the A-P axis (Srinivas 2006) (Takaoka, Yamamoto et al. 2007). Nodal signalling is required to induce the movements of AVE cells (Brennan, Lu et al. 2001) (Norris, Brennan et al. 2002) by driving differential proliferation within the VE (Yamamoto, Saijoh et al. 2004) . (Paragraph extracted from (Mazari, Zhao et al. 2014), see the articles in Annexes).

The definition of the A-P axis is then followed by gastrulation, between E 6.5 and E 7.5, and organogenesis starts around E8.

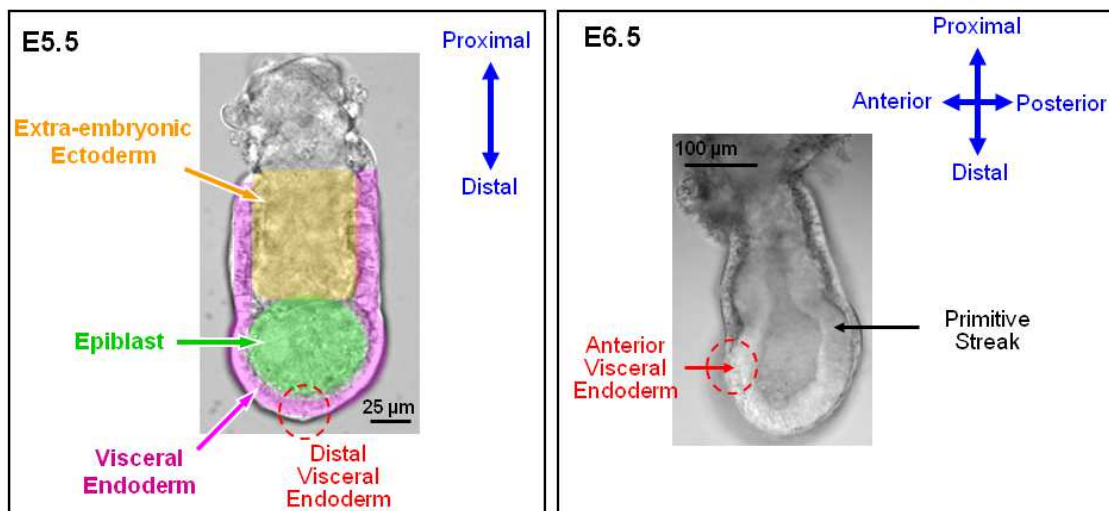


Figure II - 9. Structures of a mouse embryo at E5.5 and E6.5.

IV.2. The project and the collaboration

The main spirit of our research was to introduce numerical simulations in order to save biological materials and resources. As shown in Figure II - 10, based on an initial idea, the first version of the device was put into service after fabrication. Next, on one hand, simulations were used to give approximate values for the required electrical parameters, while, on the other hand, biological experiments were carried out. These two investigations backed up each other in order to converge on effective settings. In parallel, some technological and operational issues discovered during experiments prompted us to refine the design and we therefore entered a new cycle of simulations

and experiments. Finally, once optimal solutions were found, both device design and fabrication process were validated fully by performing embryology studies.

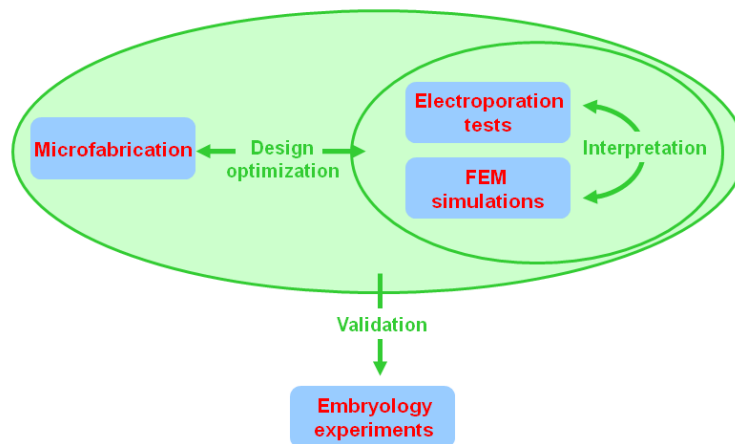


Figure II - 10. Strategy that we adopted during the project, in order to articulate at best the different tasks.

In this project, the conception step, which was assisted by numerical simulations, and the production of the microdevice took place at the LPN. On the other hand, the biological experiments were realized first by Aitana Perea-Gomez at Université Paris-Diderot and later by Diana Suárez-Boomgaard and Isabelle Migeotte at the Université Libre de Bruxelles. My contribution was at the beginning to support the production of the EM6 disposable devices. I was at this time employed as an engineer and manpower was strongly needed because several new microsystems were required for each biological experiment. Then, during my PhD I took in charge the totality of the processes yielding the EM7 prototypes, from design improvements to production. In addition, I also participated in some of the numerical simulations studies.

IV.3. The dielectric guide devices

IV.3.1. General architecture

All microsystems that will be introduced in the following obey a similar design (Figure II - 11). They include an embryo chamber, several mm long and wide, which is connected to the electrode reservoirs by connecting channels, around a few mm of long and less than 1 mm wide. The electrode reservoirs are about 1 mm in radius. The dielectric guide has the shape of a tunnel that opens on one side in the embryo chamber and on the other in the cathodic connecting channel. Its height varies between 50 and 110 μm and its width between 60 and 140 μm , which correspond to the

representative dimensions of mouse embryo at stage of interest. In fact, its exact geometry is partly dictated by the technology used for fabrication.

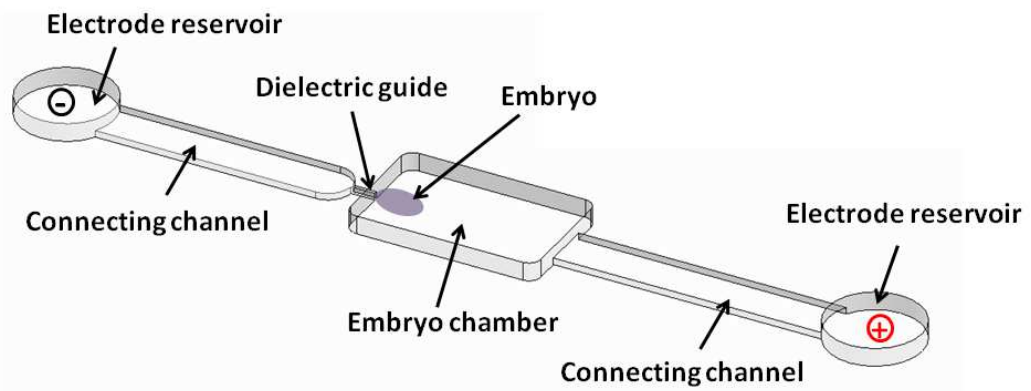


Figure II - 11. General structure of the electroporation device and a positioning of mouse embryo in front of the cathodic dielectric guide.

These tunnels make it possible to confine and guide the current in electrolyte generated from remote electrodes towards the embryo located in the embryo chamber. The embryo chamber is open in order to manipulate the organism with forceps and position it in front of the guide. The difference of pressure between the drops in the embryo chamber and in the reservoirs allows immobilizing the embryo at the dielectric guide opening, which prevents any movement during the application of the electrical pulses. The reservoirs are open because it permits to release the bubbles generated upon electrolysis.

IV.3.2 List of the various demonstrators and prototypes

To produce a complex semi-closed structure, in which there are channels and access holes, one generally has to rely on the elimination of matter and bonding of substrates. From EM5 to EM7, various technologies have been employed, which imposed a given guide design as well as given material, or vice-versa.

EM5 was conceived by E. Mazari the previous PhD student. It used the soft-lithography to make NOA 81 stickers. After bonding of this structures made of photoreticulable glue with glass, a dielectric guide channel was formed.

EM6 also relied on the technologies also developed by E. Mazari. Its key feature was a planar stacking of layers, using glass, gold, SU-8 negative photoresist, and parafilm. Different patterns applied on different planar materials and the overall assembly formed the dielectric guide structure.

From the **EM7** versions of the device we endeavored to develop reusable chips, the goal of my PhD. The first improvement was to change material. Because of its hydrophilicity and

transparency, glass was chosen as substrate and Pt wires were used as electrodes (see Chapter II, Section I.2.3 for details). Obtained by etching, the main structure was completed by drilling and bonding. Two layers of glass were needed, instead of three for the previous EM5 and EM6. More precisely, the **EM7-01** chip was based on glass wet etching, sand blasting, and UV-sensitive glue bonding. **EM7-02** made the cover glass machining more precise by introducing a new technology to realize openings: laser ablation. However, bonding still relied on the UV-sensitive glue. In **EM7-11**, the alignment step between the accesses and the channels took place during laser ablation, and not during bonding as before. More specifically, by reserving the alignment marks, the laser ablated directly the wafer side that has been etched. Furthermore, assembly was completed by simply bonding of a plain bottom substrate with HSQ. Finally, **EM7-21** was the monolithic reusable version, its fabrication by selective laser-induced etching was externalized, no bonding was necessary.

We can see that EM6 was realized according to a strategy that was suitable at an exploratory stage. Indeed, at the time the design was not totally settled and parameters like the distance between electrodes, the dielectric guide length, and the chamber dimensions were still not fixed. Once the geometry had been determined, we entered the stage of development of reusable devices which can be disseminated in the biologist community. This step made use of industrial processes and thus allowed less flexibility.

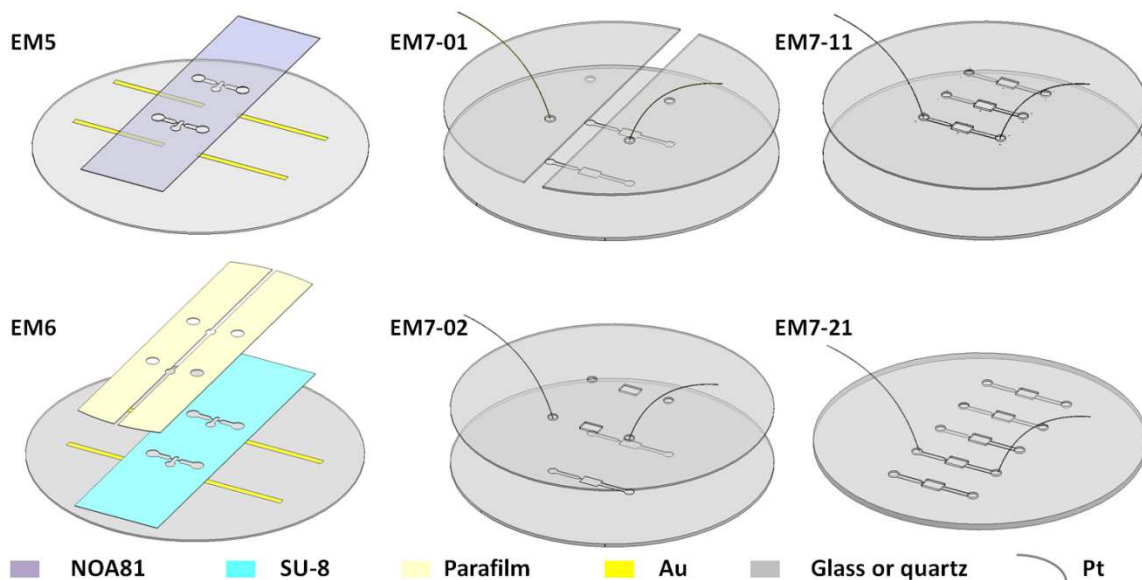


Figure II - 12. Layouts of the dielectric guide device that have been fabricated during E. Mazari's PhD and during the present doctoral studies. See Table II - 1 for details on the used material and technologies. See Figure II - 13 and Figure II - 14 for details on the dielectric guide and cross-section views

Model number	Material		Technology			Ref.
	Electrode	Guide	Guide fabrication	Chamber and reservoir opening	Bonding	
EM5	Au thin film	NOA 81	Replicate patterning (Sticker) + cutting		NOA 81	Mazari et al. 2011
EM6	Au thin film	SU-8 + parafilm	Lithography	Cutting + punching	Thermal	Mazari et al. 2012
EM7-01	Pt wire	Glass	Wet etching	Dicing + Sand blasting	Vitralit 6127	Zhao et al. 2014 ^a
EM7-02	Pt wire	Glass	Wet etching	Laser ablation	Vitralit 6127	Zhao et al. 2015 ^a
EM7-11	Pt wire	Glass	Wet etching	Laser ablation	HSQ	Zhao et al. 2017 ^a
EM7-21	Pt wire	Quartz	Selective laser-induced etching			Zhao et al. 2017 ^a

Table II - 1. Material and technologies that have been used during E. Mazari's PhD and during the present doctoral studies. See Figure II - 12, Figure II - 13, and Figure II - 14 for details on the dielectric guide devices layouts and cross-section views. (^a see the articles in Annexes)

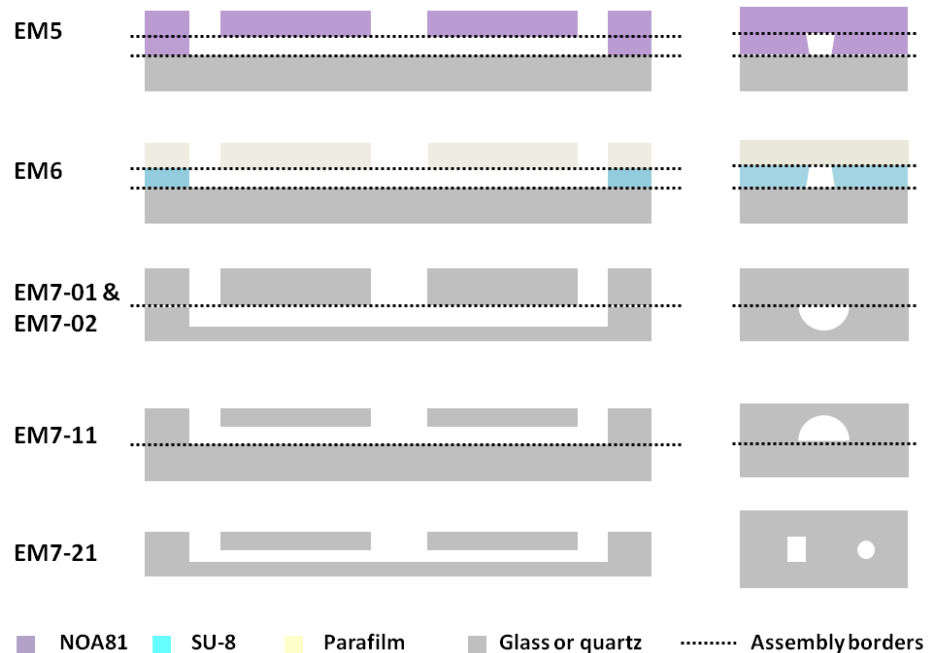


Figure II - 13. Longitudinal and transverse cross-sectional views of the dielectric guide devices that have been developed during E. Mazari's PhD and during the present doctoral studies. See Table II - 1 for details on the used material and technologies, see Figure II - 12 and Figure II - 14 for details on the layouts and cross-section views.

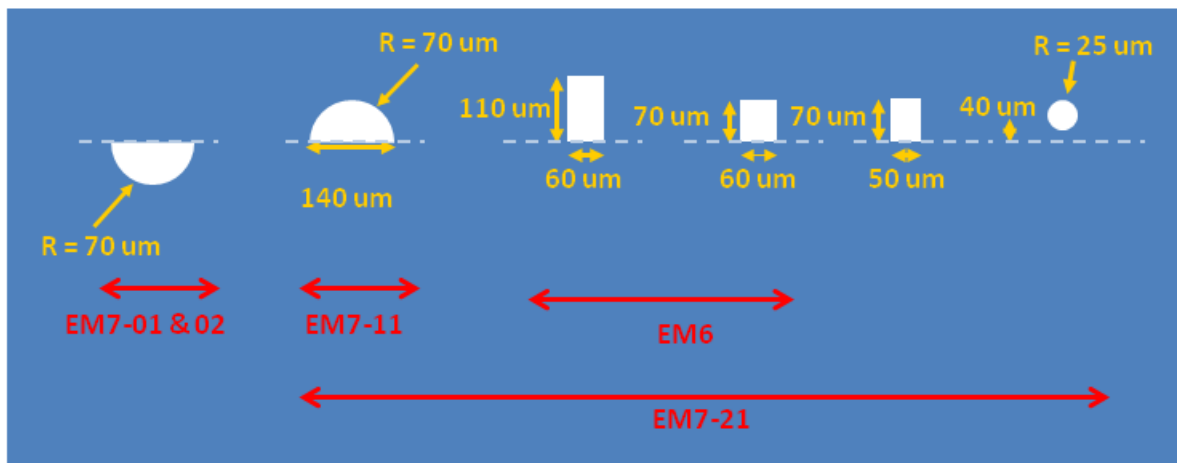


Figure II - 14. Cross-section of the dielectric guides fabricated in the series EM6 to EM7-21. The length of the channel was always 400 μm . See Table II - 1 for details on the used material and technologies. See Figure II - 12 and Figure II - 13 for details on the layouts and longitudinal and transverse cross-sectional views.

Chapter II. Microdevice design and processing

I. Choice of materials and microfabrication technologies

Historically, the development of microfluidic tools for analytical and life sciences has benefited from technologies issued from the mature semiconductor industry. The used materials were then silicon and glass, as in the case of the first microfluidic device fabricated in 1979 by the Electronic Laboratory of Stanford University: a miniature gas chromatograph (Terry, Jerman et al. 1979).

Nowadays, many different materials can be chosen to fabricate microfluidic chips. For instance, in soft lithography, it is just necessary to pour liquid oligomers and initiators onto a rigid mold, reticulate the mixture, and peel off the soft replica. This process can be repeated many times on the same mold, which is a relatively low-cost technology from the equipment point of view. At the beginning the material used for this technology was a type of organic silicone: polydimethylsiloxane (PDMS). Later on, other polymers were included, like photosensitive adhesive (Bartolo, Degré et al. 2008), which are liquid before polymerization. From the mold point of view, there are also many materials: structures can be obtained by etching in silicon or glass, patterns can be created by photolithography, or mold can be processed by micromilling.

In parallel, polymer manufacturing techniques were introduced to produce microfluidic chips industrially. For instance, use was made of hot bossing and injection molding, processes already utilized to fabricate disposable plastic petri dish and culture flask. In order for this technique to be available for microfluidic tool production, it is necessary to make sure that the metal master can faithfully keep the feature size of every fine component, and that the required accuracy could be obtained over thousands of replication cycles.

I.1 The laboratory demonstrators so far realized

First, we relied on some of the accessible techniques in laboratory conditions to make demonstrators, in order to verify the rationality of our design. Because soft lithography can be quickly and efficiently applied to transform patterns into a demonstrator, it was used in the work of the former PhD student to realize EM5 the first dielectric guide device. EM6, the second demonstrator, also used some common clean room academic techniques.

I.1.1 Soft lithography (EM5)

Soft lithography is a technique used to transfer a fine three-dimensional structures by pouring fluids such as PDMS base or NOA (Norland optical adhesive) onto a mold and curing it. Since the initial material is often liquid, it lays on the mold with a perfect conformability. Once the polymerization is triggered, the shape of the mold is perfectly copied.

The EM5 demonstrator was made of NOA 81, inspired from the work of Vincent Studer (Bartolo, Degré et al. 2008). The workflow is summarized in Figure II - 15.

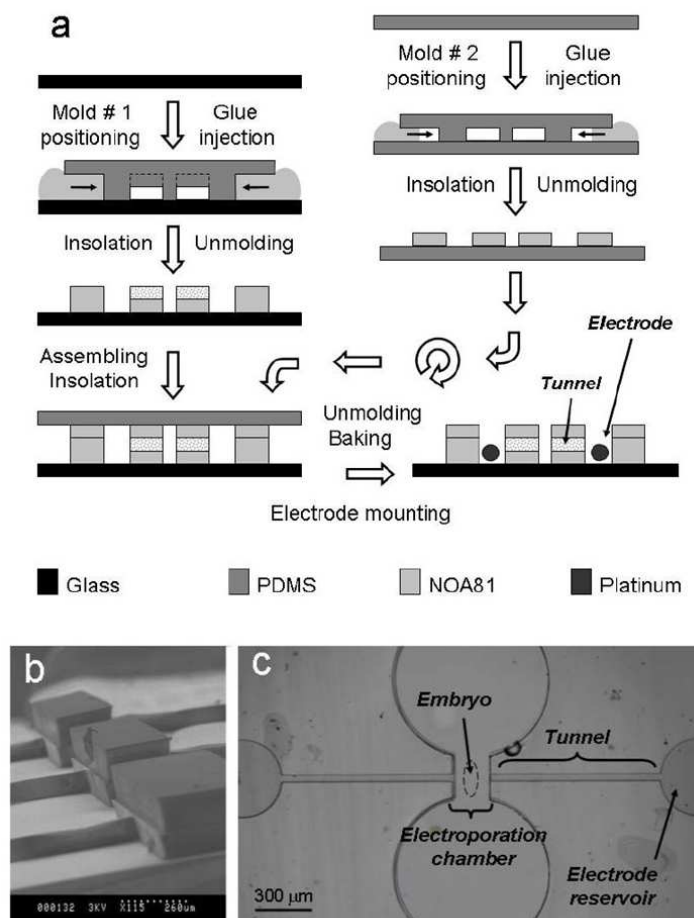


Figure II - 15. Device fabrication by soft UV imprint. (a) Process flow – the guides are first patterned on a glass substrate and then closed by a stencil which has been prepared on a flat PDMS wafer. (b) SEM picture

of the SU-8 template used to obtain a PDMS mold #1. (c) View of the complete microdevice. Image taken from (Mazari, Mantelet et al. 2011).

1.1.2 Mix “craft” technologies (EM6)

In the mix “craft” version that we denoted EM6, electrodes were produced thanks to standard microfabrication, the SU-8 epoxy photoresist was adopted to make the guide walls, parafilm was used to close the assembly, and electrical connectors were welded at the ends of the metal pads. This layer stacking strategy is clearly shown in Figure II - 16 and device pictures, with or without embryo, are displayed in Figure II - 17.

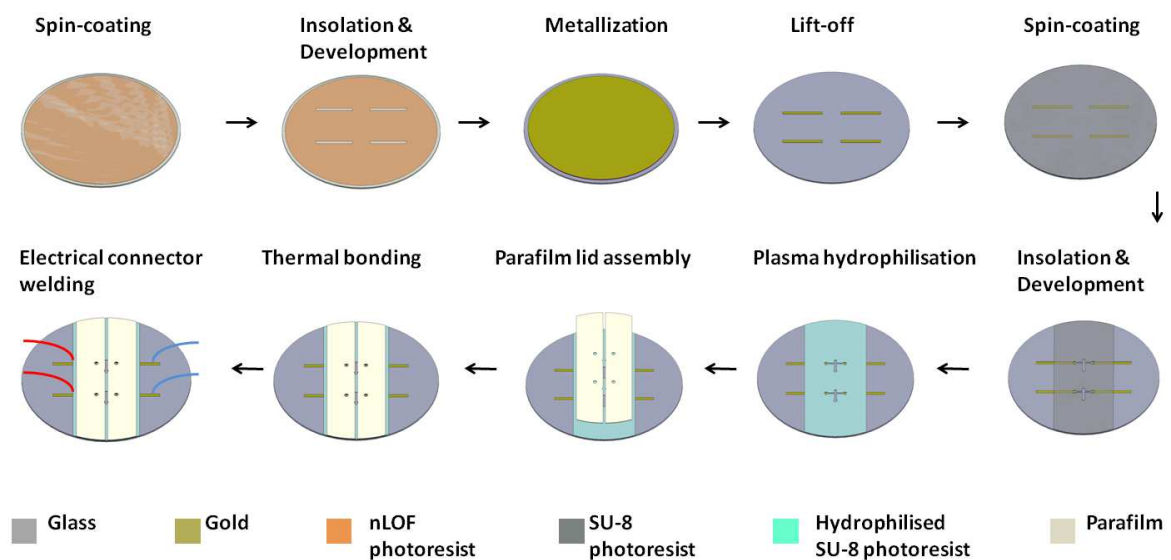


Figure II - 16. Summary of the workflow used to fabricate the EM6 single-use SU-8/Parafilm microdevice. Image adapted from (Mazari, Zhao et al. 2014).

1.1.3. Achievements and limitations

Proof-of-concept experiments were successful. The EM5 and EM6 devices validated the dielectric guide concept. Results were reproducible and the success rate was guaranteed. However, there were still many limitations.

First, the microfabrication procedure was complicated. Technologies used were quite specific, they were not industrializable for mass production. The device was designed for single-use, when the experimental schedule was busy and dense, tedious production was unable to meet the consumption rate in the biology laboratory.

Second, materials were poorly suitable. The dielectric materials (i.e. NOA81 and SU-8) used in these demonstrators were not easily accepted by biologists. Especially, the harmfulness and deleteriousness of the photoresist solvent resulted in biocompatibility and biosafety issues (Mazari,

Mantelet et al. 2011). Moreover, hydrophilicity is a prerequisite for the use of this device, but materials are here basically hydrophobic. A step of hydrophilization by plasma was necessary but this surface treatment was time-consuming and its effects decay in the following 48 h.

Therefore the diffusion of this device in the biological community was not easy, these technologies had been finally abandoned.

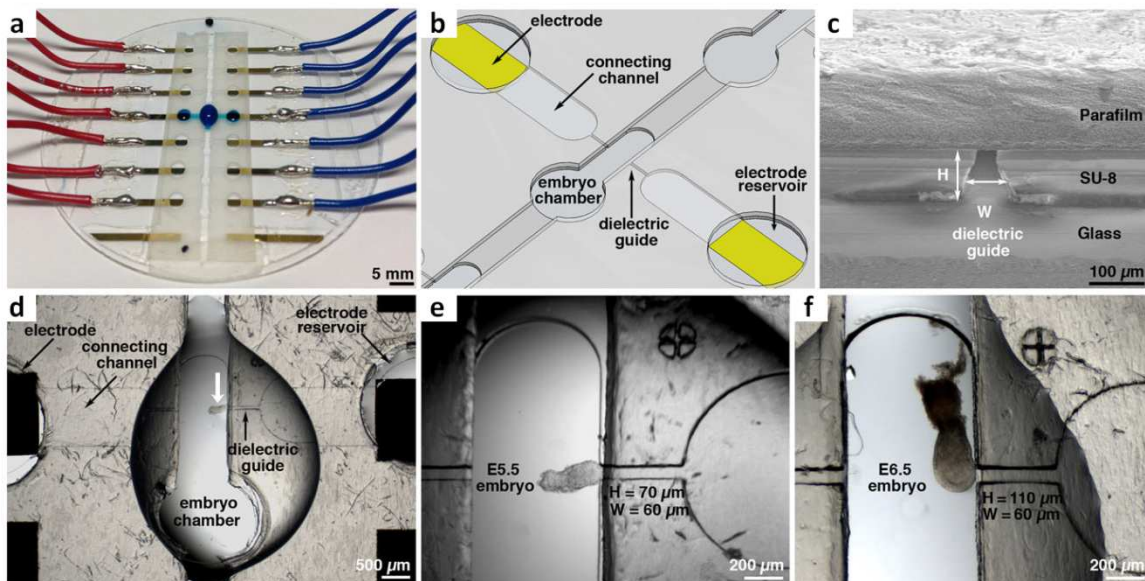


Figure II - 17. Layout and use of the EM6 electroporation device. (a) Global view of the microsystem, one of the fluidic networks being filled with a Bromophenol Blue solution to highlight connectivity. **(b)** Diagram showing a pair of electrodes with the corresponding connecting channels, dielectric guides, and embryo chamber. **(c)** Scanning electron microscopy micrograph of a dielectric guide of height $H = 110 \mu\text{m}$ and width $W = 60 \mu\text{m}$, as observed from the embryo chamber. **(d)** View of the whole fluidic system included between the electrodes. An E5.5 embryo (white arrow) is positioned so as to target its DVE, this tissue facing the dielectric guide connected to the cathode. **(e)** Zoom on the E5.5 embryo. **(f)** Similar enlarged view of an E6.5 embryo positioned so as to target its AVE. Images taken from (Mazari, Zhao et al. 2014).

1.2. The industrial prototypes

Because of the above limitations, we looked for other ways to realize the prototypes easy to use and well accepted by biologists. Furthermore, the involved processes had to be available from various companies, in order for life scientist not to be dependent on a single provider, either academic or industrial.

1.2.1 Thermoplastic manufacturing

Amorphous thermoplastic polymers have a lot of advantages: low density, low cost, and ease to manufacture. Nowadays, thermoplastic polymers are widely used in microstructure replication: when they reach a temperature above the glass transition they can be molded and they keep the

acquired shape when they return to the solid stage upon cooling. Several cycles of heating and cooling can be performed with limited damage (Biron 2012) (Worgull, Kolew et al. 2011). Some representative polymers that are used in the microchip industry, include PS (polystyrene), PMMA (poly(methyl methacrylate)), PC (polycarbonate), and COC (cyclic olefin copolymer) (Jena, Yue et al. 2010).

From the technology point of view, two processes issued from the plastic industry seem promising: injection molding and compression molding, also called hot embossing (Heckele and Schomburg 2003).

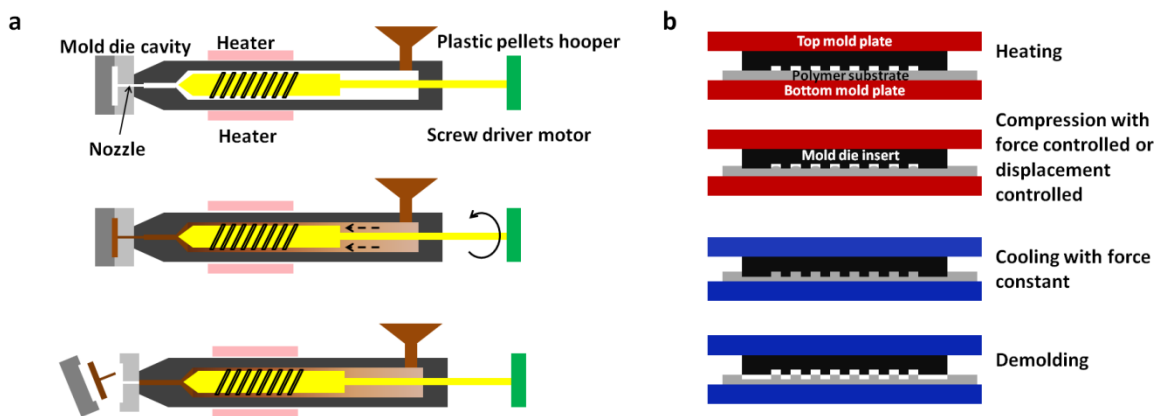


Figure II - 18. Examples of thermoplastic processing: (a) Injection molding. (b) Hot embossing.

The injection molding was first used to make plastic toys. The principle of this technique is to inject into a mold a thermoplastic heated in order to become a viscous liquid. When this thermoplastic cools, it retains the shape of the mold. Since the mold is formed by two structures, it is sufficient, at the end of the process, to separate them in order to recover the plastic component (Figure II - 18 a). The main plastics used are polymethylmethacrylate (PMMA) and polycarbonate (PC). An injection molding machine is capable of producing more than 100 devices per hour. However, this type of equipment is expensive to purchase and install; the development of molds with micrometric resolution further increases the cost.

The hot embossing technique is quite similar to the injection. The mold is also divided into two parts. The thermoformable material is placed on the bottom mold. This material may be a powder, a viscous liquid, or a solid plate. Once the bottom mold is loaded, the material is pressed with the other part of the mold and heated, so that it takes their shape. One has only to cold down the whole setup and re-open the mold to extract the device (Figure II - 18 b). This process is simpler and cheaper than injection, but the manufacturing cycle is longer. On the other hand, it has the advantage of being compatible with a wide choice of materials and of course it is already industrial.

1.2.2 MEMS-type manufacturing

Silicon and glass are materials commonly used in the MEMS industry, mainly because they are widely available and not too expensive, but also because their processing technology benefit from the experience accumulated in the integrated circuit industry – for instance, lithography, etching, metallization, dielectric deposition can all be adapted.

Although silicon is a good material for MEMS and semiconductor industries, its application to the field of biology had suffered from several drawbacks. For instance, its surface is naturally hydrophobic whereas many biological studies are performed in an aqueous environment. It is also opaque whereas transparency is most of the time required to follow phenomena in optical microscopy.

Besides silicon, various types of glass are widely used in microfluidic technologies, including borosilicates and fused silica. They are amorphous solids which displays several advantageous properties: natural hydrophilicity, good mechanical strength, bio-friendliness, chemical inertia, optical transparency, low autofluorescence, electrical insulation, and thermal stability.

1.2.3 Strategy selection

The two types of processes mentioned in the two preceding Sections significantly differ. Microfluidic Petri dishes are single-use and disposable, but they are also very cheap. Microfluidic glass beakers are expensive but they can be cleaned repeatedly. All in all the cost per experiment would thus be quite similar.

However, our design is still at an exploratory stage, and our design can still be modified. Certainly the single-use plastic devices can finally be cheap, but fabrication is constraining when one considers the uncertainties associated with the surface modification as well as the cost of an expensive mold insert. If during the development process we find that some pattern is inappropriate, we will need to change the material or the mold, which is an expensive and long cycle. Hence, thermoplastic technologies do not permit device evolution while carrying out experiments. While a single glass device is expensive, recycling is possible as long as cleaning is efficient. Its fabrication is flexible, whether it is manufactured in our laboratory or externalized to a company. Furthermore, the process for production is quite fast, which allows design improvement at any time.

Therefore, we choose to continue on the way of the reusable all-in-glass device.

II. Overview of the different processes available to make a glass micro chip

In the last section we have determined that glass will be the material selected for further elaboration. Now we will review the available technologies for its processing, from through holes and channels machining to wafer bonding.

II.1. Etching

Etching refers to a chemical, physical, or physico-chemical method that selectively removes the unprotected part of a film (such as SiO_2 , Si_3N_4 , αSi , or Al) or of a substrate. The final goal is to transfer the pattern from the mask to the film or substrate. An ideal etching technology must have the following characteristics: it must be anisotropic since the vertical etching guarantees accurate geometric transfer of the pattern from the mask to the substrate. It must be selective, with an etching rate of the mask slower than that of material to be etched, in order to ensure the effectiveness of the mask during etching process. It will be better if it is suitable for industrial production. That means the process should be easy to control for large quantities, of low cost, less environmental pollution.

Etching methods can be generally divided into two categories: dry etching and wet etching.

II.1.1 Dry etching

Dry etching is a process of micromachining which relies on reactive species in gaseous phase. The interaction between the gas etchants and the targeted materials (e.g. metals, semiconductors, insulators) may be dominated by three regimes:

- Physical process. Ion beam of high energy bombards onto the surface of target material to eject its particles, that is very similar to the sputtering process. This highly directional etching method is able to achieve anisotropic features.
- Chemical process. Reactive radicals in plasma chemically erode the targeted material. Its effects are similar to that of wet etching, the anisotropy is poor.
- A mixture of physical and chemical processes. The physical bombardment of reactive particles on the substrate plus the chemical reactions of ions have both the advantages of anisotropy and selectivity.

In my thesis, the research and development object is the devices suitable for biological study above micrometer level, the use of RIE can satisfy our requirements.

Reactive ion etching (RIE)

RIE uses the physico-chemical regime mentioned above. When a gas is transformed in a plasma, it has two characteristics: on one hand it presents a chemical activity stronger than under the normal gas state; on the other hand, the electric field can be present in the plasma sheath and used to guide and accelerate the ions towards the substrate. Both the volatile matter produced by the chemical reaction and the products issued from the physical bombardment are pumped away thanks to the vacuum system.

Figure II - 19 is a schematic diagram of the fundamental steps of plasma etching : generation of reactive species, reactive species diffusion to the substrate surface and adsorption, chemical reaction between the reactive species and the substrate material, desorption of the reactive species, and then elimination of the volatile reaction products (Jansen, Gardeniers et al. 1996).

Fluorine containing gases (e.g. SF_6 and CHF_3) are mainly used to Si-based materials (Si, SiO_2 , Si_3N_4 , SiC). The reaction product is the volatile molecules SiF_4 (Jansen, Gardeniers et al. 1996) (Campbell 2001). Particularly, fluorocarbons and fluorinated hydrocarbons (such as CF_4 , CHF_3 , CH_2F_2) are commonly used gases for silica reactive ion etching (Campbell 2001). The carbon they contain can help to remove oxygen from the oxide layer, through the production of CO and CO_2 .

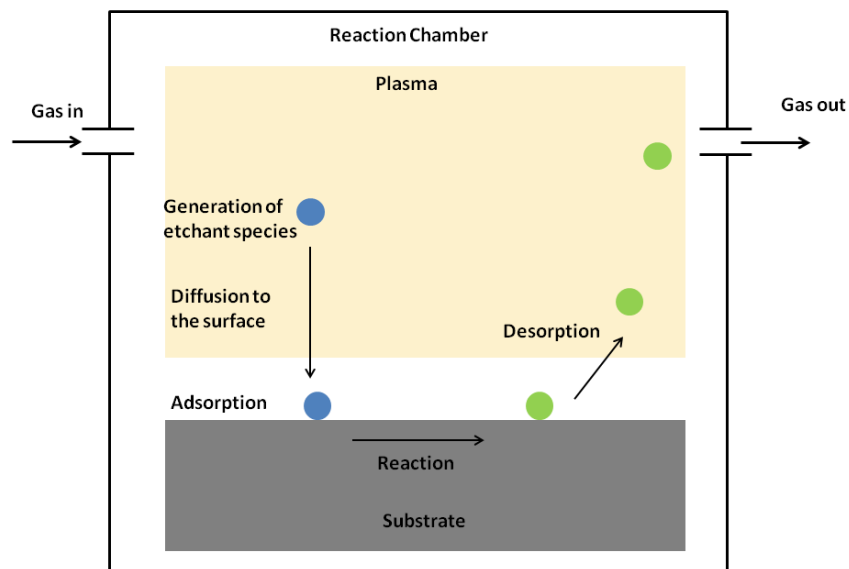


Figure II - 19. Scheme of the fundamental steps of plasma etching.

Although this technology is widely used in micro-nano fabrication, it was not used in this thesis because of its low etching rate (3-60 nm/min) (Thiénot, Domingo et al. 2006), a redhibitory

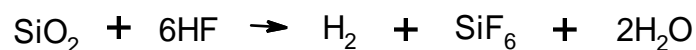
drawback when considering the up to 100 µm depth of the chamber and reservoirs we have to fabricate.

If it is required to make high aspect ratio feature by dry etching, inductively coupled plasma-RIE (ICP-RIE) can be used. Silica and glass can be etched with plasma formed from C₄F₈ precursor, but other precursors such as CHF₃, CF₄ and SF₆ can be used (Li, Abe et al. 2001) (Rueger, Doemling et al. 1999) (Akashi and Yoshimura 2006). Additional gases such as H₂, Ar, and He are also used to improve the stability of the plasma and hence to get vertical etching (Li, Ling et al. 2003). Low pressure, in the range of a few mTorr, is provided by ICP sources and a high substrate voltage bias is often needed (up to thousand volts (Kolari 2008)). High etch rate (~0.6 µm/min), aspect ratio > 10 for a depth of 200 µm was possible to be obtained in Pyrex (Li, Abe et al. 2001).

II.1.2 Wet etching

Wet chemical etching is a traditional method employing a corrosive solution to remove unwanted materials on a substrate. The wafer is immersed in an appropriate chemical solution, the reagent diffuses to the surface of the material to be etched, the reaction takes place, and the soluble product is eliminated from the etching surface into the solution. The part of the material which is not protected by the mask is chemically decomposed by the reagent. This etching in the liquid environment has the advantages of simple operation, low equipment requirement, easy application in mass production, fairly good selectivity, possibility of control of the etching rate by changing parameters such as the composition of the etchant, the temperature. But its disadvantages are also obvious (Campbell 2001): i) Poor anisotropy: lateral undercutting will change the graphical profile, resulting in geometric deformation. ii) Masks that loose adhesion in liquid environment. iii) Bubbles that prevent a homogeneous contact between the chemical solution and surface to be etched. iv) Safety problem regarding gas and liquid wastes.

Whereas, silicon exhibits anisotropic etching in certain chemicals due to different etching rates along different crystallography directions, etching of SiO₂ is isotropic because it is an amorphous material. The overall reaction of silica wet etching in HF is



The concentration of industrial HF can as high as 40 %. However, this product cannot be used as such since SiO₂ will be etched too quickly and too unevenly. The reaction consumes HF and the reaction rate will decrease with time. To avoid this problem, one solution is to use HF with a buffer such as NH₄F, which prevents the depletion of F⁻ through a dissolution reaction and hence maintain the etch rate stability. The reaction is:



HCl added to the HF solution is also a common recipe for wet etching of glass. In addition to the primary reaction between the HF and SiO₂, HF reacts with the metal ions contained in the glass, such as Ca²⁺, Mg²⁺, Al³⁺. Their fluorides are insoluble in water and accumulates on the surface, the role of HCl is to transform them into their soluble chlorides counterpart (Iliescu, Chen et al. 2008) (Iliescu, Jing et al. 2005). Doing so, the roughness of the etched area can be guaranteed.

In wet etching, the endpoint determination relies rather on etch time calculation based on a calibration curve. Of course, it is important to ensure that the etching solution is always fresh. Since our targeted depth is 70 or 110 μm, fresh etching solution is frequently added into the container and the mixture is stirred regularly.

In this thesis, HF wet etching is used to manufacture the main structure of the channel. Although controlling the fidelity of pattern dimensions can be difficult with this method, the process is satisfactory as long as the most important part of the device, i.e. the guide has its length, width, and section shape well preserved. The rest of design does not influence much on the final biological results and experimental parameters can be slightly adjusted according to the deformation of channel.

II.2. Electrochemical discharged machining

Electrochemical discharge machining (ECDM), which is also called also spark assisted chemical engraving, was first reported by Shoji et al. in 1990 (Shoji 1990). The essence of this technology is actually chemical erosion, but locally accelerated by high temperature.

We know that the glass can be eroded or etched by alkaline solution, according to the reaction



Like many other reactions, it can be accelerated by increasing temperature. The sample to be machined is immersed in an appropriate alkaline solution (typically NaOH). A constant DC voltage is applied between the tool-electrode (cathode) and the counter-electrode (anode). The counter-electrode, which could be a flat plate, much bigger than the tool-electrode, is far away from the tool-electrode and the workpiece. DC voltage is applied between the counter-electrode and the tool-electrode (Figure II - 20 a). When the voltage is increased, the tool electrode is completely coated by H₂ bubbles generated by water electrolysis. The electrical discharge breaks through the layer of gas bubbles. Electrolytically-generated heat effect of electrical discharge accelerates the erosion reaction,

the workpiece in glass is etched by NaOH. ECDM can process on insulating materials such as glass and ceramics.

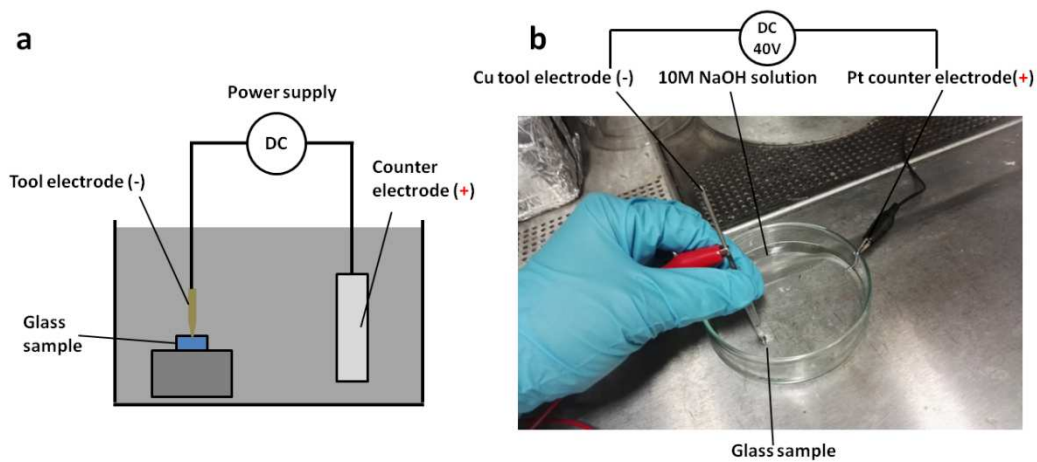


Figure II - 20. Scheme of Electrochemical Discharge Machining. (a) Diagram of the setup. (b) Corresponding picture in our studies.

In our studies, a Cu stick of ϕ 1mm is used as tool-electrode in contact with glass and a thin Pt wire is kept to the edge of petri dish as counter-electrode. A 10M NaOH is used to favor the erosion reaction and a 40 V DC power is applied to generate the breakdown voltage (Figure II - 20).

Compared with laser processings (Section II.4), which require expensive equipments and skilled personnel, this method is quite cheap. If the profile of the hole is not strictly imposed, ECDM might be a simple and practical method. However, strictly speaking, some defects have been noticed: i). The shape of holes depends on the shape and diameter of the tool-electrode, in most cases a stick. SEM images (Figure II - 21) show that it gives different results. Because the Cu is tapered in cone during the reaction, the profile of hole is thus a cone, but from time to time it varies. Moreover, the low resolution of the naked eye causes a bias in location. The Figure II - 21 a shows an etching in wrong place, and the whole device has to be abandoned.

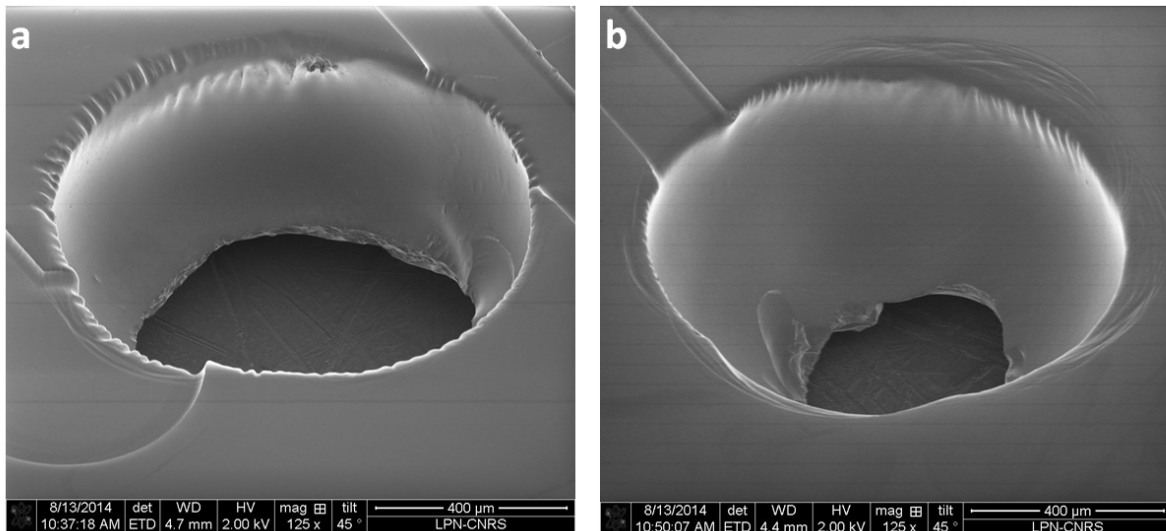


Figure II - 21. Scanning electron micrographs of two holes made by electrochemical discharge machining method (see text for experimental details).

II.3. Sand blasting

Sand blasting refers to the processing of a surface by the delivery of a stream of abrasive material under high pressure, usually relying on the compressed air. It is a pure physical process. As the abrasive particles ablate the surface of the processed substrate by shocking and cutting it, its aspect is significantly altered (Smil 2005).

In practice, a thick metal mask is first fabricated, some holes being drilled at the appropriate locations. The glass substrate is then roughly and intently fixed on the metal mask with tape. The mask and substrate are brought in the sand chamber and the material is ablated only where opening allows some exposure (Figure II - 22 b).

It has to be admitted that this method is a rough one because of its macroscopic nature — we do not deny that if particles are miniaturized, the mask protection is refined, and the alignment is precised, this will be a way to achieve accurate processing. Modern sand blasting equipment can utilize powders with fine particles (3 – 30 μm), which allows the fabrication of well-defined features with lateral dimensions as small as 10 μm . The lateral walls present slightly taper shape typically of about 5 - 15°, which limits the aspect ratio of the structure below 10 (Wensink, Berenschot et al. 2000) (Angelescu 2011).

We use sand blasting to open through holes in the glass cover, before assembling it with another piece in order to yield fully functional microdevice. The technique yields holes indeed generally displaying a positive taper shape, but the angle of the cone (Figure II - 22 c) cannot be repeatedly defined and controlled. Similarly, the diameter of the holes cannot be faithful reproduced.

This is partly due to the mask itself: with the sand-flow, its holes are deformed and expanded (Figure II - 22 a).

Importantly, the strength of the air flow may lead to the breakage of the glass wafer in halves, which is a pity when other structures have been patterned.

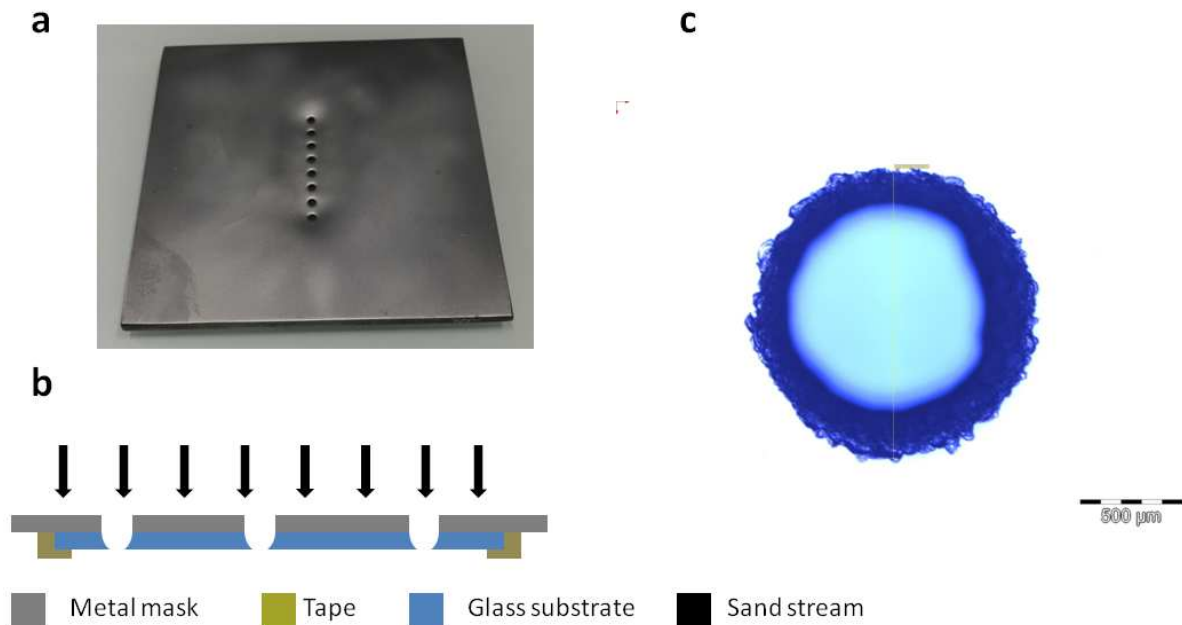


Figure II - 22. Process of sand blasting. (a) A metal mask with holes in appropriate places. (b) Scheme of the process. (c) Optical micrograph of a processed hole.

II.4. Femtosecond laser ablation

According to the theory in the report of von der Linde et al. (Von der Linde, Sokolowski-Tinten et al. 1997), in the interaction between a laser and a material, whether it is a long or short pulse, the first step is the deposition of a certain amount of energy in the material, and the second step is the modification of the spatial and temporal distribution of energy. That will determine what kind of final modification will be obtained. Figure II - 23 shows that the interaction mechanisms that can be divided in three steps depending on the scrutinized time-scale: carrier excitation, thermalization, various relaxation mechanisms as well as thermal and structural events.

When femtosecond laser pulses are strongly focused in a transparent dielectric material like silica, a large quantity of energy (10^{13} - 10^{14} W / cm²) is deposited in the material over a time much smaller than the typical thermalization times, i.e. the time to transfer of the energy to the mass of the material (a few picoseconds). It explains why effects can be located in an extremely confined area located in the mass of the material (Misawa and Juodkazis 2006). With ultra-short and ultra-

intense pulses, energy is absorbed by electrons more quickly before it can be transferred by electrons to the crystal lattice, the ions are still cold. After absorption, atoms are ionized in a way highly non-linear by multi-photon ionization or tunnel ionization (Temnov, Sokolowski-Tinten et al. 2006), and then by collisional avalanche (Marcinkevičius, Juodkazis et al. 2001). This ionization leads to electronic density up to 10^{21} - 10^{22} cm^{-3} in the volume concerned (Hallo, Bourgeade et al. 2007). On the scale of ten picoseconds, a part of the laser energy absorbed by the electrons is transferred to the network by electron-phonon collision, and both systems reach a thermal equilibrium at a temperature of about several 10^3 K (Rajesh and Bellouard 2010). After about ten nanoseconds, electrons and ions recombine. After plasma relaxation, the residual energy in the material is then evacuated from the focal zone by various energy relaxation paths, whether by thermal diffusion, mechanical shockwave or other mechanisms, leading the system back to thermodynamic equilibrium. Structural modifications in the material are generated when energy is transferred to the ions. At high enough energy, these processes can cause non-thermal permanent structural modifications such as inelastic deformation (densification or expansion, depending on the irradiation conditions and on the composition of the material) (Mao, Quéré et al. 2004), the appearance of an elastic response (stresses) in and around the irradiated zone etc. Thus, quality machining can be carried out on a surface with micrometric dimensions. In transparent materials, the interaction can occur inside the material, thus enabling the creation of cavities or zones structurally modified in volume.

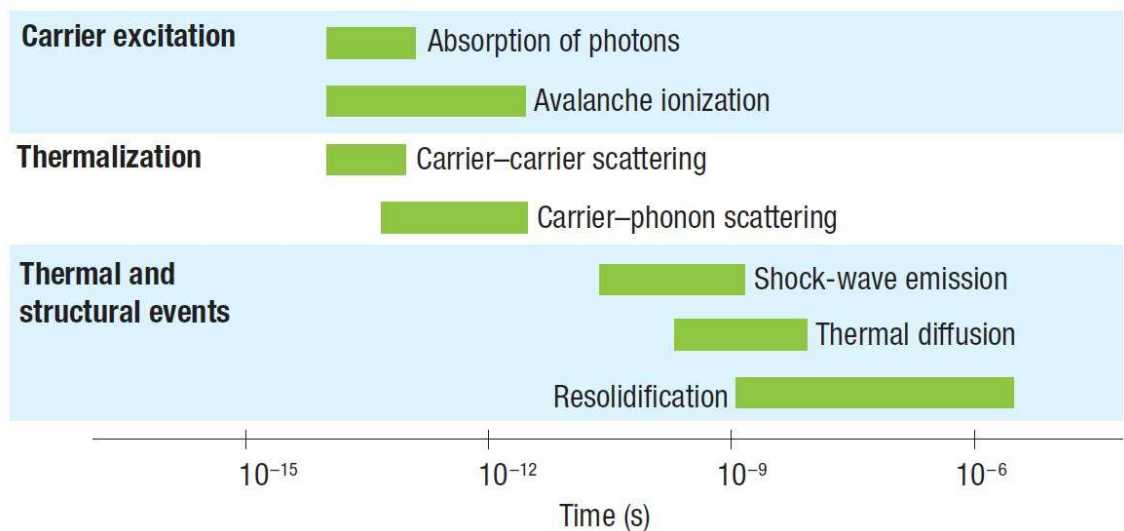


Figure II - 23. Timescale of the physical phenomena associated with the interaction of a femtosecond laser pulse with transparent materials. Note that although the absorption of light occurs on the femtosecond timescale, the material can continue to undergo changes microseconds later (Gattass and Mazur 2008).

In our studies, femtosecond laser processing was entrusted to the FEMTO ST at Besançon. Holes corresponding to the electrode reservoirs and to the embryo chamber were subsequently opened by femtosecond laser ablation. A Tangerine ytterbium femtosecond fiber laser (Amplitude Systèmes) operating at a nominal wavelength of 1030 nm was used. The beam at the exit of the laser head had approximately a Gaussian profile, with a M^2 factor of 1.23 and a full diameter of 3.5 mm at $1/e^2$. Specific optics were then added to obtain a non-diffracting Bessel beam with a 3 μm diameter and a 130 μm length (Bhuyan, Courvoisier et al. 2010). The repetition rate and the pulse duration were tuned around 5 kHz and 220 fs, respectively, and the laser power at the sample was adjusted to ~ 100 mW by combining a half-wave plate and a linear polarizer. Focusing on the sample was performed with achromatic lenses, the wet etched side of the wafer being the one exposed to the laser beam. The material was ablated along a predefined contour thanks to a 3-axis translation stage, alignment onto the gold marks being achieved with a better than 10 μm accuracy. Each hole was realized relying on 3 successive infeeds, which took between 2 and 5 min.

II.5. Selective laser-induced Etching (SLE)

The principle of selective laser-induced etching is femtosecond laser processing combined with chemical etching. This technology was first reported by Marcinkevicius et al. for fused silica (Marcinkevičius, Juodkazis et al. 2001). The main difference with femtosecond laser processing is that SLE uses relative low energy femtosecond laser irradiation, in fact just enough to induce structural modifications in order to improve wet etching selectivity. The pulse energy levels are set weak ($\leq 1 \mu\text{J}$) so no material is removed but structural modifications of the material takes place at the laser focal zone, the irradiated areas thus acquire an increased solubility to etchant such as hydrofluoric acid (HF). There is no direct ablation. Secondly, preferential chemical etching of the laser processed region is performed by immersing the substrate in an etching agent. Low concentration HF (typically less than 10%) is generally used, and heated KOH is also developed to be an etchant, increasing the aspect ratio up to 1:200 (Kiyama, Matsuo et al. 2009) (Figure II - 24).

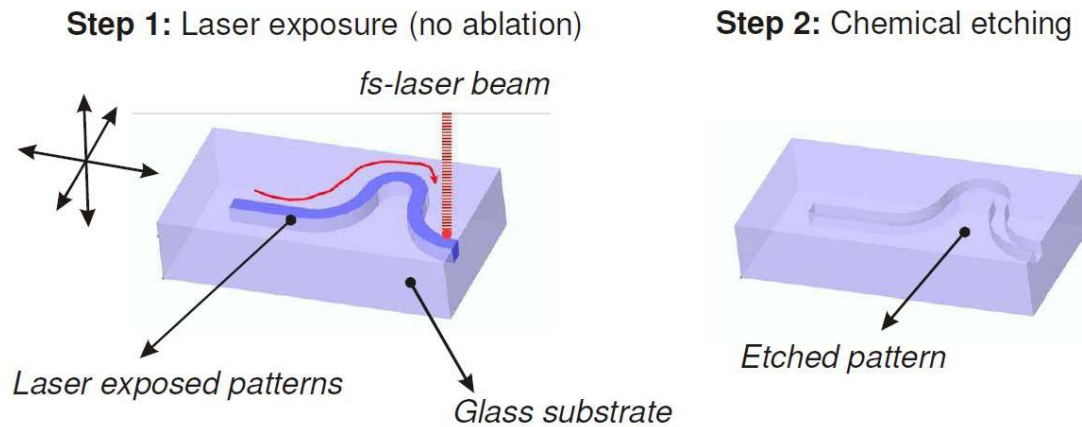


Figure II - 24. Illustration of the selective laser-induced etching. In a first step, the material is irradiated by the laser beam of low energy pulses. So no ablation is performed but the internal structure of the material is modified. In a second step, the irradiated patterns are etched by dipping the glass device in a chemical etchant. Image taken from (Rajesh and Bellouard 2010).

It is a promising processing method, thanks to the 3D structures directly shaped inside the monolithic substrate with this technology, bonding process, including tedious alignment, is not necessary anymore. This guarantees the production accuracy and the integrity of the device, ensuring long-lasting stability. It can be applied to integrated optic devices (Nolte, Will et al. 2003) (Minoshima, Kowalevicz et al. 2001) and lab on chip (Applegate Jr, Squier et al. 2006) (Hanada, Sugioka et al. 2008), that allows combination of several function, fluidics, mechanics and optics in a single substrate (Bellouard, Said et al. 2009). There have been reported about the application onto other photosensitive glass such as Foturan (Hanada, Sugioka et al. 2008), but fused silica offers excellent properties such as low self-fluorescence, high chemical stability and wide transmission spectrum, making it a suitable substrate commonly and widely used for SLE processing.

In our studies, the monolithic device in fused silica is ordered from LightFab GmbH. Based on a given design, they fabricate the device. The detailed process is described in Chapter II, Section IV.2.2.

II.6 Bonding

Bonding temporarily or permanently joins two wafers using a suitable process, either a physical or a chemical one. Glass wafer bonding is the technique to connect two glass pieces together or one glass with another material. Techniques can be divided into two categories, based on the presence, or not, of an intermediate layer.

II.6.1. Direct bonding

Direct bonding is a widely used wafer bonding technology because of its simplicity. In this method, the two hydrophilic surfaces are brought into tight contact, under pressure and annealed at high temperature. The prerequisites of smoothness, flatness, and cleanliness are strict. Furthermore, the surface must absolutely be covered by $-OH$ groups. The bonding of the two wafers relies on the formation of Si-O-Si bond upon polycondensation between two hydroxyl groups, which takes place after the evacuation of the adsorbed water (Figure II - 25). Although some studies revealed that condensation reactions between $-OH$ groups start to occur at room temperature, when the two wafers are in sufficient proximity (Tong and Goesele 1999), many of these Si-O-Si bonds are still reversible where temperature is below $425^{\circ}C$. In order to achieve a fracture strength similar to the bulk one, annealing must typically be performed at temperature higher than $1000^{\circ}C$ (Tong 2001).

The high temperatures needed for the annealing can be seen as a major drawback. For example, the bonding is often the last step in the microchip fabrication, and such high temperature can possibly damage the functional layers that have already been deposited. Therefore, one has looked to decrease the bonding temperature by depositing an intermediate layer, for instance a borophosphosilicate glass (Sukas, Schreuder et al. 2014), or a layer of HSQ ((Gosnet-Haghir and Nanteuil 2014) (see Section I.6.5).

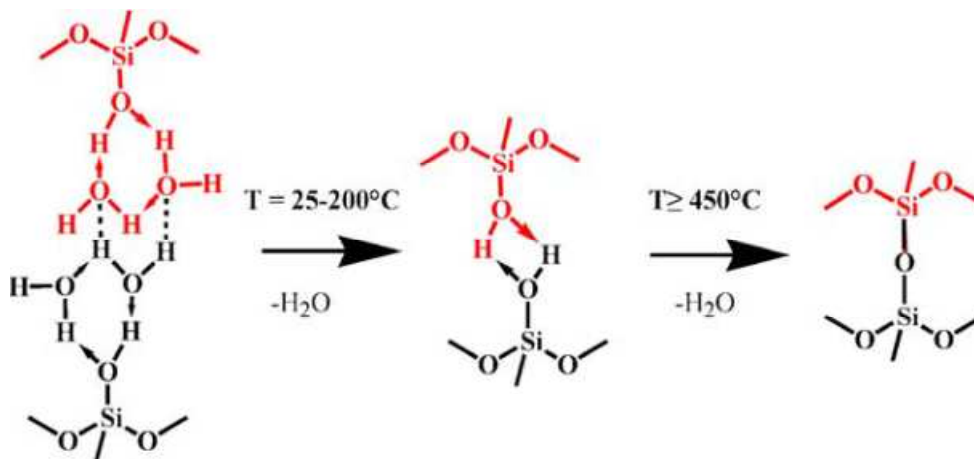


Figure II - 25. Direct bonding mechanism. Image taken from (Barbé, Cassidy et al. 2005).

II.6.2. Anodic bonding

Anodic bonding was introduced by Wallis and Pomerantz in 1968 as an assembly technique that could theoretically bond any metal, alloy, or semiconductor to a glass substrate that contains sodium and that is slightly conductive (Wallis and Pomerantz 1969). This technique has been recognized as simple, robust, and reliable. It can be carried out in air, under an inert atmosphere, or

under vacuum (Blasquez and Favaro 2002). From the technological point of view, the glass wafer can be micro-structured. Its optical transparency is also useful to allow inspection of microstructures. Thus, the anodic bonding has become one of the major techniques for the encapsulation of micro/nano electromechanical systems (Figure II - 26) (Hsieh, Tsai et al. 2005).

The principle of anodic bonding can be summarized as follow: the silicon wafer is connected to a positive electrode, the glass is connected to a negative electrode, and the two wafers are tightly pressed and heated. Sodium ions present in the glass migrate towards the negative pole under the external electric field, so that a depletion layer of a few microns is formed at the bond. This depletion layer is negatively charged whereas the silicon surface is positively charged, hence an electrostatic attraction occurs between the silicon substrate and the glass one. At a certain temperature, strong Si-O chemical bonds form. In addition to the direct use of silicon wafer, it is also possible to deposit a dielectric like SiC to perform bonding (Tudryn, Schweizer et al. 2005).

In comparison with direct bonding, the requirements of anodic bonding in terms of surface quality and environmental cleanliness are less severe. The process is realized at lower temperatures, from 200 to 400 °C. Below this range there is no conductive current, above the glass can soften (Chiao 2008). The applied voltage is generally between 200 and 1000 V (Chen, Yuan et al. 2007). Under lower voltage the electrostatic force is weak, and under higher voltage there is a possibility of dielectric breakdown. Typically, the bonding operation lasts for about 5 to 20 min (Wallis 1975).

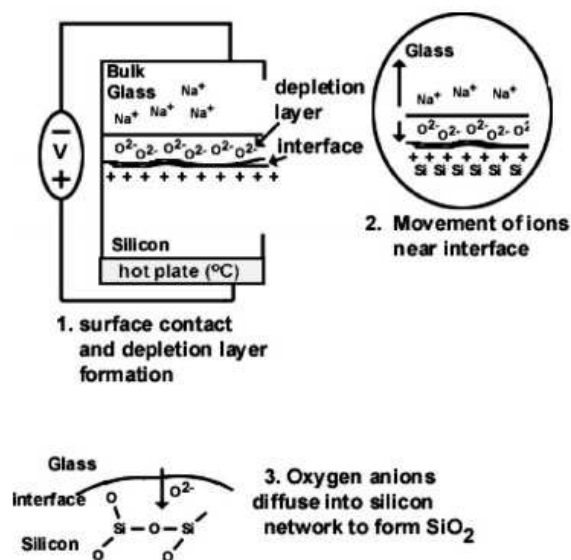


Figure II - 26. Processes occurring at the interface during anodic bonding. Image taken from (Tudryn, Schweizer et al. 2005).

II.6.3. Adhesive bonding

The method is cost-effective since it relies on inexpensive polymeric adhesives. During polymerization, the organic monomers will form long polymer chains. The polymerization reaction can be initiated by a thermal treatment (e.g. for benzocyclobutene) (Niklaus, Enoksson et al. 2001) or by ultraviolet irradiation (e.g. for Vitralit 6127 in current thesis). After cross-linking, the adhesive becomes a solid layer of polymer, which forms the basis of adhesive bonding.

The polymer adhesive is used as an intermediate layer which is deposited on one or both of the surfaces to be bonded. Pressure should be applied to ensure some intimate contact. The bonding temperature depends on the type of adhesive, it can vary from 1000 °C down to room temperature. Besides its advantages, adhesive bonding has some drawbacks. The coefficient of thermal expansion of adhesives is often different from the one of the substrates; therefore, the temperature stability is limited and the mechanical reliability cannot be guaranteed. For a microfluidic chip, which is often used in aqueous phase and undergoes pressure by liquid injection, the hermeticity of the whole device cannot be guaranteed if the adhesive layer is not solid. In our case, some version of the chip is achieved by the adhesive bonding, but due to the instability of the adhesive layer, the device cannot be completely cleaned which was a problem.

II.6.4. Eutectic bonding

Eutectic bonding relies on an intermediate metal layer that can form an eutectic with the wafer material. It makes use of the fact that the eutectic temperature can be much lower than the melting temperature of each of the component. An alloy can thus be formed at the intersurface upon moderate heating.

In industry, the Au-Si (e.g. 19% Si, 81% Au with a melting temperature of 363°C) (Wolffenbuttel 1997) and the Al-Ge (e.g. 72% Al, 28% Ge with a melting temperature of 420°C) (Sood, Farrens et al. 2010) combinations are the most commonly used. Metallization is several hundreds of nanometers to micrometer thick. As the temperature of the compressed material stack is raised and passes the eutectic point, interdiffusion of atoms occurs, leading to the eutectic alloy formation. When the temperature decreases, the eutectic alloy solidifies, serving as a solid bonding layer between the substrates.

This approach does not meet our requirements, since metal layers must be deposited between two wafers that may block the optical pathway of biological experiment. Furthermore, a conductive intermediate layer would be a problem for electroporation.

II.6.5. Sol-gel bonding

The sol-gel process is a wet-chemical technique for the synthesis of glass, ceramics, and organic-mineral hybrid materials. Precursors in solution react to form a sol, i.e. a suspension of oxide colloids, and the sol gradually transforms into an oxide network by additional polymerization reactions. In microfabrication, the sol-gel method is often used to deposit silicon dioxide. The method is thus known as the spin-on glass method (SOG). SOG is in general Si-O network polymers in organic solvents, and prepared through the hydrolysis-condensation reaction that implied the sol-gel technology.

HSQ (hydrogen silsesquioxane) is a similar material originally developed for its dielectric properties by Dow Corning. It is an inorganic silicon based photoresist. The first paper describes its use as an electronic resist in 1998 (Namatsu, Yamaguchi et al. 1998). HSQ is now frequently used in laboratory for nanofabrication of devices with extreme resolution, in e-beam lithography down to 10 nm.

HSQ consists of cage-shaped oligomers of general formula $(\text{HSiO}_{1.5})_n$ (Figure II - 27) dissolved in methyl isobutyl ketone. This resin has the consistency of a gel, which can be deposited by spin-coating. If it is annealed above 300 °C, the condensation and the oligomerization reactions confer it a network structure in which oligomers are covalently attached by Si-O-Si bonds (Figure II - 28) (Yang and Chen 2002).

To realize the bonding, we entrust the device to Klearia, they anneals the resin HSQ at 300 ° C. The bonding result is shown in Figure II - 31.

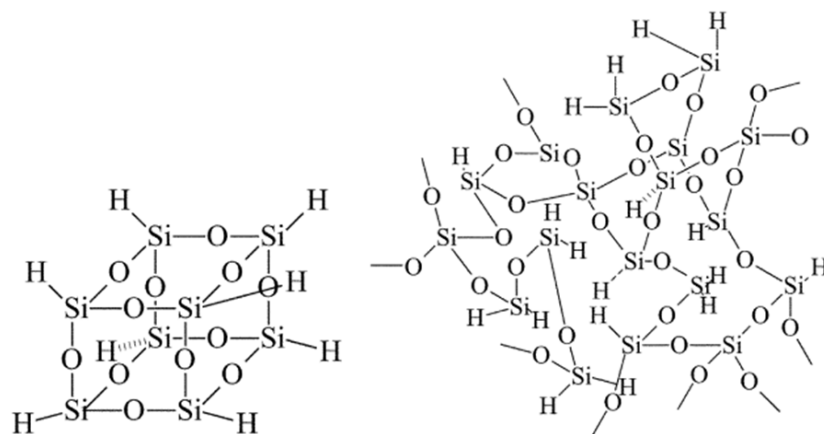


Figure II - 27. HSQ photoresist. (a) Caged-shaped oligomer. (b) Polymerized oligomers. Image taken from (Yang and Chen 2002).

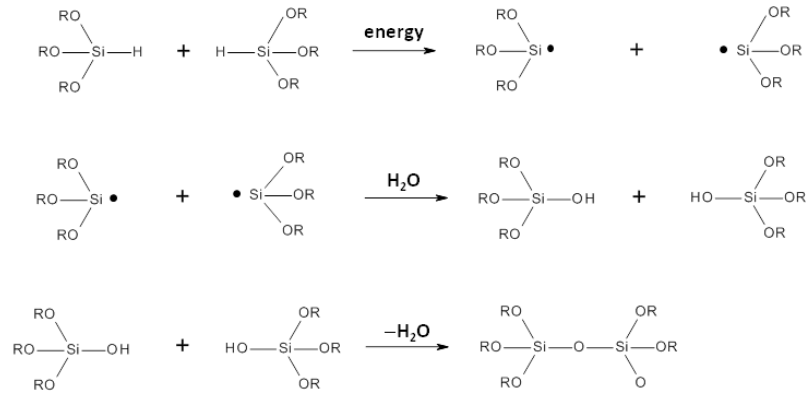


Figure II - 28. The principle of transformation of HSQ under energy. Image adapted from (Namatsu, Yamaguchi et al. 1998).

II.7. Summary of the possibilities offered by the various techniques

Different techniques can be used to process channels or holes in glass (Table II - 1). The general standards are, for instance, to ensure the pattern accuracy without increasing the roughness of the surface, to present convenient operation and low cost. In these methods only SLE is appropriate for holes and channel shaping at the same time, it is a good way to process the monolithic piece.

Among all of the introduced bonding methods (Table II - 2), only the direct and sol-gel bonding meet all the following conditions: the intermediate layer is non conductive, both cleaning with organic solvent or the some acid/base solution is possible, optical transparency and surface hydrophilicity are ensured. Moreover, sol-gel bonding does not required high temperature nor a specific setup to apply pressure. It is consequently the most suitable method and it is part of one of the last two processes we finally retain (Zhao et al. 2017).

Feature	Dry etching	Wet etching	ECDM	Sand blasting	Laser ablation	SLE
Through -hole			suitable	suitable	suitable	suitable
Shallow to medium depth channel	suitable	suitable				suitable

Table II - 2. Suitability of the various fabrication technologies, for channel or hole machining.

Bonding	Intermediate	Temperature	Electrical conductivity of	Resistance to
---------	--------------	-------------	----------------------------	---------------

techniques	layer		the intermediate layer	organic solvents or acid/base solution
Direct	no	> 1000 °C	no	yes
Anodic	yes/no	200-400 °C	yes	yes
Adhesive	yes	< 1000 °C	no	no
Eutectic	yes	300-400 °c	yes	yes
Sol-gel	yes	~300 °C	no	yes

Table II - 3. Comparison of the various bonding methods.

III. Comparative experiments on individual technological steps

III.1 Through hole manufacturing

In this thesis, five methods to realize holes have be tried (Figure II - 29). Their suitability depends on the scale and on the required accuracy. Sand blasting, ECDM, and wet etching are practical and easy techniques, but results are rough, and dimensions cannot be guaranteed at all. If one only needs a fluidic entry and if its dimensions are not important, then these methods can be adopted. Nevertheless, laser technologies are more precise. They can yield vertical and precisely positioned walls.

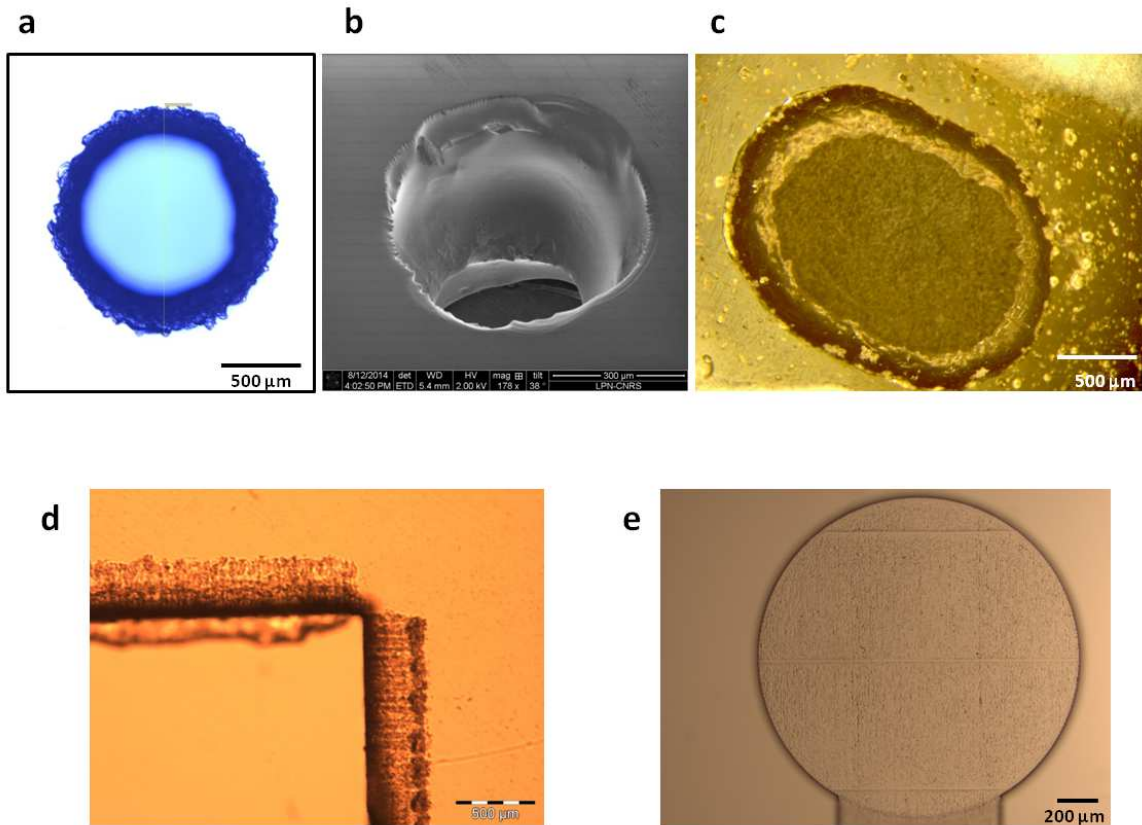


Figure II - 29. Optical or electron micrographs of through-holes obtained by various techniques. (a) Sand blasting. (b) ECDM. (c) Wet etching. (d) Laser ablation. (e) Selective laser-induced etching.

III.2 Wafer bonding

In this thesis, we tried two assembly methods, relying on either the photosensitive Vitralit 6127 glue or on the sol-gel HSQ resist.

The use of photosensitive adhesive bonding implies a rinsing step with isopropanol to clean the Vitralit that was in contact with air during the irradiation. However, this solvent will degrade part of the cured layer, resulting in some air gap (Figure II - 30 a).

Moreover, the bonding layer is composed of organic polymers. Thus, its sensitivity to organic solvents and strong acid or basic solution (e.g. KOH, piranha) makes it impossible to easily wash the device after each experiment. This results in the accumulation of salts and culture medium proteins at the interface of the adhesive layer. So in the end we turned to HSQ sol-gel bonding because after baking the intermediate layer is basically similar to silica. It is hence possible to use of acid or basic solutions.

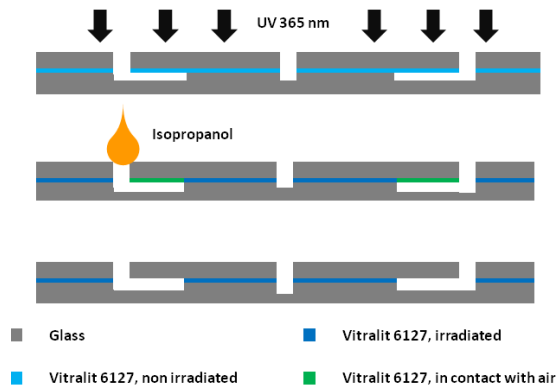


Figure II - 30. The process of Vitralit 6127 bonding.

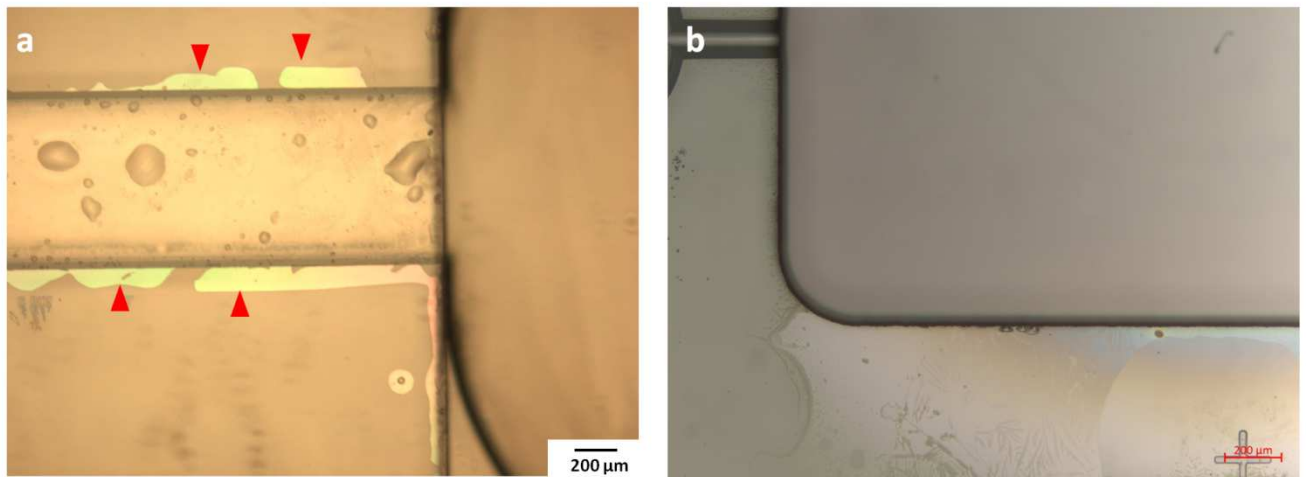


Figure II - 31. Optical micrographs of wafer bonding results. (a) Vitralit 6127 bonding. (b) HSQ bonding. Arrow heads indicate air gaps.

IV. Validation of the two protocols selected to produce an all-in-glass device

IV.1 Design update between the EM6 and EM7 devices

In order to facilitate fabrication and to ease electroporation, the chamber and connecting channel shapes were modified between the two microsystem generations (Figure II - 33).

First, EM6 devices included an embryo chamber with a key hole shape, the disk being dedicated to embryo storage. It was easily fabricated thanks to photolithography and parafilm punching and cutting. We tried to implement this process in glass but results were not satisfying (Figure II - 32). Indeed, sand blasting provided very rough patterns. Independently, we also found that this key hole pattern was not absolutely necessary for the electroporation experiments.

Second, from an ergonomic point of view, in order to ease micromanipulation of the embryo with tweezers and pipettes, the embryo chamber was widened and the space between the electrodes reservoirs was increased (Figure II - 33).

Third, as one of the two guides is often unusable due to lid alignment problems, we introduced an asymmetric layout where focus will be put on only one guide. Because the guide is the most sensitive part of the structure, this strategy also diminished the risk of fabrication failure during the photolithography and etching steps.

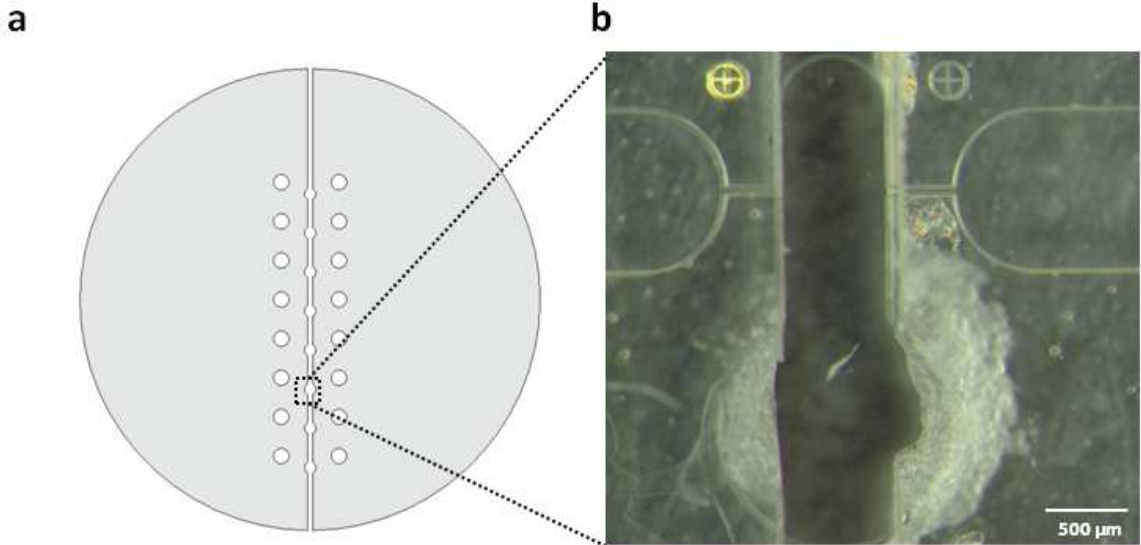


Figure II - 32. Key hole manufacturing by sand blasting and dicing of the top wafer.

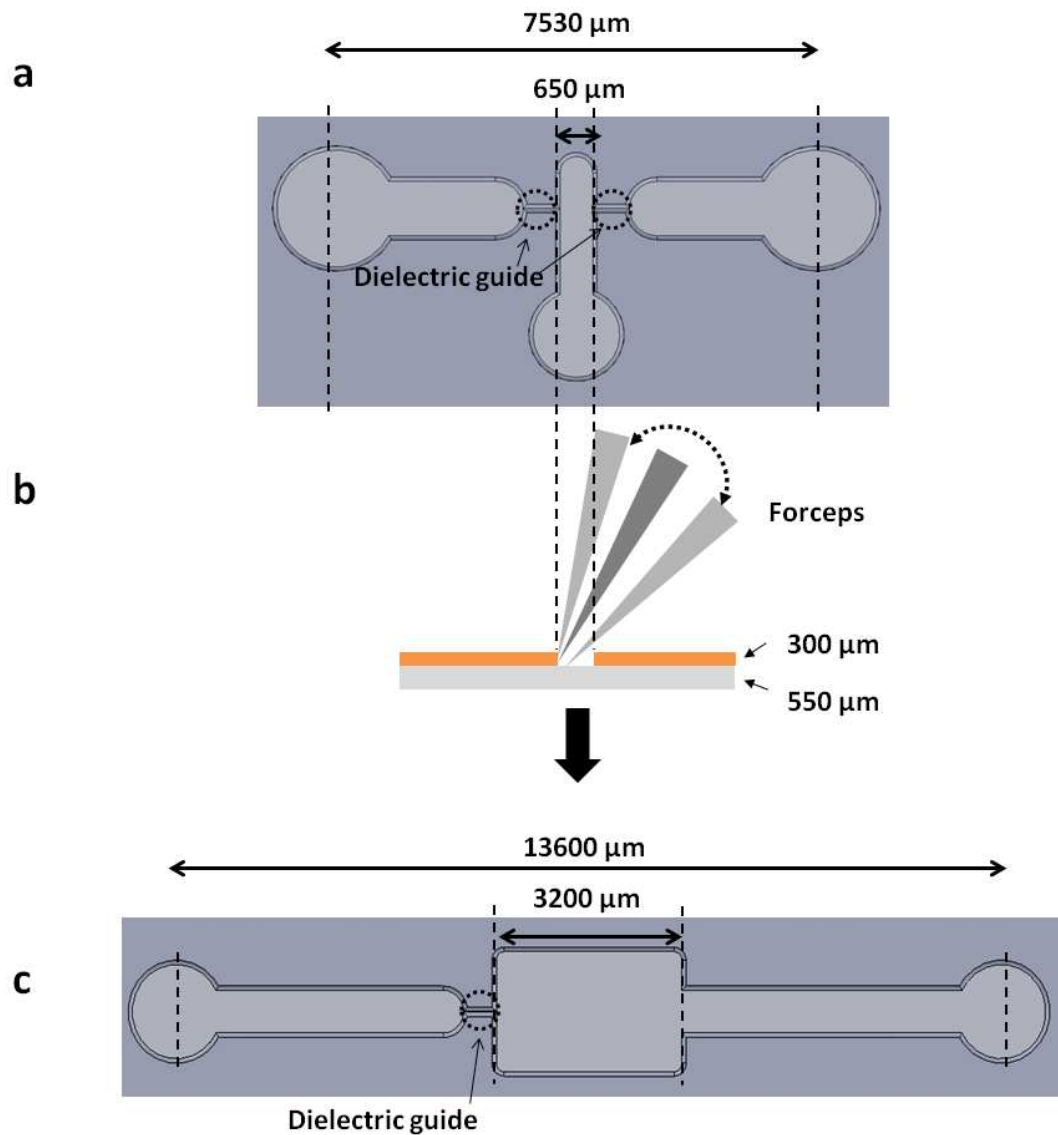


Figure II - 33. Diagram showing the design improvements between the EM6 and EM7 devices. (a) EM6 design. (b) Accessibility of the embryo chamber to manipulation tools. (c) EM7 design.

IV.2 Workflow selection and evaluation

After version of EM7-01, EM7-02, we found two main problems and laser micromachining was finally selected to open the embryo chamber in the glass wafer thanks to its accuracy. Indeed, this technique can yield vertical and precisely positioned walls.

IV.2.1. Microfabrication process by wet etching, laser ablation and bonding

In the EM7-01 and 02 versions, the two substrates were structured separately and joined together by bonding. The accuracy of the alignment was still an issue — it was manually done under a binocular. The main goal was to align on the “extremity of the channel” with the edge of the cover.

We have to admit that the alignment was rough. Because of the thickness of the cover glass and of the impact of lateral undercutting, the accuracy of alignment could not be very good (Figure II - 34).

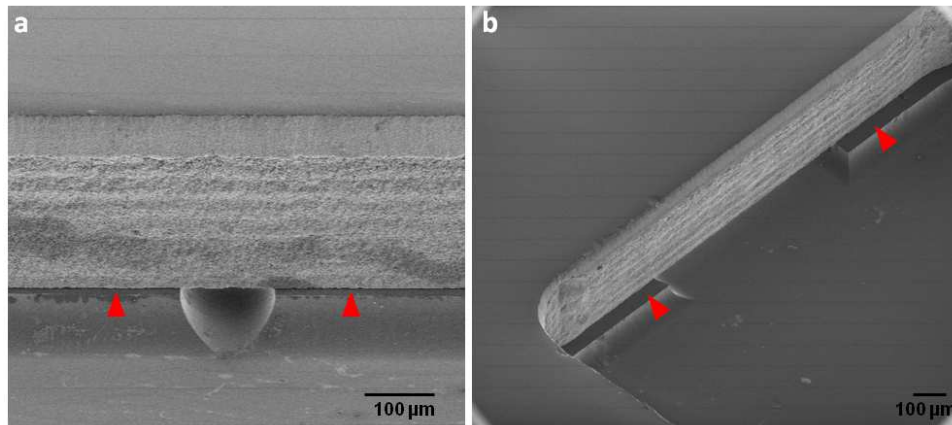


Figure II - 34. SEM pictures showing alignment mismatches when the latter step is done by eyes under binocular (red arrow heads). (a) View of the dielectric guide side. (b) View of the connecting channel side.

This issue was better solved in the EM7-11 device. After having finishing channel etching, we think about keeping some metal alignment marks visible (Figure II - 31 b, the cross at the bottom right corner), so as to indicate the position to cut with laser ablation. A better way to solve the alignment problem is thus to combine it with laser ablation, which takes place on a 3-axis translation stage. An accuracy of 30 μm is achieved. In this way, the cover glass includes all the structures, and it is only necessary to bond it to plain glass wafer (Figure II - 35). More precisely, the latter bottom wafer was activated in an oxygen plasma for 30 s and covered with a 500 nm thick layer of hydrogensilsesquioxane (HSQ) using a spin-coater (Gosnet-Haghir and Nanteuil 2014). On the other hand, the top wafer was activated using the SC-1 procedure (NH_4OH 28% / H_2O_2 30% / H_2O , 1:1:5, at 80 °C). The two parts were next put in contact and the assembly was baked at 300 °C for 5 h.

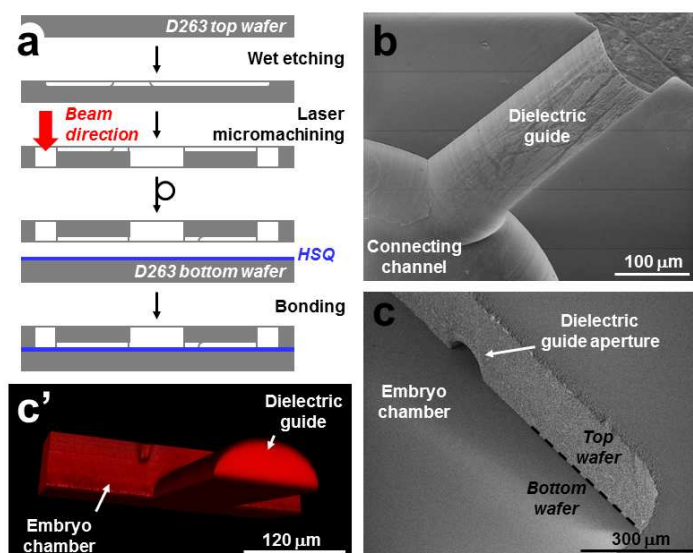


Figure II - 35. Microfabrication process by wet etching, laser ablation and bonding. (a) Workflow. (b) Scanning electron microscope view of the top wafer after wet etching and laser micromachining. (c-c') Scanning electron microscope and confocal laser scanning microscopy views of the semicircular guide of radius 70 μm obtained after bonding to the bottom wafer.

IV.2.2. Microfabrication process by SLE

In EM7-21, both channels and cavities were fabricated at once in fused silica by selective laser-induced etching (SLE) (Hermans, Gottmann et al. 2014). More precisely, the LightFab 3D Printer was first used to irradiate the transparent material line-by-line and layer-by-layer, according to the desired features. In fact, the latter apparatus includes a Satsuma fiber laser (Amplitude Systèmes) working at 1030 nm and which repetition rate and pulse duration can be adjusted in the 0.1–10 MHz and 0.4–5 ps ranges, respectively (Hermans, Gottmann et al. 2014). When the intensity of the tightly focused ultrashort pulses exceeds the nonlinear absorption threshold, photons are absorbed and permanent internal modifications are induced through heating and quenching. Besides other characteristics the resulting modified glass is more susceptible to wet chemical etching than the pristine material. Therefore, in a second step the microfluidic structures can be developed by immersing the irradiated wafer in an 8 M KOH solution, at 85 °C for 48 h (Zhao et al. 2017).

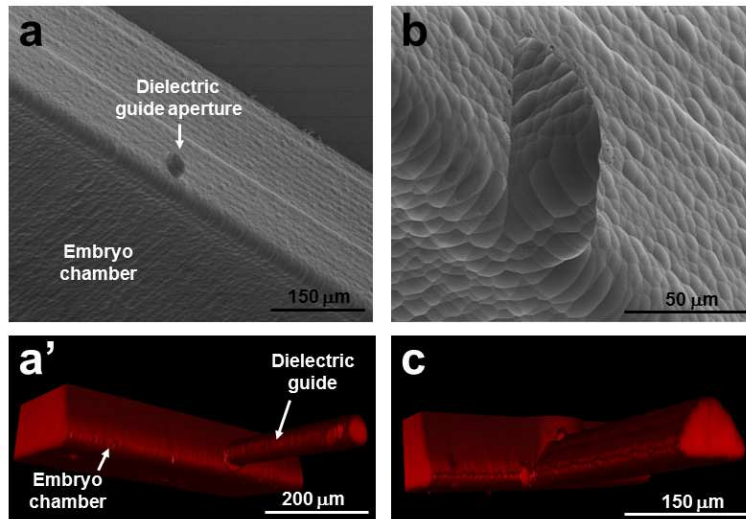


Figure II - 36. Microfabrication process by SLE – scanning electron microscope and confocal laser scanning microscopy, views of various devices. (a-a') Circular guide of radius 50 μm located 40 μm above the embryo chamber bottom. (b) Rectangular guide of section 110 μm x 60 μm. (c) Semicircular guide of radius 70 μm.

Chapter III. Microfabrication protocols

I. The SU-8/parafilm single-use device (EM6)

Cleaning: 30min for 6 pieces

Substrate	D263, diameter 54mm, thickness 550 μm
Piranha	$\frac{2}{3}$ H_2SO_4 (95%) + $\frac{1}{3}$ H_2O_2 (30%) (volume ratio), 30min
Rinse	Water
Drying	N_2 stream

Lithography of electrodes: 1h for 6 pieces

Spin-coating	Machine : RC-8 Gyrset Photoresist: nLof 2070 Speed : 4000 rpm / 2000 rpm.s ⁻¹ / 30 s
Pre-baking	1 min at 118 °C
Insolation	MJB3 40 s Mask: Chrome mask, pattern "electrodes"
Post-baking	1 min at 118 °C
Development	MF26A, 1 min 10s
Rinsing	water, 1 min 20s

Drying N₂

Metallization of electrodes: around 1 day for 6 pieces

Equipment	Alcatel SCM 600
Metallization	Ti/Au 10/120nm
Lift-off	Acetone for 2.5 hours, rinsed in isopropanol, dried by N ₂ stream
Rinsing	water, 1 min 20s
Drying	N ₂

Lithography of SU-8 layer: around 2h for 3 pieces

Spin-coating	Photoresist: SU-8 2050 (Microchem) Machine : RC-8 Gyrset Speed : 500 rpm ~1300 rpm / 400 rpm.s ⁻¹ / 30 s
Pre-baking	3 min at 65°C , 9 min at 95°C
Insolation	MJB3 18 s Mask: Chrome mask, pattern "guide"
Post-baking	2 min at 65°C , 7 min at 95°C
Development	SU-8 developer, 4 min
Rinsing	Isopropanol, 2 min
Drying	N ₂

Treatment by Plasma : around 2 min per piece

Cleaning	SU-8 developer 2-3 min
Plasma treatment	Pumping under 300 mTorr, N ₂ maintained in the chamber for 50 s, (Plasma sterilizer Harrick)

Parafilm alignment and thermal bonding: around 1h30 min for 3 pieces

Parafilm cutting	Parafilm "M" (Pechiney)
Equipment	binocular
Bonding	The "lid" layer of parafilm is deposited on the wafer on which lies the layer of SU-8 forming the tunnels thermal bonding on a thermal plate at 65 °C for 2 minutes 30 seconds.

Connectors welding: around 15 min per piece

Welding the electrodes with a banana plug set 2mm (RadioSpare) copper wire at a temperature of 230 ° C, Tin wire (alloy solders Multicore 60/40 \varnothing 0.7 mm crystal 5 channels) for soldering at 220 ° C. Well protecting the center of device by a piece of aluminum paper.

II. The reusable all-in-glass device series (EM7)

II.1. EM7-01

Cleaning: 30min for 6 pieces

Substrate	D263, diameter 54mm, thickness 550 μ m
Piranha	$\frac{2}{3}$ H ₂ SO ₄ (95%)+ $\frac{1}{3}$ H ₂ O ₂ (30%) (volume ratio), 30min
Rinse	Water
Drying	N ₂

Metallization of wet etching mask: around 1 jour for 6 pieces

Equipment	Alcatel SCM 600
Metallization	Cr/Au 10/200 nm

Lithography of window opening: around 30min for 3 pieces

Spin-coating	Machine : RC-8 Gyrset Photoresist: nLof 2070 Speed : 4000 rpm / 2000 rpm.s ⁻¹ / 30 s
Pre-baking	1 min at 118 °C
Insolation	MJB3 40 s Mask: Chrome mask, pattern "guide"
Post-baking	1 min at 118 °C
Development	MF26A, 1 min 10s
Rinsing	water, 1 min 20s
Drying	N ₂

IBE etching to open the channel pattern: around 10 min for 3 pieces

Equipment	IonSys500
Process	Tilt 20° ; Rotation 3 rpm ; Temperature -20°C P 350 W ; Acc. 350 V ; Extract. -500 V Ar 13 sccm ; 20 mbar
Duration	10 min
Target thickness	Total opening of metallization layer

Protection of the substrate back: around 1 h for 3 pieces

Material	PDMS base/initiator=10/1 (w/w)
Temperature	70°C
Duration	30 min

Wet etching in HF: around 50 min for 3 pieces

Solution	100 mL HF (40%)/200 mL deionized H ₂ O/30 mL HCl (37%)
Duration	35-40 min
Cleaning	10 min deionized water bath

Etched substrate cleaning: around 30 min for 3 pieces

PDMS	Peel-off
nLOF2070	Piranha solution 5 min
Au	Regia aqua 10 min
Cr	Cr etchant solution 5 min
Rinse	Deionized water

Sand blasting for piecing cover: around 15 min per piece

The same D263 substrates are first diced into half-disk. Then they are stuck on the back side of the “sand blasting holes” mask. The assembly is put in the sand blasting chamber and the latter one is performed (for about 10 min).

Alignment and binding: around 30 min per piece

Vitralit 6127 is spun-coated onto the half-disk covers (4000 rpm/2000 rpm·s⁻¹/30 s), the cover is flipped and aligned with the edge of the guide. They are exposed under the Hamamatsu LC5 UV light for 2 min to solidify the adhesive.

II.2. EM7-02 and EM7-11

From “substrate cleaning” to “wet etching in HF”, steps are the same as for EM7-01. At the step of “etched substrate cleaning”, the markers are protected by drops of photoresist, the remaining part of metallization is removed.

Femtosecond laser micromachining of the through holes in the cover

This step was realized by J. Safioui at FEMTO Engineering (Besançon) (See Chapter II, Section II.4.)

III. The use of protection layers during glass micromachining

III.1. Wet etching

At the beginning, amorphous silicon (α Si) deposited by PECVD was used as mask for wet etching of glass. Since silicon cannot be dissolved by HF, it should have provided an effective protection mask if a layer thick enough was deposited and the negative photoresist nLOF2070 was not removed. However, in practice, we found that this layer of α Si cannot be thicker than 300 nm. Even though, annealing in a furnace (4 h, 400 °C) was necessary to release the internal stress of the film. More problematically, with the protection of α Si and nLOF2070, pinholes phenomenon appeared after etching (Figure II - 37 a). With the improvement of the fabrication process, the protective layer was changed for 200 nm Au deposited on 10 nm Cr, and the nLOF2070 still continued to be preserved. There was no pinhole anymore because the protection of Au layer was dense.

However, another phenomenon appeared: notching (Figure II - 37 b). These defects were generated either by breakage of the mask edges or by a stress gradient between multiple layers (Iliescu, Tay et al. 2007), such as Cr/Au in the current situation. Our solution was to clean the glass surface very carefully to increase the adhesion between the glass and the metallization mask. We started by organic solvent baths (ultrasound of acetone and then isopropanol) and later shifted to a piranha solution ($\text{H}_2\text{SO}_4/\text{H}_2\text{O}_2$).

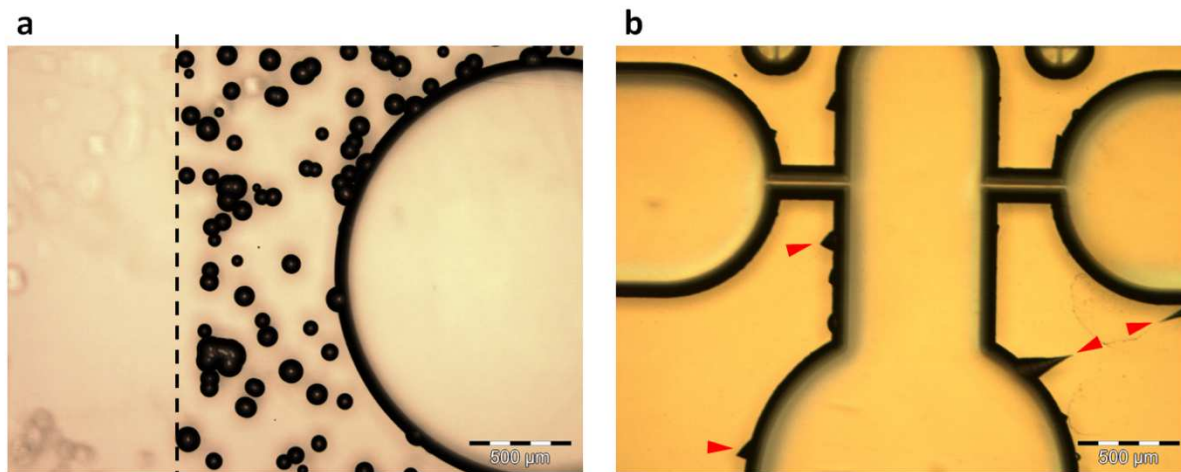


Figure II - 37. Pictures of two kinds of defects observed during glass wet etching. (a) Pinholes. The dashed line indicates the frontier of the PDMS protection (see the next paragraph and Figure II - 38). (b) Notching. Arrow heads indicate where it has occurred usually at the edge of patterns.

Nevertheless, an ever-present problem is that the front side of the sample is protected, here both by the metallization and the photoresist, but the backside is still exposed to the HF solution, and thus, etched at the same rate as the front side. To solve this problem, some colleagues melted wax on the back side to insulate it from the HF solution. Here, we suggest to use PDMS as a physical protective layer (Figure II - 38). When the PDMS is solidified, it forms a film that is completely impermeable to liquids. The backside, but also the edges of the front side, can be all protected at once. One particular observation seems important, due to the structure of PDMS (with its $-\text{Si-O-Si-O}-$ backbone), it is likely to be also attacked by HF. In fact, each time a sample was removed from the etching bath, both the protection layer of PDMS looked opaque. This also implies that some HF is lost by reaction with polymer and that it must be prepared in large quantity.

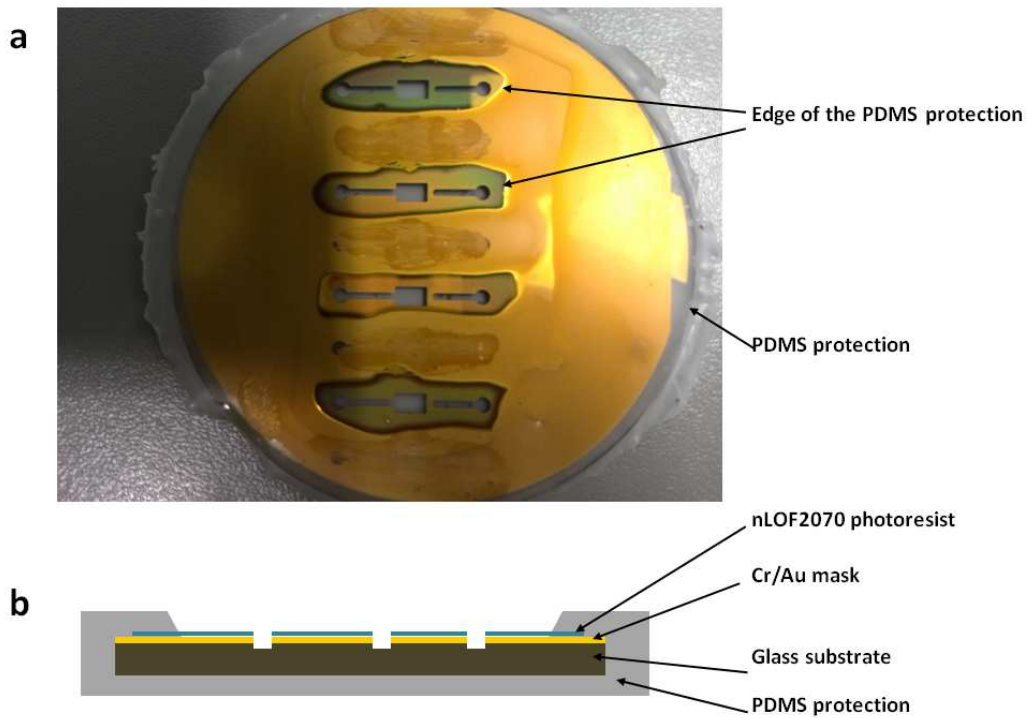


Figure II - 38. Use of a PDMS protection layer during glass wet-etching in HF. (a) Picture of a substrate ready to be processed. (b) Corresponding cross-section diagram.

III.2. Laser ablation

We found that around the edge of the opened holes, some defects were present, such as deposit of ablated matter (Figure II - 29 d). Therefore, we have tried to apply to two kinds of protective layers before laser processing: photoresist and ITO. More precisely, AZ 9260 was spun-coated on both sides of the glass and baked at 120 °C. ITO was deposited only on the side of entrance of the laser. After laser ablation, the method for removing the protective layer was also different. The photoresist was removed using a piranha solution whereas ITO was removed with an ITO etching solution. However, neither of these methods yielded satisfactory result since removal of the protective material was not complete, surely because its structure had been modified by the exposure to the high energy flux of the laser beam.

Chapter IV. Results and discussion

I. Simulations

I.1 Description of the models

In the work of a former PhD student, a simulation model was established. It describes the main shape of the device. In the EM7 series, this description is maintained and the dimensions of parts can vary, especially the cross-sectional of the guide (Figure II - 39).

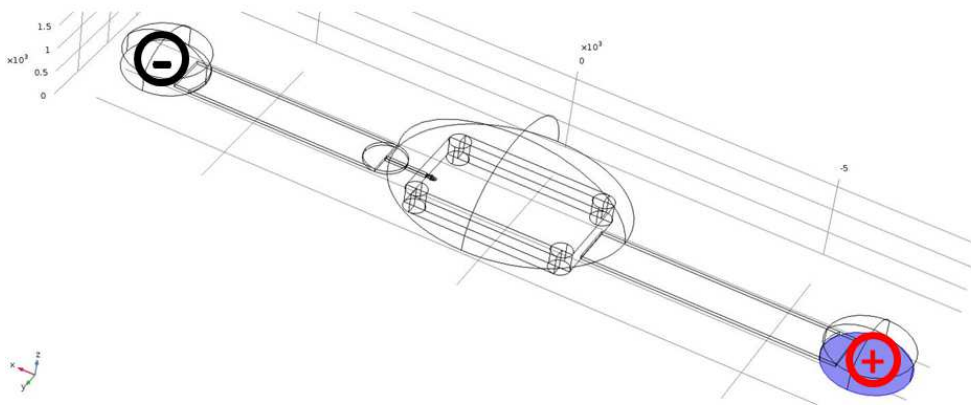


Figure II - 39. Complete general model of EM7 series.

The main shape of the embryo chamber in the EM6 version was of the keyhole shape, and in EM7 versions it was decided to be rectangle. The main dimension of the channel is shown in the Figure II - 40. The blue parts are opening and the red parts are buried fluidic channels.

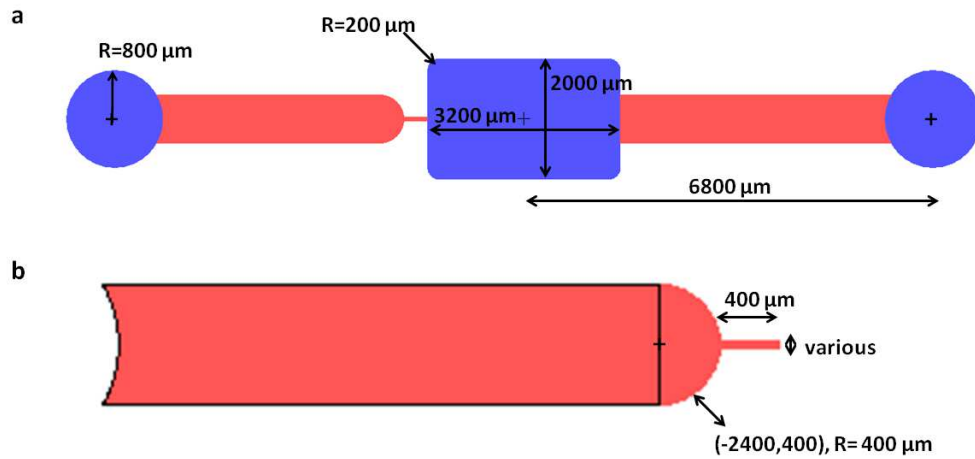


Figure II - 40. The plan of the channel. The concrete dimension of dielectric guide is shown in Figure II - 14.

Early post-implantation embryos were modelled as two concentric prolate ellipsoids (Figure II - 41), the outer one representing the organism external boundary and the inner one the periphery of the proamniotic cavity. The outer one, 200 by 100 μm large, represents the buffer/VE interface and the inner one, 140 by 40 μm large, is for the PAC/Epi+ExE. Solid lines depict those two liquid/tissue interfaces, whereas dashed lines represent tissue/tissue junctions not considered in computations. Cells were not considered individually, as they are electrically connected by GAP junctions (Pucihar, Miklavcic et al. 2009), present in all tissues at these developmental stages (Kalimi and Lo 1988) (Viotti, Niu et al. 2012). No data being available for the electrical properties of mouse embryos, values reported for various cell types were used (Gowrishankar and Weaver 2003) (Hibino, Itoh et al. 1993) (Pucihar, Kotnik et al. 2006) (Sudsiri, Wachner et al. 2007).

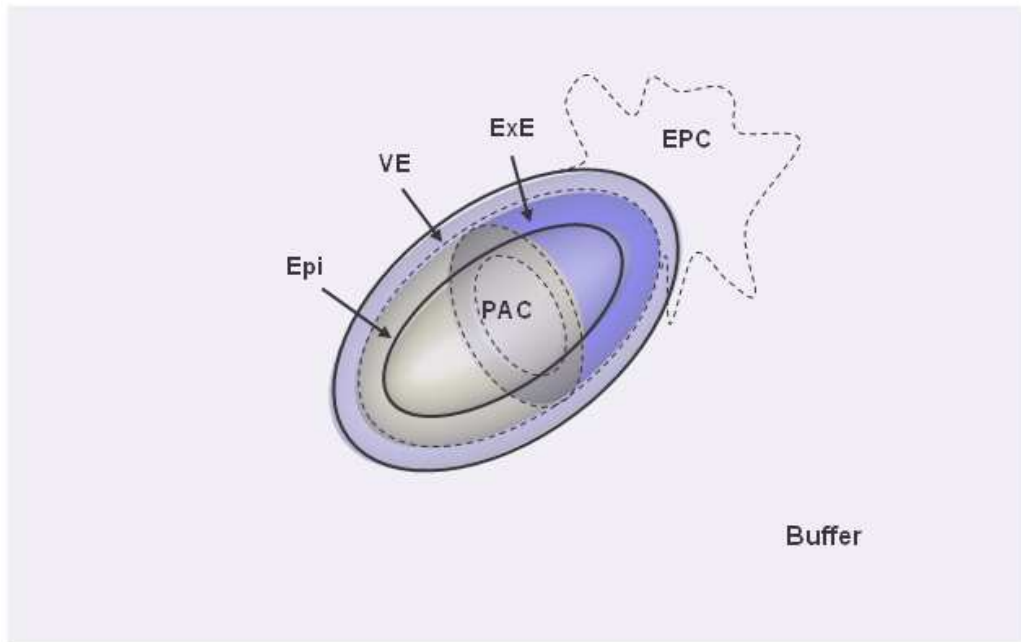


Figure II - 41. Electrical model of an E5.5, as used in FEM simulations. The embryo is approximated by two concentric prolate ellipsoids of respective length and width 200 and 100 μm for the buffer/VE interface and 140 and 40 μm for the PAC/Epi+ExE one.

The channel is filled by the electroporation buffer which conductivity was measured at 1.5 S/m, using a CDM210 conductimeter (Radiometer analytical). The two ellipsoids were described as resistive membranes having 3×10^{-7} S/m conductivity and 5 nm thickness. The conductivity of the proamniotic fluid was assumed identical to that of the cytoplasm and fixed at 0.3 S/m. The glass, polymer, and air boundaries were insulating. The cathode surface was grounded and the anode one had its potential corresponding to the pulse amplitude.

Comsol Multiphysics was run in the “Stationary” “Electric Currents” mode (Pucihar, Kotnik et al. 2006). Simple time-independent modeling was here relevant because pulses were longer than the characteristic charging time associated with phospholipidic membranes (Valič, Golzio et al. 2003).

I.2 Determination of the permeation threshold

As the guide has always a slightly smaller diameter than the embryo, a focusing effect is obtained, which restricts the area over which the induced transmembrane voltage (ITV) exceeds the poration threshold. In order to evaluate this threshold, experimental results were compared to stimulation studies. The premise is that pores are assumed to form each time the ITV exceeds a given threshold (Escoffre, Portet et al. 2009) (Rols and Teissié 1998).

In an experiment using the EM6 device, which guide is $110 \mu\text{m} \times 60 \mu\text{m}$, the length of tissue marked by FITC-Dextran after electroporation was determined and the ratio with respect to the total

length of embryo was calculated. This proportion was next applied in the simulation model, and the lowest ITV in this delineated area was determined. This ITV_{pore} value was confirmed to be 0.65 V in our studies (Figure II - 42), which agreed with published data (Valič, Golzio et al. 2003) (Escoffre, Portet et al. 2009) (Hibino, Itoh et al. 1993). At the same time it was found that the maximal ITV reached in the electroporated zone was 0.72 V. These two values are important for our following applications.

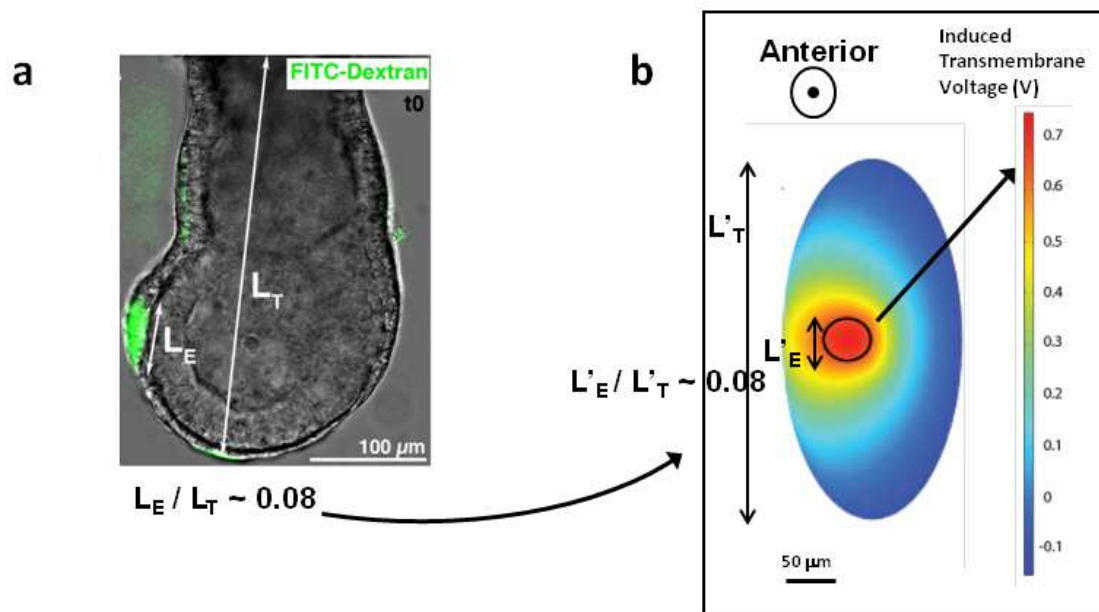


Figure II - 42. Determination of the permeation threshold by comparison. (a) Results of electroporation inform us on the relationship between the applied voltage and the length of tissue being marked. (b) The same voltage is applied in simulations in order to determine the same area electroporated and further the lowest voltage in this area.

In the subsequent experiments, we fully applied simulations to assist the design of the device and to set the electrical parameters. After each design change, it is necessary to determine the range of the voltage to apply. Giving the premise that on the exposed area to the guide opening the ITV endured should not exceed 0.72V, then the voltage applied at anode can be estimated.

II. Electroporation experiments

From the EM7-01 prototype, devices were sent to the IRIBHM at the Université Libre de Bruxelles for biological validation. We also communicated to our collaborators the parameters determined by simulations.

In general, there are three works involved in determining the electrical parameters. First, the simulation gives roughly the range, as explained in the previous section. Second, before real

experiment, the use of dyes to characterize the opening of pores delimits the minimal voltage value; Third, propidium iodide (PI) is used to mark the eventual dead cells by electroporation, it gives the information on the maximal value.

It is necessary to determine the localization of the zones where the transmembrane potential is greater than the electroporation threshold, fluorescein labeled Dextran solutions were used. Indeed, the latter make it possible to reveal the existence of the pores by dyeing the cytoplasm of the electroporated cells (Sukharev, Klenchin et al. 1992). They provide information about the predictability of our models.

When addressing cell death, embryos were electroporated in HBS, allowed to recover for 30 minutes in culture, and stained for 20 minutes at 37 °C in dissection medium containing 25 µg/mL of propidium iodide. Control embryos submitted to the whole protocol with the exception of the pulse application did not show any PI incorporation. The analysis of the electroporated embryos is done by conventional approaches, in full field epifluorescence and in particular by video microscopy.

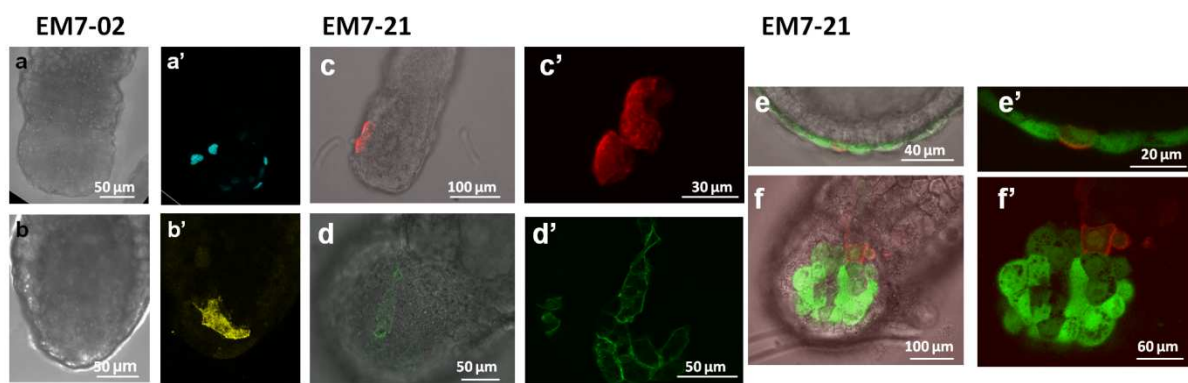


Figure II - 43. Expression of various proteins observed in both bright field and confocal laser scanning microcopies after electroporation of E5.5 embryo with the corresponding plasmid. (a-a') pCMV-H2B-CFP is used to label histones in the nuclei. (b-b') pCMV-YFP-actin, (c-c') mApple-actin, (e-f') FusionRed-Lifact are used to label actin filaments in the cytoskeleton – in the two latter cases embryos are Hex-GFP transgenics which DVE is constitutively labeled in green. (d-d') GFP- α -catenin is used to label the cell-cell adherence junction. (a-b') Electroporation are performed using the EM7-02 device and applying 3 pulses, 50 ms long and 23 V high, separated by 1 s. (c-f') Electroporation are performed using the EM7-21 device the semicircular guide of radius 70 µm and applying 3 pulses, 50 ms long and 20 V high, separated by 1 s.

Thanks to these devices and to the parameters obtained from numerical simulations, our collaborators at the Université Libre de Bruxelles have led successfully some eletroporations. As shown in Figure II - 43 , they are pCMV-H2B-CFPnes which is used for labelling histones in the nuclei, pCMV-YFP-actin, mApple-actin, and FusionRed-Lifact for labelling actin filaments in the cytoskeleton, and GFP- α -catenin for labelling cell-cell junction. These successful examples demonstrate the efficacy and validity of our device concept and the procedure in which design is assisted by numerical simulations. Of course, it can also be extended for the electroporation of other plasmids.

Chapter V. Perspectives

I. Post-electroporation culture

It has been demonstrated that external mechanical cues exerted by maternal tissues on the embryo are crucial for the specification of the anterior-posterior axis, between E5 and E6.5 (Hiramatsu, Matsuoka *et al.* 2013). In the body of the mouse, this external cue is provided by the uterine wall which, thanks to the pressure it applies, enables the embryo to elongate (Figure II - 44 a). In turn, this elongation yields a well-defined distribution of internal molecular signals and indirectly results in the differentiation of the DVE cell (Figure II - 44 b). If embryos are cultured *in vitro*, the elongation process does not take place and cells at the distal tip do not migrate in anterior position. Following Hiramatsu *et al.*, we propose to use elastomeric pit to mimic the uterine wall (Figure II - 44 a). Accordingly, we will be able to electroporate the DVE at a very early stage while still having embryos that elongate normally and in which the DVE migration occurs as expected.

Hiramatsu *et al.* adopted SU-8 lithography to fabricate the molds that were used to cast the PDMS pits. We propose to rely on PMMA micromilling, which can manufacture different sizes of pattern simply, provided features not too small. The molds contain a positive cylinder of diameter 70 μm to 150 μm located in a negative cylinder of diameter 1.2 mm; the depth reaches 300 μm (Figure II - 44 c).

After electroporation, the embryo is put into the pit vertically, and culture lasts for 8 h at 37 °C. When harvested, the embryo adopts an elongated shape like in Figure II - 44 d.

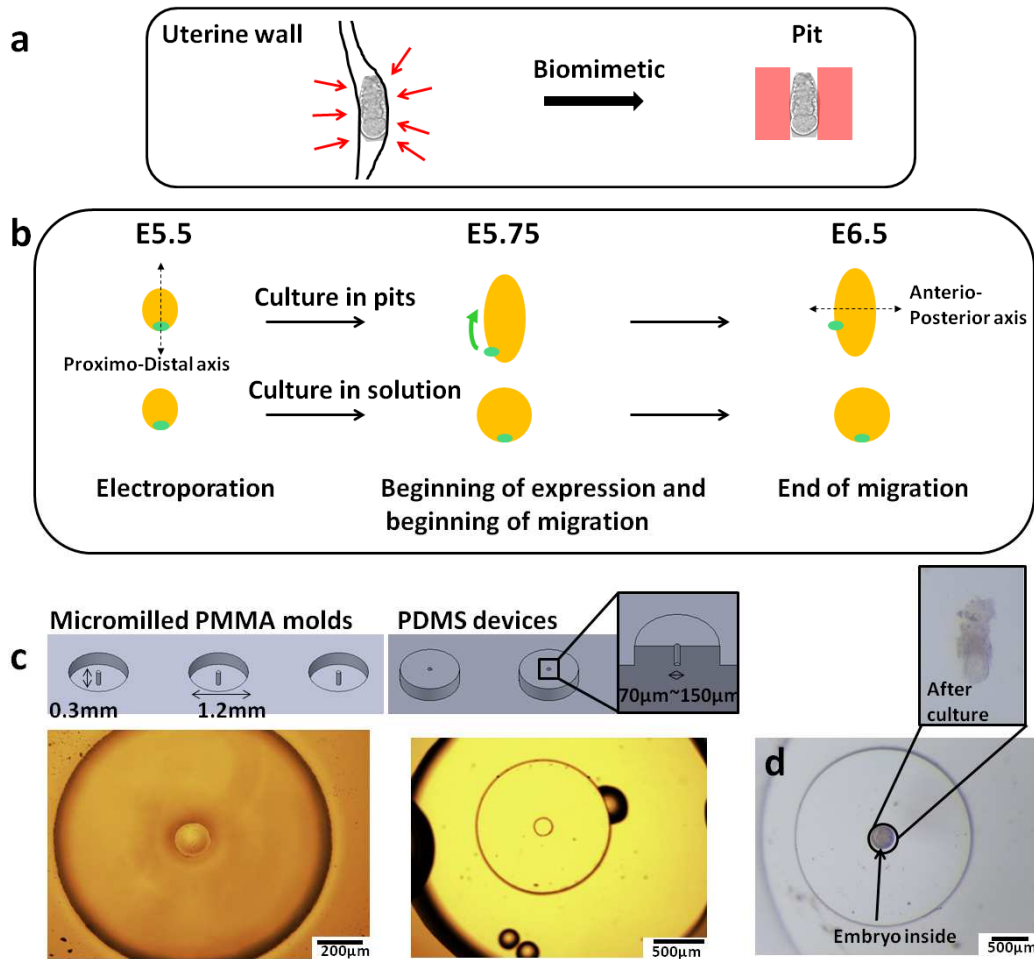


Figure II - 44. Biomimetic devices used to trigger embryo elongation. (a) Scheme explaining the force exerted on embryos by the uterine wall, this mechanism will be imitated by installing the embryo in elastomeric pits. (b) Scheme explaining the coupling between elongation and DVE migration. (c) Scheme and photo showing the micromilled molds fabricated in PMMA as well as the PDMS pits. (d) Picture of an embryo cultured in a pit.

II. Measurement of temperature and pH jumps

As discussed in Chapter I, Section III.1, oxido-reduction reactions take place at the electrodes. It may then result in the production of highly reactive chemical species, such as free radicals, or the release of metal ions (Friedrich, Stachowicz et al. 1998). The nature of the electrolytic reactions depends on the chemical nature of the electrodes (e.g. steel, stainless steel, aluminum), the composition of the medium, and the applied electrical parameters. However, the solution at the anode always becomes acid and the one at the cathode basic. Since these pH variations may have adverse consequences on embryos, it would be of interest to evaluate their amplitude in our microsystem (Loste, Eynard et al. 1998). Of course our device has been especially devised to avoid

such effect, so these measurements will surely emphasize on the benefits of using a dielectric guide. More specifically, we propose to make pH measurements relying on the ratiometric fluorescent probes that have been conceived by the group of L. Jullien (Charier, Ruel et al. 2004). In addition, these data could be backed up by FEM simulations taking into account the generation of chemical species at the electrodes as well as their molecular diffusion in the connecting channel and in the dielectric guide.

Another physical parameter needing to be monitored is temperature. As the entire channel is filled and connected by electrolyte solution, when the voltage is applied, Joule effect results in a temperature increase. For the biological object soaked in the chamber it is not a favorable condition. To measure this temperature changes in microfluidic devices, the use of molecular probes seems appropriate (Gosse, Bergaud et al. 2009).

More precisely, we plan to use the molecular beacons that we have developed in collaboration with L. Jullien at the ENS. Such molecule has two different fluorescent groups, one is fluorescein, and the other texas red; they are attached to the ends of a DNA strand which can fold in a hairpin thanks to base pairing. These fluorophores can undergo Foster resonance energy transfer (FRET) and thus the luminescent state of the beacon characterizes the state of the DNA: in the open configuration – at relative high temperature – the excited fluorescein emits light; in the closed configuration – at relative low temperature – the excited fluorescein transfers its energy by FRET to the texas red group which emits light (Barilero, Le Saux et al. 2009). The quotient between the fluorescein and the texas red emission is monotonic as a function of temperature. In this way, the fluorescence emission spectrum of the molecular beacon is able to report on temperature. Once more, experimental data will be correlated with the results issued from FEM simulations.

References

- Adamo, A., Arione, A., Sharei, A., and Jensen, K. F. (2013). "Flow-through comb electroporation device for delivery of macromolecules." Analytical chemistry **85**(3): 1637-1641.
- Akashi, T., and Yoshimura, Y. (2006). "Deep reactive ion etching of borosilicate glass using an anodically bonded silicon wafer as an etching mask." Journal of Micromechanics and Microengineering **16**(5): 1051.
- Albini, A., and Monti, S. (2003). "Photophysics and photochemistry of fluoroquinolones." Chemical Society Reviews **32**(4): 238.
- America, I. D. S. o. (2004). "Bad bugs, no drugs: As antibiotic discovery stagnates." A public health crisis brews.
- Aminov, R. I. (2010). "A brief history of the antibiotic era: lessons learned and challenges for the future." Frontiers in microbiology **1**: 134.
- Ammor, M. S., Flórez, A. B., Margolles, A., and Mayo, B. (2006). "Fluorescence spectroscopy: a rapid tool for assessing tetracycline resistance in *Bifidobacterium longum*." Canadian Journal of Microbiology **52**(8): 740-746.
- Angelescu, D. E. (2011). Highly integrated microfluidics design, Artech House.
- Applegate Jr, R. W., Squier, J., Vestad, T., Oakey, J., Marr, D. W., Bado, P., Dugan, M. A., and Said, A. A. (2006). "Microfluidic sorting system based on optical waveguide integration and diode laser bar trapping." Lab on a Chip **6**(3): 422-426.
- Ashkin, A. (1970). "Acceleration and trapping of particles by radiation pressure." Physical Review Letters **24**(4): 156-159.
- Ashkin, A. (1997). "Optical trapping and manipulation of neutral particles using lasers." Proceedings of the National Academy of Sciences **94**(10): 4853-4860.
- Ashkin, A., Dziedzic, J. M., Bjorkholm, J. E., and Chu, S. (1986). "Observation of a single-beam gradient force optical trap for dielectric particles." Optics letters **11**(5): 288-290.
- Balagaddé, F. K., You, L., Hansen, C. L., Arnold, F. H., and Quake, S. R. (2005). "Long-term monitoring of bacteria undergoing programmed population control in a microchemostat." Science **309**(5731): 137-140.
- Ball, P. (2000). "Quinolone generations: natural history or natural selection?" Journal of Antimicrobial Chemotherapy **46**(Suppl 3): 17-24.
- Barbé, C., Cassidy, D., Triani, G., Latella, B., Mitchell, D., Finnie, K., Short, K., Bartlett, J., Woolfrey, J., and Collins, G. (2005). "Sol-gel bonding of silicon wafers: Part 1: Influence of the processing temperature on final bond morphology and interfacial energy." Thin Solid Films **488**(1): 153-159.
- Barilero, T., Le Saux, T., Gosse, C., and Jullien, L. (2009). "Fluorescent thermometers for dual-emission-wavelength measurements: Molecular engineering and application to thermal imaging in a microsystem." Analytical chemistry **81**(19): 7988-8000.
- Bartolo, D., Degré, G., Nghe, P., and Studer, V. (2008). "Microfluidic stickers." Lab on a Chip **8**(2): 274-279.
- Basle, A., Rummel, G., Storici, P., Rosenbusch, J. P., and Schirmer, T. (2006). "Crystal structure of osmoporin OmpC from *E. coli* at 2.0 Å." Journal of Molecular Biology **362**(5): 933-942.
- Batchelor, E., Walthers, D., Kenney, L. J., and Goulian, M. (2005). "The *Escherichia coli* CpxA-CpxR envelope stress response system regulates expression of the porins ompF and ompC." Journal of Bacteriology **187**(16): 5723-5731.
- Bates, S. R., and Quake, S. R. (2009). "Highly parallel measurements of interaction kinetic constants with a microfabricated optomechanical device." Applied Physics Letters **95**(7): 73705.
- Bedard, J., Wong, S., and Bryan, L. E. (1987). "Accumulation of enoxacin by *Escherichia coli* and *Bacillus subtilis*." Antimicrobial Agents and Chemotherapy **31**(9): 1348-1354.

- Bellouard, Y., Said, A. A., Dugan, M., and Bado, P. (2009). Monolithic integration in fused silica: When fluidics, mechanics and optics meet in a single substrate. Optomechatronic Technologies, 2009. ISOT 2009. International Symposium on, IEEE.
- Bennett, P. M. (2008). "Plasmid encoded antibiotic resistance: acquisition and transfer of antibiotic resistance genes in bacteria." British Journal of Pharmacology **153 Suppl 1**: S347-357.
- Berg, R. D. (1996). "The indigenous gastrointestinal microflora." Trends in Microbiology **4**(11): 430-435.
- Bertrand, L., Réfrégiers, M., Berrie, B., Échard, J.-P., and Thoury, M. (2013). "A multiscale photoluminescence approach to discriminate among semiconducting historical zinc white pigments." Analyst **138**(16): 4463-4469.
- Bhuyan, M. K., Courvoisier, F., Lacourt, P.-A., Jacquot, M., Furfaro, L., Withford, M., and Dudley, J. (2010). "High aspect ratio taper-free microchannel fabrication using femtosecond Bessel beams." Optics express **18**(2): 566-574.
- Biron, M. (2012). Thermoplastics and thermoplastic composites, William Andrew.
- Blasquez, G., and Favaro, P. (2002). "Silicon glass anodic bonding under partial vacuum conditions: problems and solutions." Sensors and Actuators A: Physical **101**(1): 156-159.
- Blount, Z. D. (2015). "The unexhausted potential of *E. coli*." eLife **4**.
- Boukany, P. E., Morss, A., Liao, W.-c., Henslee, B., Jung, H., Zhang, X., Yu, B., Wang, X., Wu, Y., and Li, L. (2011). "Nanochannel electroporation delivers precise amounts of biomolecules into living cells." Nature nanotechnology **6**(11): 747-754.
- Brennan, J., Lu, C. C., Norris, D. P., Rodriguez, T. A., Beddington, R. S., and Robertson, E. J. (2001). "Nodal signalling in the epiblast patterns the early mouse embryo." Nature **411**(6840): 965-969.
- Brenner, D. J., Davis, B. R., Steigerwalt, A. G., Riddle, C. F., McWhorter, A. C., Allen, S. D., Farmer III, J. J., Saitoh, Y., and Fanning, G. R. (1982). "Atypical biogroups of *Escherichia coli* found in clinical specimens and description of *Escherichia hermannii* sp. nov." Journal of Clinical Microbiology **15**(4): 703-713.
- Brenner, D. J., McWhorter, A. C., Leete Knutson, J. K., and Steigerwalt, A. G. (1982). "*Escherichia vulneris*: a new species of Enterobacteriaceae associated with human wounds." Journal of Clinical Microbiology **15**(6): 1133-1140.
- Bruus, H. (2008). Theoretical microfluidics. Oxford master series in condensed matter physics, Oxford University Press Oxford.
- Buono, R., and Linser, P. (1991). "Transient expression of RSV-CAT in transgenic zebrafish made by electroporation." Molecular marine biology and biotechnology **1**(4-5): 271-275.
- Bureau, M., Gehl, J., Deleuze, V., Mir, L., and Scherman, D. (2000). "Importance of association between permeabilization and electrophoretic forces for intramuscular DNA electrotransfer." Biochimica et Biophysica Acta (BBA)-General Subjects **1474**(3): 353-359.
- Cai, H., Rose, K., Liang, L.-H., Dunham, S., and Stover, C. (2009). "Development of a liquid chromatography/mass spectrometry-based drug accumulation assay in *Pseudomonas aeruginosa*." Analytical Biochemistry **385**(2): 321-325.
- Cain, C. (2012). "Rediscovering antibiotics." SciBX: Science-Business eXchange **5**(46).
- Calvori, C., Frontali, L., Leoni, L., and Tecce, G. (1965). "Effect of rifamycin on protein synthesis." Nature **207**: 417-418.
- Cama, J., Bajaj, H., Pagliara, S., Maier, T., Braun, Y., Winterhalter, M., and Keyser, U. F. (2015). "Quantification of Fluoroquinolone Uptake through the Outer Membrane Channel OmpF of *Escherichia coli*." Journal of American Chemical Society **137**(43): 13836-13843.
- Cama, J., Chimerel, C., Pagliara, S., Javer, A., and Keyser, U. F. (2014). "A label-free microfluidic assay to quantitatively study antibiotic diffusion through lipid membranes." Lab on a Chip **14**(13): 2303-2308.
- Cama, J., Schaich, M., Al Nahas, K., Hernandez-Ainsa, S., Pagliara, S., and Keyser, U. F. (2016). "Direct Optofluidic Measurement of the Lipid Permeability of Fluoroquinolones." Scientific Reports **6**: 32824.

- Cama, J., Schaich, M., Al Nahas, K., Hernández-Ainsa, S., Pagliara, S., and Keyser, U. F. (2016). "Direct Optofluidic Measurement of the Lipid Permeability of Fluoroquinolones." *Scientific Reports* **6**.
- Campbell, N. A., and Reece, J. B. (2002). *Biology*. 6th, Menlo Park, California: Benjamin/Cummings Publishing Company, Inc.
- Campbell, S. A. (2001). *The science and engineering of microelectronic fabrication*, Oxford university press.
- Cantor, C. R., and Schimmel, P. R. (1981). "Biophysical Chemistry: Part II "Techniques for the study of Biological Structure and Function"." *Biochemical Education* **9**: 4.
- Carslaw, H. S., and Jaeger, J. C. (1959). "Conduction of heat in solids." *Oxford: Clarendon Press, 1959, 2nd ed.*
- Chapman, J. S., and Georgopapadakou, N. H. (1988). "Routes of quinolone permeation in *Escherichia coli*." *Antimicrobial Agents and Chemotherapy* **32**(4): 438-442.
- Chapman, J. S., and Georgopapadakou, N. H. (1989). "Fluorometric assay for fleroxacin uptake by bacterial cells." *Antimicrobial Agents and Chemotherapy* **33**(1): 27-29.
- Charier, S., Ruel, O., Baudin, J. B., Alcor, D., Allemand, J. F., Meglio, A., and Jullien, L. (2004). "An efficient fluorescent probe for ratiometric pH measurements in aqueous solutions." *Angewandte Chemie International Edition* **43**(36): 4785-4788.
- Chen, M., Yuan, L., and Liu, S. (2007). "Research on low-temperature anodic bonding using induction heating." *Sensors and Actuators A: Physical* **133**(1): 266-269.
- Chevalier, J., Atifi, S., Eyraud, A., Mahamoud, A., Barbe, J., and Pagès, J.-M. (2001). "New Pyridoquinoline Derivatives as Potential Inhibitors of the Fluoroquinolone Efflux Pump in Resistant *Enterobacter aerogenes* Strains." *Journal of Medicinal Chemistry* **44**(23): 4023-4026.
- Chevalier, J., Bredin, J., Mahamoud, A., Mallea, M., Barbe, J., and Pages, J. M. (2004). "Inhibitors of Antibiotic Efflux in Resistant *Enterobacter aerogenes* and *Klebsiella pneumoniae* Strains." *Antimicrobial Agents and Chemotherapy* **48**(3): 1043-1046.
- Chiao, M. (2008). Packaging (and Wire Bonding). *Encyclopedia of Microfluidics and Nanofluidics*. Li, D., SpringerUS.
- Choi, J., Jung, Y.-G., Kim, J., Kim, S., Jung, Y., Na, H., and Kwon, S. (2013). "Rapid antibiotic susceptibility testing by tracking single cell growth in a microfluidic agarose channel system." *Lab on a Chip* **13**(2): 280-287.
- Choi, J., Yoo, J., Kim, K.-j., Kim, E.-G., Park, K. O., Kim, H., Kim, H., Jung, H., Kim, T., and Choi, M. (2016). "Rapid drug susceptibility test of *Mycobacterium tuberculosis* using microscopic time-lapse imaging in an agarose matrix." *Applied Microbiology and Biotechnology* **100**(5): 2355-2365.
- Chou, H.-P., Unger, M. A., Scherer, A., and Quake, S. R. (2000). *Integrated Elastomer Fluidic Lab-On-A-Chip-Surface Patterning and DNA Diagnostics*. Proceedings of the Solid State Actuator and Sensor Workshop, Hilton Head, South Carolina, Citeseer.
- Cinquin, B., Maigre, L., Pinet, E., Chevalier, J., Stavenger, R. A., Mills, S., Réfrégiers, M., and Pagès, J.-M. (2015). "Microspectrometric insights on the uptake of antibiotics at the single bacterial cell level." *Scientific Reports* **5**: 17968.
- Coster, H. (1965). "A quantitative analysis of the voltage-current relationships of fixed charge membranes and the associated property of "punch-through"." *Biophysical journal* **5**(5): 669-686.
- Cowan, S. W., Schirmer, T., Rummel, G., Steiert, M., Ghosh, R., Pauptit, R. A., Jansonius, J. N., and Rosenbusch, J. P. (1992). "Crystal structures explain functional properties of two *E. coli* porins." *Nature* **358**(6389): 727-733.
- Craighead, H. (2006). "Future lab-on-a-chip technologies for interrogating individual molecules." *Nature* **442**(7101): 387-393.
- Crowley, J. M. (1973). "Electrical breakdown of bimolecular lipid membranes as an electromechanical instability." *Biophysical journal* **13**(7): 711-724.
- Darribère, T. (2003). *Le développement d'un mammifère: la souris*, Belin.
- Delcour, A. H. (1997). "Function and modulation of bacterial porins: insights from electrophysiology." *FEMS Microbiology Letters* **151**(2): 115-123.

- Delcour, A. H. (2009). "Outer membrane permeability and antibiotic resistance." Biochim Biophys Acta **1794**(5): 808-816.
- Delince, M. J., Bureau, J.-B., Lopez-Jiménez, A. T., Cosson, P., Soldati, T., and McKinney, J. D. (2016). "A microfluidic cell-trapping device for single-cell tracking of host-microbe interactions." Lab on a Chip **16**(17): 3276-3285.
- deMello, A. J. (2006). "Control and detection of chemical reactions in microfluidic systems." Nature **442**(7101): 394-402.
- Diver, J. M., Piddock, L. J. V., and Wise, R. (1990). "The accumulation of five quinolone antibacterial agents by *Escherichia coli*." Journal of Antimicrobial Chemotherapy **25**(3): 319-333.
- Doh, I., and Cho, Y.-H. (2005). "A continuous cell separation chip using hydrodynamic dielectrophoresis (DEP) process." Sensors and Actuators A: Physical **121**(1): 59-65.
- Drlica, K., and Zhao, X. (1997). "DNA gyrase, topoisomerase IV, and the 4-quinolones." Microbiology and Molecular Biology Reviews **61**(3): 377-392.
- Dusny, C., Grunberger, A., Probst, C., Wiechert, W., Kohlheyer, D., and Schmid, A. (2015). "Technical bias of microcultivation environments on single-cell physiology." Lab on a Chip **15**(8): 1822-1834.
- Edelstein, A., Amodaj, N., Hoover, K., Vale, R., and Stuurman, N. (2010). "Computer control of microscopes using microManager." Curr Protoc Mol Biol **Chapter 14**: Unit14 20.
- El-Ali, J., Sorger, P. K., and Jensen, K. F. (2006). "Cells on chips." Nature **442**(7101): 403.
- Elfving, A., LeMarc, Y., Baranyi, J., and Ballagi, A. (2004). "Observing Growth and Division of Large Numbers of Individual Bacteria by Image Analysis." Applied and Environmental Microbiology **70**(2): 675-678.
- Escoffre, J.-M., Portet, T., Wasungu, L., Teissié, J., Dean, D., and Rols, M.-P. (2009). "What is (still not) known of the mechanism by which electroporation mediates gene transfer and expression in cells and tissues." Molecular biotechnology **41**(3): 286-295.
- Eyer, K., Kuhn, P., Hanke, C., and Dittrich, P. S. (2012). "A microchamber array for single cell isolation and analysis of intracellular biomolecules." Lab on a Chip **12**(4): 765-772.
- Eyer, K., Stratz, S., Kuhn, P., Kuster, S. K., and Dittrich, P. S. (2013). "Implementing enzyme-linked immunosorbent assays on a microfluidic chip to quantify intracellular molecules in single cells." Analytical Chemistry **85**(6): 3280-3287.
- Eykyn, S. (1971). "Use and control of cephalosporins." Journal of Clinical Pathology **24**(5): 419.
- Eynard, N., Rols, M., Ganeva, V., Galutzov, B., Sabri, N., and Teissié, J. (1997). "Electrotransformation pathways of procaryotic and eucaryotic cells: recent developments." Bioelectrochemistry and Bioenergetics **44**(1): 103-110.
- Farmer III, J. J., Fanning, G. R., Davis, B. R., O'hara, C. M., Riddle, C., Hickman-Brenner, F. W., Asbury, M. A., Lowery, V. A., and Brenner, D. J. (1985). "*Escherichia fergusonii* and *Enterobacter taylorae*, two new species of *Enterobacteriaceae* isolated from clinical specimens." Journal of Clinical Microbiology **21**(1): 77-81.
- Faurie, C., Rebersek, M., Golzio, M., Kanduser, M., Escoffre, J. M., Pavlin, M., Teissie, J., Miklavcic, D., and Rols, M. P. (2010). "Electro - mediated gene transfer and expression are controlled by the life - time of DNA/membrane complex formation." The journal of gene medicine **12**(1): 117-125.
- Fertig, N., Blick, R. H., and Behrends, J. C. (2002). "Whole cell patch clamp recording performed on a planar glass chip." Biophysical Journal **82**(6): 3056-3062.
- Fleming, A. (1929). "On the antibacterial action of cultures of a penicillium, with special reference to their use in the isolation of B. influenzae." British Journal of Experimental Pathology **10**(3): 226.
- Fox, M., Esveld, D., Valero, A., Luttge, R., Mastwijk, H., Bartels, P., Van Den Berg, A., and Boom, R. (2006). "Electroporation of cells in microfluidic devices: a review." Analytical and bioanalytical chemistry **385**(3): 474.
- Freter, R., Brickner, H., Fekete, J., Vickerman, M. M., and Carey, K. E. (1983). "Survival and implantation of *Escherichia coli* in the intestinal tract." Infection and Immunity **39**(2): 686-703.

- Friedrich, U., Stachowicz, N., Simm, A., Fuhr, G., Lucas, K., and Zimmermann, U. (1998). "High efficiency electrotransfection with aluminum electrodes using microsecond controlled pulses." Bioelectrochemistry and bioenergetics **47**(1): 103-111.
- Fritzsche, F. S., Rosenthal, K., Kampert, A., Howitz, S., Dusny, C., Blank, L. M., and Schmid, A. (2013). "Picoliter nDEP traps enable time-resolved contactless single bacterial cell analysis in controlled microenvironments." Lab on a Chip **13**(3): 397-408.
- Galas, J. C., Haghiri-Gosnet, A. M., and Estevez-Torres, A. (2013). "A nanoliter-scale open chemical reactor." Lab on a Chip **13**(3): 415-423.
- Gallo, G. G., Lancini, G., and Parenti, F. (2013). Antibiotics: a multidisciplinary approach, Springer Science & Business Media.
- Gattass, R. R., and Mazur, E. (2008). "Femtosecond laser micromachining in transparent materials." Nature photonics **2**(4): 219-225.
- Geertz, M., Shore, D., and Maerkl, S. J. (2012). "Massively parallel measurements of molecular interaction kinetics on a microfluidic platform." Proceedings of the National Academy of Sciences **109**(41): 16540-16545.
- Gerber, D., Maerkl, S. J., and Quake, S. R. (2009). "An in vitro microfluidic approach to generating protein-interaction networks." Nature Methods **6**(1): 71-74.
- Ghale, G., Lanctôt, A. G., Kreissl, H. T., Jacob, M. H., Weingart, H., Winterhalter, M., and Nau, W. M. (2014). "Chemosensing ensembles for monitoring biomembrane transport in real time." Angewandte Chemie International Edition **53**(10): 2762-2765.
- Giuliani, A., Jamme, F., Rouam, V., Wien, F., Giorgetta, J. L., Lagarde, B., Chubar, O., Bac, S., Yao, I., Rey, S., Herbeaux, C., Marlats, J. L., Zerbib, D., Polack, F., and Refregiers, M. (2009). "DISCO: a low-energy multipurpose beamline at synchrotron SOLEIL." J Synchrotron Radiat **16**(Pt 6): 835-841.
- Golzio, M., Teissié, J., and Rols, M.-P. (2002). "Direct visualization at the single-cell level of electrically mediated gene delivery." Proceedings of the National Academy of Sciences **99**(3): 1292-1297.
- Goodman, M. B., and Lockery, S. R. (2000). "Pressure polishing: a method for re-shaping patch pipettes during fire polishing." Journal of Neuroscience Methods **100**(1): 13-15.
- Gosnet-Haghiri, A.-M., and Nanteuil, C. (2014). Method for manufacturing a microfluidic chip, and related chip and plate, Google Patents.
- Gosse, C., Bergaud, C., and Löw, P. (2009). Molecular probes for thermometry in microfluidic devices. Thermal Nanosystems and Nanomaterials, Springer: 301-341.
- Gowrishankar, T. R., and Weaver, J. C. (2003). "An approach to electrical modeling of single and multiple cells." Proceedings of the National Academy of Sciences **100**(6): 3203-3208.
- Greatorex, J. S., and Thorne, G. M. (1994). "Humoral immune responses to Shiga-like toxins and *Escherichia coli* O157 lipopolysaccharide in hemolytic-uremic syndrome patients and healthy subjects." Journal of Clinical Microbiology **32**(5): 1172-1178.
- Grunberger, A., Paczia, N., Probst, C., Schendzielorz, G., Eggeling, L., Noack, S., Wiechert, W., and Kohlheyer, D. (2012). "A disposable picolitre bioreactor for cultivation and investigation of industrially relevant bacteria on the single cell level." Lab on a Chip **12**(11): 2060-2068.
- Grünberger, A., Probst, C., Helfrich, S., Nanda, A., Stute, B., Wiechert, W., von Lieres, E., Nöh, K., Frunzke, J., and Kohlheyer, D. (2015). "Spatiotemporal microbial single - cell analysis using a high - throughput microfluidics cultivation platform." Cytometry Part A **87**(12): 1101-1115.
- Grunberger, A., Wiechert, W., and Kohlheyer, D. (2014). "Single-cell microfluidics: opportunity for bioprocess development." Current Opinion of Biotechnology **29**: 15-23.
- Hall, R. M., and Collis, C. M. (1995). "Mobile gene cassettes and integrons: capture and spread of genes by site - specific recombination." Molecular Microbiology **15**(4): 593-600.
- Hallo, L., Bourgeade, A., Tikhonchuk, V. T., Mezel, C., and Breil, J. (2007). "Model and numerical simulations of the propagation and absorption of a short laser pulse in a transparent dielectric material: Blast-wave launch and cavity formation." Physical Review B **76**(2): 024101.

- Hamdi, F. S., Français, O., Subra, F., Dufour-Gergam, E., and Le Pioufle, B. (2013). "Microarray of non-connected gold pads used as high density electric traps for parallelized pairing and fusion of cells." Biomicrofluidics **7**(4): 044101.
- Hanada, Y., Sugioka, K., Kawano, H., Ishikawa, I. S., Miyawaki, A., and Midorikawa, K. (2008). "Nano-aquarium for dynamic observation of living cells fabricated by femtosecond laser direct writing of photostructurable glass." Biomedical Microdevices **10**(3): 403-410.
- Hancock, R. E. W. (1987). "Role of porins in outer membrane permeability." Journal of Bacteriology **169**(3): 929.
- Hartl, D., Medhora, M., Green, L., and Dykhuizen, D. (1986). "The evolution of DNA sequences in *Escherichia coli*." Philosophical Transactions of the Royal Society of London B: Biological Sciences **312**(1154): 191-204.
- Hawkey, P. M. (1998). "The origins and molecular basis of antibiotic resistance." British Medical Journal **317**(7159): 657.
- Hays, E. E., Wells, I. C., Katzman, P. A., Cain, C. K., Jacobs, F. A., Thayer, S. A., Doisy, E. A., Gaby, W. L., Roberts, E. C., Muir, R. D., Carroll, C. J., and Jones, L. R. (1945). "Antibiotic Substances produced by *Pseudo-monas aeruginosa*." Biological Chemistry **159**(3): 725-750.
- He, Y.-Y., and Häder, D. P. (2002). "UV-B-induced formation of reactive oxygen species and oxidative damage of the cyanobacterium *Anabaena sp.*: protective effects of ascorbic acid and *N-acetyl-L-cysteine*." Journal of Photochemistry and Photobiology B: Biology **66**(2): 115-124.
- Health, U. D. o., and Services, H. (2013). "Antibiotic resistance threats in the United States, 2013." Atlanta: CDC.
- Heck, D. E., Vetrano, A. M., Mariano, T. M., and Laskin, J. D. (2003). "UVB light stimulates production of reactive oxygen species: unexpected role for catalase." Journal of Biological Chemistry **278**(25): 22432-22436.
- Heckele, M., and Schomburg, W. (2003). "Review on micro molding of thermoplastic polymers." Journal of Micromechanics and Microengineering **14**(3): R1.
- Hecker, M. T., Aron, D. C., Patel, N. P., Lehmann, M. K., and Donskey, C. J. (2003). "Unnecessary use of antimicrobials in hospitalized patients: current patterns of misuse with an emphasis on the antianaerobic spectrum of activity." Archives of Internal Medicine **163**(8): 972-978.
- Hermans, M., Gottmann, J., and Riedel, F. (2014). "Selective, laser-induced etching of fused silica at high scan-speeds using KOH." Journal of Laser Micro Nanoengineering **9**(2): 126.
- Hibino, M., Itoh, H., and Kinosita, K. (1993). "Time courses of cell electroporation as revealed by submicrosecond imaging of transmembrane potential." Biophysical journal **64**(6): 1789-1800.
- Hiramatsu, R., Matsuoka, T., Kimura-Yoshida, C., Han, S.-W., Mochida, K., Adachi, T., Takayama, S., and Matsuo, I. (2013). "External mechanical cues trigger the establishment of the anterior-posterior axis in early mouse embryos." Developmental cell **27**(2): 131-144.
- Hogg, S. (2013). Essential microbiology, John Wiley & Sons.
- Hooper, D., and Rubinstein, E. (2003). "Quinolone antimicrobial agents, ASM Press." Washington, DC.
- Hooper, D. C. (2000). "Mechanisms of action and resistance of older and newer fluoroquinolones." Clinical infectious diseases **31**(Supplement 2): S24-S28.
- Hooper, D. C. (2001). "Mechanisms of action of antimicrobials: focus on fluoroquinolones." Clinical infectious diseases **32**(Supplement 1): S9-S15.
- Hsieh, G.-W., Tsai, C.-H., and Lin, W.-C. (2005). "Anodic bonding of glass and silicon wafers with an intermediate silicon nitride film and its application to batch fabrication of SPM tip arrays." Microelectronics journal **36**(7): 678-682.
- Huys, G., Cnockaert, M., Janda, J. M., and Swings, J. (2003). "*Escherichia albertii* sp. nov., a diarrhoeagenic species isolated from stool specimens of Bangladeshi children." International Journal of Systematic and Evolutionary Microbiology **53**: 807-810.
- Iliescu, C., Chen, B., and Miao, J. (2008). "On the wet etching of Pyrex glass." Sensors and actuators A: Physical **143**(1): 154-161.

- Iliescu, C., Jing, J., Tay, F. E., Miao, J., and Sun, T. (2005). "Characterization of masking layers for deep wet etching of glass in an improved HF/HCl solution." Surface and Coatings Technology **198**(1): 314-318.
- Iliescu, C., Tay, F. E., and Miao, J. (2007). "Strategies in deep wet etching of Pyrex glass." Sensors and Actuators A: Physical **133**(2): 395-400.
- Inoue, I., Wakamoto, Y., Moriguchi, H., Okano, K., and Yasuda, K. (2001). "On-chip culture system for observation of isolated individual cells." Lab on a Chip **1**(1): 50-55.
- Ionescu-Zanetti, C., Blatz, A., and Khine, M. (2008). "Electrophoresis-assisted single-cell electroporation for efficient intracellular delivery." Biomedical microdevices **10**(1): 113-116.
- Ishii, Y., and Yanagida, T. (2000). "Single molecule detection in life sciences." Single Molecules **1**(1): 5-16.
- Jamme, F., Kascakova, S., Villette, S., Allouche, F., Pallu, S., Rouam, V., and Réfrégiers, M. (2013). "Deep UV autofluorescence microscopy for cell biology and tissue histology." Biologu of the Cell **105**(7): 277-288.
- Jamme, F., Villette, S., Giuliani, A., Rouam, V., Wien, F., Lagarde, B., and Réfrégiers, M. (2010). "Synchrotron UV fluorescence microscopy uncovers new probes in cells and tissues." Microscopy and Microanalysis **16**(5): 507-514.
- Janasek, D., Franzke, J., and Manz, A. (2006). "Scaling and the design of miniaturized chemical-analysis systems." Nature **442**(7101): 374.
- Jansen, H., Gardeniers, H., de Boer, M., Elwenspoek, M., and Fluitman, J. (1996). "A survey on the reactive ion etching of silicon in microtechnology." Journal of micromechanics and microengineering **6**(1): 14.
- Jena, R. K., Yue, C., Lam, Y., and Wang, Z. (2010). "High fidelity hot-embossing of COC microdevices using a one-step process without pre-annealing of polymer substrate." Sensors and Actuators B: Chemical **150**(2): 692-699.
- Jordan, C. A., Neumann, E., and Sowers, A. E. (2013). Electroporation and electrofusion in cell biology, Springer Science & Business Media.
- Kalimi, G. H., and Lo, C. W. (1988). "Communication compartments in the gastrulating mouse embryo." J Cell Biol **107**(1): 241-255.
- Kaper, J. B., Nataro, J. P., and Mobley, H. L. (2004). "Pathogenic *Escherichia coli*." Nature Reviews Microbiology **2**(2): 123-140.
- Karch, H., Tarr, P. I., and Bielaszewska, M. (2005). "Enterohaemorrhagic *Escherichia coli* in human medicine." International Journal of Medical Microbiology **295**(6-7): 405-418.
- Kascakova, S., Maigre, L., Chevalier, J., Réfrégiers, M., and Pagès, J.-M. (2012). "Antibiotic transport in resistant bacteria: synchrotron UV fluorescence microscopy to determine antibiotic accumulation with single cell resolution." PLoS One **7**(6): e38624.
- Kennedy, D. (2013). "Time to deal with antibiotics." Science **342**(6160): 777-777.
- Khine, M., Lau, A., Ionescu-Zanetti, C., Seo, J., and Lee, L. P. (2005). "A single cell electroporation chip." Lab on a Chip **5**(1): 38-43.
- King, D. E., Malone, R., and Lilley, S. H. (2000). "New classification and update on the quinolone antibiotics." American Family Physician **61**(9): 2741-2748.
- Kinosita, K., and Tsong, T. (1977). "Hemolysis of human erythrocytes by transient electric field." Proceedings of the National Academy of Sciences **74**(5): 1923-1927.
- Kitamura, K., Tokunaga, M., Iwane, A. H., and Yanagida, T. (1999). "A single myosin head moves along an actin filament with regular steps of 5.3 nanometres." Nature **397**(6715): 129-134.
- Kiyama, S., Matsuo, S., Hashimoto, S., and Morihira, Y. (2009). "Examination of etching agent and etching mechanism on femtosecond laser microfabrication of channels inside vitreous silica substrates." The Journal of Physical Chemistry C **113**(27): 11560-11566.
- Koebnik, R., Locher, K. P., and Van Gelder, P. (2000). "Structure and function of bacterial outer membrane proteins: barrels in a nutshell." Molecular Microbiology **37**(2): 239-253.
- Kohanski, M. A., Dwyer, D. J., and Collins, J. J. (2010). "How antibiotics kill bacteria: from targets to networks." Nature Reviews Microbiology **8**(6): 423-435.

- Kolari, K. (2008). "Deep plasma etching of glass with a silicon shadow mask." Sensors and Actuators A: Physical **141**(2): 677-684.
- Koronakis, V., Eswaran, J., and Hughes, C. (2004). "Structure and function of TolC: the bacterial exit duct for proteins and drugs." Annual Review of Biochemistry **73**: 467-489.
- Kortmann, H., Chasanis, P., Blank, L. M., Franzke, J., Kenig, E. Y., and Schmid, A. (2009). "The Envirostat - a new bioreactor concept." Lab on a Chip **9**(4): 576-585.
- Kramer, C. E., Singh, A., Helfrich, S., Grunberger, A., Wiechert, W., Noh, K., and Kohlheyer, D. (2015). "Non-Invasive Microbial Metabolic Activity Sensing at Single Cell Level by Perfusion of Calcein Acetoxymethyl Ester." PLoS One **10**(10): e0141768.
- Kresge, N., Simoni, R. D., and Hill, R. L. (2004). "Selman Waksman: the father of antibiotics." Journal of Biological Chemistry **279**(48): e7-e7.
- Leekha, S., Terrell, C. L., and Edson, R. S. (2011). "General principles of antimicrobial therapy." Mayo Clin Proc **86**(2): 156-167.
- Lesch, J. E. (2007). The first miracle drugs: how the sulfa drugs transformed medicine, Oxford University Press, USA.
- Leshner, G. Y., Froelich, E. J., Gruett, M. D., Bailey, J. H., and Brundage, R. P. (1962). "1, 8-Naphthyridine derivatives. A new class of chemotherapeutic agents." Journal of Medicinal Chemistry **5**(5): 1063-1065.
- Levine, D. P. (2006). "Vancomycin: a history." Clinical Infectious Diseases **42**(Supplement 1): S5-S12.
- Li, B., Yao, Q., Pan, X. C., Wang, N., Zhang, R., Li, J., Ding, G., Liu, X., Wu, C., Ran, D., Zheng, J., and Zhou, H. (2011). "Artesunate enhances the antibacterial effect of β -lactam antibiotics against *Escherichia coli* by increasing antibiotic accumulation via inhibition of the multidrug efflux pump system AcrAB-TolC." Journal of Antimicrobial Chemotherapy **66**(4): 769-777.
- Li, X., Abe, T., and Esashi, M. (2001). "Deep reactive ion etching of Pyrex glass using SF₆ plasma." Sensors and actuators A: Physical **87**(3): 139-145.
- Li, X., Ling, L., Hua, X., Fukasawa, M., Oehrlein, G. S., Barela, M., and Anderson, H. M. (2003). "Effects of Ar and O₂ additives on SiO₂ etching in C₄F₈-based plasmas." Journal of Vacuum Science & Technology A: Vacuum, Surfaces, and Films **21**(1): 284-293.
- Lim, S. P., and Nikaido, H. (2010). "Kinetic parameters of efflux of penicillins by the multidrug efflux transporter AcrAB-TolC of *Escherichia coli*." Antimicrobial Agents and Chemotherapy **54**(5): 1800-1806.
- Lin, Y.-C., Jen, C.-M., Huang, M.-Y., Wu, C.-Y., and Lin, X.-Z. (2001). "Electroporation microchips for continuous gene transfection." Sensors and Actuators B: Chemical **79**(2): 137-143.
- Liu, S., Jin, D., Lan, R., Wang, Y., Meng, Q., Dai, H., Lu, S., Hu, S., and Xu, J. (2015). "*Escherichia marmotae* sp. nov., isolated from faeces of *Marmota himalayana* in Qinghai-Tibet Plateau China." International Journal of Systematic and Evolutionary Microbiology **65**(7): 2130-2134.
- Livermore, D. (2004). "The need for new antibiotics." Clinical Microbiology and Infection **10**(s4): 1-9.
- Loder, B., Newton, G. G. F., and Abraham, E. P. (1961). "The cephalosporin C nucleus (7-aminocephalosporanic acid) and some of its derivatives." Biochemical Journal **79**(2): 408.
- Lomovskaya, O., Warren, M. S., Lee, A., Galazzo, J., Fronko, R., Lee, M., Blais, J., Cho, D., Chamberland, S., Renau, T., Leger, R., Hecker, S., Watkins, W., Hoshino, K., Ishida, H., and Lee, V. J. (2001). "Identification and characterization of inhibitors of multidrug resistance efflux pumps in *Pseudomonas aeruginosa*: novel agents for combination therapy." Antimicrob Agents and Chemotherapy **45**(1): 105-116.
- Long, Z., Nugent, E., Javer, A., Cicuta, P., Sclavi, B., Lagomarsino, M. C., and Dorfman, K. D. (2013). "Microfluidic chemostat for measuring single cell dynamics in bacteria." Lab on a Chip **13**(5): 947-954.
- Loste, F., Eynard, N., and Teissie, J. (1998). "Direct monitoring of the field strength during electropulsation." Bioelectrochemistry and bioenergetics **47**(1): 119-127.
- Lu, H., Schmidt, M. A., and Jensen, K. F. (2005). "A microfluidic electroporation device for cell lysis." Lab on a Chip **5**(1): 23-29.
- MacDonald, J. (1967). Pyocyanine. Biosynthesis, Springer: 52-65.

- Macfarlane, G., and Taylor, F. (1979). Howard Florey: the making of a great scientist, Oxford University Press Oxford.
- Maerkl, S. J., and Quake, S. R. (2007). "A systems approach to measuring the binding energy landscapes of transcription factors." Science **315**(5809): 233-237.
- Mao, S., Quéré, F., Guizard, S., Mao, X., Russo, R., Petite, G., and Martin, P. (2004). "Dynamics of femtosecond laser interactions with dielectrics." Applied Physics A: Materials Science & Processing **79**(7): 1695-1709.
- Marcinkevičius, A., Juodkakis, S., Watanabe, M., Miwa, M., Matsuo, S., Misawa, H., and Nishii, J. (2001). "Femtosecond laser-assisted three-dimensional microfabrication in silica." Optics Letters **26**(5): 277-279.
- Markx, G. H., Talary, M. S., and Pethig, R. (1994). "Separation of viable and non-viable yeast using dielectrophoresis." Journal of Biotechnology **32**(1): 29-37.
- Matchette, L. S., Agrawal, A., and Pfefer, T. J. (2007). "Fluoroquinolone Antibiotics Having the Potential to Interfere with Fluorescence-Based Diagnosis." Photochemistry and Photobiology **83**(6): 1386-1393.
- Mather, W., Mondragon-Palomino, O., Danino, T., Hasty, J., and Tsimring, L. S. (2010). "Streaming instability in growing cell populations." Physical Review Letters **104**(20): 208101.
- Mazari, E., Mantelet, M., Iranzo, J., Perea-Gomez, A., and Gosse, C. (2011). Localized electroporation of mouse embryo using dielectric guides. Solid-State Sensors, Actuators and Microsystems Conference (TRANSDUCERS), 2011 16th International, IEEE.
- Mazari, E., Zhao, X., Collignon, J., Perea-Gomez, A., and Gosse, C. "ON CHIP SPATIOTEMPORAL ELECTRIC FIELD SHAPING TO LOCALLY ELECTROPORATE CELL MARKERS INTO MOUSE EMBRYONIC TISSUES."
- Mazari, E., Zhao, X., Migeotte, I., Collignon, J., Gosse, C., and Perea-Gomez, A. (2014). "A microdevice to locally electroporate embryos with high efficiency and reduced cell damage." Development **141**(11): 2349-2359.
- Meulemans, C. C. E. (1987). "The Basic Principles of UV–Disinfection of Water." Ozone: Science & Engineering **9**(4): 299-313.
- Minoshima, K., Kowalevicz, A. M., Hartl, I., Ippen, E. P., and Fujimoto, J. G. (2001). "Photonic device fabrication in glass by use of nonlinear materials processing with a femtosecond laser oscillator." Optics Letters **26**(19): 1516-1518.
- Mir, L. M., Banoun, H., and Paoletti, C. (1988). "Introduction of definite amounts of nonpermeant molecules into living cells after electropermeabilization: direct access to the cytosol." Experimental cell research **175**(1): 15-25.
- Misawa, H., and Juodkakis, S. (2006). 3D laser microfabrication: principles and applications, John Wiley & Sons.
- Moffitt, J. R., Lee, J. B., and Cluzel, P. (2012). "The single-cell chemostat: an agarose-based, microfluidic device for high-throughput, single-cell studies of bacteria and bacterial communities." Lab on a Chip **12**(8): 1487-1494.
- Morel, M., Galas, J.-C., Dahan, M., and Studer, V. (2012). "Concentration landscape generators for shear free dynamic chemical stimulation." Lab on a Chip **12**(7): 1340-1346.
- Mortimer, P. G., and Piddok, L. J. (1993). "The accumulation of five antibacterial agents in porin-deficient mutants of *Escherichia coli*." Journal of Antimicrobial Chemotherapy **32**(2): 195-213.
- Mortimer, P. G. S., and Piddock, L. J. V. (1991). "A comparison of methods used for measuring the accumulation of quinolones by Enterobacteriaceae, *Pseudomonas aeruginosa* and *Staphylococcus aureus*." Journal of Antimicrobial Chemotherapy **28**(5): 639-653.
- Mustafi, N., Grunberger, A., Mahr, R., Helfrich, S., Noh, K., Blombach, B., Kohlheyer, D., and Frunzke, J. (2014). "Application of a genetically encoded biosensor for live cell imaging of L-valine production in pyruvate dehydrogenase complex-deficient *Corynebacterium glutamicum* strains." PLoS One **9**(1): e85731.
- Nakamura, H. (2009). Electroporation and sonoporation in developmental biology, Springer Science & Business Media.

- Namatsu, H., Yamaguchi, T., Nagase, M., Yamazaki, K., and Kurihara, K. (1998). "Nano-patterning of a hydrogen silsesquioxane resist with reduced linewidth fluctuations." Microelectronic Engineering **41**: 331-334.
- Nesme, J., Cecillon, S., Delmont, T. O., Monier, J.-M., Vogel, T. M., and Simonet, P. (2014). "Large-scale metagenomic-based study of antibiotic resistance in the environment." Current Biology **24**(10): 1096-1100.
- Neumann, E., and Rosenheck, K. (1972). "Permeability changes induced by electric impulses in vesicular membranes." Journal of Membrane Biology **10**(1): 279-290.
- Neumann, E., Schaefer-Ridder, M., Wang, Y., and Hofschneider, P. (1982). "Gene transfer into mouse lymphoma cells by electroporation in high electric fields." The EMBO journal **1**(7): 841.
- Nikaido, H. (1989). "Outer membrane barrier as a mechanism of antimicrobial resistance." Antimicrobial Agents and Chemotherapy **33**(11): 1831.
- Nikaido, H., and Rosenberg, E. Y. (1981). "Effect on solute size on diffusion rates through the transmembrane pores of the outer membrane of *Escherichia coli*." Journal of General Physiology **77**(2): 121-135.
- Nikaido, H., and Rosenberg, E. Y. (1983). "Porin channels in *Escherichia coli*: studies with beta-lactams in intact cells." Journal of Bacteriology **153**(1): 232-240.
- Nikaido, H., and Rosenberg, E. Y. (1983). "Porin channels in *Escherichia coli*: studies with liposomes reconstituted from purified proteins." Journal of Bacteriology **153**(1): 241-252.
- Nikaido, H., and Takatsuka, Y. (2009). "Mechanisms of RND multidrug efflux pumps." Biochim Biophys Acta **1794**(5): 769-781.
- Nikaido, H., and Takatsuka, Y. (2009). "Mechanisms of RND multidrug efflux pumps." Biochimica et Biophysica Acta **1794**(5): 769-781.
- Niklaus, F., Enoksson, P., Griss, P., Kalvesten, E., and Stemme, G. (2001). "Low-temperature wafer-level transfer bonding." Journal of microelectromechanical systems **10**(4): 525-531.
- Noguchi, H., Matsuhashi, M., and Mitsuhashi, S. (1979). "Comparative Studies of Penicillin - Binding Proteins in *Pseudomonas aeruginosa* and *Escherichia coli*." The FEBS Journal **100**(1): 41-49.
- Nolte, S., Will, M., Burghoff, J., and Tuennermann, A. (2003). "Femtosecond waveguide writing: a new avenue to three-dimensional integrated optics." Applied Physics A: Materials Science & Processing **77**(1): 109-111.
- Nomenclature, J. C. o. t. I. C. o. B. (1958). "Conservation of the family name Enterobacteriaceae, of the name of the type genus, and designation of the type species, Opinion No. 15." International Bulletin of Bacteriological Nomenclature and Taxonomy **8**: 73-74.
- Norman, T. M., Lord, N. D., Paulsson, J., and Losick, R. (2013). "Memory and modularity in cell-fate decision making." Nature **503**(7477): 481-486.
- Norris, D. P., Brennan, J., Bikoff, E. K., and Robertson, E. J. (2002). "The Foxh1-dependent autoregulatory enhancer controls the level of Nodal signals in the mouse embryo." Development **129**(14): 3455-3468.
- O'Neill, J. (2015). "Antimicrobials in agriculture and the environment: reducing unnecessary use and waste." The review on antimicrobial resistance.
- Okada, Y., and Hirokawa, N. (1999). "A processive single-headed motor: kinesin superfamily protein KIF1A." Science **283**(5405): 1152-1157.
- Okusu, H., Ma, D., and Nikaido, H. (1996). "AcrAB efflux pump plays a major role in the antibiotic resistance phenotype of *Escherichia coli* multiple-antibiotic-resistance (Mar) mutants." Journal of bacteriology **178**(1): 306-308.
- Organization, W. H. (2014). Antimicrobial resistance: global report on surveillance, World Health Organization.
- Orlowski, S., and Mir, L. M. (1993). "Cell electropermeabilization: a new tool for biochemical and pharmacological studies." Biochimica et Biophysica Acta (BBA)-Reviews on Biomembranes **1154**(1): 51-63.

- Pages, J.-M., James, C. E., and Winterhalter, M. (2008). "The porin and the permeating antibiotic: a selective diffusion barrier in Gram-negative bacteria." Nature Reviews Microbiology **6**(12): 893-903.
- Pagès, J.-M., James, C. E., and Winterhalter, M. (2008). "The porin and the permeating antibiotic: a selective diffusion barrier in Gram-negative bacteria." Nature Reviews Microbiology **6**(12): 893-903.
- Pagès, J. M., and Amaral, L. (2009). "Mechanisms of drug efflux and strategies to combat them: challenging the efflux pump of Gram-negative bacteria." Biochim Biophys Acta **1794**(5): 826-833.
- Park, J., Wu, J., Polymenis, M., and Han, A. (2013). "Microchemostat array with small-volume fraction replenishment for steady-state microbial culture." Lab on a Chip **13**(21): 4217-4224.
- Pasteur, L., and Vallery-Radot, P. (1933). Oeuvres de Pasteur: Maladies virulentes, virus-vaccins et prophylaxie de la rage, Masson et Cie.
- Pattison, D. I., and Davies, M. J. (2006). Actions of ultraviolet light on cellular structures. Cancer: cell structures, carcinogens and genomic instability. Bignold, L. P., Springer: 131-157.
- Peitz, I., and van Leeuwen, R. (2010). "Single-cell bacteria growth monitoring by automated DEP-facilitated image analysis." Lab on a Chip **10**(21): 2944-2951.
- Phetsang, W., Blaskovich, M. A., Butler, M. S., Huang, J. X., Zuegg, J., Mamidyala, S. K., Ramu, S., Kavanagh, A. M., and Cooper, M. A. (2014). "An azido-oxazolidinone antibiotic for live bacterial cell imaging and generation of antibiotic variants." Bioorganic and Medicinal Chemistry **22**(16): 4490-4498.
- Phetsang, W., Pelingon, R., Butler, M. S., KC, S., Pitt, M., Kaeslin, G., Cooper, M. A., and Blaskovich, M. A. T. (2016). "Fluorescent Trimethoprim Conjugate Probes To Assess Drug Accumulation in Wild Type and Mutant Escherichia coli." ACS Infectious Diseases **2**(10): 688-701.
- Piddock, L. J. (2006). "Clinically relevant chromosomally encoded multidrug resistance efflux pumps in bacteria." Clinical Microbiology Reviews **19**(2): 382-402.
- Piddock, L. J. V. (2006). "Multidrug-resistance efflux pumps? not just for resistance." Nature Reviews Microbiology **4**(8): 629-636.
- Pohl, H. A. (1978). Dielectrophoresis: the behavior of neutral matter in nonuniform electric fields, Cambridge university press Cambridge.
- Poulsen, L. K., Lan, F., Kristensen, C. S., Hobolth, P., Molin, S., and Krogfelt, K. A. (1994). "Spatial distribution of Escherichia coli in the mouse large intestine inferred from rRNA in situ hybridization." Infection and Immunity **62**(11): 5191-5194.
- Pray, L. A. (2008). "Transposons: The jumping genes." Nature Education **1**(1): 204.
- Prevention, C. f. D. C. (2013). Antibiotic resistance threats in the United States, 2013, Centres for Disease Control and Prevention, US Department of Health and Human Services.
- Probst, C., Grünberger, A., Braun, N., Helfrich, S., Nöh, K., Wiechert, W., and Kohlheyer, D. (2015). "Rapid inoculation of single bacteria into parallel picoliter fermentation chambers." Analytical Methods **7**(1): 91-98.
- Probst, C., Grünberger, A., Wiechert, W., and Kohlheyer, D. (2013). "Microfluidic growth chambers with optical tweezers for full spatial single-cell control and analysis of evolving microbes." Journal of Microbiological Methods **95**(3): 470-476.
- Psaltis, D., Quake, S. R., and Yang, C. (2006). "Developing optofluidic technology through the fusion of microfluidics and optics." nature **442**(7101): 381.
- Pu, Y., Zhao, Z., Li, Y., Zou, J., Ma, Q., Zhao, Y., Ke, Y., Zhu, Y., Chen, H., and Baker, M. A. B. (2016). "Enhanced efflux activity facilitates drug tolerance in dormant bacterial cells." Molecular cell **62**(2): 284-294.
- Pu, Y., Zhao, Z., Li, Y., Zou, J., Ma, Q., Zhao, Y., Ke, Y., Zhu, Y., Chen, H., Baker, M. A. B., Ge, H., Sun, Y., Xie, X. S., and Bai, F. (2016). "Enhanced Efflux Activity Facilitates Drug Tolerance in Dormant Bacterial Cells." Molecular Cell **62**(2): 284-294.
- Pucihar, G., Kotnik, T., Miklavčič, D., and Teissié, J. (2008). "Kinetics of transmembrane transport of small molecules into electroporabilized cells." Biophysical journal **95**(6): 2837-2848.

- Pucihar, G., Kotnik, T., Valič, B., and Miklavčič, D. (2006). "Numerical determination of transmembrane voltage induced on irregularly shaped cells." Annals of biomedical engineering **34**(4): 642.
- Pucihar, G., Miklavcic, D., and Kotnik, T. (2009). "A time-dependent numerical model of transmembrane voltage inducement and electroporation of irregularly shaped cells." IEEE Transactions on Biomedical Engineering **56**(5): 1491-1501.
- Raja, S. B., Murali, M. R., and Devaraj, S. N. (2008). "Differential expression of ompC and ompF in multidrug-resistant *Shigella dysenteriae* and *Shigella flexneri* by aqueous extract of *Aegle marmelos*, altering its susceptibility toward beta-lactam antibiotics." Diagnostic Microbiology and Infectious Disease **61**(3): 321-328.
- Rajesh, S., and Bellouard, Y. (2010). "Towards fast femtosecond laser micromachining of fused silica: The effect of deposited energy." Optics express **18**(20): 21490-21497.
- Roberts, W. (1874). "Studies on biogenesis." Philosophical Transactions of the Royal Society of London **164**: 457-477.
- Rols, M.-P. (2016). *Gene Delivery by Electroporation In Vitro: Mechanisms*, Springer International Publishing.
- Rols, M.-P., Delteil, C., Golzio, M., Dumond, P., Cros, S., and Teissie, J. (1998). "In vivo electrically mediated protein and gene transfer in murine melanoma." Nature biotechnology **16**(2): 168-171.
- Rols, M.-P., Golzio, M., Delteil, C., and Teissie, J. (2000). "In vitro delivery of drugs and other molecules to cells." Electrochemotherapy, Electrogenotherapy, and Transdermal Drug Delivery: Electrically Mediated Delivery of Molecules to Cells: 83-97.
- Rols, M.-P., and Teissie, J. (1990). "Electropermeabilization of mammalian cells. Quantitative analysis of the phenomenon." Biophysical journal **58**(5): 1089-1098.
- Rols, M.-P., and Teissie, J. (1998). "Electropermeabilization of mammalian cells to macromolecules: control by pulse duration." Biophysical journal **75**(3): 1415-1423.
- Rubinstein, E. (2001). "History of quinolones and their side effects." Chemotherapy **47**(Suppl 3): 3-8.
- Rueger, N., Doemling, M., Schaepkens, M., Beulens, J., Standaert, T., and Oehrlein, G. (1999). "Selective etching of SiO₂ over polycrystalline silicon using CHF₃ in an inductively coupled plasma reactor." Journal of Vacuum Science & Technology A: Vacuum, Surfaces, and Films **17**(5): 2492-2502.
- Ruiz, N., Kahne, D., and Silhavy, T. J. (2006). "Advances in understanding bacterial outer-membrane biogenesis." Nature Reviews Microbiology **4**(1): 57-66.
- Sale, A., and Hamilton, W. (1968). "Effects of high electric fields on micro-organisms: III. Lysis of erythrocytes and protoplasts." Biochimica et Biophysica Acta (BBA)-Biomembranes **163**(1): 37-43.
- Santos, A. L., Moreirinha, C., Lopes, D., Esteves, A. C., Henriques, I., Almeida, A., Domingues, M. R. r. M., Delgado, I., Correia, A. n., and Cunha, A. n. (2013). "Effects of UV radiation on the lipids and proteins of bacteria studied by mid-infrared spectroscopy." Environmental Science and Technology **47**(12): 6306-6315.
- Schatz, A., and Waksman, S. A. (1944). "Effect of Streptomycin and Other Antibiotic Substances upon *Mycobacterium tuberculosis* and Related Organisms." Experimental Biology and Medicine **57**(2): 244-248.
- Schindelin, J., Arganda-Carreras, I., Frise, E., Kaynig, V., Longair, M., Pietzsch, T., Preibisch, S., Rueden, C., Saalfeld, S., Schmid, B., Tinevez, J. Y., White, D. J., Hartenstein, V., Eliceiri, K., Tomancak, P., and Cardona, A. (2012). "Fiji: an open-source platform for biological-image analysis." Nat Methods **9**(7): 676-682.
- Schirmer, T. (1998). "General and specific porins from bacterial outer membranes." Journal of Structural Biology **121**(2): 101-109.
- Selander, R. K., Caugant, D. A., and Whittam, T. S. (1987). Genetic structure and variation in natural populations of *Escherichia coli*.

- Shales, S. W., Chopra, I., and Ball, P. R. (1980). "Evidence for more than one mechanism of plasmid-determined tetracycline resistance in *Escherichia coli*." Journal of General Microbiology **121**(1): 221-229.
- Sheehan, J. C. (1967). "The chemistry of synthetic and semisynthetic penicillins." Annals of the New York Academy of Sciences **145**(1): 216-223.
- Shoji, S. (1990). Photoetching and electrochemical discharge drilling of Pyrex glass. Technical Digest of the 9th Sensor Symposium.
- Si, F., Li, B., Margolin, W., and Sun, S. X. (2015). "Bacterial growth and form under mechanical compression." Scientific Reports **5**: 11367.
- Silver, L. L. (2011). "Challenges of antibacterial discovery." Clinical Microbiology Reviews **24**(1): 71-109.
- Smil, V. (2005). Creating the twentieth century: Technical innovations of 1867-1914 and their lasting impact, Oxford University Press.
- Sood, S., Farrens, S., Pinker, R., Xie, J., and Cataby, W. (2010). "Al-Ge eutectic wafer bonding and bond characterization for CMOS compatible wafer packaging." ECS Transactions **33**(4): 93-101.
- Spratt, B. G. (1977). "Properties of the Penicillin - Binding Proteins of *Escherichia coli* K12." European Journal of Biochemistry **72**(2): 341-352.
- Srinivas, S. (2006). "The anterior visceral endoderm—turning heads." Genesis **44**(11): 565-572.
- Stapulionis, R. (1999). "Electric pulse-induced precipitation of biological macromolecules in electroporation." Bioelectrochemistry and bioenergetics **48**(1): 249-254.
- Stewart, P. S. (1996). "Theoretical aspects of antibiotic diffusion into microbial biofilms." Antimicrobial Agents and Chemotherapy **40**(11): 2517-2522.
- Stone, H. A., Stroock, A. D., and Ajdari, A. (2004). "Engineering flows in small devices: microfluidics toward a lab-on-a-chip." Annu. Rev. Fluid Mech. **36**: 381-411.
- Stratz, S., Eyer, K., Kurth, F., and Dittrich, P. S. (2014). "On-chip enzyme quantification of single *Escherichia coli* bacteria by immunoassay-based analysis." Analytical Chemistry **86**(24): 12375-12381.
- Sudsiri, J., Wachner, D., and Gimsa, J. (2007). "On the temperature dependence of the dielectric membrane properties of human red blood cells." Bioelectrochemistry **70**(1): 134-140.
- Suginaka, H., Blumberg, P. M., and Strominger, J. L. (1972). "Multiple penicillin-binding components in *Bacillus subtilis*, *Bacillus cereus*, *Staphylococcus aureus*, and *Escherichia coli*." Journal of Biological Chemistry **247**(17): 5279-5288.
- Sukas, S., Schreuder, E., de Wagenaar, B., Swennenhuis, J., van den Berg, A., Terstappen, L., and Le Gac, S. (2014). "A novel side electrode configuration integrated in fused silica microsystems for synchronous optical and electrical spectroscopy." Lab on a Chip **14**(11): 1821-1825.
- Sukharev, S., Klenchin, V., Serov, S., Chernomordik, L., and YuA, C. (1992). "Electroporation and electrophoretic DNA transfer into cells. The effect of DNA interaction with electropores." Biophysical journal **63**(5): 1320-1327.
- Swingle, W. T., and Briggs, L. J. (1907). "Improvements in the Ultra-Violet Microscope." Science: 180-183.
- Tabeling, P. (2006). Introduction to Microfluidics Oxford University Press, Oxford, England ISBN.
- Takaoka, K., Yamamoto, M., and Hamada, H. (2007). "Origin of body axes in the mouse embryo." Current opinion in genetics & development **17**(4): 344-350.
- Teissie, J., and Rols, M.-P. (1993). "An experimental evaluation of the critical potential difference inducing cell membrane electroporation." Biophysical journal **65**(1): 409-413.
- Temnov, V., Sokolowski-Tinten, K., Zhou, P., El-Khamhawy, A., and Von Der Linde, D. (2006). "Multiphoton ionization in dielectrics: comparison of circular and linear polarization." Physical review letters **97**(23): 237403.
- Tenaillon, O., Skurnik, D., Picard, B., and Denamur, E. (2010). "The population genetics of commensal *Escherichia coli*." Nature Reviews Microbiology **8**(3): 207-217.

- Teng, S.-W., Mukherji, S., Moffitt, J. R., De Buyl, S., and O'shea, E. K. (2013). "Robust circadian oscillations in growing cyanobacteria require transcriptional feedback." Science **340**(6133): 737-740.
- Terry, S. C., Jerman, J. H., and Angell, J. B. (1979). "A gas chromatographic air analyzer fabricated on a silicon wafer." IEEE Transactions on Electron Devices **26**(12): 1880-1886.
- Thiénot, E., Domingo, F., Cambril, E., and Gosse, C. (2006). "Reactive ion etching of glass for biochip applications: Composition effects and surface damages." Microelectronic engineering **83**(4): 1155-1158.
- Tomov, T., and Tsoneva, I. (2000). "Are the stainless steel electrodes inert?" Bioelectrochemistry **51**(2): 207-209.
- Tong, Q.-Y. (2001). "Wafer bonding for integrated materials." Materials Science and Engineering: B **87**(3): 323-328.
- Tong, Q.-Y., and Goesele, U. (1999). Semiconductor wafer bonding: science and technology, John Wiley.
- Tudryn, C., Schweizer, S., Hopkins, R., Hobbs, L., and Garratt-Reed, A. J. (2005). "Characterization of Si and CVD SiC to glass anodic bonding using TEM and STEM analysis." Journal of the Electrochemical Society **152**(4): E131-E134.
- Tyndall, J. (1876). "The optical department of the atmosphere in relation to the phenomena of putrefaction and infection." Philosophical Transactions of the Royal Society of London **166**: 27-74.
- Ullman, G., Wallden, M., Marklund, E. G., Mahmutovic, A., Razinkov, I., and Elf, J. (2013). "High-throughput gene expression analysis at the level of single proteins using a microfluidic turbidostat and automated cell tracking." Philosophical Transactions of the Royal Society of London B: Biological Sciences **368**(1611): 20120025.
- Ullman, G., Wallden, M., Marklund, E. G., Mahmutovic, A., Razinkov, I., and Elf, J. (2013). "High-throughput gene expression analysis at the level of single proteins using a microfluidic turbidostat and automated cell tracking." Philosophical Transactions of the Royal Society B: Biological **368**(1611): 20120025.
- Unger, M. A. (2000). "Monolithic Microfabricated Valves and Pumps by Multilayer Soft Lithography." Science **288**(5463): 113-116.
- Valič, B., Golzio, M., Pavlin, M., Schatz, A., Faurie, C., Gabriel, B., Teissié, J., Rols, M.-P., and Miklavčič, D. (2003). "Effect of electric field induced transmembrane potential on spheroidal cells: theory and experiment." European Biophysics Journal **32**(6): 519-528.
- van Leest, T., and Caro, J. (2013). "Cavity-enhanced optical trapping of bacteria using a silicon photonic crystal." Lab on a Chip **13**(22): 4358-4365.
- Verchère, A., Dezi, M., Adrien, V., Broutin, I., and Picard, M. (2015). "*In vitro* transport activity of the fully assembled MexAB-OprM efflux pump from *Pseudomonas aeruginosa*." Nature Communications **6**.
- Viotti, M., Niu, L., Shi, S.-H., and Hadjantonakis, A.-K. (2012). "Role of the gut endoderm in relaying left-right patterning in mice." PLoS Biol **10**(3): e1001276.
- Visscher, K., Schnitzer, M. J., and Block, S. M. (1999). "Single kinesin molecules studied with a molecular force clamp." Nature **400**(6740): 184-189.
- Viveiros, M., Jesus, A., Brito, M., Leandro, C., Martins, M., Ordway, D., Molnar, A. M., Molnar, J., and Amaral, L. (2005). "Inducement and reversal of tetracycline resistance in *Escherichia coli* K-12 and expression of proton gradient-dependent multidrug efflux pump genes." Antimicrobial Agents and Chemotherapy **49**(8): 3578-3582.
- Viveiros, M., Jesus, A., Brito, M., Leandro, C., Martins, M., Ordway, D., Molnar, A. M., Molnar, J., and Amaral, L. (2005). "Inducement and reversal of tetracycline resistance in *Escherichia coli* K-12 and expression of proton gradient-dependent multidrug efflux pump genes." Antimicrob Agents Chemother **49**(8): 3578-3582.
- Voldman, J., Gray, M. L., and Schmidt, M. A. (1999). "Microfabrication in biology and medicine." Annual review of biomedical engineering **1**(1): 401-425.

- Von der Linde, D., Sokolowski-Tinten, K., and Bialkowski, J. (1997). "Laser–solid interaction in the femtosecond time regime." *Applied Surface Science* **109**: 1-10.
- Wagnières, G. A., Star, W. M., and Wilson, B. C. (1998). "In vivo fluorescence spectroscopy and imaging for oncological applications." *Photochemistry and Photobiology* **68**(5): 603-632.
- Wakamoto, Y., Ramsden, J., and Yasuda, K. (2005). "Single-cell growth and division dynamics showing epigenetic correlations." *Analyst* **130**(3): 311-317.
- Wallis, G. (1975). "Field assisted glass sealing." *Active and Passive Electronic Components* **2**(1): 45-53.
- Wallis, G., and Pomerantz, D. I. (1969). "Field assisted glass - metal sealing." *Journal of applied physics* **40**(10): 3946-3949.
- Wang, P., Robert, L., Pelletier, J., Dang, W. L., Taddei, F., Wright, A., and Jun, S. (2010). "Robust growth of Escherichia coli." *Current Biology* **20**(12): 1099-1103.
- Wang, Y., Ran, M., Wang, J., Ouyang, Q., and Luo, C. (2015). "Studies of Antibiotic Resistance of Beta-Lactamase Bacteria under Different Nutrition Limitations at the Single-Cell Level." *PLoS One* **10**(5): e0127115.
- Watson, J. D. (1992). *Recombinant Dna*, Macmillan.
- Weaver, J. C. (1993). "Electroporation: a general phenomenon for manipulating cells and tissues." *Journal of cellular biochemistry* **51**(4): 426-435.
- Wensink, H., Berenschot, J., Jansen, H. V., and Elwenspoek, M. C. (2000). *High resolution powder blast micromachining*. Micro Electro Mechanical Systems, 2000. MEMS 2000. The Thirteenth Annual International Conference on, IEEE.
- Westerwalbesloh, C., Grünberger, A., Stute, B., Weber, S., Wiechert, W., Kohlheyer, D., and von Lieres, E. (2015). "Modeling and CFD simulation of nutrient distribution in picoliter bioreactors for bacterial growth studies on single-cell level." *Lab on a Chip* **15**(21): 4177-4186.
- Whitesides, G. M. (2006). "The origins and the future of microfluidics." *Nature* **442**(7101): 368.
- Willmott, C. J. R., and Maxwell, A. (1993). "A single point mutation in the DNA gyrase A protein greatly reduces binding of fluoroquinolones to the gyrase-DNA complex." *Antimicrobial Agents and Chemotherapy* **37**(1): 126-127.
- Wolf, H., Rols, M., Boldt, E., Neumann, E., and Teissie, J. (1994). "Control by pulse parameters of electric field-mediated gene transfer in mammalian cells." *Biophysical journal* **66**(2): 524-531.
- Wolffenbuttel, R. (1997). "Low-temperature intermediate Au-Si wafer bonding; eutectic or silicide bond." *Sensors and Actuators A: Physical* **62**(1-3): 680-686.
- Worgull, M., Kolew, A., Heilig, M., Schneider, M., Dingreiter, H., and Rapp, B. (2011). "Hot embossing of high performance polymers." *Microsystem technologies* **17**(4): 585-592.
- Xia, Y., and Whitesides, G. M. (1998). "Soft lithography." *Annual review of materials science* **28**(1): 153-184.
- Xin, H., Liu, Q., and Li, B. (2014). "Non-contact fiber-optical trapping of motile bacteria: dynamics observation and energy estimation." *Scientific Reports* **4**: 6576.
- Xin, H., Xu, R., and Li, B. (2012). "Optical trapping, driving, and arrangement of particles using a tapered fibre probe." *Scientific Reports* **2**: 818.
- Yager, P., Edwards, T., Fu, E., Helton, K., Nelson, K., Tam, M. R., and Weigl, B. H. (2006). "Microfluidic diagnostic technologies for global public health." *Nature* **442**(7101): 412.
- Yamamoto, M., Saijoh, Y., Perea-Gomez, A., Shawlot, W., Behringer, R. R., Ang, S.-L., Hamada, H., and Meno, C. (2004). "Nodal antagonists regulate formation of the anteroposterior axis of the mouse embryo." *Nature* **428**(6981): 387-392.
- Yang, C.-C., and Chen, W.-C. (2002). "The structures and properties of hydrogen silsesquioxane (HSQ) films produced by thermal curing." *Journal of Materials Chemistry* **12**(4): 1138-1141.
- Yang, L. (2009). "Dielectrophoresis assisted immuno-capture and detection of foodborne pathogenic bacteria in biochips." *Talanta* **80**(2): 551-558.
- Yang, L., Banada, P. P., Bhunia, A. K., and Bashir, R. (2008). "Effects of Dielectrophoresis on Growth, Viability and Immuno-reactivity of Listeria monocytogenes." *Journal of Biological Engineering* **2**: 6.

- Yarmush, M. L., Golberg, A., Serša, G., Kotnik, T., and Miklavčič, D. (2014). "Electroporation-based technologies for medicine: principles, applications, and challenges." Annual review of biomedical engineering **16**: 295-320.
- Yoshida, T., Qin, L., Egger, L. A., and Inouye, M. (2006). "Transcription regulation of ompF and ompC by a single transcription factor, OmpR." Journal of Biological Chemistry **281**(25): 17114-17123.
- Yoshimura, F., and Nikaido, H. (1985). "Diffusion of beta-lactam antibiotics through the porin channels of *Escherichia coli* K-12." Antimicrobial Agents and Chemotherapy **27**(1): 84-92.
- Zeller, R. W. (2004). "Generation and use of transgenic ascidian embryos." Methods in cell biology **74**: 713-730.
- Zhao, G., Meier, T. I., Kahl, S. D., Gee, K. R., and Blaszcak, L. C. (1999). "BOCILLIN FL, a sensitive and commercially available reagent for detection of Penicillin-Binding Proteins." Antimicrobial Agents and Chemotherapy **43**(5): 1124-1128.
- Zimmermann, U., Pilwat, G., and Riemann, F. (1974). "Dielectric breakdown of cell membranes." Biophysical journal **14**(11): 881-899.
- Zimmermann, W., and Rosselet, A. (1977). "Function of the Outer Membrane of *Escherichia Coli* as a Permeability Barrier to Beta-Lactam Antibiotics." Antimicrobial Agents and Chemotherapy **12**(3): 368-372.
- Zhao X., Suárez-Boomgaard D., Saykali B., Safioui J., Hermans M., Louër A.-C., Migeotte I., and Gosse C. 'LASER MICROMACHINING OF REUSABLE GLASS DEVICES DEDICATED TO THE TARGETED ELECTROPORATION OF CELL ASSEMBLIES', *Transducer 2017*.
- George de Hevesy, 1943: <http://www.su.se/english/about/prizes-awards/nobel-prize/george-de-hevesy>
- Ibidi chemotaxis: <http://ibidi.com/applications/chemotaxis/u-slide-chemotaxis/>
- UN 2016 SEP media: <https://www.un.org/press/en/2016/ga11825.doc.htm>
- WHO Antimicrobial Resistance 2014: World Health Organization, April 2014.
<http://www.who.int/mediacentre/factsheets/fs194/en/>.
- WHO Drug Resistance: World Health Organization. http://www.who.int/topics/drug_resistance/en/
- WHO World Health Day 2011: antimicrobial resistance: no action today, no cure tomorrow.
<http://www.who.int/world-health-day/2011/en/>
- WHO World Health Day 2015: From farm to plate, make food safe.
<http://www.who.int/mediacentre/news/releases/2015/food-safety/en/>
- WHO 2017 FEB media: <http://www.who.int/mediacentre/news/releases/2017/bacteria-antibiotics-needed/en/>
- Wikilectures Resting Membrane Potential: http://www.wikilectures.eu/index.php/Resting_Membrane_Potential

RESEARCH ARTICLE

TECHNIQUES AND RESOURCES

A microdevice to locally electroporate embryos with high efficiency and reduced cell damage

 Elsa Mazari¹, Xuan Zhao¹, Isabelle Migeotte², Jérôme Collignon³, Charlie Gosse^{1,*} and Aitana Perea-Gomez^{3,*}
ABSTRACT

The ability to follow and modify cell behaviour with accurate spatiotemporal resolution is a prerequisite to study morphogenesis in developing organisms. Electroporation, the delivery of exogenous molecules into targeted cell populations through electric permeation of the plasma membrane, has been used with this aim in different model systems. However, current localised electroporation strategies suffer from insufficient reproducibility and mediocre survival when applied to small and delicate organisms such as early post-implantation mouse embryos. We introduce here a microdevice to achieve localised electroporation with high efficiency and reduced cell damage. *In silico* simulations using a simple electrical model of mouse embryos indicated that a dielectric guide-based design would improve on existing alternatives. Such a device was microfabricated and its capacities tested by targeting the distal visceral endoderm (DVE), a migrating cell population essential for anterior-posterior axis establishment. Transfection was efficiently and reproducibly restricted to fewer than four visceral endoderm cells without compromising cell behaviour and embryo survival. Combining targeted mosaic expression of fluorescent markers with live imaging in transgenic embryos revealed that, like leading DVE cells, non-leading ones send long basal projections and intercalate during their migration. Finally, we show that the use of our microsystem can be extended to a variety of embryological contexts, from preimplantation stages to organ explants. Hence, we have experimentally validated an approach delivering a tailor-made tool for the study of morphogenesis in the mouse embryo. Furthermore, we have delineated a comprehensive strategy for the development of ad hoc electroporation devices.

KEY WORDS: Localised electroporation, Mouse embryo, Microsystem, Visceral endoderm, Migration, Organ explant, Finite element model simulations

INTRODUCTION

During embryonic development, morphogenesis is the result of dynamic and complex cellular events controlled by signalling networks finely regulated in space and time. Understanding these processes requires the ability to label discrete cell populations in order to characterise their lineage and fate and to modify gene expression with precise spatiotemporal resolution.

Electroporation consists in delivering exogenous molecules into cells via the electric permeabilisation of the plasma membrane. It

has been widely used to introduce nucleic acids in model organisms (Calegari et al., 2004; Escoffre et al., 2009; Nakamura and Funahashi, 2012; Swartz et al., 2001). Unlike viral infection and lipofection, electroporation does not require specific sample preparation. Moreover, spatial and temporal control of gene expression is achieved without the obligatory identification of tissue-specific regulatory sequences, nor the time- and resource-consuming production of genetically modified animals.

Targeting electroporation to specific tissues often involves local application of the exogenous molecule and generation of an electric field with large electrodes, either commercially available or home-made. This approach has been implemented most successfully when the tissue of interest surrounds a natural body cavity in which microinjection is possible, for example the neural tube lumen or the proamniotic cavity of vertebrate embryos (Itasaki et al., 1999; Soares et al., 2008). In other situations, such as experiments involving epithelial tissues lying at the periphery of embryos or organs, the geometry and the position of the targeted area do not allow local concentration of the exogenous molecule. The latter compound is then homogeneously distributed, and localised electroporation can only be achieved if the electric field is spatially restricted, for instance by using needle-shaped electrodes placed close to the targeted area (Davidson et al., 2003; Momose et al., 1999). The main limitation of this strategy is that electrolysis at the surface of the needles leads to pH variations and gas bubble generation that can be detrimental to the adjacent cells (Kim et al., 2008; Wang et al., 2010; Wang and Lee, 2013). This problem can be circumvented by relying on electrodes placed at a distance from the organism while channelling the electric field through narrow dielectric guides filled with an electrolyte, a technique notably applied to label single neurons with electroporation micropipettes (Haas et al., 2001; Nolkrantz et al., 2001; Wang et al., 2010). Recently, dielectric guide-based electroporation has also been adapted to the on-chip format, with microfabricated electrodes and fluidic channels (Fox et al., 2006; Wang et al., 2010; Wang and Lee, 2013). Although the use of such devices has so far been restricted to single cells in culture, one could in principle devise similar microsystems to target small embryos or organ explants that face poor survival in traditional electroporation experiments. This is the case for mouse embryos at early post-implantation stages, a crucial time-window for anterior-posterior axis formation (Rossant and Tam, 2009; Takaoka and Hamada, 2012).

Shortly after implantation, at embryonic day 5 of development (E5), the mouse embryo has the shape of an elongated cylinder, less than 200 μm long, and displays radial symmetry around the proximo-distal axis. The pluripotent epiblast (Epi) in the distal region is associated to two extra-embryonic tissues, the extra-embryonic ectoderm (ExE), which abuts the epiblast proximally, and the visceral endoderm (VE), an absorptive epithelium essential for nutrient exchange that forms the outer layer of the conceptus. Dynamic reciprocal signalling between the epiblast and the extra-embryonic tissues results in radial symmetry

¹Laboratoire de Photonique et de Nanostructures, LPN-CNRS, route de Nozay, 91460 Marcoussis, France. ²Institut de Recherche Interdisciplinaire en Biologie Humaine et Moléculaire, Université Libre de Bruxelles, Brussels 1070, Belgium. ³Institut Jacques Monod, CNRS, UMR7592, Univ Paris Diderot, Sorbonne Paris Cité, F-75205 Paris, France.

*Authors for correspondence (charlie.gosse@lpn.cnrs.fr; pereagomez.aitana@ijm.univ-paris-diderot.fr)

breaking, specification of the anterior-posterior axis, gastrulation initiation, and formation of the definitive germ layers. Central to these processes is a VE subpopulation identified at E5.5 by a specific morphology and the expression of a distinct gene repertoire: the distal visceral endoderm (DVE). These cells will move proximally towards one side of the embryo, where they will define the future anterior pole and hence take the name of anterior visceral endoderm (AVE) at E6.5 (Rossant and Tam, 2009; Takaoka and Hamada, 2012).

DVE migration has been followed by live imaging of transgenic embryos where this cell population is selectively marked by the expression of fluorescent proteins, e.g. Hex-GFP (Rodriguez et al., 2001). This approach has demonstrated that DVE cells migrate while keeping epithelial integrity by intercalating between other VE cells (Migeotte et al., 2010; Srinivas et al., 2004; Trichas et al., 2011, 2012). Moreover, cell tracking has shown that the whole VE layer is involved in a global reorganisation initiated by DVE motion (Rivera-Perez et al., 2003; Takaoka et al., 2011; Trichas et al., 2011). Detailed observation of DVE cells at the migration front revealed that they send long actin-dependent projections, which possibly sense the environment for orientation cues (Migeotte et al., 2010; Srinivas et al., 2004). Ablation experiments during the initial phase of migration indicated that front row cells act as leading cells and are essential for subsequent movements in the VE (Morris et al., 2012; Takaoka et al., 2011). By contrast, it has been difficult to scrutinise the shape and behaviour of DVE cells located in the midst of the migrating fluorescent population or of other non-labelled VE cells. It is thus currently unknown whether they also send long extensions and intercalate or whether they are dragged by the leading DVE cells. Answering these questions requires new tools to specifically target chosen populations and create cell mosaics in the VE layer.

We here describe an on-chip approach based on dielectric guides that makes localised electroporation efficient, reproducible and safe. As a proof of principle, we have chosen to target small cell populations in the VE of mouse embryos at E5.5-E6.5, a crucial stage for which existing electroporation procedures face poor reproducibility and poor

embryo survival. By combining our new electroporation strategy with live imaging in transgenic embryos, we provide evidence that, during anterior-posterior axis formation, active migration and intercalation are not restricted to leading DVE cells. Finally, we demonstrate that the microdevice we designed can be used to electroporate tissues in a wide range of embryonic contexts.

RESULTS

Numerical simulations validate a design based on dielectric guides to locally permeate the outer epithelium of embryos

Electroporation of early post-implantation mouse embryos has first been achieved in a chamber with parallel plate electrodes (Fig. 1B) (Mellitzer et al., 2002; Soares et al., 2008). However, it can be inferred from computations of the electric potential at the surface of an ellipsoid model that although permeation localisation is optimal when the longer axis of the embryo is perpendicular to both electrodes, it degrades as soon as a tilt angle exists, becoming nearly impossible after a 90° rotation (Valic et al., 2003). This limitation has been overcome by replacing one of the plates by a needle (Fig. 1C), thereby creating a significant variation of the electric potential over a small area (Davidson et al., 2003; Khoo et al., 2007). Importantly, permeation is efficiently restricted in space only if the needle is close enough to the targeted tissue, which may result in cell damage. To circumvent this problem, we considered a third approach where the electric field generated by large electrodes is conveyed to the targeted zone by dielectric guides (Fig. 1D) (Wang et al., 2010; Wang and Lee, 2013).

In order to compare the three strategies, a simple electrical model of the embryo was conceived (Fig. 1A) and numerical simulations were undertaken to evaluate the extent of membrane permeation for each setup. It was here assumed that exogenous molecules could enter the cells of the outer epithelium only if the absolute value of the induced transmembrane voltage (ITV) exceeded a given threshold (Escoffre et al., 2009; Rols and Teissie, 1998). To determine the latter parameter, the ITV value on the anterior surface of E6.5 embryos was first plotted in the dielectric guide case

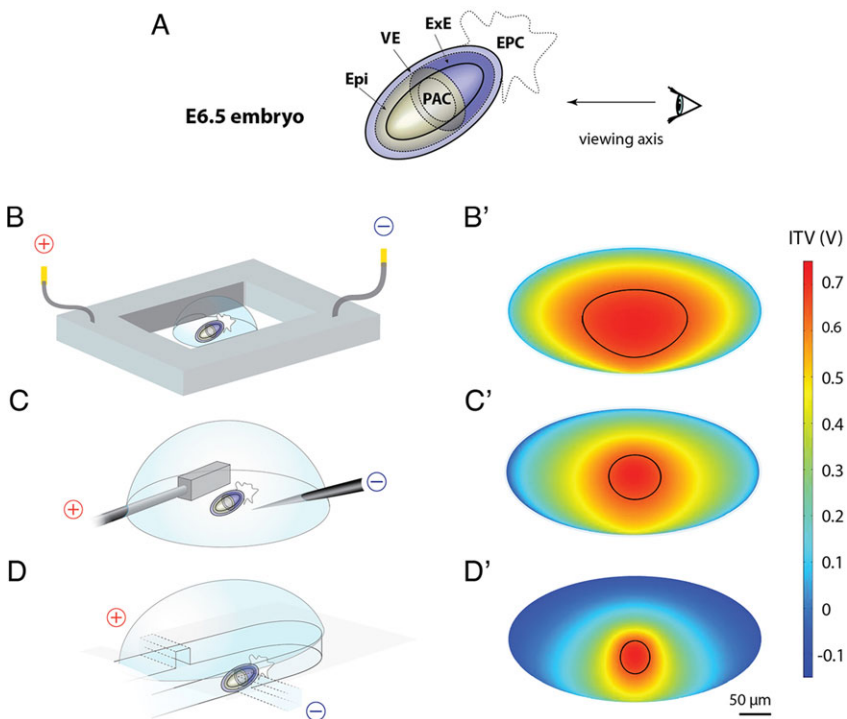


Fig. 1. Numerical simulations for the electroporation of the outer epithelial cells located on the anterior half of E6.5 embryos. (A) The embryo is approximated by two concentric prolate ellipsoids of respective length and width 400 and 200 μm for the buffer/VE interface and 300 and 100 μm for the PAC/Epi+ExE one (dimensions established according to our observations, Fig. 3A,C,D and Fig. 4A). Solid lines depict those two liquid/tissue interfaces, whereas dashed lines represent tissue/tissue junctions not considered in computations. Techniques relying on (B,B') parallel plate electrodes, (C,C') plate and needle electrodes and (D,D') $110 \times 60 \mu\text{m}^2$ dielectric guides are compared. The geometries used to simulate the experimental situations schematised in B, C and D are detailed in supplementary material Fig. S2. B', C' and D' display the ITV on flattened views of the anterior half of E6.5 embryos, using 34, 2 and 15 V pulse amplitudes, respectively. The same 0.72 V maximal ITV value is then reached in all three cases. Black lines delimitate the areas where the ITV is superior to the 0.65 V permeation threshold. Epi, epiblast; EPC, ectoplacental cone; ExE, extra-embryonic ectoderm; PAC, proamniotic cavity; VE, visceral endoderm.

(Fig. 1D') and the results of these computations were analysed with respect to experimental data on FITC-Dextran incorporation. As measurements provided an electroporated length corresponding to 8% of the total proximo-distal length (see below, Fig. 4A), the permeation threshold was fixed at 0.65 V in order to achieve consistency. Incidentally, this value is within the range of those reported for isolated cells (Escoffre et al., 2009; Hibino et al., 1993; Valic et al., 2003; Wang et al., 2010). Next, the parallel plates and the plate and needle setups were simulated. The pulse amplitudes were chosen to yield ITV maxima identical to the 0.72 V obtained with the dielectric guides, thereby allowing the comparison of the three approaches. When targeting the AVE at E6.5 with parallel plate electrodes, up to 14% of the embryo anterior half displayed an ITV beyond the permeation threshold (Fig. 1B'). The extent of the electroporated area was reduced to 4% when using the plate and needle electrodes (Fig. 1C'), and further decreased to 2% with the dielectric guides (Fig. 1D').

Keeping the same permeation threshold, similar conclusions were reached when targeting the DVE at E5.5: parallel plate electrodes, plate and needle electrodes, and dielectric guides respectively yielded electroporation of 7%, 4% and 2% of the embryo distal half (supplementary material Fig. S1).

Microfabrication techniques enable to easily and reproducibly fabricate dielectric guides

Both the single-use SU-8/Parafilm devices and the subsequent reusable glass/Parafilm ones were designed following a similar layout (Fig. 2A,B; supplementary material Figs S5 and S7). A keyhole-shaped open chamber at the centre enables easy embryo manipulation. At both extremities, large electrodes are located at the bottom of open circular reservoirs that allow the evacuation of

bubbles produced by electrolysis, thus preventing these insulating objects from disrupting current flow and hindering membrane permeation. Each reservoir is connected to the chamber by a fluidic system including a narrow dielectric guide and a wider connecting channel. The shape of the aperture in front of which the embryo is placed is the most important parameter affecting electroporation localisation. Geometry was here adjusted to the size of the developing organism (Fig. 2C-F). On the other hand, the dielectric guide length was set so as to achieve ITV in the order of 0.5 to 1 V while applying voltage pulses with amplitudes remaining in the electroporator working range, i.e. 10 to 90 V.

Materials were first selected according to considerations related to microfabrication: glass is cheap and widely used in microfluidics; SU-8 is a well-known high-aspect-ratio epoxy-photoresist that allows features up to 200 μm high; Parafilm is easy to pattern with cutters and punchers, it can also be straightforwardly bonded under moderate heating. Regarding biocompatibility, SU-8 and gold were favoured as their innocuousness has been demonstrated for numerous cell and tissue types (Ereifej et al., 2011; Kotzar et al., 2002).

Dielectric guide-based devices allow efficient electroporation with reduced cell damage

Validation of the design and functionality of our chip was performed by electroporating the VE of E6.5 and E5.5 mouse embryos. Efficient membrane permeabilisation was assessed by FITC-Dextran penetration (Fig. 3A,F). Cell transfection by nucleic acids was evaluated through the expression of fluorescent proteins 24 h after electroporation of plasmids encoding Venus or mCherry (Fig. 3B,G). Finally, electrically induced cell damage was asserted when at least one cell displayed PI incorporation shortly after pulse

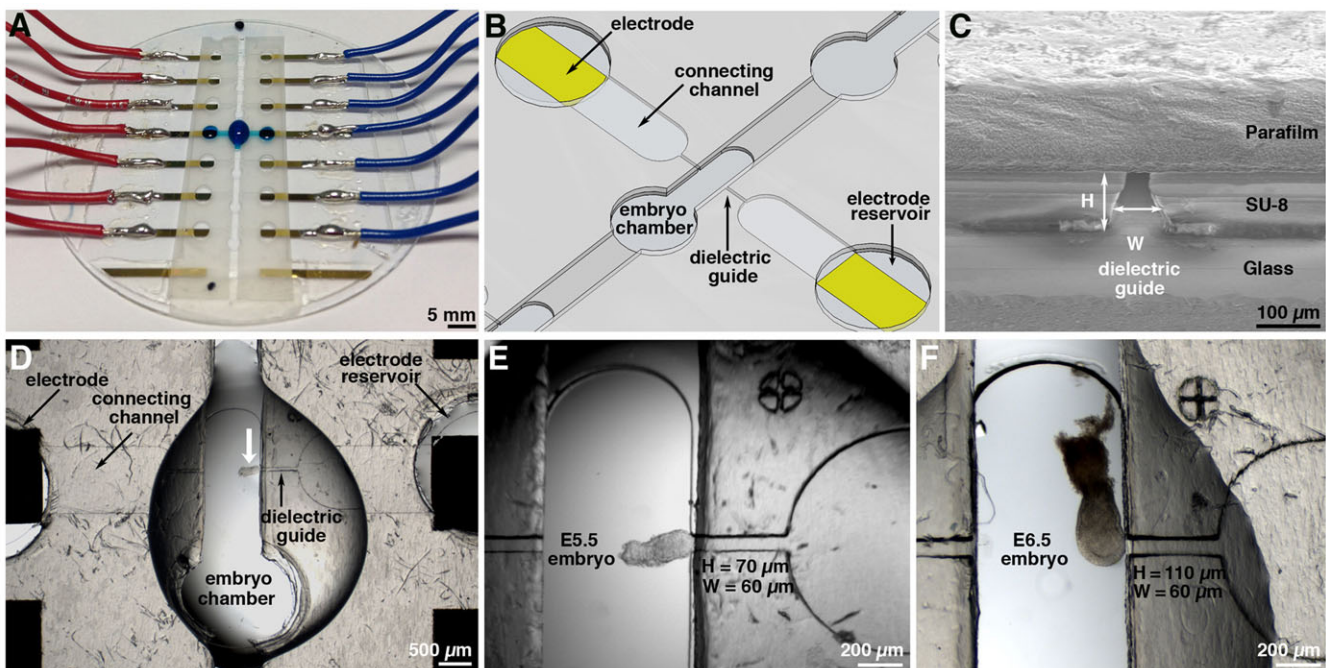


Fig. 2. Layout and use of the dielectric guide-based electroporation device. (A) Global view of the microsystem, one of the fluidic networks being filled with a Bromophenol Blue solution to highlight connectivity. (B) Diagram showing a pair of electrodes with the corresponding connecting channels, dielectric guides and embryo chamber. (C) Scanning electron microscopy micrograph of a dielectric guide of height $H=110\ \mu\text{m}$ and width $W=60\ \mu\text{m}$, as observed from the embryo chamber. (D) View of the whole fluidic system included between the electrodes. An E5.5 embryo (white arrow) is positioned so as to target its DVE, this tissue facing the dielectric guide connected to the cathode. (E) Zoom on the E5.5 embryo. (F) Similar enlarged view of an E6.5 embryo positioned so as to target its AVE.

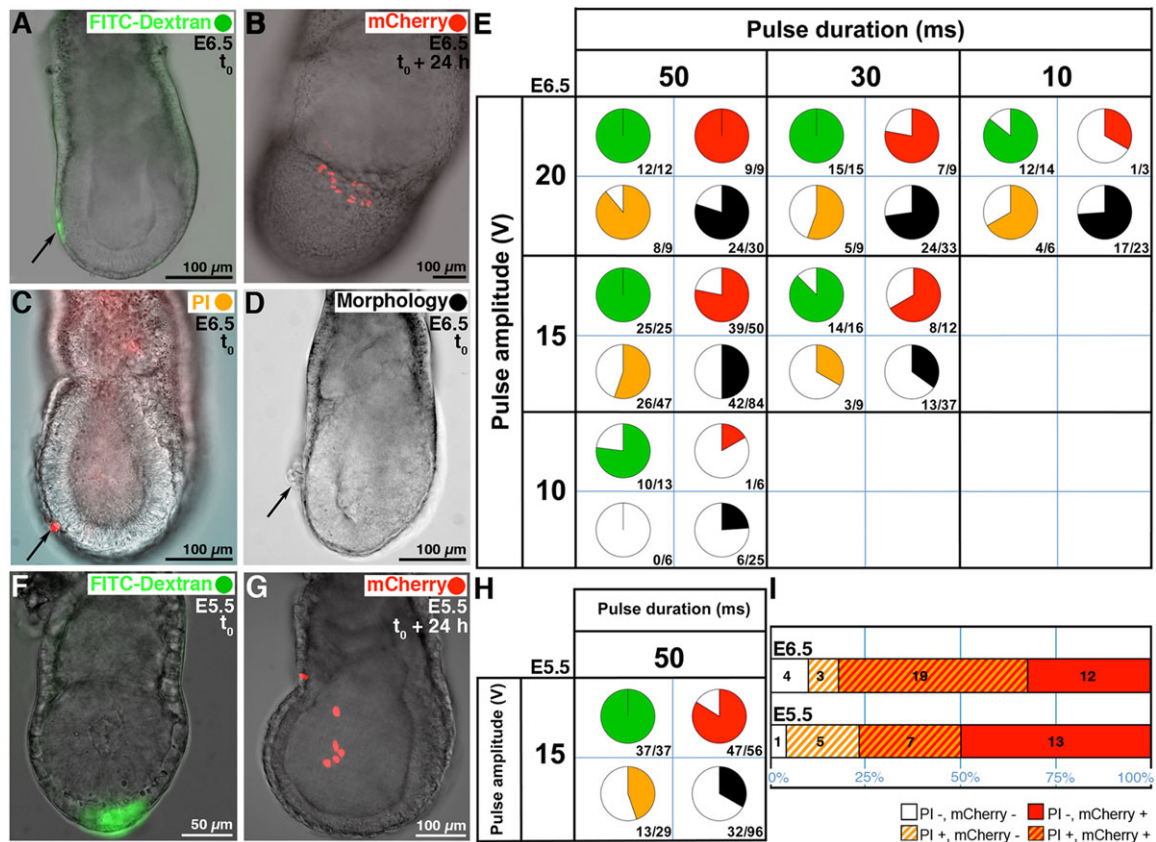


Fig. 3. Electroporation outcome for E6.5 and E5.5 embryos submitted to a series of three identical square voltage pulses of various amplitude and duration, and separated by 1 s. Representative examples for the criteria used to define electrical conditions suitable to electroporate AVE cells at E6.5: (A) FITC-Dextran incorporation (black arrow); (B) nuclear mCherry expression; (C) PI incorporation (black arrow); (D) abnormal morphology such as cell swelling or destruction (black arrow). (E) Results for E6.5 embryos electroporated using $110 \times 60 \mu\text{m}^2$ dielectric guides. Coloured sectors report on the percentage of embryos in which at least one cell of the VE displays the following characteristics: (green) FITC-Dextran incorporation; (red) Venus or mCherry expression; (orange) PI incorporation; (black) abnormal morphology. The p/n fraction indicated below each pie chart corresponds to the number of positive results, p , over the total number of electroporated embryos, n . Representative examples for the criteria used to define electrical conditions suitable to electroporate DVE cells at E5.5: (F) FITC-Dextran incorporation; (G) nuclear mCherry expression. (H) Results for E5.5 embryos electroporated using $70 \times 60 \mu\text{m}^2$ dielectric guides. (I) Analysis of the co-appearance in single embryos of cell death (PI incorporation) and efficient transfection (mCherry expression) after electroporation with 15 V and 50 ms pulses at E6.5 ($n=38$) and E5.5 ($n=26$). Anterior is to the left in A-D and G.

application (Fig. 3C). Distinct batches of embryos were used to score these three outputs, whereas morphological alterations were monitored for all groups (Fig. 3D).

E6.5 embryos, early to mid-streak stage, were electroporated with their AVE facing a $110 \mu\text{m}$ high and $60 \mu\text{m}$ wide dielectric guide (Fig. 2F), using a range of electrical conditions close to those predicted by numerical simulations (Fig. 3E). Efficient pore opening occurred in all cases as revealed by FITC-Dextran incorporation. Moreover, embryo survival was not impaired as 100% of the electroporated embryos reached the late bud to head fold stage after 24 h of *in vitro* culture, irrespective of the presence of local cell damages ($n=232$, Fig. 3E). For 20 V pulses, local cell death was induced in the majority of the embryos as evidenced by PI incorporation. Reducing pulse duration at this voltage did not improve cell viability while DNA transfection was dramatically reduced, an effect likely to be due to insufficient electrophoretic transport of the plasmids to the permeabilised membrane (Escoffre et al., 2009; Rols and Teissie, 1998). By contrast, 10 V pulses preserved cell viability but failed to trigger transfection. Applying three pulses of 15 V, 50 or 30 ms long and spaced by 1 s yielded high transfection efficiency and good cell viability. These conditions were also optimal for the electroporation of DVE cells at E5.5 (Fig. 3F-H; data not shown), with the height of the dielectric

guides being reduced to $70 \mu\text{m}$, so as to maintain localisation in these smaller organisms (Fig. 2E).

The co-appearance of efficient DNA transfection and cell damage in individual embryos was next analysed for electroporation with the 15 V and 50 ms conditions. The percentage of embryos expressing mCherry that showed no cell death was 39% and 65% at E6.5 and E5.5, respectively (Fig. 3I; supplementary material Figs S8 and S9). For both stages, DNA transfection and PI incorporation were independent events (Fisher's exact test, two-tailed, $P=0.42$ and $P=0.07$, Fig. 3I). PI incorporation strongly correlated to the appearance of morphological abnormalities upon pulse application (supplementary material Figs S8 and S9), indicating that visual scoring alone can allow the identification of embryos with irreversible local cell damage.

Dielectric guide-based devices allow reproducible localised electroporation

Two approaches were undertaken to address the size of the electroporated area with the previously established 15 V and 50 ms conditions. First, the length of the zone showing FITC-Dextran fluorescence along the proximo-distal axis was measured in a subset of E6.5 embryos shortly after electroporation (Fig. 4A). The signal extended over $33 \pm 7 \mu\text{m}$ ($n=13$), representing 3-4 cell

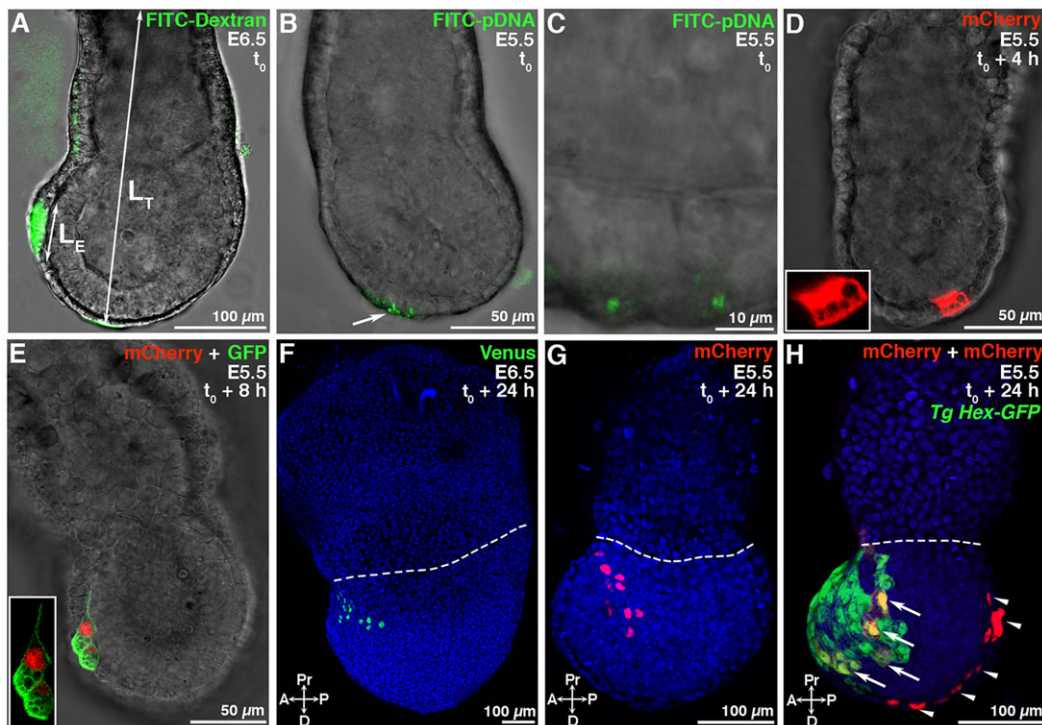


Fig. 4. Localised VE electroporation of E6.5 and E5.5 embryos with 15 V and 50 ms pulses, using 110×60 μm² and 70×60 μm² dielectric guides, respectively. (A) FITC-Dextran incorporation after AVE electroporation at E6.5. The fluorescent signal extends over a length L_E, and the total embryo length L_T is measured from the basis of the ectoplacental cone to the distal tip. (B) FITC-labelled pCAG-nls-mCherry plasmid interacting with the plasma membrane 45 min after DVE electroporation at E5.5. Superposition of the maximum intensity projection of a confocal stack comprising 19 slices spaced by 2 μm and of a single transmission plane. (C) Single plane view of the region indicated by the white arrow in B. (D) Cytoplasmic mCherry expression 4 h after DVE electroporation at E5.5. Single confocal plane. (E) Fluorescent protein expression targeted to the nucleus and to the plasma membrane 8 h after co-electroporation of pCAG-nls-mCherry and pCMV-GAP43myr-EGFP in the DVE at E5.5. Single confocal plane. (F) Nuclear Venus distribution 24 h after AVE electroporation at E6.5. Maximum intensity projection of a confocal stack comprising 81 slices spaced by 3 μm. (G) Nuclear mCherry distribution 24 h after DVE electroporation at E5.5. Maximum intensity projection of a confocal stack comprising 29 slices spaced by 5 μm. (H) Cytoplasmic (arrows) and nuclear (arrowheads) mCherry expression 24 h after double electroporation of pCAG-mCherry and pCAG-nls-mCherry, respectively, in the DVE and in the posterior visceral endoderm of a E5.5 Hex-GFP transgenic embryo. Maximum intensity projection of a confocal stack comprising 34 slices spaced by 5 μm. Inserts show close up views in D,E. Hoechst-stained nuclei are shown in blue and white dashed lines highlight the embryonic/extra-embryonic boundary in F-H. A, anterior; D, distal; P, posterior; Pr, proximal.

diameters and 8±2% of the total embryo length. Second, FITC or Cy3-labelled plasmids were used to electroporate the DVE at E5.5. These molecules were visible as spots at the surface of the targeted cells just after pulse application and up to 4 h later (Fig. 4B,C). Such fluorescent spots have previously been observed when electroporating isolated cells and probably correspond to plasmids that form a stable complex with the plasma membrane before being internalised into the cytoplasm (Escoffre et al., 2009; Golzio et al., 2002). Confocal imaging indicated that in all cases four cells were marked under these conditions ($n=6$, Fig. 4B,C).

Fluorescent protein expression was detected in one to four VE cells 4 h after plasmid electroporation (Fig. 4D, $n=14$), a timing in agreement with previous observations (Davidson et al., 2003; Khoo et al., 2007). Prominent apical vacuoles and basal projections in migrating DVE cells were observed when cytoplasmic or membrane-targeted fluorescent proteins were used (Fig. 4D,E; supplementary material Movie 1), indicating that transfected cells show similar characteristics to unmanipulated ones (Migeotte et al., 2010; Rivera-Perez et al., 2003; Srinivas et al., 2004; Wada et al., 2013).

After 24 h of whole embryo culture, the spatial distribution of the fluorescent cells was consistent with the morphogenetic displacements reported for each subpopulation. AVE cells targeted at E6.5 were found at proximal anterior positions (Fig. 4F). For E5.5 embryos, labelled DVE cells had migrated anteriorly and laterally (Fig. 4G,H), whereas electroporated posterior visceral endoderm

cells were found at posterior and distal positions (Fig. 4H) (Lawson and Pedersen, 1987; Perea-Gomez et al., 2001; Rivera-Perez et al., 2003; Srinivas et al., 2004; Takaoka et al., 2011). Transfection of E6.5 AVE and E5.5 DVE respectively yielded 12±7 and 9±5 fluorescent cells after 24 h ($n=14$ and $n=26$, respectively). These results are compatible with a VE population doubling time previously estimated to 10-12 h by clonal analysis (Lawson and Pedersen, 1987; Perea-Gomez et al., 2001).

Localised electroporation reveals the behaviour of VE cells in the mouse embryo

The analysis of transgenic embryos in which DVE cells specifically express a fluorescent protein has shed light on the behaviour of cells at the migration front. However, these studies only dealt with the initial phase of DVE movement and did not address in detail the characteristics of DVE cells located in the midst of the GFP-expressing population, where the outlines of individual cells could not be distinguished (Migeotte et al., 2010; Srinivas et al., 2004; Takaoka et al., 2011; Trichas et al., 2011). We combined localised electroporation, transgenic lines and live imaging to tackle this question.

E5.5-5.75 Hex-GFP transgenic embryos were electroporated distally with a plasmid encoding cytoplasmic mCherry and imaged by live confocal microscopy from 10 to 20 h after electroporation (Fig. 5; supplementary material Movies 2 and 3). All embryos

developed normally ($n=5$), as assessed by the stereotyped anterior and lateral movement of Hex-GFP expressing cells. When electroporated cells divided, they did so only once during the 10 h imaging, in line with the cell cycle length in the VE at this stage. In all cases, divisions were characterised by rounding of cells and mitosis was completed in less than 30 min ($n=9$ divisions observed in three embryos, Fig. 5B-C''). Moreover, nearby labelled cells divided synchronously, indicating some degree of coordination in clonally related neighbours (Fig. 5B''-C'').

We focused our analysis on the behaviour of electroporated cells found in the anterior region of the VE, once the Hex-GFP positive migration front had reached the embryonic/extra-embryonic (Emb-Xemb) border (Fig. 5; supplementary material Movies 2 and 3). The anterior VE comprises Hex-GFP-positive and Hex-GFP-negative cellular clusters (Migeotte et al., 2010; Srinivas et al., 2004) and we could target both populations. Labelled cells expressing mCherry showed a net distal to proximal displacement corresponding to 2 to 4 cell diameters ($38\pm 16\ \mu\text{m}$, displacement of $n=5$ cells measured in two embryos) during the 10 h culture period (Fig. 5; supplementary material Movies 2 and 3). This observation is in agreement with the

finding that VE cells in the anterior region continue to undergo a proximal movement after leading DVE cells have reached the Emb-Xemb border at E5.75 (Takaoka et al., 2011).

Prominent basal projections were observed for both Hex-GFP-positive and -negative mCherry-expressing cells as they moved forward and intercalated (Fig. 5). These projections were oriented towards the proximal region, had an average length of $13\pm 7\ \mu\text{m}$, and lasted from 15 min to 1.5 h ($n=30$ measurements performed on 11 cells in the embryos shown in Fig. 5; supplementary material Movies 2 and 3). The longer, up to $30\ \mu\text{m}$, and more stable projections were observed in cells reaching the proximity of the Emb-Xemb border. Thin extensions, longer than two cell diameters, appeared to contact the first or second row of Hex-GFP positive cells in the proximal region, through filopodial-like tips (Fig. 5E,E'',F,F''; supplementary material Movies 2 and 3).

Previous studies had shown that after the initial phase of migration, DVE cells make an abrupt halt when they reach the Emb-Xemb border, become elongated with their long axis parallel to the border and spread on the anterior surface of the embryo (Migeotte et al., 2010; Srinivas et al., 2004; Trichas et al., 2011). We

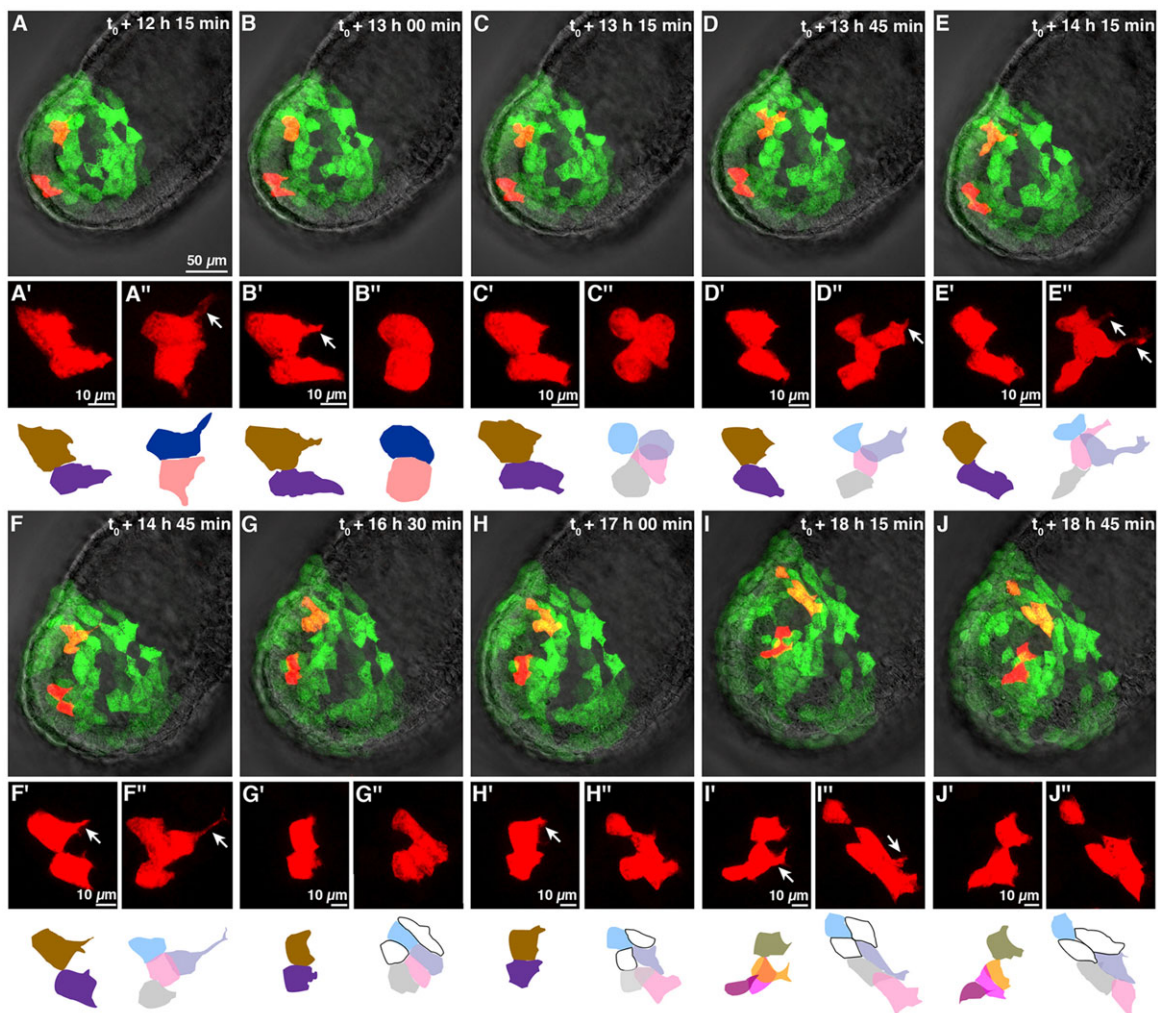


Fig. 5. Confocal live imaging of a Hex-GFP E5.5 embryo electroporated in the VE with pCAG-mCherry with 15 V and 50 ms pulses, using $70\times 60\ \mu\text{m}^2$ dielectric guides. Images were acquired every 15 min for 10 h. (A-J) Superpositions of a single transmission plane with the maximum intensity projection of mCherry and GFP fluorescence from a stack comprising 25 slices spaced by $4\ \mu\text{m}$. (A'-J'') Close-up fluorescence views at each time point of the distal Hex-GFP negative (A'-J') and proximal Hex-GFP positive (A''-J'') mCherry-expressing cells. White arrows show cell projections. Maximal intensity projections and individual confocal sections were used to draw diagrams where the electroporated cells are coloured and the outlines of some of the Hex-GFP expressing cells are shown in black.

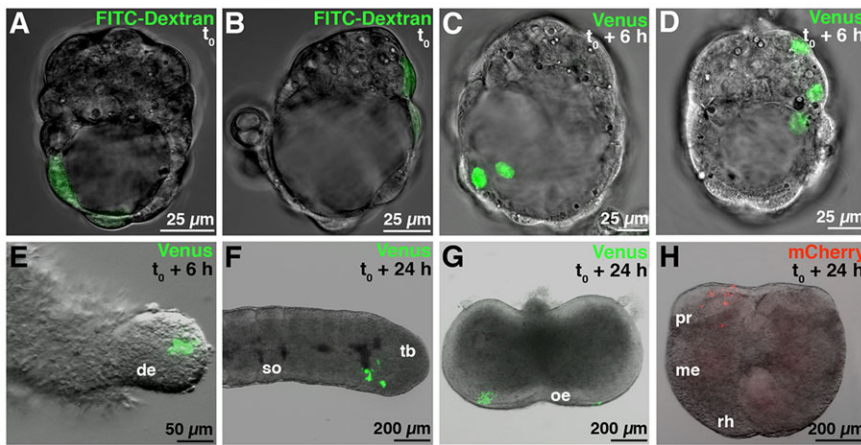


Fig. 6. Electroporation of E3.5 blastocysts and organ explants with 20 V and 50 ms pulses, using $60 \times 50 \mu\text{m}^2$ and $110 \times 60 \mu\text{m}^2$ dielectric guides, respectively. In E3.5 blastocysts, FITC-Dextran incorporation (A,B) and nuclear Venus expression (C,D) in mural (A,C) and polar (B,D) trophectoderm. In organ explants, nuclear Venus expression after electroporation of an E11.5 lung endodermal bud explant (E), an E11.5 tail bud explant (F), and an E9.5 mandibular arch explant (G). (H) Nuclear mCherry expression after electroporation of an E8.5 anterior neural plate explant. de, distal endoderm; me, mesencephalon; oe, oral epithelium; pr, prosencephalon; rh, rhombencephalon; so, somite; tb, tail bud.

observed that non-leading Hex-GFP-positive cells also ceased forward movement and adopted elongated shapes, but they did so before reaching the Emb-Xemb border, stopping just distally to the first rows of leading Hex-GFP-positive cells (Fig. 5G-J''; supplementary material Movie 2). In addition, lateral spreading of the non-leading cells also involved intercalation and junction remodelling (Fig. 5G-J'').

Dielectric guide-based devices allow the localised electroporation of external epithelia in embryos and explants

By adapting the dimensions of the dielectric guides, smaller or larger samples could also be targeted with the new microsystem. E3.5 blastocysts were electroporated using $60 \mu\text{m}$ high and $50 \mu\text{m}$ wide guides, and upon appropriate orientation mural or polar trophectoderm were always selectively labelled with FITC-Dextran ($n=9$, Fig. 6A,B). Venus expression was observed in 83% of the cases 6 h after electroporation (positive embryos/analysed embryos, $p/n=10/12$, 3 ± 1 labelled cells, Fig. 6C,D; supplementary material Movie 4). By using dielectric guides $110 \mu\text{m}$ high and $60 \mu\text{m}$ wide, localised electroporation was successfully achieved in several organ explants: E11.5 lung endoderm buds (Fig. 6E, $p/n=8/8$), E11.5 tail buds (Fig. 6F, $p/n=10/10$), E9.5 mandibular arches (Fig. 6G, $p/n=6/6$) and E8.5 anterior neural plates (Fig. 6H, $p/n=4/6$).

Dielectric guide-based devices fabricated in glass can be reused

The above results demonstrate that the proposed microsystem design allows an efficient and reproducible localised electroporation. During performance optimisation, which was achieved by sequential improvements of prototypes, we favoured ease of fabrication over robustness. Indeed, the microfluidic network was patterned in SU-8, a material difficult to clean and regenerate after use. In order to overcome this limitation, an alternative glass-based fabrication

protocol was implemented (Fig. 7A,B; supplementary material Figs S6 and S7). Despite some differences in the geometry due to the use of a wet etching technique, a comparable design yielded similar electroporation results when E5.5 DVE cells were targeted. All the electroporated embryos reached the early streak stage after one day of *in vitro* culture ($n=20$). Localised FITC-Dextran incorporation was each time successful ($n=11$, Fig. 7C). Upon plasmid electroporation, 67% of the embryos expressed nuclear Venus and showed 9 ± 2 fluorescent cells after 18 to 20 h in culture ($p/n=6/9$, Fig. 7D). Importantly, no difference in results was noticed when the glass wafer was reused after being cleaned.

DISCUSSION

We have produced a chip to locally electroporate small embryos and explants in an efficient, reproducible and safe way. Although the advantages of miniaturisation have been widely recognised when dealing with single cells (Boukany et al., 2011; Fox et al., 2006; Wang et al., 2010; Wang and Lee, 2013), microfabrication techniques have only rarely been adopted for the electroporation of developing organisms (Bansal et al., 2009; Huang et al., 2007). To our knowledge this work validates for the first time the superiority of dielectric guide based designs when targeting small cell populations in embryos. When applied to early post-implantation stages in mouse, our microsystem offers important benefits over the approaches relying on plate and/or needle electrodes (Davidson et al., 2003; Khoo et al., 2007): embryo survival is always assured and small populations of fewer than four cells can be transfected without noticeable modification of their behaviour. Moreover, immobilisation of the sample by suction in front of the dielectric guide and targeting of one or more selected regions can be performed under a conventional dissecting microscope with no need for micromanipulation, unlike in the lipofection or microinjection approaches (Lawson and Pedersen, 1987; Yamamoto et al., 2004).

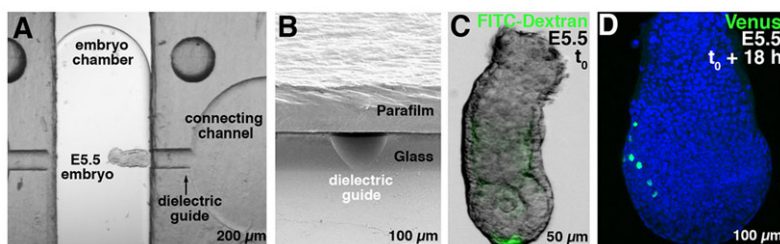


Fig. 7. Electroporation experiments performed with the reusable glass microdevice, using 15 V and 50 ms pulses. (A) Close-up view of a chip with an E5.5 embryo positioned so as to target its DVE. (B) Scanning electron microscopy micrograph of a dielectric guide of height $H=70 \mu\text{m}$, as observed from the embryo chamber. (C) Example of an E5.5 embryo showing FITC-Dextran incorporation in the DVE. (D) Nuclear Venus distribution 18 h after electroporation. Superposition of the maximum intensity projection of a confocal stack comprising 56 slices spaced by $3 \mu\text{m}$. Anterior is to the left in D. Hoechst-stained nuclei are shown in blue.

Combining localised electroporation with the use of transgenic mouse lines and live imaging revealed new behaviours of VE cells during anterior-posterior axis formation. Previous studies had reported that DVE cells at the migration front are required to initiate DVE movement, therefore acting as a leading population (Morris et al., 2012; Takaoka et al., 2011). Their displacement involves intercalation and production of long and stable basal projections (Migeotte et al., 2010; Srinivas et al., 2004). Our results show that non-leading DVE cells behave similarly, indicating that they are not passively dragged and that they potentially sense cues to regulate their progression. In addition, upon reaching the proximity of the Emb/Xemb border, non-leading DVE cells extend very long projections that appear to contact the first or second cell rows of the migration front. It is tempting to speculate that distally located Emb VE cells need to make contact with the subpopulation of leading DVE cells, which is characterised by a distinct origin and specific expression of the markers *Cer1* and *Lefty1* (Morris et al., 2012; Takaoka et al., 2011), in order to receive the signals that regulate their migration and/or arrest.

The optimisation process leading to the design of the new electroporation microsystem first involved soft-lithography (Mazari et al., 2011) before a fabrication protocol based on the SU-8 photoresist could yield effective prototypes. However, at this stage, chips remained single-use. In order to make our transfection technique accessible to a wide community of users, we have developed, as an intermediate milestone, a reusable hybrid device composed of a removable Parafilm lid and of a glass wafer in which the dielectric guides have been etched. The latter part, the sole including features realised thanks to microtechnologies, can be recycled through washing and hydrophilisation procedures easy to perform on any wet bench. Future work will aim at obtaining a complete glass-based chip, for which no assembly will be necessary and only simple cleaning will be required before use.

The present comprehensive strategy coupling numerical simulations, prototype microfabrication and *in vivo* testing, provides a framework that will be helpful for the realisation of electroporation devices tailor-made for a variety of samples: whole embryos from different species, e.g. *Xenopus* (Chernet and Levin, 2012; Falk et al., 2007), chick (Nakamura et al., 2004; Voiculescu et al., 2008), zebrafish (Bansal et al., 2009; Huang et al., 2007), insects (Ando and Fujiwara, 2013); organ explants, e.g. brain (Barker et al., 2009; del Rio and Soriano, 2010), retina (Matsuda and Cepko, 2004), cochlea (Driver and Kelley, 2010), gut (Abud et al., 2008), gonads (Gao et al., 2011); or *in vitro* reconstituted tissues, e.g. spheroids (Chopin et al., 2011; Mellor et al., 2006). Here, by adjusting the dimensions of the dielectric guides, the microsystem dedicated to early post-implantation mouse embryos was straightforwardly adapted to blastocysts and mouse embryonic organ explants, which had different sizes and shapes. Future implementations at either smaller or larger scales can thus easily be foreseen (Bansal et al., 2009; Boukany et al., 2011; Falk et al., 2007; Voiculescu et al., 2008). Likewise, the size of the targeted region can be modulated by modifying the dielectric guide cross-section. Finally, in the present design efficient electric field focusing ensures excellent electroporation localisation for external tissues. However, our localisation strategy cannot be applied to internal tissues, located further away from the dielectric guides. Our preliminary results issued from numerical simulations indicate that the pulse amplitude required to reach the permeabilisation threshold for inner cells would be deleterious for outer ones (data not shown). Combining local injection of DNA with the use of very large dielectric apertures (Falk et al., 2007), or relying on more invasive

guides to penetrate the internal tissue and reach the targeted area (Haas et al., 2001; Nolkrantz et al., 2001), would provide alternative approaches to circumvent this problem.

A variety of molecules can be efficiently introduced into cells by electroporation, including DNA, mRNA (Cerdeira et al., 2006; Chernet and Levin, 2012), dsRNA (Mellitzer et al., 2002; Soares et al., 2008), morpholinos (Falk et al., 2007; Mellitzer et al., 2002; Voiculescu et al., 2008), siRNA (Calegari et al., 2004; Paganin-Gioanni et al., 2011), proteins (Rols et al., 1998; Rols and Teissie, 1998) and drugs (Teissie et al., 2012). In this work we concentrated on DNA electroporation to provide a readout for transfection. Incidentally, we confirmed for the first time in a live organism the formation of transient DNA aggregates at the plasma membrane. This observation highlights the interest of coupling our safe electroporation protocol with live imaging to investigate the mechanistic aspects of DNA electrotransfer in complex *in vivo* environments, such as the ones faced in clinical applications of electromediated nucleic acid delivery (Andre and Mir, 2010; Chabot et al., 2013; Mir et al., 1999; Rols et al., 1998).

Finally, associating efficient localised electroporation with the rapidly evolving fluorescent protein-based tools for optogenetics (Nowotschin and Hadjantonakis, 2009; Tang et al., 2013; Yin and Wu, 2013) will surely provide new powerful approaches for the investigation of the cellular bases of morphogenesis.

MATERIALS AND METHODS

Numerical simulations

In order to evaluate which cells are permeated upon voltage application we built simplified models of experimental situations (Fig. 1; supplementary material Figs S1-S3) and used the Comsol Multiphysics 4.2a software (Comsol) to compute the electric potential both outside and inside the embryo. The ITV at the VE surface was calculated by subtracting the extracellular potential at the embryo periphery to its cytoplasmic counterpart (Fig. 1; supplementary material Fig. S1). Each time this parameter exceeded a given threshold, pores were assumed to form (Escarotte et al., 2009; Rols and Teissie, 1998). Incidentally, the contribution of the resting potential to the total transmembrane voltage was neglected because its -20 to -60 mV value (Valic et al., 2003; Wang et al., 2010) was smaller than the uncertainty evaluated for threshold determination.

Early post-implantation embryos were modelled as two concentric prolate ellipsoids, the outer one representing the organism external boundary and the inner one the periphery of the proamniotic cavity (Fig. 1; supplementary material Fig. S1). Cells were not considered individually, as they are electrically connected by GAP junctions (Pucihar et al., 2009), present in all tissues at these developmental stages (Kalimi and Lo, 1988; Viotti et al., 2012). No data being available for the electrical properties of mouse embryos, values reported for various cell types were used (Gowrishankar and Weaver, 2003; Hibino et al., 1993; Pucihar et al., 2006; Sudsiri et al., 2007). The two ellipsoids were described as resistive membranes having a 3×10^{-7} S/m conductivity and a 5 nm thickness. The conductivity of the proamniotic fluid was assumed identical to that of the cytoplasm and fixed at 0.3 S/m. For the electroporation buffer a 1.5 S/m value was measured using a CDM210 conductimeter (Radiometer analytical). The glass, polymer and air boundaries were insulating. The cathode surface was grounded and the anode one had its potential corresponding to the pulse amplitude.

Microfabrication

Devices were realized in the LPN clean room using standard microfabrication techniques (Abgrall and Gue, 2007). An abbreviated version of these lengthy processes is given below, and the detailed procedures and dimensions can be found in supplementary material Figs S4-S7.

The single-use SU-8/Parafilm chips were produced on D263 glass substrates, 50 mm in diameter and 550 μ m thick (Opticad) (Fig. 2; supplementary material Fig. S4). Gold thin-film electrodes, spaced by 5.8 mm, were first obtained using a lift-off procedure. Then, the walls of the 650 μ m wide embryo chamber and of the 415 μ m long dielectric guides

were patterned in SU-8 2050 (MicroChem). The thickness H of the epoxy-resist layer and the width W of the dielectric guides were adjusted to the size of the electroporated organism, varying from 60 to 110 μm and from 50 to 60 μm , respectively (supplementary material Fig. S5). Next, the polymer surface was hydrophilised by plasma treatment. Finally, the fluidic system was closed by thermal bonding of a 130 μm thick ceiling made of Parafilm 'M' (Pechiney) including the necessary access holes.

For fabrication of the reusable glass/Parafilm device (Fig. 7; supplementary material Figs S6 and S7) a chromium mask was first patterned on the D263 substrate by optical lithography followed by ion beam etching. Hydrofluoric acid was subsequently used to selectively etch the fluidic network in the wafer bulk up to $H=70\ \mu\text{m}$, which resulted in guides with a rounder profile. After electrodes were deposited, the glass surface was hydrophilised in a basic solution. Finally, the Parafilm lid was assembled. Following electroporation, glass substrate recycling was performed by peeling off the Parafilm, cleaning the organic traces in trichloroethylene and the mineral ones in a caustic soda solution. A new surface activation and the bonding of a new lid could then be undertaken.

Mouse strains, embryo collection, *in vitro* culture of whole embryos and explants

Embryos were obtained from natural matings of wild-type Swiss females with either Swiss males or transgenic Hex-GFP males maintained on a mixed C57Bl/6 CBA/J and Swiss background (embryos obtained from males of the C57Bl/6 CBA/J background alone were less resistant to the electroporation procedure, data not shown). E5.5 and E6.5 embryos were dissected in DMEM, 10% fetal calf serum, 25 mM Hepes buffer pH 7.0 (Gibco) and cultured at 37°C and 5% CO_2 in, respectively, 50% or 75% heat-inactivated rat serum in DMEM/F12, 100 $\mu\text{g}/\text{ml}$ streptomycin, 100 U/ml penicillin, by groups of three in 200 μl or individually in 30 μl . E3.5 blastocysts were flushed from uterine horns in M2 medium (Sigma), depellucidated in acid Tyrode's solution, and cultured in 10 μl of G2 medium (Vitrolife) covered with mineral oil. E11.5 lung endodermal bud explants, obtained after removal of mesenchyme with pancreatin/trypsin treatment, were cultured in Matrigel (Becton Dickinson) (Weaver et al., 2000). E11.5 tail buds, E9.5 mandibular arches, and E8.5 anterior neural plate explants were cultured on Millicell organotypic inserts (Millipore) (Chai et al., 1998; Shimamura and Rubenstein, 1997). Experiments were performed in accordance with French Agricultural Ministry and European guidelines for the care and use of laboratory animals (certificate CEB-35-2012 delivered by ethical committee CEEA-40).

Markers for electroporation

Fluorescein-labelled dextran (FITC-Dextran, 4 kDa, Sigma) was dissolved at 2 mg/ml in HBS (150 mM NaCl, 20 mM Hepes buffer pH 7.0). pCAG-mCherry, pCAG-nls-mCherry, pCMV-GAP43myr-EGFP (the myristoylation sequence of GAP43 targets EGFP to the plasma membrane), and pCAG-nls-Venus endotoxin-free plasmids were diluted at 1 to 1.5 $\mu\text{g}/\mu\text{l}$ in HBS. Concentrations were selected according to literature (Davidson et al., 2003; Khoo et al., 2007; Rols and Teissie, 1998). For immediate visualisation of DNA electroporation, plasmids were labelled with either Cy3 or fluorescein using the Label IT Tracker kit (Mirus) (Boukany et al., 2011). Incubating the embryos in FITC-Dextran or in fluorescently labelled plasmid solutions for 5 min did not result in any fluorescence above background (data not shown), ruling out any significant endocytic uptake of these markers by VE cells during the procedure. Furthermore, marker molecular weights above 1 kDa precluded diffusion from cell to cell through GAP junctions (Kalimi and Lo, 1988).

Electroporation protocols

For each electroporation, 15 μl of solution containing the exogenous molecule were applied to the device, starting with the electrode reservoirs to easily achieve dielectric guide filling. Individual embryos or explants were briefly rinsed in HBS and transferred to the central chamber, with the targeted area facing the cathodic channel (Fig. 2D-F). A small residual flow, probably due to pressure differences between droplets of different volumes in the electrode reservoirs and the embryo chamber, kept the organism steady in front of the guide opening during the procedure (2 to 3 min per sample). A train of three

square pulses of duration 10 to 50 ms and amplitude 10 to 20 V, spaced by 1 s, was immediately applied using a TSS20 Ovodyne electroporator (Intracel).

When addressing cell death, electroporated embryos were cultured for 30 min and stained for 20 min at 37°C in dissection medium containing 25 $\mu\text{g}/\text{ml}$ of propidium iodide (PI, Sigma). PI staining did not modify the efficiency of transfection with plasmid DNA. Control embryos submitted to the whole protocol with the exception of pulse application did not show any PI incorporation (data not shown).

Wide-field and confocal microscopy

To document FITC-Dextran and PI incorporation, embryos were imaged 1 to 3 h after electroporation using a DMI6000B inverted microscope (Leica) equipped with 20 \times /0.7NA and 10 \times /0.4NA lenses. For detailed investigations on the position and number of electroporated cells, embryos were fixed in PBS/paraformaldehyde 4% at 4°C for 1 h and stained with 10 $\mu\text{g}/\text{ml}$ Hoechst 33342 (Molecular Probes). Confocal images were obtained using a LSM 710 confocal microscope (Zeiss) equipped with 25 \times /0.8NA and 40 \times /1.3NA lenses.

Time-lapse microscopy

Individual E5.5 electroporated embryos were transferred into wells of angiogenesis μ -slides (Ibidi) containing 30 μl of culture medium and imaged for up to 16 h on an inverted LSM 710 confocal microscope (Zeiss) equipped with a 40 \times /1.3NA lens. Cell projections were measured on 3D images by manually selecting their tip and basis and using the 'Filament tracer' function of Imaris 7.6.4 (Bitplane).

Acknowledgements

We are indebted to the staff of the LPN clean room, the ImagoSeine platform, and the IJM animal facility for excellent technical assistance. We thank L. Couraud, C. Dupuis and L. Leroy for performing metallization and electron microscopy, A.-C. Louër and W. Supatto for useful discussions, C. Papanayotou and S. Meilhac for gifts of plasmids, G. Duval for help with embryo culture, G. Dubois, J. Laniel, M. Mantelet and J. Iranzo for participating in initial experiments, A. Camus, H. Berthoumieux, C. Papanayotou, P.-H. Puech and D. Sabéran-Djoneidi for critical reading of the manuscript.

Competing interests

The authors declare no competing financial interests.

Author contributions

A.P.-G. and C.G. conceived and coordinated the project; E.M. and C.G. performed numerical simulations; C.G., E.M. and X.Z. designed and fabricated electroporation devices; A.P.-G. and E.M. carried out electroporations and analysed data with contributions of I.M.; A.P.-G. and C.G. wrote the manuscript with contributions of E.M., I.M., X.Z. and J.C.

Funding

This work was supported by ElectroMice, Biomodulator and ElectroTagMan grants from the Centre National de la Recherche Scientifique (CNRS) PI 2008, Agence Nationale de la Recherche (ANR) PNANO 2009, and C'nano IdF 2011 calls, respectively. E.M. was the recipient of PhD scholarships from the Fondation pour la Recherche Médicale (FRM) and from the Réseau Thématique de Recherche Avancée (RTRA) 'Triangle de la Physique' (ElectroMagSign project). I.M. is a research associate of the Fonds National de la Recherche Scientifique (FNRS).

Supplementary material

Supplementary material available online at <http://dev.biologists.org/lookup/suppl/doi:10.1242/dev.106633/-/DC1>

References

- Abgrall, P. and Gué, A.-M. (2007). Lab-on-chip technologies: making a microfluidic network and coupling it into a complete microsystem – a review. *J. Micromech. Microeng.* **17**, R15-R49.
- Abud, H. E., Young, H. M. and Newgreen, D. F. (2008). Analysing tissue and gene function in intestinal organ culture. *Methods Mol. Biol.* **468**, 275-286.
- Ando, T. and Fujiwara, H. (2013). Electroporation-mediated somatic transgenesis for rapid functional analysis in insects. *Development* **140**, 454-458.
- Andre, F. M. and Mir, L. M. (2010). Nucleic acids electrotransfer in vivo: mechanisms and practical aspects. *Curr. Gene Ther.* **10**, 267-280.
- Bansal, T., Lenhart, J., Kim, T., Duan, C. and Maharbiz, M. M. (2009). Patterned delivery and expression of gene constructs into zebrafish embryos using microfabricated interfaces. *Biomed. Microdevices* **11**, 633-641.

- Barker, M., Billups, B. and Hamann, M.** (2009). Focal macromolecule delivery in neuronal tissue using simultaneous pressure ejection and local electroporation. *J. Neurosci. Methods* **177**, 273-284.
- Boukany, P. E., Mors, A., Liao, W.-C., Henslee, B., Jung, H., Zhang, X., Yu, B., Wang, X., Wu, Y., Li, L. et al.** (2011). Nanochannel electroporation delivers precise amounts of biomolecules into living cells. *Nat. Nanotechnol.* **6**, 747-754.
- Calegari, F., Marzeco, A.-M., Kittler, R., Buchholz, F. and Huttner, W. B.** (2004). Tissue-specific RNA interference in post-implantation mouse embryos using directional electroporation and whole embryo culture. *Differentiation* **72**, 92-102.
- Cerda, G. A., Thomas, J. E., Allende, M. L., Karlstrom, R. O. and Palma, V.** (2006). Electroporation of DNA, RNA, and morpholinos into zebrafish embryos. *Methods* **39**, 207-211.
- Chabot, S., Rosazza, C., Golzio, M., Zumbusch, A., Teissie, J. and Rols, M.-P.** (2013). Nucleic acids electro-transfer: from bench to bedside. *Curr. Drug Metab.* **14**, 300-308.
- Chai, Y., Bringas, P., Jr, Shuler, C., Devaney, E., Grosschedl, R. and Slavkin, H. C.** (1998). A mouse mandibular culture model permits the study of neural crest cell migration and tooth development. *Int. J. Dev. Biol.* **42**, 87-94.
- Chernet, B. T. and Levin, M.** (2012). A versatile protocol for mRNA electroporation of *Xenopus laevis* embryos. *Cold Spring Harb. Protoc.* **2012**, 447-452.
- Chopin, L., Wasungu, L. and Rols, M.-P.** (2011). First explanations for differences in electrotransfection efficiency in vitro and in vivo using spheroid model. *Int. J. Pharm.* **423**, 7-15.
- Davidson, B. P., Tsang, T. E., Khoo, P.-L., Gad, J. M. and Tam, P. P. L.** (2003). Introduction of cell markers into germ layer tissues of the mouse gastrula by whole embryo electroporation. *Genesis* **35**, 57-62.
- del Rio, J. A. and Soriano, E.** (2010). Regenerating cortical connections in a dish: the entorhino-hippocampal organotypic slice co-culture as tool for pharmacological screening of molecules promoting axon regeneration. *Nat. Protoc.* **5**, 217-226.
- Driver, E. C. and Kelley, M. W.** (2010). Transfection of mouse cochlear explants by electroporation. *Curr. Protoc. Neurosci.* Chapter 4, Unit 4.34 1-10.
- Ereifej, E. S., Khan, S., Newaz, G., Zhang, J., Auner, G. W. and VandeVord, P. J.** (2011). Characterization of astrocyte reactivity and gene expression on biomaterials for neural electrodes. *J. Biomed. Mater. Res. A* **99A**, 141-150.
- Escoffre, J.-M., Portet, T., Wasungu, L., Teissie, J., Dean, D. and Rols, M.-P.** (2009). What is (still not) known of the mechanism by which electroporation mediates gene transfer and expression in cells and tissues. *Mol. Biotechnol.* **41**, 286-295.
- Falk, J., Drinjakovic, J., Leung, K. M., Dwivedy, A., Regan, A. G., Piper, M. and Holt, C. E.** (2007). Electroporation of cDNA/Morpholinos to targeted areas of embryonic CNS in *Xenopus*. *BMC Dev. Biol.* **7**, 107.
- Fox, M. B., Esveld, D. C., Valero, A., Luttge, R., Mastwijk, H. C., Bartels, P. V., van den Berg, A. and Boom, R. M.** (2006). Electroporation of cells in microfluidic devices: a review. *Anal. Bioanal. Chem.* **385**, 474-485.
- Gao, L., Kim, Y., Kim, B., Lofgren, S. M., Schultz-Norton, J. R., Nardulli, A. M., Heckert, L. L. and Jorgensen, J. S.** (2011). Two regions within the proximal steroidogenic factor 1 promoter drive somatic cell-specific activity in developing gonads of the female mouse. *Biol. Reprod.* **84**, 422-434.
- Golzio, M., Teissie, J. and Rols, M.-P.** (2002). Direct visualization at the single-cell level of electrically mediated gene delivery. *Proc. Natl. Acad. Sci. U.S.A.* **99**, 1292-1297.
- Gowrishankar, T. R. and Weaver, J. C.** (2003). An approach to electrical modeling of single and multiple cells. *Proc. Natl. Acad. Sci. U.S.A.* **100**, 3203-3208.
- Haas, K., Sin, W.-C., Javaherian, A., Li, Z. and Cline, H. T.** (2001). Single-cell electroporation for gene transfer in vivo. *Neuron* **29**, 583-591.
- Hibino, M., Itoh, H. and Kinosita, K., Jr.** (1993). Time courses of cell electroporation as revealed by submicrosecond imaging of transmembrane potential. *Biophys. J.* **64**, 1789-1800.
- Huang, K.-S., Lin, Y.-C., Su, K.-C. and Chen, H.-Y.** (2007). An electroporation microchip system for the transfection of zebrafish embryos using quantum dots and GFP genes for evaluation. *Biomed. Microdevices* **9**, 761-768.
- Itasaki, N., Bel-Vialar, S. and Krumlauf, R.** (1999). 'Shocking' developments in chick embryology: electroporation and in ovo gene expression. *Nat. Cell Biol.* **1**, E203-E207.
- Kalimi, G. H. and Lo, C. W.** (1988). Communication compartments in the gastrulating mouse embryo. *J. Cell Biol.* **107**, 241-255.
- Khoo, P. L., Franklin, V. J. and Tam, P. P.** (2007). Fate-mapping technique: targeted whole-embryo electroporation of DNA constructs into the germ layers of mouse embryos 7-7.5 days post-coitum. *CSH Protoc.* **2007**, pdb prot4893.
- Kim, J. A., Cho, K., Shin, M. S., Lee, W. G., Jung, N., Chung, C. and Chang, J. K.** (2008). A novel electroporation method using a capillary and wire-type electrode. *Biosens. Bioelectron.* **23**, 1353-1360.
- Kotzar, G., Freas, M., Abel, P., Fleischman, A., Roy, S., Zorman, C., Moran, J. M. and Melzak, J.** (2002). Evaluation of MEMS materials of construction for implantable medical devices. *Biomaterials* **23**, 2737-2750.
- Lawson, K. A. and Pedersen, R. A.** (1987). Cell fate, morphogenetic movement and population kinetics of embryonic endoderm at the time of germ layer formation in the mouse. *Development* **101**, 627-652.
- Matsuda, T. and Cepko, C. L.** (2004). Electroporation and RNA interference in the rodent retina in vivo and in vitro. *Proc. Natl. Acad. Sci. U.S.A.* **101**, 16-22.
- Mazari, E., Mantelet, M., Iranzo, J., Perea-Gomez, A. and Gosse, C.** (2011). Localized electroporation of mouse embryo using dielectric guides. *Transducers 2011, Digest of the Technical Papers of the 16th International Conference on Solid-State Sensors, Actuators, and Microsystems*, 1172-1175.
- Mellitzer, G., Hallonet, M., Chen, L. and Ang, S.-L.** (2002). Spatial and temporal 'knock down' of gene expression by electroporation of double-stranded RNA and morpholinos into early postimplantation mouse embryos. *Mech. Dev.* **118**, 57-63.
- Mellor, H. R., Davies, L. A., Caspar, H., Pringle, C. R., Hyde, S. C., Gill, D. R. and Callaghan, R.** (2006). Optimising non-viral gene delivery in a tumour spheroid model. *J. Gene Med.* **8**, 1160-1170.
- Migeotte, I., Omelchenko, T., Hall, A. and Anderson, K. V.** (2010). Rac1-dependent collective cell migration is required for specification of the anterior-posterior body axis of the mouse. *PLoS Biol.* **8**, e1000442.
- Mir, L. M., Bureau, M. F., Gehl, J., Rangara, R., Rouy, D., Caillaud, J.-M., Delaere, P., Branellec, D., Schwartz, B. and Scherman, D.** (1999). High-efficiency gene transfer into skeletal muscle mediated by electric pulses. *Proc. Natl. Acad. Sci. U.S.A.* **96**, 4262-4267.
- Momose, T., Tonegawa, A., Takeuchi, J., Ogawa, H., Umesono, K. and Yasuda, K.** (1999). Efficient targeting of gene expression in chick embryos by microelectroporation. *Dev. Growth Differ.* **41**, 335-344.
- Morris, S. A., Grewal, S., Barrios, F., Patankar, S. N., Strauss, B., Buttery, L., Alexander, M., Shakesheff, K. M. and Zernicka-Goetz, M.** (2012). Dynamics of anterior-posterior axis formation in the developing mouse embryo. *Nat. Commun.* **3**, 673.
- Nakamura, H. and Funahashi, J.** (2012). Electroporation: past, present and future. *Dev. Growth Differ.* **55**, 15-19.
- Nakamura, H., Katahira, T., Sato, T., Watanabe, Y. and Funahashi, J.** (2004). Gain- and loss-of-function in chick embryos by electroporation. *Mech. Dev.* **121**, 1137-1143.
- Nolkranz, K., Farre, C., Brederlau, A., Karlsson, R. I. D., Brennan, C., Eriksson, P. S., Weber, S. G., Sandberg, M. and Orwar, O.** (2001). Electroporation of single cells and tissues with an electrolyte-filled capillary. *Anal. Chem.* **73**, 4469-4477.
- Nowotschin, S. and Hadjantonakis, A.-K.** (2009). Photomodulatable fluorescent proteins for imaging cell dynamics and cell fate. *Organogenesis* **5**, 217-226.
- Paganin-Gioanni, A., Bellard, E., Escoffre, J. M., Rols, M. P., Teissie, J. and Golzio, M.** (2011). Direct visualization at the single-cell level of siRNA electrotransfer into cancer cells. *Proc. Natl. Acad. Sci. U.S.A.* **108**, 10443-10447.
- Perea-Gomez, A., Lawson, K. A., Rhinn, M., Zakin, L., Brulet, P., Mazan, S. and Ang, S. L.** (2001). Otx2 is required for visceral endoderm movement and for the restriction of posterior signals in the epiblast of the mouse embryo. *Development* **128**, 753-765.
- Pucihar, G., Kotnik, T., Valič, B. and Miklavčič, D.** (2006). Numerical determination of transmembrane voltage induced on irregularly shaped cells. *Ann. Biomed. Eng.* **34**, 642-652.
- Pucihar, G., Miklavcic, D. and Kotnik, T.** (2009). A time-dependent numerical model of transmembrane voltage induction and electroporation of irregularly shaped cells. *IEEE Trans. Biomed. Eng.* **56**, 1491-1501.
- Rivera-Pérez, J. A., Mager, J. and Magnuson, T.** (2003). Dynamic morphogenetic events characterize the mouse visceral endoderm. *Dev. Biol.* **261**, 470-487.
- Rodriguez, T. A., Casey, E. S., Harland, R. M., Smith, J. C. and Beddington, R. S. P.** (2001). Distinct enhancer elements control Hex expression during gastrulation and early organogenesis. *Dev. Biol.* **234**, 304-316.
- Rols, M.-P. and Teissie, J.** (1998). Electroporation of mammalian cells to macromolecules: control by pulse duration. *Biophys. J.* **75**, 1415-1423.
- Rols, M.-P., Delteil, C., Golzio, M., Dumond, P., Cros, S. and Teissie, J.** (1998). In vivo electrically mediated protein and gene transfer in murine melanoma. *Nat. Biotechnol.* **16**, 168-171.
- Rossant, J. and Tam, P. P. L.** (2009). Blastocyst lineage formation, early embryonic asymmetries and axis patterning in the mouse. *Development* **136**, 701-713.
- Shimamura, K. and Rubenstein, J. L.** (1997). Inductive interactions direct early regionalization of the mouse forebrain. *Development* **124**, 2709-2718.
- Soares, M. L., Torres-Padilla, M.-E. and Zernicka-Goetz, M.** (2008). Bone morphogenetic protein 4 signaling regulates development of the anterior visceral endoderm in the mouse embryo. *Dev. Growth Differ.* **50**, 615-621.
- Srinivas, S., Rodriguez, T., Clements, M., Smith, J. C. and Beddington, R. S. P.** (2004). Active cell migration drives the unilateral movements of the anterior visceral endoderm. *Development* **131**, 1157-1164.
- Sudsiri, J., Wachner, D. and Gimsa, J.** (2007). On the temperature dependence of the dielectric membrane properties of human red blood cells. *Bioelectrochemistry* **70**, 134-140.
- Swartz, M., Eberhart, J., Mastick, G. S. and Krull, C. E.** (2001). Sparking new frontiers: using in vivo electroporation for genetic manipulations. *Dev. Biol.* **233**, 13-21.
- Takaoka, K. and Hamada, H.** (2012). Cell fate decisions and axis determination in the early mouse embryo. *Development* **139**, 3-14.

- Takaoka, K., Yamamoto, M. and Hamada, H.** (2011). Origin and role of distal visceral endoderm, a group of cells that determines anterior-posterior polarity of the mouse embryo. *Nat. Cell Biol.* **13**, 743-752.
- Tang, J. C., Szikra, T., Kozorovitskiy, Y., Teixeira, M., Sabatini, B. L., Roska, B. and Cepko, C. L.** (2013). A nanobody-based system using fluorescent proteins as scaffolds for cell-specific gene manipulation. *Cell* **154**, 928-939.
- Teissié, J., Escoffre, J. M., Paganin, A., Chabot, S., Bellard, E., Wasungu, L., Rols, M. P. and Golzio, M.** (2012). Drug delivery by electropulsation: recent developments in oncology. *Int. J. Pharm.* **423**, 3-6.
- Trichas, G., Joyce, B., Crompton, L. A., Wilkins, V., Clements, M., Tada, M., Rodriguez, T. A. and Srinivas, S.** (2011). Nodal dependent differential localisation of dishevelled-2 demarcates regions of differing cell behaviour in the visceral endoderm. *PLoS Biol.* **9**, e1001019.
- Trichas, G., Smith, A. M., White, N., Wilkins, V., Watanabe, T., Moore, A., Joyce, B., Sugnaseelan, J., Rodriguez, T. A., Kay, D. et al.** (2012). Multi-cellular rosettes in the mouse visceral endoderm facilitate the ordered migration of anterior visceral endoderm cells. *PLoS Biol.* **10**, e1001256.
- Valic, B., Golzio, M., Pavlin, M., Schatz, A., Faurie, C., Gabriel, B., Teissié, J., Rols, M.-P. and Miklavcic, D.** (2003). Effect of electric field induced transmembrane potential on spheroidal cells: theory and experiment. *Eur. Biophys. J.* **32**, 519-528.
- Viotti, M., Niu, L., Shi, S.-H. and Hadjantonakis, A.-K.** (2012). Role of the gut endoderm in relaying left-right patterning in mice. *PLoS Biol.* **10**, e1001276.
- Voiculescu, O., Papanayotou, C. and Stern, C. D.** (2008). Spatially and temporally controlled electroporation of early chick embryos. *Nat. Protoc.* **3**, 419-426.
- Wada, Y., Sun-Wada, G.-H. and Kawamura, N.** (2013). Microautophagy in the visceral endoderm is essential for mouse early development. *Autophagy* **9**, 252-254.
- Wang, S. and Lee, L. J.** (2013). Micro-/nanofluidics based cell electroporation. *Biomicrofluidics* **7**, 11301.
- Wang, M., Orwar, O., Olofsson, J. and Weber, S. G.** (2010). Single-cell electroporation. *Anal. Bioanal. Chem.* **397**, 3235-3248.
- Weaver, M., Dunn, N. R. and Hogan, B. L.** (2000). Bmp4 and Fgf10 play opposing roles during lung bud morphogenesis. *Development* **127**, 2695-2704.
- Yamamoto, M., Saijoh, Y., Perea-Gomez, A., Shawlot, W., Behringer, R. R., Ang, S.-L., Hamada, H. and Meno, C.** (2004). Nodal antagonists regulate formation of the anteroposterior axis of the mouse embryo. *Nature* **428**, 387-392.
- Yin, T. and Wu, Y. I.** (2013). Guiding lights: recent developments in optogenetic control of biochemical signals. *PLoS Arch.* **465**, 397-408.

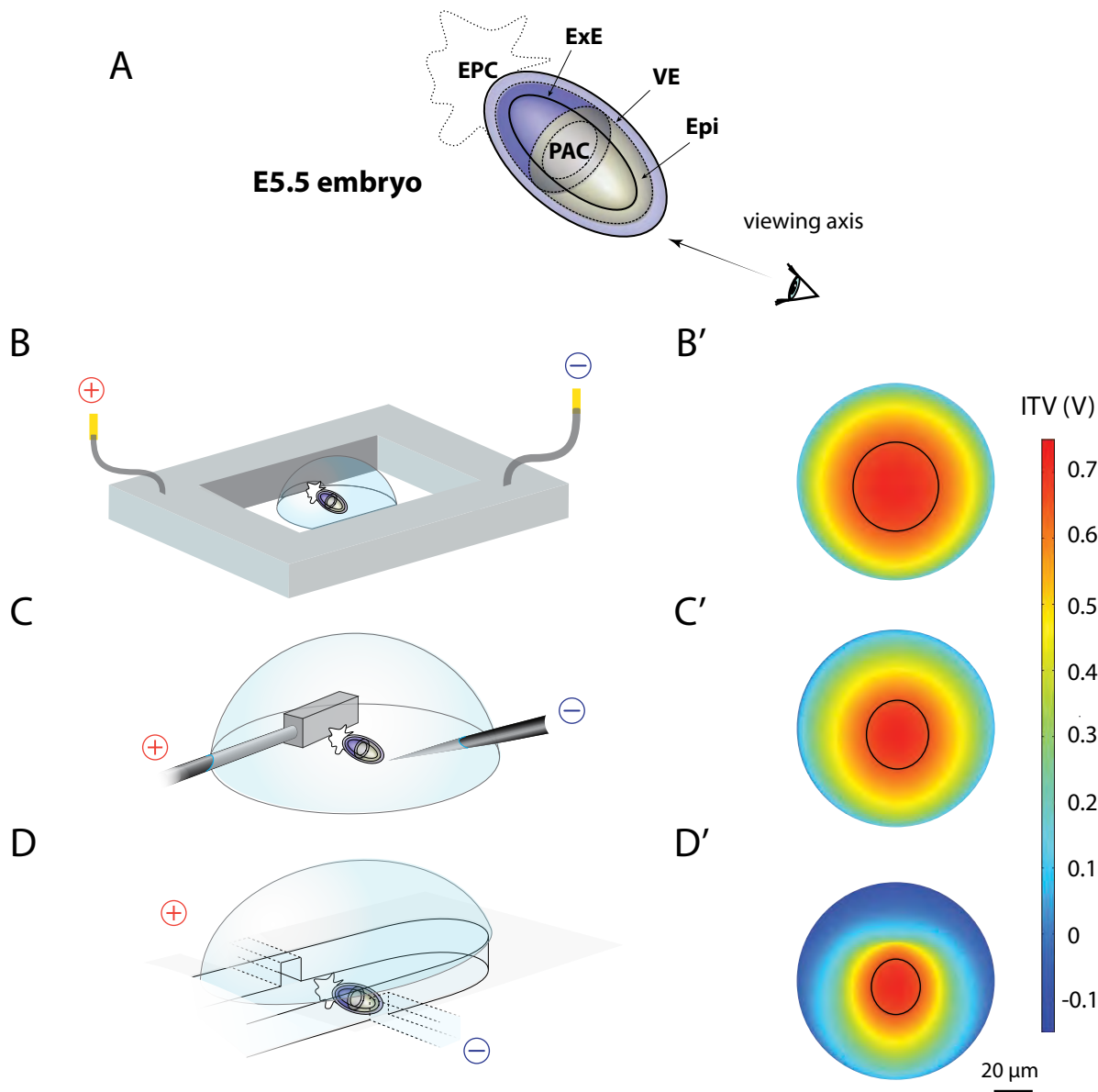


Figure S1. Numerical simulations for the electroporation of the outer epithelial cells located on the distal half of E5.5 embryos. (A) The embryo is approximated by two concentric prolate ellipsoids of respective length and width 200 and 100 μm for the buffer/VE interface and 140 and 40 μm for the PAC/Epi+ExE one, dimensions which have been established according to our own observations (Figs 3F, 4B). Those two liquid/tissue interfaces are represented by solid lines whereas dashed lines account for tissue/tissue junctions that were not considered in computations. Techniques relying on (B-B') parallel plate electrodes, (C-C') plate and needle electrodes, and (D-D') dielectric guides are compared. The geometries used to simulate the experimental situations schematised in (B), (C), and (D) are detailed in Fig. S3. (B'), (C'), and (D') display the ITV on flattened views of the distal region of E5.5 embryos. These maps have been calculated using 52, 3, and 15 V pulse amplitudes, respectively. The same 0.72 V maximal ITV value is then reached in all three cases. In (D') dielectric guides were 70 μm high and 60 μm wide. Black lines delimitate the areas where the ITV is superior to the 0.65 V permeation threshold. Epi: epiblast, EPC: ectoplacental cone, ExE: extraembryonic ectoderm, PAC: proamniotic cavity, VE: visceral endoderm.

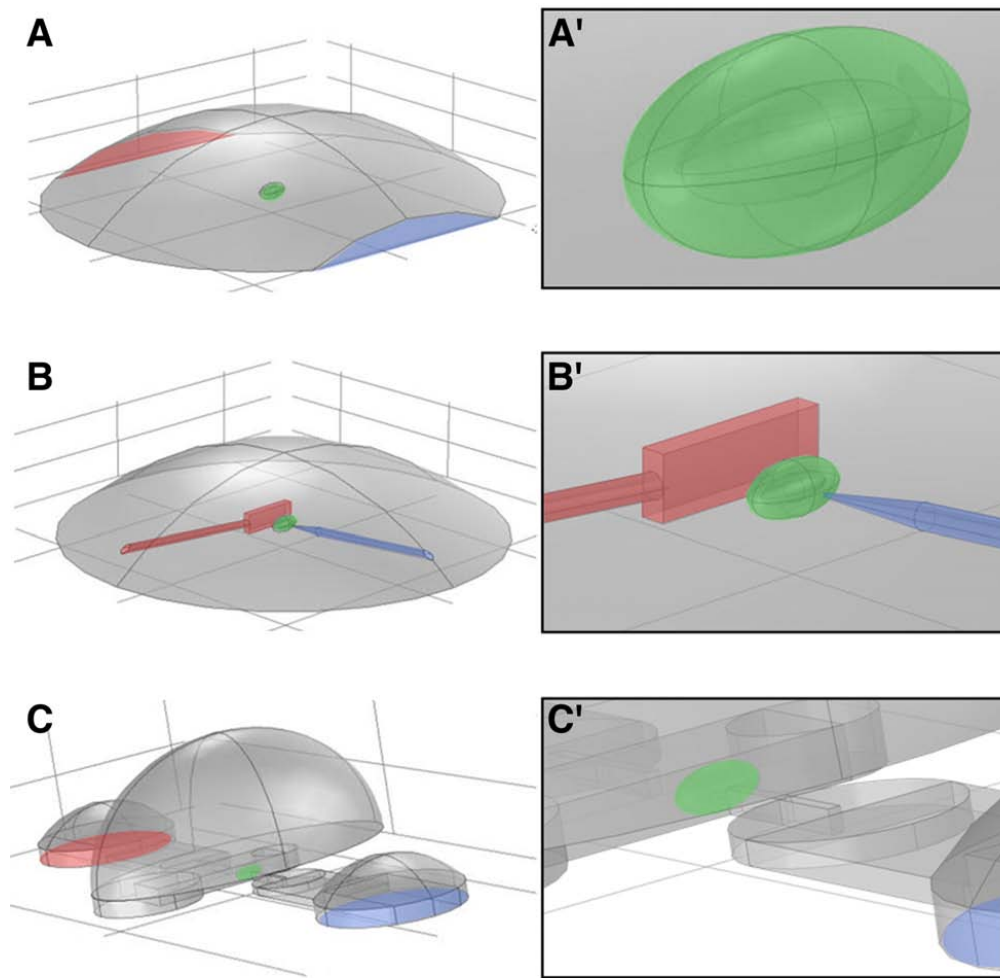


Figure S2. Snapshots of the conducting domains used to evaluate by numerical simulations the permeated area at the surface of E6.5 embryos. The three geometries, which have been entered in Comsol Multiphysics and run in the “Stationary” “Electric Currents” modes, correspond to the three schemes of Fig. 1B-D. Anodes are coloured in red whereas cathodes are in blue. Embryos, in green, rest on the setup bottom surfaces, inside drops of electroporation buffer. They are also laterally centred with respect to the electrode axis and their angular positioning is defined in order to transfect the AVE cells (the targeted area faces either an electrode or a dielectric guide, depending on the technique). The semi-axis values of the prolate ellipsoids are 200 and 100 μm long for the buffer/VE interface and 150 and 50 μm for the PAC/VE+ExE one. **(A-A’)** The parallel plates design is based on the one of the commercial “5 mm Petri dish platinum electrode chamber” (BTX Harvard Apparatus) where the cathode and the anode are spaced by 5 mm. The embryo is placed in the middle of a 15 μL liquid drop making a 40° contact angle with the glass surface (as measured by ourselves). This domain was represented by a spherical cap which other characteristics could be easily computed: it had a 1.07 mm height and a 5.86 mm base diameter. The latter dimension being slightly larger than the inter-electrode spacing, it consequently yielded to two additional vertical truncations (the variation in final buffer volume was negligible). **(B-B’)** The geometry implemented for localised electroporation with plate and needle electrodes has been established relying on the experimental details given by Khoo and collaborators (Khoo et al., 2007). The embryo is contained in a 15 μL drop similar to the above one, modelled as 1.07 mm high and 5.86 mm diameter spherical cap. The platinum plate is 750 μm long, 250 μm high, and 100 μm thick. It is connected to the macro-world by a rod, 100 μm in diameter. The tungsten needle has the shape of a 100 μm diameter cylinder which ends by a truncated cone. The corresponding tip half-angle is 5° and the radius of the terminal discoid section is 8.75 μm . Both the plate handle and the needle penetrate the buffer drop with a 5° angle with respect to the dish surface. The plate is set vertical at 150 μm from the embryo surface while the needle tip extremity is at 100 μm from the glass surface and at 50 μm from the targeted cells (volume variation due to the presence of the electrodes was negligible). **(C-C’)** The dimensions of the dielectric guide microdevice are given in Fig. S5 technical drawings. Briefly, the keyhole-shaped embryo chamber was obtained by merging a 650 μm large rectangular parallelepiped with two cylinders of radius 750 and 325 μm , respectively located at 1500 and 570 μm from the dielectric guide axis. The two electrode reservoirs are cylinders of diameter 2 mm which are 7.43 mm apart. Each of the three preceding features is open to the exterior and has a depth of 240 μm . They are joined by two 110 μm high microfluidic tunnels including the dielectric guides per se, 60 μm wide and 415 μm long, and a larger connecting channels, 1 mm wide and ~ 2 mm long. The Parafilm ceiling thickness is 130 μm . The volume defined by the latter structures is ~ 2.6 μL , which leaves ~ 12.4 μL for the three drops emerging from the embryo chamber and from the electrode reservoirs. According to our observations, the two spherical caps covering the electrode reservoirs are 2 mm in diameter and make a 50° contact angle with the Parafilm layer. Consequently, they have a height of 0.46 mm (Fig. 2A,D). For the central electroporation buffer volume the contact angle is nearly 90° and we depicted it as a half-ellipsoid 4.50 mm and 2.46 mm large, 1.80 mm high. Finally, the embryo was positioned with its anterior surface at 15 μm from the cathodic dielectric guide opening (Fig. 2F).

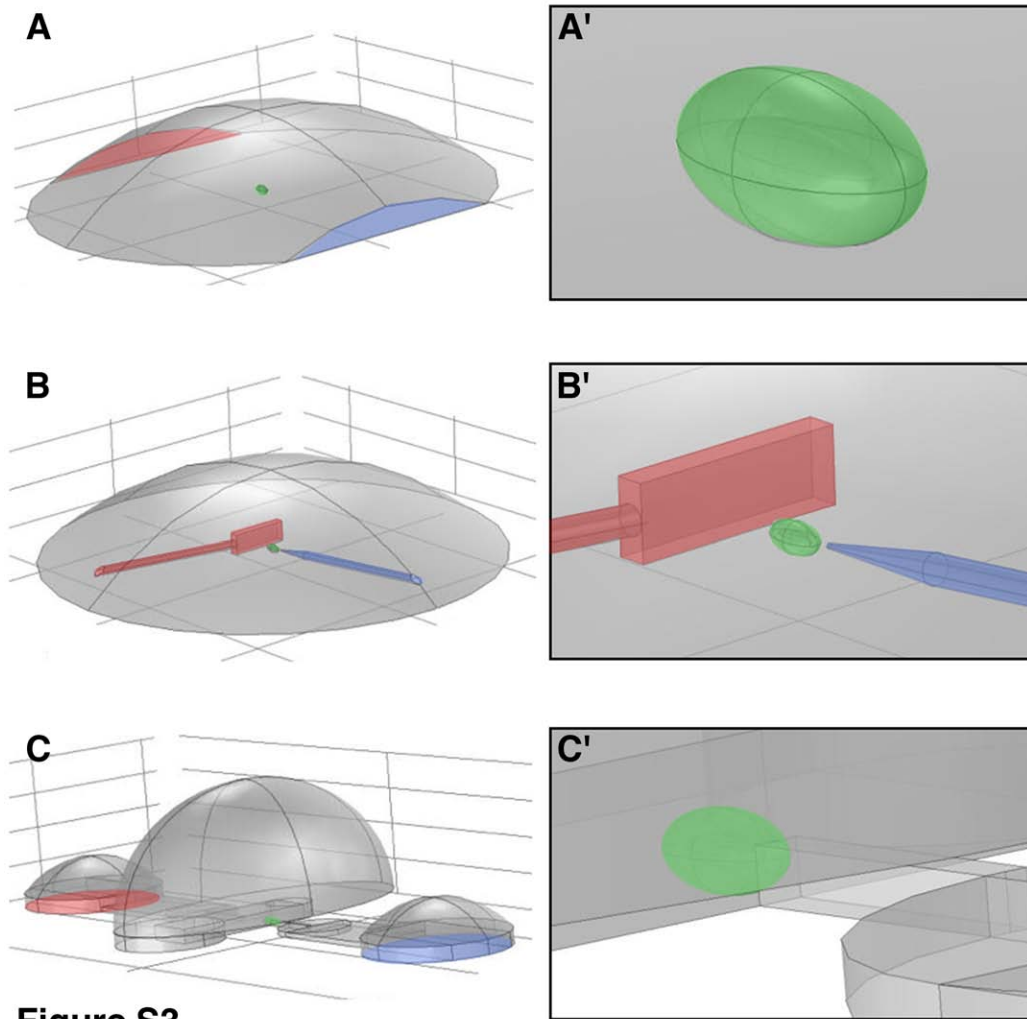


Figure S3

Figure S3. Snapshots of the conducting domains used to evaluate by numerical simulations the permeated area at the surface of E5.5 embryos. The three configurations, which have been entered in Comsol Multiphysics and run in the “Stationary” “Electric Currents” modes, correspond to the three schemes of Fig. S1B-D. The red and blue surfaces correspond respectively to anodes and cathodes. The embryo is in green and its angular positioning is set in order to target the DVE cells. The semi-axis values of the prolate ellipsoids are 100 and 50 mm long for the buffer/VE interface and 70 and 20 mm for the PAC/VE+ExE one. **(A-A’)** The device with parallel plate electrodes is identical to the one used at E6.5 and the embryo is resting halfway from the cathode and from the anode. **(B-B’)** The plate and the needle electrodes have the same dimension than at E6.5. They have not been displaced in order to maintain the same 150 mm and 50 mm respective spacing with the embryo surface. **(C-C’)** Although the dielectric guide width has been kept at 60 mm, its height has been adjusted to 70 mm. Consequently, the embryo chamber and the electrode reservoir depths are 200 mm, as displayed in Fig. S5 technical drawings. Moreover, the distal tip of the developing organism is now entering by 8 mm inside the guide opening (Fig. 2E).

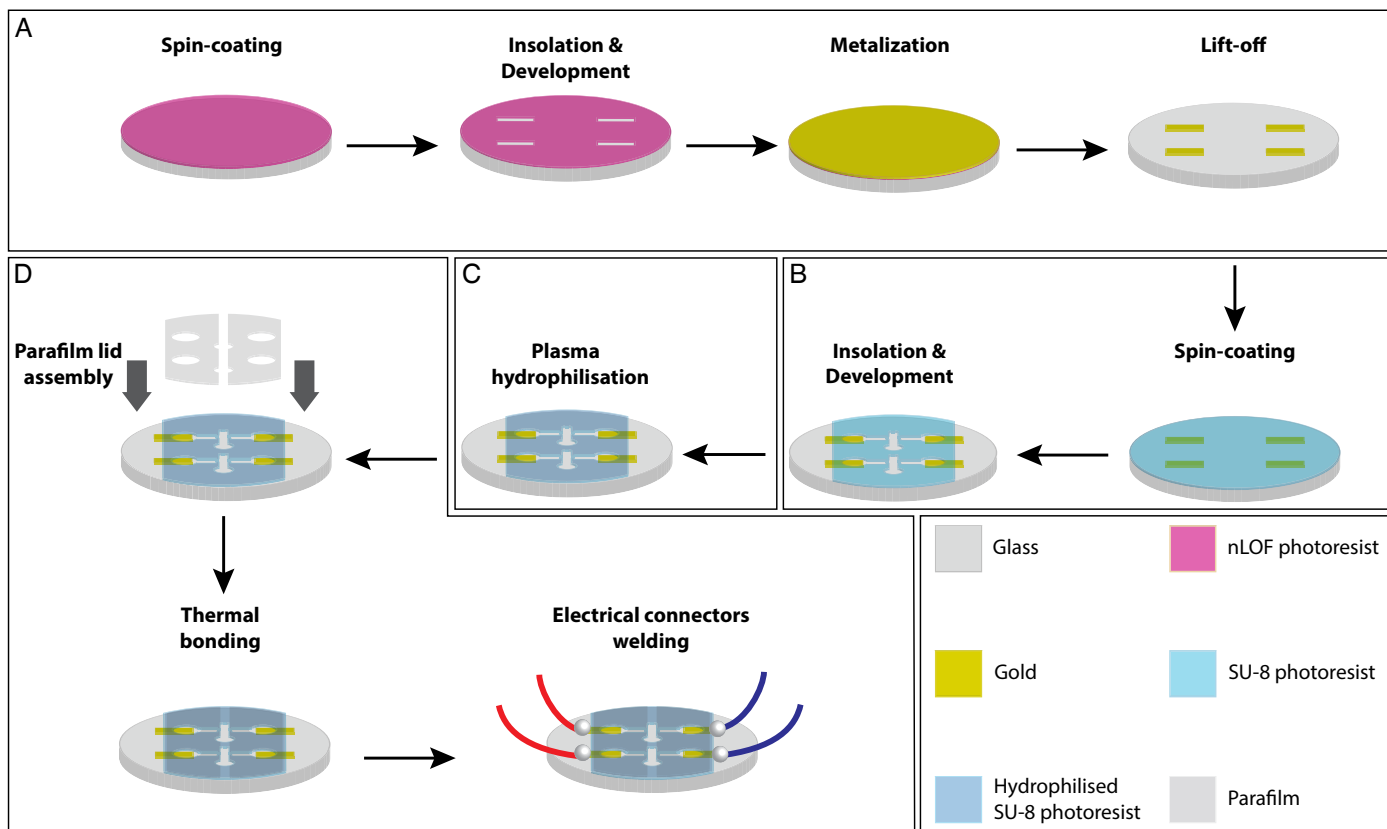


Figure S4. Fabrication of single-use SU-8/Parafilm microdevices such as the ones displayed in Fig. 2. Wafers of D263 glass (Opticad), 50 mm in diameter and 550 mm thick, are first cleaned by soaking in a fresh piranha mixture (H_2SO_4 95% / H_2O_2 30%, 2:1) for 3 hours followed by thorough rinsing with water. Then, a four-step protocol begins: **(A)** The electrodes are obtained by patterning a nLOF 2070 (MicroChemicals) layer by optical lithography, depositing by e-beam evaporation a metal film composed of 10 nm Ti / 120 nm Au, and dissolving the resist in acetone. The resulting features consist in paired stripes, 1 mm large and 12 mm long, that are separated by a 5.8 mm gap; **(B)** The dielectric guides (415 μm long for their narrowest section), the embryo chamber (650 μm wide), and the electrode reservoirs (2 mm in diameter) are photolithographed in SU-8 2050 (MicroChem), the thickness of the epoxy-resist and the width of the dielectric guides being respectively adjusted to 60 and 50 μm for E3.5 blastocysts, 70 and 60 μm for E5.5 embryos, and 110 and 60 μm for E6.5 embryos and explants; **(C)** The polymer surface is rendered hydrophilic using an ambient air plasma treatment for 50 s, at 300 mTorr in the Expanded Plasma Cleaner (Harrick); **(D)** The fluidic channels and guides are closed by thermal bonding of a thin film ceiling made of Parafilm “M” (Pechiney) in which appropriate access holes have been punched. The lid is assembled on a hot plate set at 60°C, and its final thickness is 130 μm . Finally, electrical connectors are welded to the electrodes.

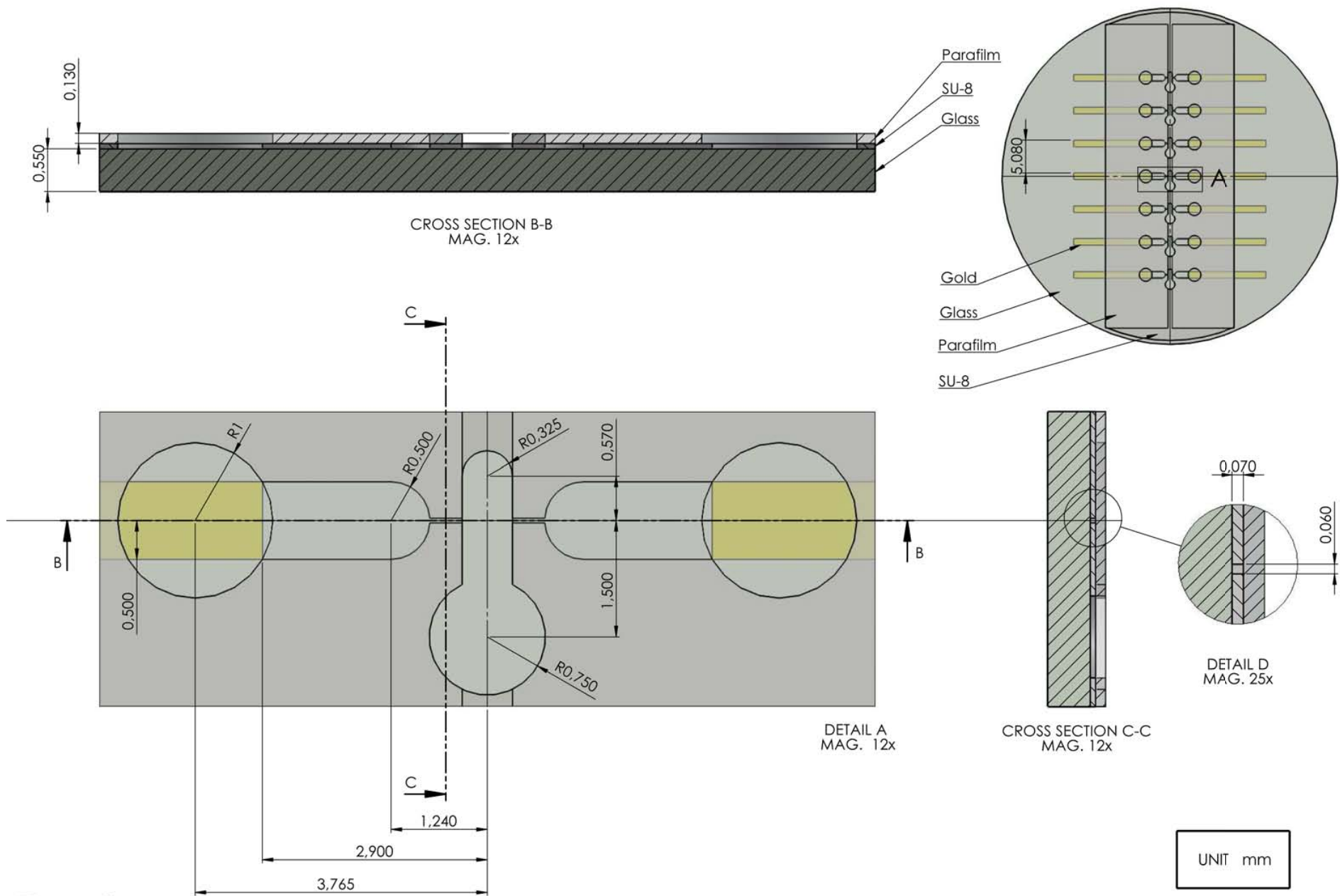


Figure S5. Technical drawing of the SU-8/Parafilm microdevice including 70 μm high and 60 μm wide dielectric guides, such as the one displayed in Fig. 2D,E. Detail A corresponds to a top view of the fluidic network whereas detail D emphasizes on the shape of the aperture in front of which the embryo is placed. The parent chip of Fig. 2F, which comprises 110 μm high and 60 μm wide dielectric guides, is obtained by simply changing the thickness of the SU-8 layer from 70 to 110 μm .

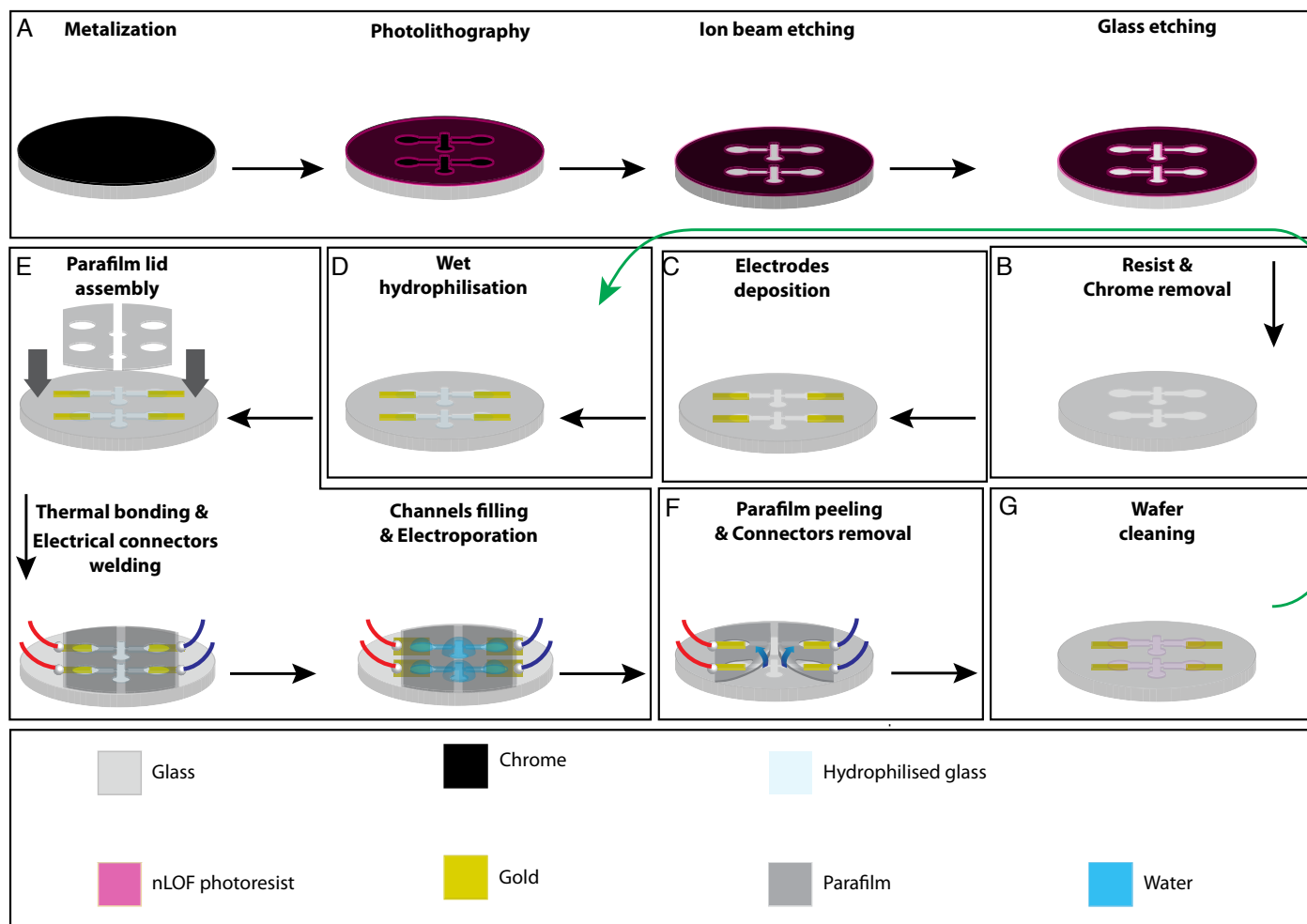


Figure S6. Fabrication and recycling procedure for reusable glass/Parafilm microdevices such as the one displayed in Fig. 7A,B. The starting glass wafers are the same than for the single-use chips, they are cleaned similarly in the piranha mixture. Then, a five-step protocol begins: **(A)** A mask is prepared by depositing by e-beam evaporation a 200 nm thin Cr film, patterning a nLOF 2070 layer by optical lithography, and attacking by ion beam etching the metal where it is unprotected. Patterns here obtained are identical to the previous SU-8 ones, except that the open trenches that will yield the dielectric guide are only 15 mm large. **(B)** Glass is next etched in a hydrofluoric acid solution (HF 40% / HCl 37% / H₂O, 10:3:20) for 40 minutes before thorough rinsing with water. Features are now 70 nm deep and they have significantly widened since wet etching is isotropic. The resist is next dissolved in acetone and the metal mask is removed in Chrome-Etch 3144 (Honeywell); **(C)** After a new piranha clean, metal electrodes are obtained thanks to a lift-off procedure identical to the one used for the SU-8/Parafilm devices; **(D)** The glass surface is then hydrophilised by dipping in a RCA1 mixture (NH₄OH 28% / H₂O₂ 30% / H₂O, 1:1:1) for 5 minutes and rinsing with water; **(E)** The Parafilm with all the necessary openings is finally thermally bonded, the connectors are welded, and the channels are filled with water within 5 minutes. Once the electroporation experiments performed, the glass part of the microsystem can be recycled according to the following four-step procedure: **(F)** The Parafilm is peeled off and the connectors are dismantled; **(G)** The wafer is soaked in trichloroethylene for 2 hours at 95°C, rinsed with acetone and isopropanol, dried under nitrogen, wiped in a 1 M NaOH solution, rinsed with water; Steps **(D)** and **(E)** are realized once more.

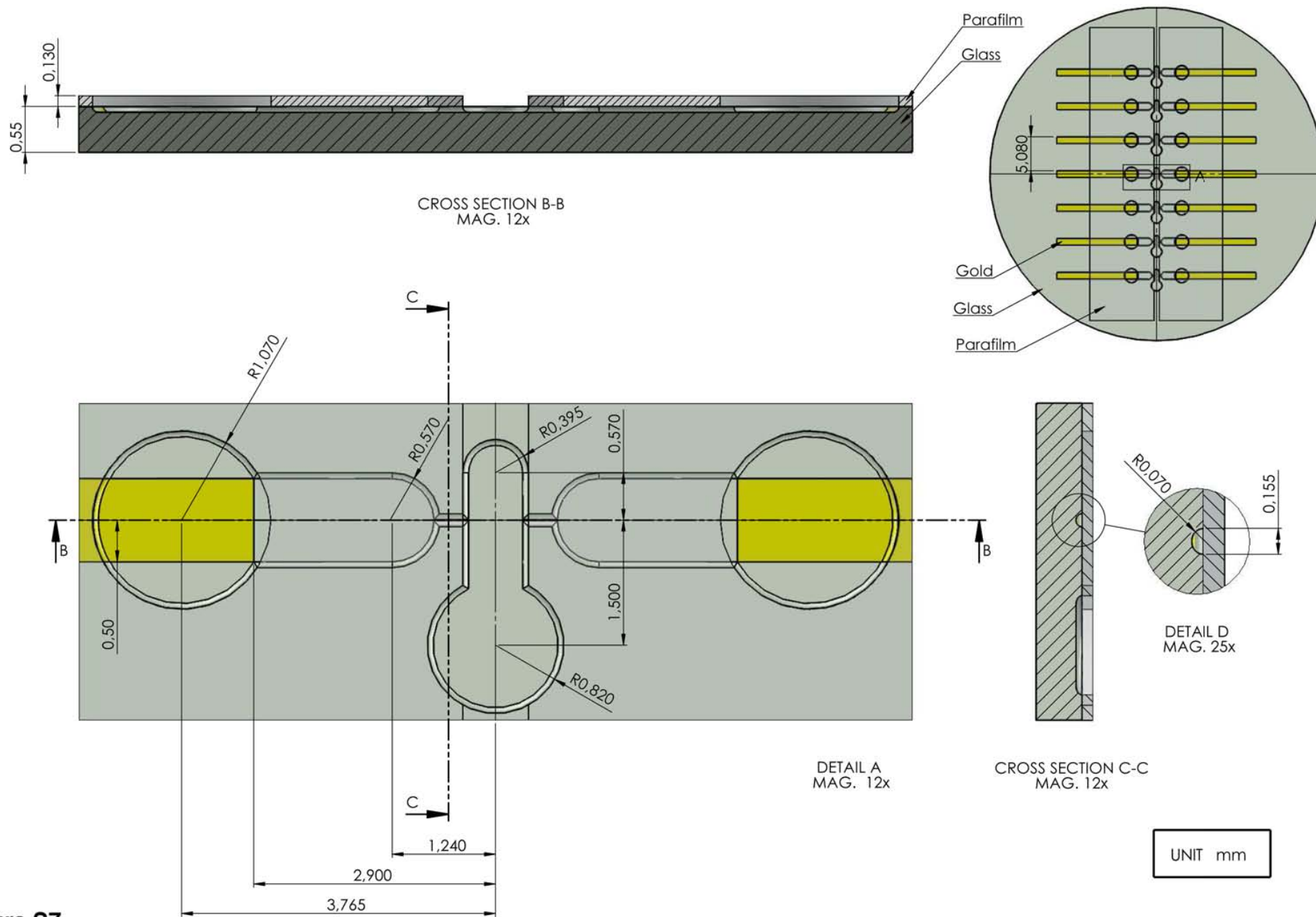


Figure S7

Figure S7. Technical drawing of the glass/Parafilm microdevice including 70 μm high dielectric guides, such as the one displayed in Fig. 7A,B. Detail A corresponds to a top view of the fluidic network whereas detail D emphasizes on the shape of the aperture in front of which the embryo is placed.

E6.5 Embryo	Abnormal Morphology	PI incorporation	mCherry expression
1	+	+	+
2	-	-	-
3	+	+	+
4	+	+	+
5	+	+	+
6	-	-	-
7	-	-	+
8	+	+	+
9	+	-	+
10	-	-	+
11	-	-	+
12	-	-	+
13	-	-	-
14	+	-	+
15	+	+	+
16	-	-	+
17	-	+	+
18	-	+	+
19	-	+	+
20	-	-	+
21	-	+	-
22	+	+	-
23	-	+	+
24	+	+	+
25	+	+	+
26	+	+	+
27	+	+	+
28	-	+	+
29	+	+	-
30	-	+	+
31	+	+	+
32	-	+	+
33	-	-	-
34	-	+	+
35	-	-	+
36	-	-	+
37	-	-	+
38	+	-	+

		mCherry expression		
		+	-	<i>Total</i>
Abnormal morphology	+	14	2	16
	-	17	5	22
<i>Total</i>		31	7	38

Fisher's exact test 2 tailed, p=0.67

		mCherry expression		
		+	-	<i>Total</i>
PI incorporation	+	19	3	22
	-	12	4	16
<i>Total</i>		31	7	38

Fisher's exact test 2 tailed, p=0.42

		Abnormal morphology		
		+	-	<i>Total</i>
PI incorporation	+	14	8	22
	-	2	14	16
<i>Total</i>		16	22	38

Fisher's exact test 2 tailed, p=0.002

Figure S8. Results of co-appearance in single E6.5 embryos of abnormal morphology, cell death, and mCherry expression after electroporation with 15 V and 50 ms pulses, using a 110 μm high and 60 μm wide dielectric guide. The results for 38 embryos electroporated with pCAG-nls-mCherry are shown. Fisher's exact test was used to determine the independence of the different parameters. Only PI incorporation and abnormal morphology displayed a p-value below 0.05.

E5.5 Embryo	Abnormal Morphology	PI incorporation	mCherry expression
1	-	-	+
2	-	-	+
3	+	-	+
4	+	+	+
5	-	-	+
6	-	+	+
7	-	-	+
8	+	+	+
9	+	-	+
10	+	+	+
11	+	-	+
12	+	+	-
13	-	-	+
14	+	-	+
15	+	+	+
16	-	-	+
17	+	+	+
18	+	+	-
19	-	-	+
20	-	-	+
21	-	-	-
22	-	-	+
23	+	+	-
24	-	+	-
25	+	+	-
26	-	+	+

		mCherry expression		Total
		+	-	
Abnormal morphology	+	9	4	13
	-	11	2	13
Total		20	6	26

Fisher's exact test 2 tailed, $p=0.64$

		mCherry expression		Total
		+	-	
PI incorporation	+	7	5	12
	-	13	1	14
Total		20	6	26

Fisher's exact test 2 tailed, $p=0.065$

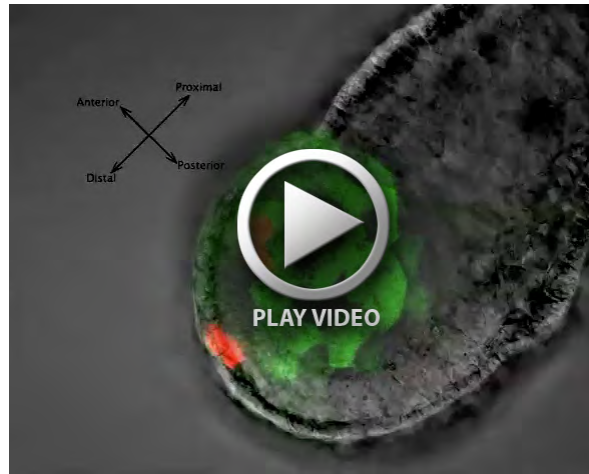
		Abnormal morphology		Total
		+	-	
PI incorporation	+	9	3	12
	-	4	10	14
Total		13	13	26

Fisher's exact test 2 tailed, $p=0.047$

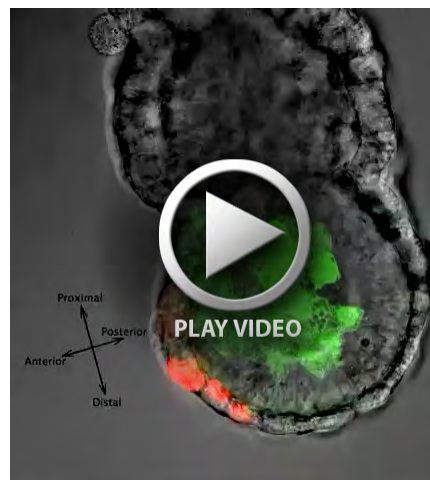
Figure S9. Results of co-appearance in single E5.5 embryos of abnormal morphology, cell death, and mCherry expression after electroporation with 15 V and 50 ms pulses, using a 70 μm high and 60 μm wide dielectric guide. The results for 26 embryos electroporated with pCAG-nls-mCherry are shown. Fisher's exact test was used to determine the independence of the different parameters. Only PI incorporation and abnormal morphology were found to be dependent displayed a p-value below 0.05.



Movie 1. Confocal live imaging on the embryo shown in Fig. 4E. pCAG-nls-mCherry and pCMV-GAP43myr-EGFP were co-electroporated in the VE with 15 V and 50 ms pulses, using a 70 μm high and 60 μm wide dielectric guide. Images were acquired starting 8 hours after electroporation, every 5 minutes for 30 minutes followed by every 15 minutes for 4 hours. The movie shows the superposition of maximum intensity projections of mCherry and GFP fluorescence from a stack comprising 18 slices spaced by 3 μm .



Movie 2. Confocal live imaging on the Hex-GFP E5.5 embryo shown in Fig. 5. pCAG-mCherry was electroporated in the VE with 15 V and 50 ms pulses, using a 70 μm high and 60 μm wide dielectric guide. Images were acquired every 15 minutes for 10 hours, starting 10 hours after electroporation. The movie shows the superposition of maximum intensity projections of mCherry and GFP fluorescence from a stack comprising 25 slices spaced by 4 μm .



Movie 3. Confocal live imaging on a Hex-GFP E5.5 embryo electroporated in the VE with pCAG-mCherry with 15 V and 50 ms pulses, using a 70 μm high and 60 μm wide dielectric guide. Images were acquired every 15 minutes for 10 hours, starting 9 hours 30 minutes after electroporation. The movie shows the superposition of maximum intensity projections of mCherry and GFP fluorescence from a stack comprising 23 slices spaced by 5 μm .



Movie 4. Confocal live imaging on a E3.5 blastocyst electroporated in the TE with pCAG-nls-Venus with 20 V and 50 ms pulses, using a 60 μm high and 50 μm wide dielectric guide. Images were acquired every 20 minutes for 18 hours, starting 6 hours after electroporation. The movie shows the superposition of the maximum intensity projection of Venus fluorescence with a single transmission plane from a stack comprising 14 slices spaced by 4 μm .

Finite Element Model Simulations to Assist the Design of Microdevices Dedicated to the Localized Electroporation of Mouse Embryos

X. Zhao^a, E. Mazari^a, D. Suárez-Boomgaard^b, I. Migeotte^b,
A. Perea-Gomez^c, and C. Gosse^a

^a Laboratoire de Photonique et de Nanostructures, CNRS UPR20,
route de Nozay, 91460 Marcoussis, France

^b Institut de Recherche Interdisciplinaire en Biologie Humaine et Moléculaire,
Université Libre de Bruxelles, route de Lennik 808, 1070 Bruxelles, Belgium

^c Institut Jacques Monod, Université Paris Diderot / CNRS UMR7592,
15 rue Hélène Brion, 75013 Paris, France

We have recently developed a microsystem to electroporate a few cells at the surface of early post-implantation mouse embryos. We could achieve the efficient, reproducible, and safe transfection of various genetic markers, which allowed single cell fate studies during morphogenesis. However, our single-use polymeric device necessitated to be fabricated in a clean room the day before each experiment. Thus, we here introduce an all-glass chip that any biologist can easily recycle in its laboratory. Most importantly, during the technological evolution process we could validate a comprehensive design strategy based on finite element model simulations. Indeed, both the embryo and the microsystem were represented as very simple electric objects and stationary computations enabled to properly predict the voltage pulse amplitude that would yield optimal device performances.

Introduction

During embryonic development interactions between cell groups enable the growth, migration, and specification of various tissues. The dynamics of these phenomena can be unraveled by manipulating gene expression with appropriate spatiotemporal resolution, in order to precisely label selected cell populations, and/or to modify their behavior. Electroporation, the delivery of exogenous molecules into the cytoplasm through electric permeation of the plasma membrane, has been harnessed to this aim. However, until recently, existing strategies suffered from insufficient reproducibility and mediocre survival when applied to early post-implantation mouse embryos. Indeed, between 5.5 and 7.5 days of development (E5.5 and E7.5) these organisms are small (between 150 and 500 μm long) and delicate.

If sharp metallic electrodes are efficient to concentrate electric field lines and permeate the plasma membrane over a restricted area, their use often results in embryo death because harmful species such as gases and protons are produced by electrolysis (1). Thereby, we recently introduced a device where the electric field is generated by remote gold electrodes and channeled towards the cells to be transfected by dielectric guides (Fig. 1) (2,3). This technique was proved efficient, reproducible, and safe. Moreover, microsystem performances could be demonstrated by addressing at E5.5 the distal

visceral endoderm (DVE), a migrating cell population essential for anterior-posterior axis establishment. Live imaging of cells discretely labeled with fluorescent proteins allowed us to reveal new facts concerning tissue rearrangement (4). Besides, we showed that the utilization of our device could be extended to a variety of embryological contexts, from preimplantation embryos to organ explants dissected from latter stage organisms (4).

Up to now, our chips are fabricated on a glass wafer by patterning the guide walls in SU-8 photoresist, hydrophilizing them with an air plasma, and closing the structure with a Parafilm lid (Fig. 1B). Despite its success, this technology is rather labor intensive since a new microsystem has to be prepared for each series of transfection experiments. Indeed, polymer surfaces cannot easily be cleaned. In addition, the hydrophobic nature of the materials soon reappears and storage for more than 48 h is impossible. In the present paper we proposed an all-in-glass device that every embryologist should be able to infinitely reuse on his own. We further illustrate how finite element model (FEM) simulations provide a cost-effective way to manage design changes.

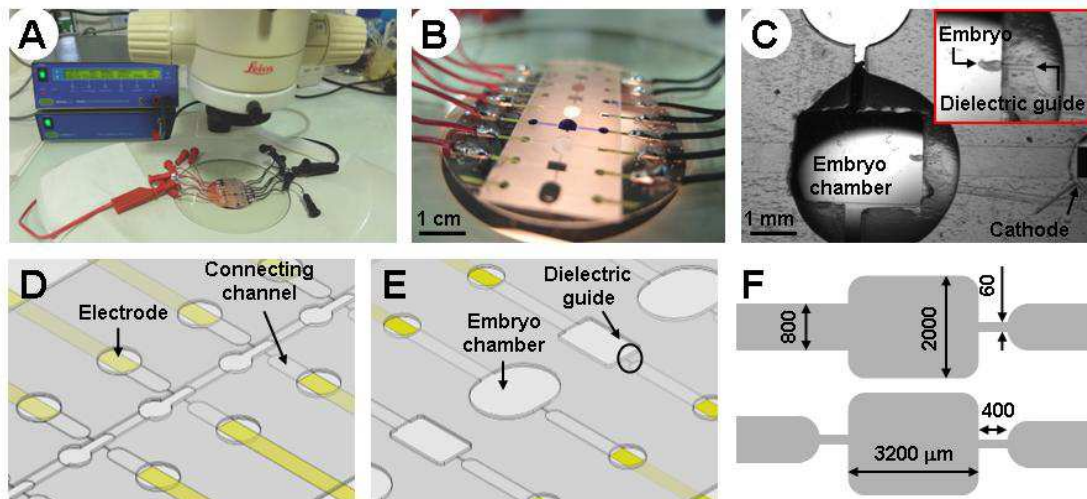


Figure 1. Layout of the various electroporation devices introduced along the upgrading procedure. Photographs evidence (A) how a SU-8 / Parafilm microsystem is integrated in the whole experimental setup, which includes a stereo microscope and the electroporator, (B) how the fluidic network is filled (here with a dye solution), and (C) how an E5.5 embryo is positioned in front of the cathodic dielectric guide. Diagrams showing SU-8 / Parafilm chips, including the electrodes, connecting channels, dielectric guides, and embryo chamber, enable to compare (D) the design used in our initial work (4) with (E) the more ergonomic asymmetric solution proposed in the present article. Dimensions for the latter microsystem, as well as for the symmetric one, are given in μm in the schematic top view (F).

Design considerations

Our present SU-8 / Parafilm device includes a keyhole-shaped embryo chamber that welcomes a droplet in which the organism to be electroporated can easily be manipulated with glass or metal tools (Fig. 1D). At both extremities are the open electrode reservoirs from which gas bubbles produced by electrolysis can escape without blocking the electric current flow. Each of the two latter chambers is linked to the central one by a closed connecting channel that narrows to yield the dielectric guide per se. The size of the

aperture in front of which the embryo is placed is the most critical part of the chip since it has to roughly match the embryo size in order to achieve proper localization of the permeation.

In addition to shifting to the all-in-glass technology, we here propose several improvements in the design of the microfluidic network (Fig. 1E,F). First, to ease micromanipulation the embryo chamber will be widened and the space between the electrodes will be increased. Second, to render fabrication simpler the keyhole shape for the central reservoir will be abandoned. Finally, as of the two guides one is often unusable due to lid alignment problems, we will introduce an asymmetric layout which will also diminish the risk of fabrication failure during photolithography steps (Fig. 1F).

Numerical simulations

Relying on the Comsol Multiphysics 4.2a software (Comsol), we determined the electric potential in both the embryo and the electroporation buffer solution, and we could then estimate the extent of the permeated area. Since they were experimentally validated in reference (4), the present electric representation, as well as the computational procedures, enabled one to assert pore opening from the value of the induced transmembrane voltage (ITV).

Model description

Two concentric prolate ellipsoids were used to figure an E5.5 embryo (Figs 2A,D and 2B,E). The outer one, 200 by 100 μm large, represents the external boundary of the organism and the inner one, 140 by 40 μm large, its proamniotic cavity. Cells were not considered individually because at the considered developmental stage they are connected by electrically conductive structures called GAP junctions (5,6). Numerical parameters were next inferred from the literature (4): we assumed the two ellipsoids to behave as resistive membranes having a $3 \cdot 10^{-7}$ S/m conductivity and a 5 nm thickness; the conductivity of the proamniotic fluid was hypothesized identical to that of the cytoplasm and fixed at 0.3 S/m. For the electroporation buffer, we measured a 1.5 S/m value. Finally, the glass, polymer, and air boundaries are insulating. The cathode surface was grounded and the anode one had its potential corresponding to the pulse amplitude, V_{anode} .

Comsol Multiphysics was run in the “Stationary” “Electric Currents” mode (7). Simple time-independent modeling was here relevant because pulses were longer than the characteristic charging time associated with phospholipidic membranes (8).

Procedures

Subtracting the electric potential on the extra-cellular side of the embryo surface to its cytoplasmic counterpart (Fig. 2B,E) yields the ITV (Fig. 2C,F). This parameter was directly used to account for the electroporated area since exogenous molecules can enter cells only when it exceeds a given threshold ITV_{pore} (9). Our previous work enabled to determine that for the DVE of early post-implantation embryos $\text{ITV}_{\text{pore}} \sim 0.65$ V (4), which agreed with published data (8,9,10). Note that we ignored the resting potential contribution to the ITV since its uncertain -20 to -60 mV value (8) is at least 10 times smaller than ITV_{pore} .

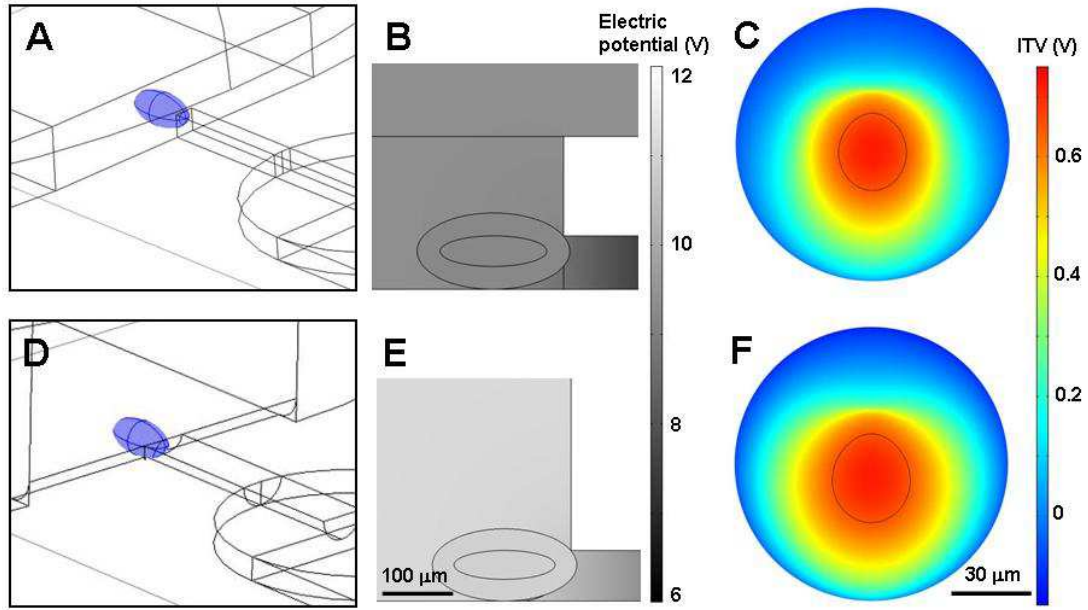


Figure 2. FEM simulations for the electroporation of E5.5 embryos. Microdevices are fabricated following the asymmetric design, using either (A-C) the SU-8 / Parafilm technology or (D-F) the glass / glass one. The applied pulse amplitudes correspond to the V_{anode} parameters given in Table I. Figure shows, for each case, (A,D) the snapshots of the conducting domains, (B,E) the electric potential in the vertical symmetry plane passing through the embryo center, as well as (C,F) the induced transmembrane voltage on flattened views of the distal half of the embryo. In the latter figures the electroporated area, where $\text{ITV} > \text{ITV}_{\text{pore}}$, is surrounded by a red line.

TABLE I. Summary of the results obtained from the FEM simulations. V_{anode} is the applied pulse amplitude, V_{dist} the outer potential at the distal tip of the embryo, ITV_{max} the maximal value of the induced transmembrane voltage, and S_{pore} the surface of the electroporated area divided by half the one of the ellipsoid.

Technology	Design	V_{anode} (V)	V_{dist} (V)	ITV_{max} (mV)	S_{pore} (%)
SU-8 / Parafilm	<i>Mazari 2014</i>	15.0	6.76	0.72	2.25
SU-8 / Parafilm	asymmetric	13.4	8.52	0.72	2.18
SU-8 / Parafilm	symmetric	18.6	8.54	0.72	2.18
glass / glass	asymmetric	17.6	10.2	0.72	2.95

Once a new microsystem had been conceived, it was drawn in Comsol Multiphysics and the embryo was positioned in front of the cathodic dielectric guide so as to target its DVE (Figs 1C and 2A,D), its distal tip entering $8 \mu\text{m}$ inside the aperture (Figs 2A,D and 2B,E). The applied pulse amplitude V_{anode} was next adjusted by hand in order to yield a maximum ITV value, ITV_{max} , similar to the 0.72 V one achieved with our previous chip (4). Indeed, both simulations and experimental observations have proved that for $\text{ITV} \sim 0.6 - 0.8 \text{ V}$ electroporation remains efficient while survival of the embryo is not at risk (4). Please be aware that it is not the value of the electric potential at cell surface which has to be limited but the one of the ITV since the latter parameter is the sole that is related to membrane disruption. Then, once the electroporation conditions had been selected according to both transfection success and safety issues, localization still remained to be investigated. We thus computed the ratio of the electroporated area to the one of the distal embryo half, S_{pore} . As can be seen in Table I, for all three new devices

we could find appropriate pulse amplitudes V_{anode} that yielded ITV_{max} and S_{pore} values similar to the ones characterizing the former SU-8 / Parafilm chip.

Device fabrication

Most of the procedures given below are fully described in reference (4), with the exception of the glass / glass bonding one which is mentioned here for the first time.

SU-8 / Parafilm technology

Microsystems were realized on D263 glass substrates, 550 μm thick and 2 inches in diameter (Fig. 1B,C). An identical four-step process was followed for both asymmetric and symmetric designs: (i) the electrodes were obtained by patterning a nLOF2070 layer (AZ Electronic Materials) by optical lithography, successively evaporating 10 nm of Ti and 120 nm Au, and dissolving the resist in acetone. The resulting features consisted in pairs of 0.8 mm large aligned stripes which will serve as electrodes; (ii) the 60 μm large dielectric guides, as well as the connecting channels, the electroporation chamber, and the electrode reservoirs were photolithographed in a 70 μm thick layer of SU8-2050 (MicroChem); (iii) the polymer surface was rendered hydrophilic using a 300 mTorr air plasma treatment for 50 s in a plasma cleaner reactor (Harrick); (iv) the fluidic network was closed by thermal bonding, at 60 $^{\circ}\text{C}$, of a 130 μm thick Parafilm 'M' lid (Pechiney) in which appropriate access holes had been cut out with a CE6000-40 cutting plotter (Graphtec).

Glass / glass technology

Starting with similar glass wafers than above, a two-step protocol yielded the lower part of the device: (i) a 200 nm Cr thin film was deposited by e-beam evaporation, the fluidic system was patterned in a nLOF 2070 layer by optical lithography, and the metal coating was opened by ion beam etching; (ii) glass was attacked in a HF 40% / HCl 37% / H_2O , 10:3:20 mixture for 40 minutes before thorough rinsing with water. The resist was next dissolved in acetone and the metal removed in Chrome-Etch 3144 (Honeywell). The lithography mask was here conceived in order to account for the widening inherent to isotropic etching. Thus, it resulted in rounded features having the same dimensions than the SU-8 ones, except for the dielectric guide which had the shape of a half-pipe with a 70 μm radius (Fig. 2D).

The upper lid was also made of 550 μm thick D263 glass. After dicing a wafer along its diameter, the ~ 1.5 mm diameter access holes for the electrode reservoirs were sand blasted. A thin layer of Vitralit 6127 (Eleco) was then spin-coated onto these parts before their assembly onto the lower wafer using a MJB3 aligner (SUSS MicroTec). Insolation of the UV-curable glue for 1 min was followed by baking at 100 $^{\circ}\text{C}$ for 3 h in order to complete the evaporation of any toxic solvents.

Experimental validation

The goal of the present section was to certify the relevance of the electroporation conditions predicted by FEM simulations (Table I), for the three devices that had been fabricated.

Electroporation

The device was filled with 15 μL of electroporation solution which had been divided in 3 droplets in order to cover both electrodes as well as the central chamber (Fig. 1B). According to the biomolecule of interest, the 150 mM NaCl 20 mM Hepes buffer, pH 7.0, was supplemented with either 2 mg/mL of FITC-dextran (FD4, Sigma) or 1 $\mu\text{g}/\mu\text{L}$ of pCAG-mCherry. Freshly dissected E5.5 mouse embryos were then placed with their DVE facing the cathodic dielectric guide, a small spontaneous liquid flow gently maintaining them in front of the opening (Fig. 1C). Transfection was subsequently carried out using a TSS20 Ovodyne electroporator (Intracell) directly connected to the microsystem (Fig. 1A). A train of three 50 ms long square pulses, spaced by 1 s, was applied, their amplitude being chosen so as to be close to the V_{anode} values predicted by the FEM simulations (Table I, Fig. 3).

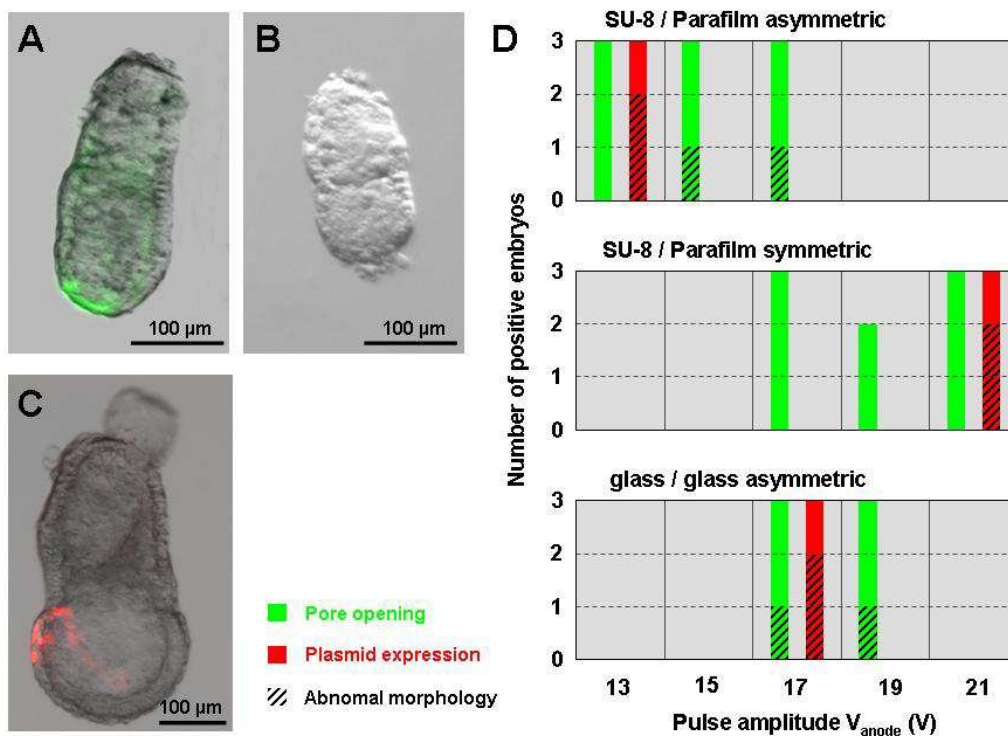


Figure 3. Electroporation outcomes for series of three E5.5 embryos submitted to voltage pulses of various amplitudes V_{anode} , in devices fabricated according to the designs and technologies listed in Table I. Representative examples are given for the criteria used to assert (A) FITC-Dextran incorporation, (B) abnormal morphology, and (C) mCherry cytoplasmic expression. In (D) colored bars report for the number of embryos where at least one of the DVE cells displayed the following characteristics: (green) FITC-Dextran incorporation, (red) mCherry expression, and (hatched black) abnormal morphology. Please note that regarding FITC-Dextran incorporation only three voltage amplitudes were tested for the SU-8 / Parafilm microsystems and two for the glass / glass one. As far as mCherry expression was concerned, only one condition was investigated for each kind of chip. The embryo anterior side is to the left in C.

Observations

After electroporation completion, embryos were rinsed in the dissection solution (DMEM-GlutaMAX, 4.5 g/L glucose – Invitrogen – supplemented with 25 mM Hepes and 10 % inactivated fetal calf serum). If relevant, observation of FITC-Dextran penetration was here performed to assert pore opening (Fig. 3A). Furthermore irrespectively of the electroporated molecule, cells of the outer periphery of the organism were always scrutinized for morphological abnormalities such as swelling or destruction (Fig. 3B). Subsequently, each group of 3 embryos was placed into 200 μ L of culture medium (DMEM-GlutaMAX, 4.5 g/L glucose, 100 μ g/ml streptomycin, 100 U/ml penicillin, supplemented with 50 % inactivated rat serum) and incubated in a 8-wells chambers slide (NUNC) under standard cell culture conditions (37 °C, 5% CO₂). In the case a plasmid was transfected, the expression of the red fluorescent protein was checked after 24 h (Fig. 3C).

Both bright field and fluorescence visualization were achieved on a M165FC stereomicroscope (Leica) equipped with GFP and Cy3 filters and connected to an Orca-R2 camera (Hamamatsu).

Discussion

The transition from the single-use polymeric device introduced in references (3,4) towards a simply recyclable microsystem was two-step. First, we changed the chip design while stacking to the effective SU-8 / Parafilm technology (Fig. 1B,C). It allowed us to notice that both asymmetric and symmetric configurations worked equally well (Figs 1F and 3D). As usually only a single dielectric guide is used in an experiment and as the fabrication of asymmetric device is less constrained during lid alignment, we consequently selected the latter design to implement the glass / glass technology. Up to now, the bottom wafer containing the fluidic system and the upper one with the access holes were assembled relying on an original gluing procedure. Although not completely optimal as far as microfabrication is concerned, our strategy has enabled to prove that the rounded shape of dielectric guides wet etched in glass is as efficient as the squared one that characterized our initial polymeric chips. Future work will include the development of glass drilling for access hole opening as well as fusion bonding for wafer assembly.

Regarding FEM simulations, we have confirmed that they represent a very helpful tool to assist device conception. Indeed, before performing any test on embryos we could devise microsystems which operating range will match the electroporator one. Later on we successfully predicted the pulse amplitude to apply for each of the fabricated chips. Indeed, conditions distant by less than 2 V from the V_{anode} parameters recommended in Table I yielded very satisfactory outcomes with respect to electroporation efficiency and safety (Fig. 3D). Although relying on a limited number of samples, our results indicate that in a large majority of cases a restricted cell population integrates the exogeneous molecules, either FITC-Dextran or plasmid DNA, while deleterious effects remain limited to 30 – 50 % of the processed embryos. These data are similar to the one associated with the best conditions used to run our original SU-8 / Parafilm chip (4). However, thanks to the simulations the present optimal parameters were obtained after a very limited number of tests, ~ 12 per device, whereas in our initial screening work on the first design we performed more than 200 electroporations (4). Finally, it is worth noting that permeation localization also stayed satisfactory since the shape of the dielectric guides was roughly kept constant during the technological evolution process.

Acknowledgments

This work was supported by the grants *BioModulator* (ANR Pnano 2008), *ElectroMice* (CNRS PI: Physique Chimie Biologie 2008), *ElectroTagMam* (Cnano IdF 2011), *ElectroMagSign* (RTRA Triangle de la Physique 2012), and *ElectroDev* (PHC Tournesol 2013). E.M. was recipient of a PhD scholarship from the FRM, I.M. is a research associate of the FNRS, and D.S.B is supported by the FNRS under grant n° MIS F.4525.14. We thank J.-C. Galas for technical assistance with the cutting plotter.

References

1. B. P. Davidson, T. E. Tsang, P.-L. Khoo, J. M. Gad, and P. P. L. Tam, *Genesis*, **35**, 57 (2003).
2. E. Mazari, M. Mantelet, J. Iranzo, A. Perea-Gomez, and C. Gosse, *Transducers 2011, Digest of the Technical Papers of the 16th International Conference on Solid-State Sensors, Actuators, and Microsystems*, 1172 (2011).
3. E. Mazari, X. Zhao, J. Collignon, A. Perea-Gomez, and C. Gosse, *MicroTAS 2012, Proceedings of the 16th International Conference on Miniaturized Systems for Chemistry and Life Sciences*, 1729 (2012).
4. E. Mazari, X. Zhao, I. Migeotte, J. Collignon, C. Gosse, and A. Perea-Gomez, *Development*, **141**, 2349 (2014).
5. G. H. Kalimi and C. W. Lo, *J. Cell Biol.*, **107**, 241 (1988).
6. G. Pucihar, D. Miklavcic, and T. Kotnik, *IEEE Trans. Biomed. Eng.*, **56**, 1491 (2009).
7. G. Pucihar, T. Kotnik, B. Valic, and D. Miklavcic, *Ann. Biomed. Eng.*, **34**, 642 (2006).
8. B. Valic, M. Golzio, M. Pavlin, A. Schatz, C. Faurie, B. Gabriel, J. Teissié, M.-P. Rols, and D. Miklavcic, *Eur. Biophys. J.*, **32**, 519 (2003).
9. J.-M. Escoffre, T. Portet, L. Wasungu, J. Teissié, D. Dean, and M.-P. Rols, *Mol. Biotechnol.*, **41**, 286 (2009).
10. M. Hibino, H. Itoh, and K. Kinoshita Jr, *Biophys. J.*, **64**, 1789 (1993).

ENGINEERING A REUSABLE GLASS DEVICE TO ELECTROPORATE A FEW CELLS AND TO STUDY THEIR MIGRATION IN THE DEVELOPING MOUSE EMBRYO

Xuan Zhao,[†] D. Suárez-Boomgaard,[#] Elsa Mazari,[†] Jassem Safioui,[§]
Isabelle Migeotte,[#] Aitana Perea-Gomez,^{*} Charlie Gosse[†]

[†] *Laboratoire de Photonique et de Nanostructures, LPN-CNRS, Marcoussis, FRANCE*

[#] *IRIBHM, Université Libre de Bruxelles, Bruxelles, BELGIUM*

[§] *Femto Engineering, Besançon, FRANCE*

^{*} *Institut Jacques Monod, Université Paris Diderot – CNRS, Paris, FRANCE*

ABSTRACT

The localized introduction of transgenic constructs in early post-implantation mouse embryos can be achieved thanks to electroporation microdevices including dielectric guides. To make this technique more accessible we here transform our single-use home-made demonstrator in a reusable prototype complying with standard micromachining processes and user-inspired ergonomic choices. Design changes were assisted by numerical simulations and validated using fluorescent markers. Biological relevance was demonstrated by analyzing the migration of previously unobservable cell populations.

KEYWORDS: Transfection, Developmental biology, Laser micromachining

INTRODUCTION

Specification of the mouse anterior-posterior axis starts after 5.5 days of development (E5.5). Cells belonging to the distal visceral endoderm (DVE) leave their position at the tip of the embryo for a more lateral one, as observed in Hex-GFP transgenic animals where this tissue is labeled in green [1]. However, the involved migration mechanism as well as the fate of all the unlabeled cells still remain unclear. We therefore proposed an electroporation microsystem able to focus electric field lines at the surface of those tiny organisms and dispense plasmids encoding fluorescent proteins (FP) in only 2 to 4 cells, at any selected location [2]. Compared to the utilization of sharp metallic electrodes [3], our technique is safe, efficient, and reproducible. Nevertheless, up to now it depended on a chip which fabrication involved non-standard and operator-dependent steps such as Parafilm punching and bonding. Furthermore, the microsystem had to be utilized within 48 hours because the hydrophilization of the fluidic channels faded. Thus, in the present paper we introduce a device entirely realized from hydrophilic and easy-to-clean glass substrates, which stays functional after more than 6 months of intensive use.

EXPERIMENTAL

In our previous microsystem the dielectric guides were parallelepipeds, 70 μm high and 60 μm large, fabricated by photolithographing two SU-8 photoresist walls on a glass slide and covering them with a Parafilm ceiling [2]. Guides are now hemi-cylinders of radius 70 μm obtained by closing a first BF33 glass wafer including wet-etched patterns with a second substrate in which access holes for electrodes insertion and embryo manipulation have been realized by laser micromachining [4] (Fig. 1). A thin layer of Vitralit 6127, a photo-curable glue that can be spin-coated on the lid before assembly and hardened under UV once the two glass parts are in contact, enables watertight bonding [5].

More specifically, the via holes in the 300 μm thick BF33 lid were drilled with a Ti:Sapphire system emitting, with a 5 kHz repetition rate, 200 fs long Gaussian laser pulses centered at 800 nm. Focusing on the sample top surface was performed with achromatic lenses and the material was ablated layer by layer along a predefined contour thanks to a 3-axis translation stage. Satisfactory edge roughness as well as substrate surfaces with nearly no debris redistribution could be obtained by appropriately selecting the

pulse energy and duration, and the machining speed (Fig. 1d). However, we observed that trying to further improve edge quality resulted in crevices forming on the exit surface of the wafer.

Finite element model (FEM) simulations based on a validated electrical model of the embryo [2,5] were subsequently undertaken to determine which voltage to apply at the anode of the glass device. We found that slightly increasing the pulse amplitude, in comparison to reference [2] settings, yield roughly the same permeated area for an identical maximum induced transmembrane voltage (ITV) (Fig. 2). To validate this new parameter value, we first looked for pore opening and protein expression respectively employing FITC-dextran, a membrane impermeant fluorophore, and pCAG-mCherry, a plasmid encoding a red FP. Signs of necrosis at the visceral endoderm (VE) surface were also recorded [2]. As anticipated from FEM simulations the new microsystem performed as well as the old one (Table 1).

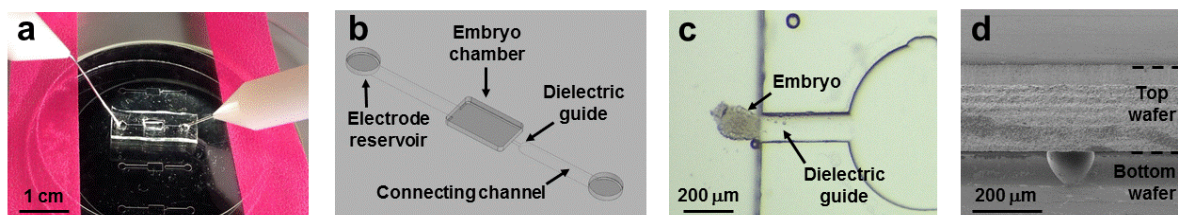


Figure 1. (a) View of the glass microsystem positioned on the stereo microscope stage and connected to the electroporator through macroscopic platinum electrodes. A PDMS stamp helps to contain the electroporation buffer in the electrode reservoirs and in the embryo chamber. (b) Diagram detailing the device structure. (c) Close up picture of an E5.5 embryo positioned in front of the cathodic dielectric guide. (d) Scanning electron micrograph of the dielectric guide aperture.

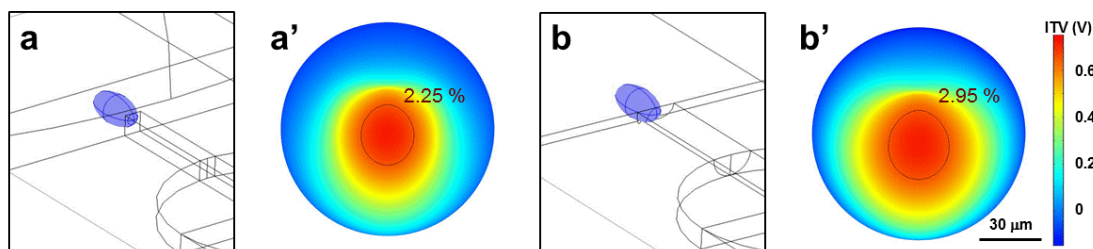


Figure 2. FEM simulations for the electroporation of E5.5 embryos in microsystems fabricated using either (a-a') the SU-8 / Parafilm technology and the reference [2] design or (b-b') the glass technology and the Fig. 1 design. The applied pulse amplitudes were 15 and 17.6 V, respectively. For each case are displayed (a, b) a snapshot of the conducting domains established according to our previously validated electrical model [2] and (a', b') the ITV on flattened views of the distal half of the embryo – the electroporated area, where the ITV exceeds the 0.65 V threshold, is delimited by a red line and the percentage represents the one of the enclosed surface.

Table 1. Experimental outcomes for E5.5 embryos electroporated in the VE with 3 voltage pulses of 50 ms separated by 1 s, using either the single-use demonstrator or the reusable prototype – we provide the ratio between the number of positive embryos, for which at least one cell displays the examined criteria, and the total number of electroporations. An abnormal morphology corresponds to dead cells “bubbling” out of the VE epithelium.

Design	Technology	Voltage amplitude (V)	Criteria		
			FITC-dextran incorporation	mCherry expression	Abnormal morphology
Ref. [2]	SU-8 / Parafilm	15	37/37	47/56	32/96
Fig. 1	Glass	17	3/3	3/3	3/6

RESULTS

We first targeted different regions of the visceral endoderm of Hex-GFP transgenic embryos with the mCherry plasmid. Indeed, Hex-GFP allows the visualization of cell behavior at the DVE migration front (Fig. 3a-a') but does not provide information on all the other VE cells. Lifetime imaging revealed that

active motion associated with the extension of filopodial projections to sense the environment is not a behavior restricted to the DVE leader cells; instead, it characterizes the whole VE (Fig. 3).

Second, to image the subcellular structures involved in migration, we are currently electroporating plasmids encoding constructs in which a protein of interest is fused with a FP. Preliminary trials enabled to observe histones in nuclei (Fig. 4a-a') and actin microfilaments in the cytoskeleton (Fig. 4b-b').

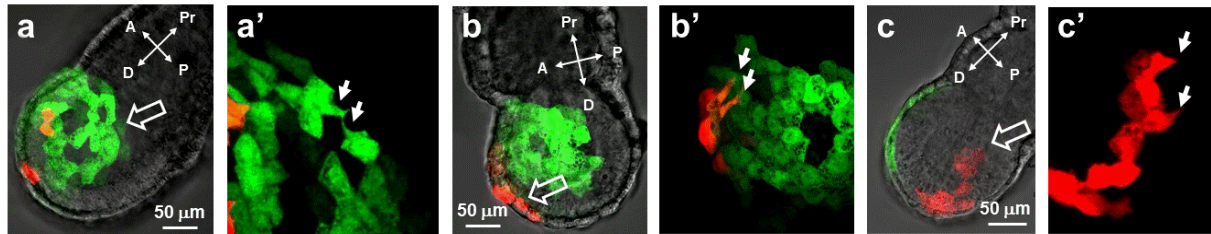


Figure 3. Cell migration observed by live imaging in E5.5 Hex-GFP embryos electroporated into their (a-a', b-b') distal or (c-c') posterior VE with the pCAG-mCherry plasmid. (a-c) Superposition of the bright field and fluorescence views of the embryos a few hours after transfection – the single-use demonstrator and 20 V pulses were used. Big arrows indicate the cells that will display filopodial projections later on. A = anterior, P = posterior, D = distal, Pr = proximal. (a'-c') Close up fluorescence views on the projections, highlighted with small white arrows, for (a') two DVE leader cells, (b') two DVE non-leader cells, and (c') two non-DVE cells.

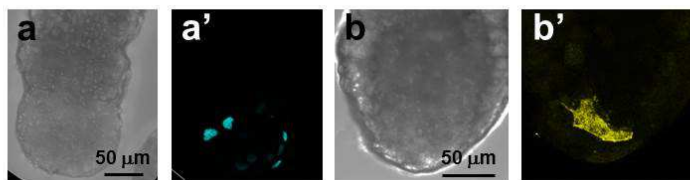


Figure 4. Molecular structures observed in E5.5 embryos electroporated with plasmids encoding two fusion proteins: (a-a') pCMV-H2B-CFP and (b-b') pCMV-YFP-actin. (a-b) are bright field views and (a'-b') the corresponding epifluorescence observations.

CONCLUSIONS

We have defined a methodological framework that will for sure ease the conception of simple and robust electroporation devices dedicated to embryos at other stages or from other species: standard microfabrication protocols favor reproducibility; FEM simulations facilitate design optimization and help to decrease the number of tests performed on animals. Localized transfection was here used to label cells and investigate migration mechanisms but we also plan to harness it so as to modulate morphogen expression and study migration cues.

ACKNOWLEDGEMENTS

We thank the staff of the LPN clean room, of the ImagoSeine platform, and of the ULB LiMiF platform for technical assistance. This work has been supported by the grants “ElectroMice” (CNRS PI: Physique Chimie Biologie 2008), “ElectroTagMam” (Cnano IdF 2011), “ElectroDev” (PHC Tournesol 2014), and FNRS MIS 2013.

REFERENCES

- [1] S. Srinivas, *et al.*, *Development*, **131**, 1157 (2004) ; I. Migeotte, *et al.*, *PLoS Biol.*, **8**, e1000442 (2010) ; T. Omelchenko, *et al.*, *Genes Dev.*, **28**, 2764 (2014).
- [2] E. Mazari, *et al.*, *Proc. MicroTAS 2012*, 1729 ; E. Mazari, *et al.*, *Development*, **141**, 2349 (2014).
- [3] B. P. Davidson, *et al.*, *Genesis*, **35**, 57 (2003); P. L. Khoo, *et al.*, *CHS Protoc.*, pdb prot4893 (2007).
- [4] R. R. Gattass and E. Mazur, *Nature Photonics*, **2**, 219 (2008).
- [5] X. Zhao, *et al.*, *ECS Trans.*, **64**, 7 (2014).

CONTACT

*C. Gosse; phone +33-1-69-63-61-55; charlie.gosse@lpn.cnrs.fr

LASER MICROMACHINING OF REUSABLE GLASS DEVICES DEDICATED TO THE TARGETED ELECTROPORATION OF CELL ASSEMBLIES

Xuan Zhao¹, Diana Suárez-Boomgaard², Bechara Saykali², Jassem Safioui³, Martin Hermans⁴,
Anne-Claire Louër⁵, Isabelle Migeotte², and Charlie Gosse¹

¹Laboratoire de Photonique et de Nanostructures, LPN-CNRS, Marcoussis, FRANCE

²IRIBHM, Université Libre de Bruxelles, Bruxelles, BELGIUM

³Femto Engineering, Besançon, FRANCE

⁴LightFab GmbH, Aachen, GERMANY

⁵Klearia SAS, Marcoussis, FRANCE

ABSTRACT

We demonstrate that the localized introduction of cell markers by electroporation can be efficiently and safely achieved with reusable glass chips complying with industrial micromachining techniques. Consequently, any biologist can now rely on contract manufacturing to easily implement this transfection approach at moderate cost.

KEYWORDS

Femtosecond laser ablation, selective laser-induced etching, hydrogensilsesquioxane, dielectric guide, transfection, embryology.

INTRODUCTION

Following and/or modifying the fate of specific cell populations are key issues in developmental biology. Therefore, life scientists aim at techniques able to locally introduce transgenic constructs into tissues of model organisms [1]. As an example, we focus here on the labeling with fluorescent proteins of the distal visceral endoderm (DVE) of 5.5 days old (E5.5) mouse embryos. The 12 hours long collective migration of this group of cells is of importance since it is required for the specification of the anterior-posterior axis.

Electroporation depends on voltage pulses that charge and eventually permeabilize the plasma membrane, enabling DNA to enter the cytoplasm. Sharp metallic electrodes have traditionally been used to induce strong transmembrane potential variations at the tissue surface (Fig. 1a) [1,2]. However, harmful chemical species (e.g. gas, protons) generated by electrolysis compromise the survival of the cells located close to the tip of the electrodes. Therefore, using dielectric guides to focus the electric field created by remote metal wires appears safer. Efficient and reproducible results have been obtained with both glass micropipettes (Fig. 1b) [1,3] and fluidic channels [1,4,5]. We recently showed that microfabrication allows one to better control the shape and size of the guide aperture, as well as to create a design compatible with easy and fast embryo manipulation [4,5]. Yet, specialized equipment and know-how were necessary to produce chips that were only single-use. In our prototype dielectric guides were parallelepipeds, 70 μm high and 60 μm large, fabricated by photolithography of two SU-8 walls on a glass slide, plasma hydrophilization of the photoresist, and thermal bonding of a Parafilm lid [5]. The surface activation lasted only 24h, and channel filling was thus impossible after this delay.

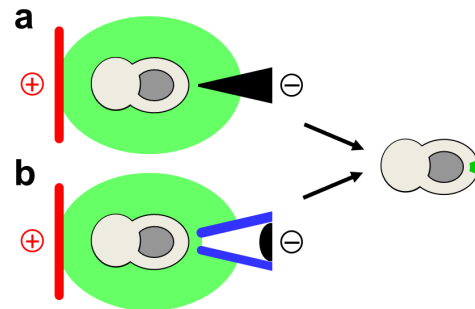


Figure 1: Previous strategies employed to locally electroporate the DVE of early post-implantation mouse embryos. The electric field is focused with either (a) a metallic microneedle or (b) a micropipette. The plasmid solution is represented in clear green and the encoded protein in dark green.

In this paper we rely on glass micromachining to disseminate the dielectric guide approach. Indeed, all life scientists agree on glass biocompatibility. Moreover, chips can be easily cleaned and reused, which compensates for the ~ 200 \$ cost per functional unit (Fig. 2a-b). Finally, many companies propose single-piece contract manufacturing, hence enabling biologists to engage in a rapid prototyping cycle.

EXPERIMENTAL SECTION

General considerations

The device consists in a buried fluidic network and in large open cavities; the connecting channels and the dielectric guide bring the electric field from the electrode reservoirs to the chamber where the embryo is positioned (Fig. 2a-d). As the guide has a slightly smaller diameter than the embryo, a focusing effect is obtained, which restricts the area over which the induced transmembrane voltage (ITV) exceeds the poration threshold. However, the success of localized electroporation is highly dependent on the shape of the aperture, as demonstrated by finite element method (FEM) simulations (Fig. 2e-e') [6]. Therefore, laser micromachining was selected to open the embryo chamber in the glass wafer. Indeed, this technique can yield vertical and precisely positioned walls. Furthermore, to demonstrate the variety of the technological offer, we here explore two different fabrication processes.

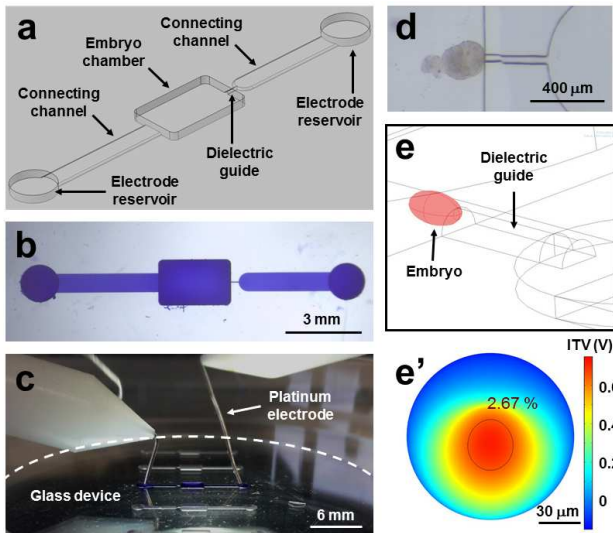


Figure 2: Working principle of the electroporation devices. (a) Chip layout. A semicircular guide of radius $70\ \mu\text{m}$, realized according to the microfabrication process No. 1, is here taken as example. (b) Top view with the channels filled with a bromophenol blue solution. (c) Picture of the microsystem mounted on a dissection microscope, the two macroscopic electrodes in place. (d) Zoom on an E5.5 embryo with his distal part facing the dielectric guide, ready to get electroporated. (e) Snapshot of the conducting domains used to compute by FEM simulations the ITV at the surface of an E5.5 embryo when 19 V pulses are applied. (e') ITV on a flattened view of the distal half of the embryo. The porated area, where the ITV exceeds the 0.65 V threshold, is delimited by a red line (the percentage corresponds to the enclosed surface).

Microfabrication process No. 1

A D263 glass wafer, 50 mm in diameter and $300\ \mu\text{m}$ in thickness, was cleaned in a piranha mixture (H_2SO_4 95% / H_2O_2 30%, 2:1). A mask delineating the connecting channels and the dielectric guide was next prepared by e-beam physical vapor deposition of 10 nm Cr / 200 nm Au, patterning of a nLOF2070 photoresist layer, and ion beam etching of the unprotected metal with an Ar plasma. In addition, both the back side of the wafer and areas far from any features on the front side were protected with PDMS. Glass was subsequently etched in hydrofluoric acid (HF 40% / H_2O / HCl 30%, 10:20:3) for ~ 35 min (Fig. 3a). PDMS was finally peeled off, the photoresist cleaned in piranha, and the Au and Cr layers respectively dissolved in aqua regia and in Cr-etch. Note that, during both the glass and the metal wet etching steps, alignment marks that had been opened in the Cr/Au layer were protected by drops of photoresist deposited with a brush.

Through holes corresponding to the electrode reservoirs and to the embryo chamber were subsequently opened by femtosecond laser ablation (Fig. 3a-b). A Tangerine ytterbium femtosecond fiber laser (Amplitude Systèmes) operating at a nominal wavelength of 1030 nm was used. The beam at the exit of the laser head had approximately a Gaussian profile, with a M^2 factor of 1.23 and a full diameter of 3.5 mm at $1/e^2$. Specific optics were then added to obtain a non-diffracting Bessel beam with a $3\ \mu\text{m}$ diameter and a $130\ \mu\text{m}$ length [7]. The repetition

rate and the pulse duration were tuned around 5 kHz and 220 fs, respectively, and the laser power at the sample was adjusted to ~ 100 mW by combining a half-wave plate and a linear polarizer. Focusing on the sample was performed with achromatic lenses, the wet etched side of the wafer being the one exposed to the laser beam. The material was ablated along a predefined contour thanks to a 3-axis translation stage, alignment onto the gold marks being achieved with a better than $10\ \mu\text{m}$ accuracy. Each hole was realized relying on 3 successive infeeds, which took between 2 and 5 min.

Finally, the microfluidic structures were closed by bonding the processed wafer onto an unprocessed one having the same dimensions (Fig. 3a,c-c'). The latter bottom wafer was activated in an oxygen plasma for 30 s and covered with a 500 nm thick layer of hydrogen silsesquioxane (HSQ) using a spin-coater [8]. On the other hand, the top wafer was activated using the SC-1 procedure (NH_4OH 28% / H_2O_2 30% / H_2O , 1:1:5, at $80\ ^\circ\text{C}$). The two parts were next put in contact and the assembly was baked at $300\ ^\circ\text{C}$ for 5 h.

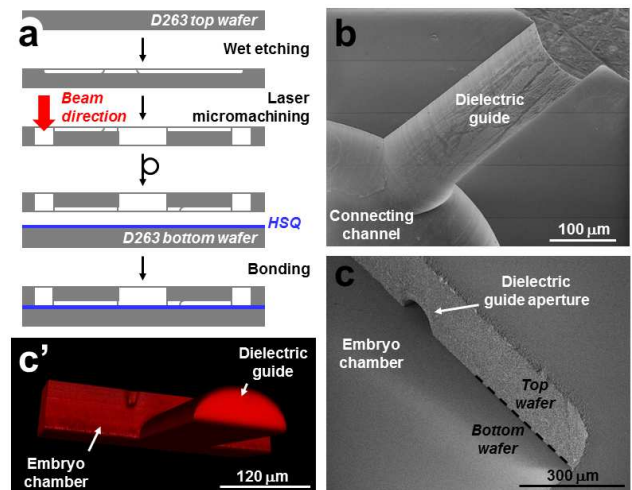


Figure 3: Microfabrication process No. 1. (a) Workflow. (b) SEM view of the top wafer after wet etching and laser micromachining. (c-c') SEM and CLSM views of the semicircular guide of radius $70\ \mu\text{m}$ obtained after bonding to the bottom wafer.

Microfabrication process No. 2

Both channels and cavities were fabricated at once in fused silica by selective laser-induced etching (SLE) [9]. More precisely, the LightFab 3D Printer was first used to irradiate the transparent material line-by-line and layer-by-layer, according to the desired features. In fact, the latter apparatus includes a Satsuma fiber laser (Amplitude Systèmes) working at 1030 nm and which repetition rate and pulse duration can be adjusted in the 0.1 – 10 MHz and 0.4 – 5 ps ranges, respectively (see reference [9] for details on the settings). When the intensity of the tightly focused ultrashort pulses exceeds the nonlinear absorption threshold photons are absorbed and permanent internal modifications are induced through heating and quenching. Besides other characteristics the resulting modified glass is more susceptible to wet chemical etching than the pristine material. Therefore, in a second step the

microfluidic structures can be developed by immersing the irradiated wafer in an 8 M KOH solution, at 85 °C for 48 hours.

Microdevice characterization

Scanning electron microscopy (SEM) was achieved on a Magellan 400L (FEI) working at 2 kV and 50 pA.

Confocal laser scanning microscopy (CLSM) was performed on a LSM 780 (Zeiss) equipped with a HeNe laser (543 nm) and a 10× EC Plan Neofluar objective (NA 0.3, WD 5.2 mm). The fluidic structures were filled with 100 μM Rhodamine B and Z-slices were spaced by 1 μm.

Surface roughness at the bottom of the embryo chamber was measured with a Dektak 8 stylus profilometer (Veeco), the tip of which was 2.5 μm in radius. Scans were 900 μm long. On one hand, data were straightforwardly analyzed to estimate R_t , the peak-to-valley maximum. On the other hand, a low-pass filter with a cut-off at 100 μm was applied before determining R_a , the average roughness.

Electroporation and live imaging

The platinum wires (0.5 mm in diameter) used as electrodes were inserted in the corresponding reservoirs (Fig. 2a,c) and connected to a TSS20 Ovodyne electroporator coupled with an EP21 current amplifier (Intracell). Next, the device was filled with 14 μL of HBS (150 mM NaCl 20 mM Hepes buffer, pH 7.0) supplemented with 1.5 μg/μL of plasmid of interest. The latter reagent had been cloned in house and purified using an endotoxin-free kit. Mouse embryos were dissected at E5.5 according to standard protocols, rinsed in HBS, placed in the chamber, and pushed with a pipet towards the dielectric guide (Fig. 2d). The position of the DVE in front of the aperture, which was set by hand, was found very stable thanks to a naturally present hydrodynamic flow sucking the tip of the embryo into the guide. A train of 3 square pulses, 50 ms long and spaced by 1 s, was then applied, the amplitude being adjusted using the results of the FEM simulations as a starting point (Fig. 2e-e') [5,6]. For the semicircular guides of radius 70 μm fabricated according to processes No. 1 and 2 we relied on 23 and 20 V pulses, respectively. Following each electroporation the chip was emptied and refilled with fresh plasmid solution.

After electroporation completion, embryos were rinsed in the dissection solution (DMEM-GlutaMAX, 4.5 g/L glucose supplemented with 25 mM Hepes and 10 % inactivated fetal calf serum) and placed into 200 μL of culture medium (DMEM-GlutaMAX, 4.5 g/L glucose, 100 μg/ml streptomycin, 100 U/ml penicillin, supplemented with 50 % inactivated rat serum) by groups of three. Incubation was realized in 15-wells chambers slides (IBIDI) under standard cell culture conditions (37 °C, 5 % CO₂), for up to 24 h.

For live imaging, each electroporated embryo was placed in an IBIDI well containing 30 μl of culture medium and imaged on a LSM 780 (ZEISS) equipped with Argon (488 nm) and HeNe (543 nm) lasers, a 20× Plan Apochromat objective (NA 0.8, WD 5.5 mm), and an incubation chamber. Z-slices were spaced by 3 μm and

acquisition was performed every 35 min for up to 5 h.

At the end of the day, all the microsystems were washed in 2 M HCl to remove biological debris, rinsed with water, and dried for storage. This protocol also regenerated hydrophilicity and eased subsequent filling.

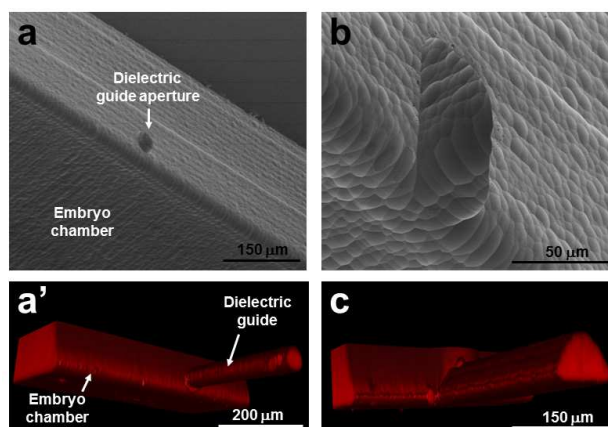


Figure 4: Microfabrication process No. 2 – SEM and CLSM views of various devices. (a-a') Circular guide of radius 50 μm located 40 μm above the embryo chamber bottom. (b) Rectangular guide of section 110 μm x 60 μm. (c) Semicircular guide of radius 70 μm.

RESULTS

Microfabrication

In process No. 1 laser ablation with non-diffracting Bessel beam was chosen in order to obtain perfectly vertical walls for the embryo chamber, without bevel (Fig. 3c). Appropriately selected repetition rate, pulse energy, pulse duration, and feeding speed yielded a satisfactory edge roughness – further improvement of this parameter was associated with the formation of crevices on the exit surface of the wafer. Debris redistribution on the entrance surface was also limited (Fig. 3b). Particles were smaller than 300 nm, as observed in SEM, which did not prevent bonding. Indeed, the HSQ layer is 500 nm thick and is still soft at the time of assembly.

Process No. 2 (SLE) also provides vertical walls and well defined guide apertures (Fig. 4). However, the combination of focused pulsed laser irradiation and wet etching is characterized by surfaces that look hammered. Bumps have a characteristic width of 5 – 10 μm and the average roughness is $R_a \sim 0.3 \mu\text{m}$. On a larger scale we measured peak-to-valley maxima $R_t \sim 2.5 \mu\text{m}$. Finally, all openings display concave fillets with a $\sim 15 \mu\text{m}$ radius, which are related to some widening of the irradiation pattern upon wet etching.

Electroporation

Both fabrication techniques resulted in devices able to target between 1 and 4 cells at the surface of E5.5 embryos, as can be assessed from the live imaging data collected 12 h after electroporation (Fig. 5) and from the ~ 10 h population doubling time for the DVE at this developmental stage [5]. Noteworthy, microsystems manufactured using process No. 1 displayed a much lower transfection yield than the one produced according to process No. 2. Indeed, percentages of labeled embryos

obtained with a semicircular guide of radius 70 μm were ~ 30 and $\sim 100\%$, respectively. We attribute this discrepancy to the larger hydrodynamic flow present in the guides made by SLE, a phenomenon possibly related to particular wetting properties. As a consequence, embryos are more tightly hold in place in front of the aperture.

Importantly, all the electroporated embryos survived. Therefore, neither the use of HSQ for bonding nor the surface roughness characterizing SLE resulted in any biocompatibility issue.

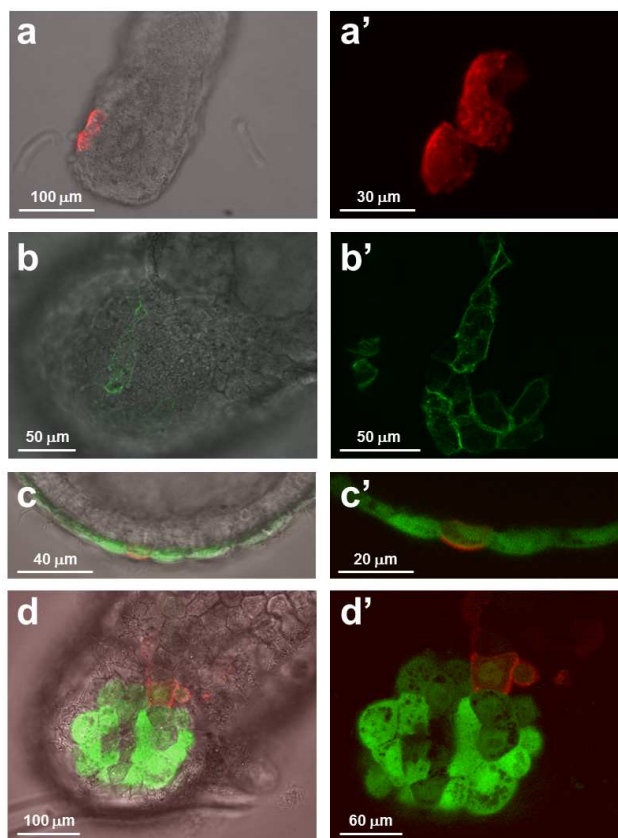


Figure 5: Expression of various proteins observed in both bright field and confocal laser scanning microcopies 12 h after E5.5 embryos have been electroporated in their DVE with the corresponding plasmids. (a-a') mApple-actin. (b-b') GFP- α -catenin. (c-d') FusionRed-Lifact – in these two cases embryos are Hex-GFP transgenics which DVE is constitutively labeled in green. For all four experiments the semicircular guide of radius 70 μm microfabricated by SLE was used.

DISCUSSION

This paper presents two ways of fabricating reusable glass devices dedicated to the localized electroporation of early-post implantation mouse embryos. Both techniques are commercially available, not only from the authors' companies but also from many other ones – although some minor variations may exist, with respect to the bonding process for instance. As far as process No. 1 is concerned dielectric guides are mostly limited to half-cylinders (Fig. 3). Interestingly, process No. 2 allows more diverse cross-sections (Fig. 4) as well as true 3D machining. Thus, it should favor the adaptation of the

proposed approach to other cell assemblies (e.g. embryos from other species, explants, cysts, organoids) or to user-inspired ergonomic choices. To do so, biologists may rely on the numerical tools we have developed to assist device conception [5,6] and on the cellular labeling protocols established to emphasize on poration, cell death, and protein expression [1,5].

ACKNOWLEDGEMENTS

We thank the staff of the LPN clean room and of the ULB LiMiF imaging facility for technical assistance, as well as C. Dupuis (LPN, Marcoussis) for help during SEM imaging, A. Perea-Gomez (IBV, Nice) for helpful discussions, and S. Le Gac (University of Twente) for advertising SLE. This work was supported by the grants “ElectroMice” (CNRS PI: Physique Chimie Biologie 2008), “ElectroTagMam” (Cnano IdF 2011), “ElectroDev” (PHC Tournesol 2014), and “RhoGTPases and collective migration” (FNRS MIS 2013).

REFERENCES

- [1] C. Gosse, et al., “The use of electroporation in developmental biology” in *Handbook of electroporation*, Springer, 2017.
- [2] B. P. Davidson, et al., “Introduction of cell markers into germ layer tissues of the mouse gastrula by whole embryo electroporation”, *Genesis*, vol. 35, pp. 57-62, 2003.
- [3] Y. Huang, et al., “Methods for precisely localized transfer of cells or DNA into early postimplantation mouse embryos”, *J. Vis. Exp.*, e 53295, 2015.
- [4] E. Mazari, et al., “Localized electroporation of mouse embryo using dielectric guides”, in *Digest Tech. Papers Transducers'11 Conference*, Beijing, June 5-9, 2011, pp. 1172-1175.
- [5] E. Mazari, et al., “A microdevice to locally electroporate embryos with high efficiency and reduced cell damage”, *Development*, vol. 141, pp. 2349-2359, 2014.
- [6] X. Zhao, et al., “Finite element model simulations to assist the design of microdevices dedicated to the localized electroporation of mouse embryos”, *ECS Trans.*, vol. 64, pp. 7-14, 2014.
- [7] M. K. Bhuyan, et al., “High aspect ratio taper-free microchannel fabrication using femtosecond Bessel beams”, *Opt. Express*, vol. 18, pp. 566-574, 2010.
- [8] A.-M. Haghiri-Gosnet, C. Nanteuil, “Method for manufacturing a microfluidic chip, and related chip and plate”, US20130071305 A1, 2010.
- [9] M. Hermans, et al., “Selective, laser-induced etching of fused silica at high scan-speeds using KOH”, *J. Laser Micro Nanoeng.*, vol. 9, pp. 126-131, 2014.

CONTACT

* C. Gosse, tel: +33-(0)1-69-63-61-55;
charlie.gosse@lpn.cnrs.fr

The Use of Electroporation in Developmental Biology

C. Gosse, X. Zhao, I. Migeotte, D. Suárez-Boomgaard, I. Hue,
S. Degrelle, A. Perea-Gomez, and E. Mazari

Abstract

During the formation of a complex organism, cells divide, die, migrate, and differentiate. Biologists have established tools to observe those phenomena but also to change their course, which subsequently enables to infer causal relationships between various events occurring in different cell groups. More precisely, present approaches mostly rely on modifications of gene expression. For instance, cells are labeled with fluorescent proteins and tracked within the embryo,

C. Gosse (✉) • X. Zhao

Laboratoire de Photonique et de Nanostructures, LPN-CNRS, Marcoussis, France

e-mail: charlie.gosse@lpn.cnrs.fr; xuan.zhao@lpn.cnrs.fr

I. Migeotte • D. Suárez-Boomgaard

Institut de Recherche Interdisciplinaire en Biologie Humaine et Moléculaire, Université Libre de Bruxelles, Bruxelles, Belgium

e-mail: imigeott@ulb.ac.be; boomgaard83@gmail.com

I. Hue

Biologie du Développement et Reproduction, UMR 1198 INRA, ENVA, Université Paris-Saclay, Jouy-en-Josas, France

e-mail: isabelle.hue@inra.fr

S. Degrelle

Physiopathologie et Pharmacotoxicologie Placentaire Humaine, INSERM UMR-S1139, Université Paris Descartes, Sorbonne Paris Cité, Paris, France

e-mail: severine.degrelle@inserm.fr

A. Perea-Gomez

Institut de Biologie Valrose, CNRS UMR7277, Inserm U1091, Université Nice Sophia Antipolis, Nice, France

e-mail: apereagomez@unice.fr

E. Mazari

Center for International Research on MicroMechatronics, Institute of Industrial Science, The University of Tokyo, Tokyo, Japan

e-mail: mazari@iis.u-tokyo.ac.jp

molecular signals are switched on and off to perturb regulatory pathways. Importantly, in all those experiments, the exogenous genetic material must be delivered at the right place and with the appropriate timing: requirements that can both be fulfilled by electroporation. After 15 years of constant refinement, this technique has now superseded methods like viral infection, microinjection, and lipofection. Applications encompass a large number of model organisms, targeted anatomical structures, and molecular biology techniques.

Keywords

Embryogenesis • Organogenesis • Cell labeling • Genetic engineering • Numerical simulations • Microfabrication

Contents

Introduction	2
Specificities Related to the Scientific Context	3
Typical Experiments	3
Organisms and Tissues	5
Molecular Biology Tools	8
Competing Techniques	10
Strategies to Spatially Restrict Transfection	13
Orientation of the Embryo	13
Containment of the Nucleic Acids Solution	15
Generation of an Electric Field Gradient	16
Combination of both Molecular Localization and Electric Field Focusing	17
Engineering Practices	18
Setup Conception	18
Material Selection	21
Reagents Preparation	23
Performances Validation	24
Conclusion	27
Cross-References	29
References	29

Introduction

The use of electroporation to study embryogenesis and organogenesis was initiated around 1995, and most of the associated technical developments took place in the following decade (Nakamura and Funahashi 2013). Therefore, the book *Electroporation and Sonoporation in Developmental Biology* edited by H. Nakamura in 2009 displays a quite complete overview of the possibilities offered by this technique, with detailed accounts on manipulations performed on model organisms such as chick and mouse (Nakamura 2009). Since then electroporation has become a widespread tool enabling embryologists to answer questions specific to their discipline.

More than a hundred of original articles have been published on the sole methodological advances. Additionally, many reviews and focus papers have already extensively summarized and discussed this large corpus of studies (Itasaki et al.

1999; Swartz et al. 2001; Ogura 2002; Krull 2004; Odani et al. 2008; Sauka-Spengler and Barembaum 2008; Takahashi et al. 2008a; Tanaka et al. 2014). Thus, the present chapter has been conceived along somewhat different lines: it aims to be a primer that presents the utilization of electroporation in developmental biology from an engineering point of view. To start with, the fundamental objectives pursued by embryologists will be described, as well as the typical experiments they carry out. How electroporation can fulfill some of the corresponding technical needs will also be explained. Next, a comprehensive summary of the realizations so far published will be provided, using the strategy devised to localize transfection as an organizing principle for the redaction. Finally, some of the practical issues related to the implementation of electroporation in this particular field of life sciences will be discussed.

The bibliography will be more illustrative than exhaustive. It will mainly focus on seminal publications and on well-detailed technical papers, leaving aside reports on biological questions in which electroporation is marginally employed. Furthermore, references for many reviews will be included, to be used as introductions to more specific parts of the literature. We will also try to discuss as much as possible the advances posterior to the 2009 publication of Nakamura's book. Noteworthy, in the last 10 years both *Nature Protocols* and the *Journal of Visualized Experiments* have released a few dozens of detailed protocols, old and new. In the case of the latter journal, each article is associated with videos that really bring a plus, because skilled manual experimentation is often a prerequisite in embryology. Finally, for complementary technical and bibliographical information, one can profitably check the websites of some of the main providers of electroporation apparatus (e.g., BTX Harvard Apparatus, NepaGene).

Specificities Related to the Scientific Context

Typical Experiments

The formation of a multicellular organism from a single cell, the fertilized egg (or zygote), involves fundamental processes like differentiation, which produces diverse cell types such as neurons or insulin producing cells, and morphogenesis, which allows their spatial and functional organization into organs such as the brain or the pancreas. During embryonic development, a tight regulation of cell division, cell death, and cell migration is also at play to control the global growth (Slack 2006; Gilbert 2013). Importantly, developmental processes are not restricted to the time of the embryonic life. Indeed, in human for instance, some organs like the skin or the surface of the intestine are constantly renewed. Moreover, in animals with high regenerative capacities like amphibians, an entire adult limb or a tail can be replaced after injury.

Understanding the development of a complex organism requires acquiring a precise knowledge of the origins and of the dynamics of the cell populations that form the different tissues of the embryo. So-called fate maps are then drawn by tracing the descendants of a particular cell population (cell lineage analysis) or even

of a single cell (clonal analysis) (Stern and Fraser 2001; Kretschmar and Watt 2012). Classically, marking selected cell populations relied on the injection of organic dyes (Bhattacharyya et al. 2008) or the grafting of cells possessing specific characters such as a pigmentation or a specific nuclear organization (Le Douarin et al. 2008 – Fig. 1a). In modern developmental biology, cells are labeled by modifying their gene expression so that they produce specific proteins like the enzyme β -galactosidase, which product can be detected in fixed tissues or fluorescent proteins, that allow live imaging experiments (Fig. 2a).

Another important experimental paradigm in developmental biology is to modify the behavior of a given cell population in order to understand its role in the formation of a given tissue. In classic embryology it was achieved by the grafting or the ablation of specific cell groups. This approach is best illustrated by the Spemann and Mangold experiment, demonstrating that grafting some specific dorsal cell population of an amphibian embryo, the organizer, is sufficient to modify the

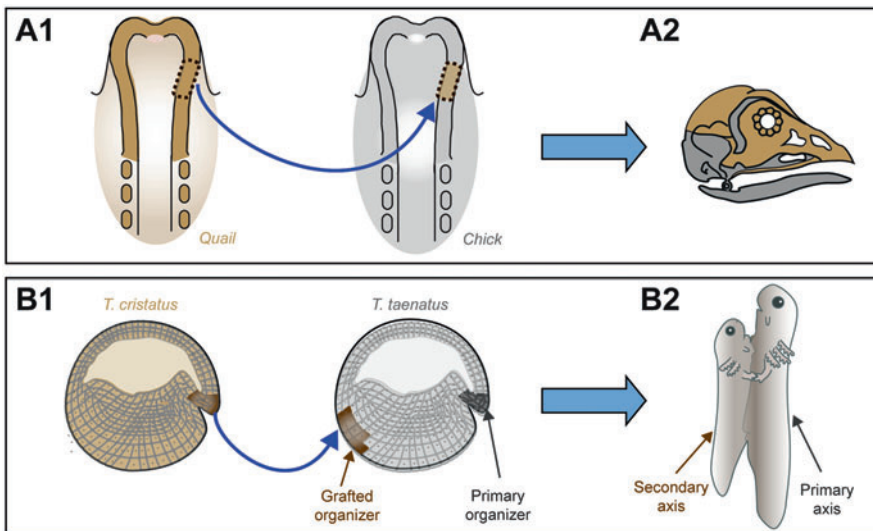


Fig. 1 Examples, in developmental biology, of seminal experiments relying on tissue transplantation. **(A1–2)** Lineage tracing performed on avian embryos to decipher the origin of the skull components (Adapted from Couly et al. 1993). **(A1)** A piece of the anterior part of the neural fold is dissected from a quail embryo at the three-somite stage and grafted in a chick one. **(A2)** The fate of the tissues issued from this isotopic and isochronic substitution is analyzed by inspection of head sections at later stages. Quail cells can indeed be distinguished from chick ones thanks to differences in the structure of their interphase nuclei. The xenograft is here at the origin of the upper part of the skull. **(B1–2)** Induction experiment evidencing the presence of the organizer in newt embryos (Adapted from Kretschmar and Watt 2012) and inspired from the work presented in (Spemann and Mangold 1924). **(B1)** A piece of tissue from above the dorsal blastopore lip is collected on a *Triton cristatus* gastrula and ectopically transplanted in the ventral marginal zone of a *Triton taeniatus* one (the two species differ by their pigmentation). **(B2)** The signals produced by the graft subsequently lead to the apparition of a secondary body axis

behavior of the adjacent tissues in the receiving host, so that a secondary axis is induced (Spemann and Mangold 1924 – Fig. 1b). Later on, the molecular nature of the communication between cell groups was further evidenced by grafting polymeric beads releasing so-called morphogens, i.e., small molecules or proteins that induce the formation of anatomical structures from a distance (Eichele et al. 1985; Stern et al. 1990). Nowadays, local modification of gene expression is commonly used to change the characteristics of targeted cells (Fig. 2b). Gain- or loss-of-function strategies result in the respective up- or downregulation of the activity of the protein of interest, by modulating its synthesis or by interfering with its normal molecular behavior (section “[Molecular Biology Tools](#)”). The consequences of these changes on the modified cell population or on the adjacent tissues can then be addressed in the context of the whole developing organism (Sauka-Spengler and Barembaum 2008; Tanaka et al. 2014). The ultimate goal of such perturbative approach is to explain morphogenesis thanks to wiring diagrams that emphasize the spatiotemporal coupling, either chemical or mechanical, between intracellular genetic regulatory networks and intercellular communication pathways (Streit et al. 2013).

Local modification of gene expression to trace cell populations or to change their behavior can be achieved in several ways. In some animal models like the *Drosophila*, powerful genetic tools allow the production of lines where clones of cells harbor stable transgenes or mutations. In contrast, some other models like the chick or the *Xenopus* do not offer such possibilities. Finally, in some cases like the mouse, genetically modified embryos can be obtained but it requires much time and labor (Itasaki et al. 1999; Slack 2006; Sharpe and Mason 2008). In addition, when a stable line can be produced, one also has to cope with the lethality associated with mutations affecting most developmental genes – a protein might have several roles at different stages and in different tissues but the death of the embryo during early regulatory processes prevents the study of the following ones. Therefore, conditional expression systems have been devised, relying on the response to an external chemical trigger (Danielian et al. 1998; Shin et al. 1999) and/or on the activation of tissue-specific *cis*-regulatory elements (Jaenisch 1988). However, these techniques are quite heavy, and alternative methods have been developed to modify gene expression with high spatial and temporal resolutions (section “[Competing Techniques](#)”). Electroporation is one of them, which enables embryologists to perform experiments that are basically the same than a century ago but in the context of functional genomics and with the incredible precision associated with modern molecular biology – compare Figs. 1 and 2.

Organisms and Tissues

As stated above, the scale of embryology is the one of cell populations and tissues. Therefore, we will not consider here transfection studies that are performed on zygotes in order to produce stable lines of transgenic animals. In a similar way, researches on isolated embryonic cells will be ignored. Conversely, we will take into account manipulations realized on explants to understand organogenesis. We will

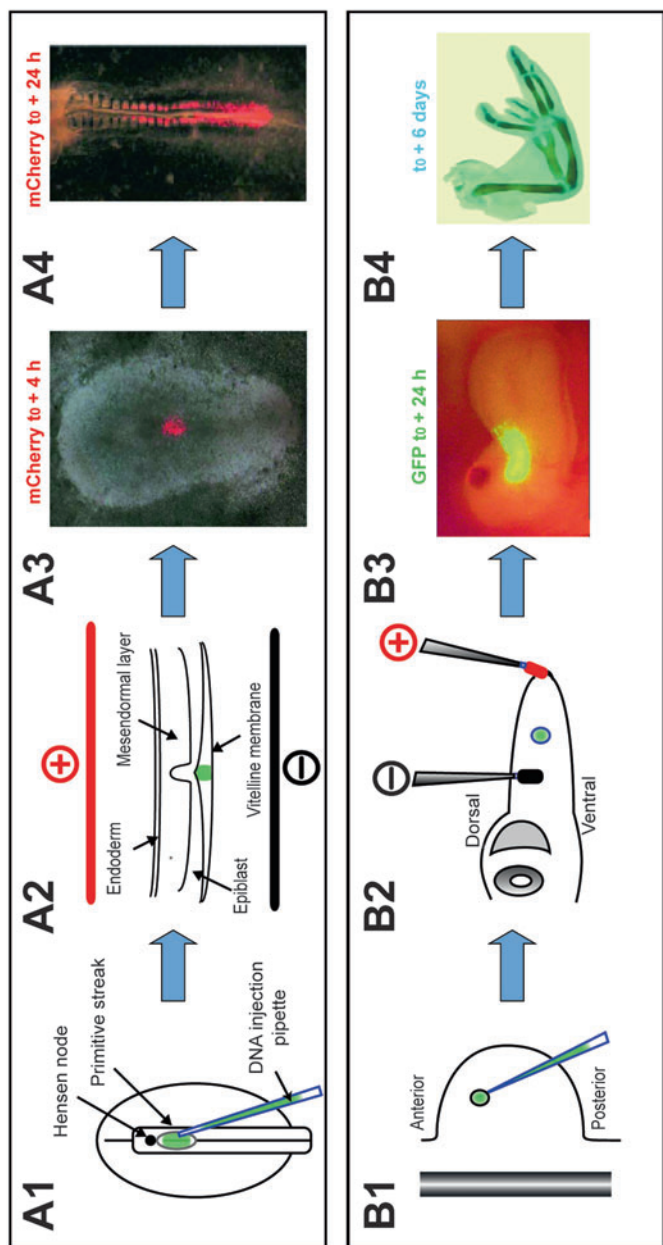


Fig. 2 Examples, in developmental biology, of contemporary experiments relying on tissue electroporation. (A1–4) Lineage tracing performed on a chick embryo to evidence somitogenesis (Adapted and reproduced from Iimura and Pourquié 2008). (A1) Schematic dorsal view of the injection of the DNA solution (in *green*) between the epiblast and the vitelline membrane at stage HH4. Using a fine glass needle, the anterior first third of the primitive streak groove is targeted. (A2) Transverse representation of the electroporation. (A3) Overlay of fluorescence and bright-field images evidencing the area over which the dsRed is protein expressed 4 h after electroporation with the corresponding plasmid. (A4) Same result after 24 h. (B1–4) Induction experiment demonstrating that the ectopic expression of the *Hoxb-8* transcription factor can yield “mirror image” digit duplication in chick (Adapted and reproduced from Oberg et al. 2002). (B1) Schematic dorsal view of the injection of the DNA solution (in *green*) into the limb bud mesoderm at stage HH19. (B2) Transverse representation of the

also include experiments related to regeneration (of tail and limb in fishes and amphibians) and neonatal development (of brain in mouse and rat).

The early implementations of electroporation in developmental biology were directly inspired by the protocols devised for cell suspensions. Transfections were mainly performed in cuvette equipped with parallel plate electrodes, relying on apparatuses providing exponentially decaying voltage pulses. This type of experiments was well adapted to very early stage embryos, containing from one to a few cells. Among the first scrutinized animals were fishes (Inoue 1992; Buono and Linser 1992; Powers et al. 1992; Müller et al. 1993; Murakami et al. 1994), insects (Kamdar et al. 1995; Leopold et al. 1996), and ascidians (Corbo et al. 1997).

Soon after, electroporation was demonstrated on chick embryos in ovo (Muramatsu et al. 1996, 1997). This advance was made possible thanks to the use of a generator delivering square voltage pulses of low amplitude and long duration (section “[Material Selection](#)”), which enabled to significantly reduce cell death (Itasaki et al. 1999; Ogura 2002; Krull 2004; Nakamura and Funahashi 2013). Naturally, the fact that chick was characterized by a long tradition in microsurgery as well as in in ovo culture was also important for those initial trials (Momose et al. 1999). Now that this animal model had become amendable to gene expression manipulation, developmental studies including gain- and loss-of-function could be performed, especially on neural tissues (Itasaki et al. 1999; Swartz et al. 2001; Odani et al. 2008). Transfection protocols adapted to other tissues (Oberge et al. 2002; Krull 2004) or to in vitro culture (Iimura and Pourquié 2008; Voiculescu et al. 2008) were further published.

Two years after the pioneering work of Muramatsu and his colleagues, mouse embryo electroporation was successfully undertaken (Akamatsu et al. 1999; Itasaki et al. 1999), once more focusing on nervous system formation. In these in vitro protocols transfection was followed by whole embryo culture (Takahashi et al. 2008a). However, not all developmental stages could be studied that way – in particular, it was impossible to obtain living pups. Consequently ex and in utero electroporation techniques were conceived (Tabata and Nakajima 2001; Saito and Nakatsuji 2001; Fukuchi-Shimogori and Grove 2001). Finally, the preimplantation (Grabarek et al. 2002; Soares et al. 2005) and the early post-implantation (Mellitzer et al. 2002; Davidson et al. 2003; Soares et al. 2008) stages were also transfected in vitro.

Until now, chick and mouse embryos are the ones that have been the most often electroporated. These two species, respectively, *Gallus domesticus* and *Mus musculus*, belong to the group of the six most popular animal models in developmental biology, with the zebrafish *Danio rerio*, the frog *Xenopus laevis*, the



Fig. 2 (continued) electroporation. **(B3)** Fluorescence image displaying the area over which the GFP is expressed 24 h after electroporation of a mixture of plasmids encoding for the latter fluorescent protein and for Hoxb-8. The *dark spot* indicates the injection site where, in this technique, some oil remains. **(B4)** Anatomical results after trichloroacetic acid fixation and alcian green staining at stage HH35-36

nematode worm *Caenorhabditis elegans*, and the fruit fly *Drosophila melanogaster* (Slack 2006; Sharpe and Mason 2008). Reports on electroporation of the two latter organisms can hardly be found in the literature because genetic tools have been available for long, and establishing a new technique was unnecessary (section “Typical Experiments”). Conversely, methods to control gene expression were also eagerly required for the two remaining species, and therefore electroporation was readily transferred to zebrafish (Tawk et al. 2002; Teh et al. 2003; Cerda et al. 2006; Hendricks and Jesuthasan 2007; Tawk et al. 2009; Kera et al. 2010) and *Xenopus* (Eide et al. 2000; Haas et al. 2001, 2002; Sasagawa et al. 2002; Falk et al. 2007; Lin et al. 2007; Chernet and Levin 2012) after it had been established in chick and mouse.

Subsequently, more confidential animal models could also be transfected by electroporation. It includes the silkworm *Bombyx mori* (Moto et al. 1999; Thomas 2003; Ando and Fujiwara 2013), the sea squirt *Ciona intestinalis* (Corbo et al. 1997), the freshwater polyps *Hydra vulgaris* and *Hydra magnipapillata* (Smith et al. 2000; Bosch et al. 2002), the axolotl *Ambystoma mexicanum* (Echeverri and Tanaka 2003, 2005), and the newt *Notophthalmus viridescens* (Kumar et al. 2007).

As far as in vitro organ electroporation is concerned, the proof of concept was realized on chick retinal explants (Pu and Young 1990) – in fact it was the first use of the technique in a developing tissue. Then, the transfection of a whole heart (Harrison et al. 1998) as well as pieces of gut (Fukuda et al. 2000) and slices of brain (Hashimoto-Torii et al. 2003) followed. To study organogenesis in mouse, protocols are now available for the intestine (Abud et al. 2004), retina (Donovan and Dyer 2006), kidney (Alie et al. 2007), palate (Lee et al. 2008), cochlear (Driver and Kelley 2010), genital ridge (Tanaka et al. 2014), mandibular arch, tail bud, neural plate, and lung endodermal bud (Mazari et al. 2014).

Finally, in regenerative biology, electroporation has enabled to better understand the regrowth of tentacle in *Hydra* (Smith et al. 2000), spinal cord in *Xenopus* tadpole (Lin et al. 2007) and axolotl (Echeverri and Tanaka 2003), limb in newt (Kumar et al. 2007) and axolotl (Echeverri and Tanaka 2005), as well as fin in zebrafish (Tawk et al. 2002).

Molecular Biology Tools

From the physicochemical point of view, there are only four kinds of molecules that are electroporated in embryos to perform gain- and loss-of-function experiments: the plasmids (pDNA) which are double-stranded circular DNA polymers (up to 14,000 base pairs long), the messenger RNA (mRNA) which are single-stranded RNA polymers (up to 1,500 nucleotides long), the small interfering RNA (siRNA) which are double-stranded RNA molecules (20–24 base pairs long), and the morpholinos (MO) which are oligomeric single-stranded analogues of DNA (around 25 morpholino units long). For the sake of simplicity, all these chemical species will be denoted as nucleic acids in the following, although morpholinos do not have a phosphate backbone. In fact, the latter oligomers are neutral, and to favor their delivery to the targeted cells by electrophoresis, they are often conjugated to a

charged dye (section “[Performances Validation](#)”). The difference in size characterizing those four reagents is also noteworthy when one considers the transfection mechanism: siRNA are small enough to first enter through the pores opened by the electric pulses and then diffuse freely in the cytoplasm before reaching their biological target (Paganin-Gioanni et al. 2011); in contrast, large plasmids form aggregates at the cell surface (Golzio et al. 2002; Mazari et al. 2014) before being actively transported to the nucleus (chapters “[Gene Delivery by Electroporation In Vitro: Mechanisms](#)” and “[Nucleic Acid Electrotransfer in Mammalian Cells: Mechanistic Description](#)”). Information on mRNA and MO are scarce (Chabot et al. 2013), although processes should be similar to the ones occurring in the siRNA case.

From the biological point of view, the nature of the obtained biological perturbation, i.e., either an up- or a downregulation, is not unambiguously related to the nature of transfected molecules, as reviewed for chick (Krull 2004; Sauka-Spengler and Barembaum 2008; Streit et al. 2013) and for mouse (Takahashi et al. 2008a; Tanaka et al. 2014).

Gain-of-function experiments consist in the overexpression of the gene of interest, either in its wild-type form or in a constitutively activated one. This is commonly achieved through the electroporation of a plasmid encoding for the corresponding protein; relying on mRNA is more expensive and thus rarer (Sasagawa et al. 2002; Cerda et al. 2006; Bansal et al. 2009; Chernet and Levin 2012).

On the other hand, the ways to realize loss-of-function experiments are more diverse. First, one can use a plasmid that encodes for a dominant-negative form of the targeted protein, e.g., a transcription factor with an inactive transactivation domain or a receptor without transmembrane domain. Consequently, the latter molecule will act as a competitive inhibitor of the wild-type form and perturb the associated regulatory pathway (Akamatsu et al. 1999; Bartkowska et al. 2007, Barembaum and Bronner-Fraser 2007). Another common strategy consists in blocking the transcription of the gene of interest, which is classically achieved through morpholino electroporation (Mellitzer et al. 2002; Kos et al. 2003). These nucleic acids are in fact antisense oligonucleotides which are either directed against the proximal region of the translation initiation site, to sterically inhibit the initiation complex, or designed to encompass the intron/exon boundaries and thus interfere with RNA splicing. The last well-established loss-of-function approach involves siRNA. These nucleic acids operate within the RNA interference pathway, a succession of several enzymatic reactions catalyzed by various protein complexes, the final result being that the sequence complementarity between one of the RNA strand and a given mRNA drives the degradation of the latter molecule and thereby prevents protein synthesis. siRNA molecules can be introduced as such in the cytoplasm by electroporation (Mellitzer et al. 2002; Calegari et al. 2002; Pekarik et al. 2003) or one may have them produced by the cell from a transfected plasmid (Katahira and Nakamura 2003; Peng et al. 2012). In this case, a promoter for RNA polymerase III is used, and the sequences are chosen to yield small hairpin RNA (shRNA) that are then processed as siRNA.

To conclude, we would like to mention that up to now, the CRISPR/Cas9 genome editing technology has only been scarcely used in embryos in conjunction with

electroporation, except for transgenic line production (Sato et al. 2016). Concerning developmental biology, knockout experiments have so far been realized in ascidia (Stolfi et al. 2014; Sasaki et al. 2014), chick (Véron et al. 2015), and mouse (Tsunekawa et al. 2016).

The differences in mechanism of action outlined above come with differences in timing of perturbation. In experiments using plasmids encoding fluorescent proteins, expression is detectable 2–4 h after electroporation, it then reaches a maximum 4–7 days later, and finally it fades within 1–2 weeks (Momose et al. 1999; Teh et al. 2003; Echeverri and Tanaka 2003; Oberg et al. 2002; Davidson et al. 2003; Falk et al. 2007; Takahashi et al. 2008a; Kera et al. 2010; Sauka-Spengler and Barembaum 2008; Simkin et al. 2014). However, these numbers may strongly vary with the cell type: for instance, a signal still measured after 4 months in postmitotic neurons (Saito 2006). Such an observation thereby indicates that pDNA displays a fair chemical stability and that the loss of expression is likely due to the dilution of the vector in the dividing cells. To tackle the latter issue, Tol2 transposon-mediated gene transfer has been devised, which provides a stable integration into the host genome (Takahashi et al. 2008b; Simkin et al. 2014).

With mRNA, expression can be observed as early as 1 h after electroporation (Sasagawa et al. 2002). Yet, this technique is more costly and more challenging due to the poor stability of mRNA and its degradation by cell nucleases. As far as siRNA are concerned, things are even worst since the dicer enzyme cut them into pieces. Therefore, to sustain the knockout activity, plasmids permanently enabling shRNA production are utilized (Katahira and Nakamura 2003; Peng et al. 2012). Finally, MO are stable but their antisense effect tends to disappear due to the dilution associated with cell division.

Competing Techniques

Different methods have been developed to introduce nucleic acids into cells, so as to produce genetically modified animals or to cure hereditary diseases (Kaestner et al. 2015; Sato et al. 2016). Among the ones listed in the first column of Table 1, four are today routinely used in embryology laboratories: viral infection, lipofection, microinjection, and electroporation. Incidentally, a few articles report on sonoporation (Ohta et al. 2003; Skachkov et al. 2014) on biolistics (Muramatsu et al. 1997; Thomas et al. 2001; Lee et al. 2005). On the other hand, the Table 1 header gives some of the parameters that have to be taken into account when selecting a technique. It is here worth noting that protocols are not exclusive. For instance, lipofection has been coupled to sonoporation (Lee et al. 2005) or to magnetofection (Svingen et al. 2009); grafting experiments, as described in Fig. 1, have been performed after transfection of the donor tissues (Iba 2000; Iimura and Pourquié 2008).

Gene transfer by viral infection has been important in chick embryology, as a way to cope with the lack of genetic tools characterizing this model (Iba 2000; Sauka-Spengler and Barembaum 2008). With retrovirus, the transgene is integrated in the

Table 1 Comparison of the various methods utilized to introduce nucleic acids in embryos or in embryonic tissues, in order to achieve gene expression modulation. This synthesis is partly based on the results and discussions presented in the following comparative studies and reviews: for chick (Muramatsu et al. 1997; Fukuda et al. 2000; Oberg et al. 2002; Ohta et al. 2003; Scaal et al. 2004; Saka-Spengler and Barembaum 2008), for mouse (Giroux et al. 2007; Sakai and Trainor 2014; Tanaka et al. 2014), and for both (Ogura 2002; deCastro et al. 2006; Geetha-Loganathan et al. 2011)

Technique	Efficacy	Possible risk for the tissue	Drawback for the researcher	Transfected molecules	Spatial resolution	Localization strategy	Timing for overexpression experiments	Problematic cell type
Biological transfection								
Retroviral infection	High	Biological toxicity; mutagenic	Labor; cost; biohazard	Insert <5 kbp	Initially 100 μm ; Ulterior spreading	Injection	Start after 12–24 h; Stable	Postmitotic cells
Lentiviral infection	High	Biological toxicity; mutagenic	Labor; cost; biohazard	Insert <8 kbp			Stable	
Adenoviral infection	Variable		Labor; cost	Insert <8 kbp			Transient	
Chemical transfection								
Lipofection		Chemical toxicity		pDNA; siRNA	100 μm	Injection	Start after 2–3 h; Stop within days	
Physical transfection								
Gene biolistics		Mechanical damage		pDNA	500 μm	Focusing	Start after 2–3 h; Stop within days	Buried cells
Microinjection	Good	Mechanical damage	Labor	All	Single cell	Injection		Small cells
Electroporation	High	Electrical damage		All	Single cell	Injection; focusing		Mesenchyme
Sonoporation	Good	Mechanical damage		pDNA; dye	500 μm	Injection; focusing		

host genome, which leads to a stable expression. However, such initial process is only possible when cells are dividing. It also significantly delays the onset of expression. Furthermore, the infectious nature of the method results in spreading outside the initially targeted area and limits the possibility of subsequent gene transfer (through a phenomenon called interference). The latter issue becomes problematic when associated with the reduced space available for the inserts. The use of other types of viruses has enabled to overcome numbers of the preceding shortcomings: lentivirus can carry two genes (Semple-Rowland and Berry 2014) and replication-defective vectors cannot infect neighboring cells (Iba 2000). Despite all these progresses, the viral infection technique is getting superseded. Indeed, virus production remains too demanding in time, money, and expertise. Additionally, stable gene integration can now also be achieved with the other transfection techniques, relying for instance on the Tol2 transposon-mediated gene transfer (Takahashi et al. 2008b; Simkin et al. 2014).

Chemical and physical transfection protocols are in fact much easier to implement, from both an economical and a practical point of view: only basic embryology laboratory equipment is necessary, plus a machine costing less than 15,000 € for electroporation and sonoporation. These methods are also more polyvalent since they are not restricted to any organism, or even cell type, for biological reasons. Similarly, the variety of molecules they can deal with is larger (Table 1). For lipofection all negatively charged nucleic acids can be used since they all assemble with cationic lipids to form transfection complexes that will cross the cell membrane (deCastro et al. 2006). In comparison, electroporation suffers even less limitations since many molecular species are actually able to diffuse through the electropores (chapters “► [Fluorescent Indicators of Membrane Permeabilization Due to Electroporation](#)” “► [Nucleic Acid Electrotransfer in Mammalian Cells: Mechanistic Description](#)”). Finally, microinjection is adapted to any kind of marker since the apertures created in plasma membranes by micropipettes are larger than a micron. Accordingly, fluorescently labeled polymers like dextrans, proteins like the horseradish peroxidase, and small cyanine dyes like DiI have all been microinjected into embryonic tissues to establish fate maps (Bhattacharyya et al. 2008). Nevertheless, this technique is quite time consuming and is better suited to target large cells, as in the classical manipulations on early *Xenopus* embryos, that involved mRNA injection (Slack 2006).

To end, the different methods can be compared with respect to their temporal and spatial targeting abilities (Table 1). In fact, the former property mostly depends on molecular biology as modern constructs allow the sustained or the conditional production of both proteins and interfering RNA, independently of the utilized transfection technique (sections “[Molecular Biology Tools](#)” and “[Conclusion](#)”). Concerning the spatial resolution, because some intimate contact between the nucleic acids and the cells is necessary, locally injecting the reagent always offers an opportunity to restrict the transfected area to a given tissue. However, molecular diffusion prevents the precision to be better than 100 μm , as observed for viral infection and for lipofection. Electroporation further permits to focus the electric field and to approach the single cell resolution. Interestingly, this limit is more surely

reached when the DNA solution fills a patch-clamp pipette and when the tip of the latter is in close contact with the plasma membrane: microinjection driven by iontophoresis and focal electroporation then become surprisingly similar.

Strategies to Spatially Restrict Transfection

Orientation of the Embryo

Whereas electroporation provides a straightforward control of the timing of gene expression (section “[Molecular Biology Tools](#)”), managing the spatial extent over which transfection is achieved is more complicated. In the following, the case of a 6.5-day-old (E6.5) mouse embryo placed between parallel plate electrodes will be considered as an illustration (Fig. 3a, b). The latter organism roughly consists of a closed double-layered epithelium and can be modeled by two concentric prolate spheroids (section “[Setup Conception](#)”); the first one corresponds to the interface of the embryonic tissues with the buffer and the second one with the proamniotic cavity content (Mazari et al. 2014; Zhao et al. 2014). Pores will open at the surface of cells only if the induced transmembrane voltage (ITV) generated upon electric field application exceeds a given threshold, ITV_{pore} (chapters “[► Transmembrane Voltage Induced by Applied Electric Fields](#)” and “[► Critical Electric Field and Transmembrane Voltage for Lipid Pore Formation in Experiments](#)”). Since the ITV is maximal for plasma membrane regions facing the electrodes, it is possible to selectively transfect a given area by adjusting the orientation of the biological object (Fig. 3c). However, controlling the extent of the porated zone additionally requires to tune the amplitude of the voltage pulses, V_{anode} (Fig. 3d). Unfortunately, this adjustment may not be easy to achieve because, in comparison with what occurs on clearly bumped tissues, ITV variations are gentle on flat surfaces. As a consequence, to significantly restrict poration, the ITV_{pore} threshold should not be exceeded by much, which in turn may result in suboptimal transfection efficiency.

The former example shows how problematic localized transfection may become when the embryo, or the explant, is simply soaked in the solution of nucleic acids and when a homogeneous electric field is applied. Therefore, cuvettes with parallel plate electrodes is mainly used to electroporate early embryos, from zygotes to cleaving stages and blastocysts (Powers et al. 1992; Buono and Linser 1992; Corbo et al. 1997; Grabarek et al. 2002; Soares et al. 2005; Peng et al. 2012). Data analysis is here often performed while taking into account the mosaic nature of the transfection, and a precise localization of the expression at the surface of those spherical objects is not a prerequisite. Moreover, cuvette protocols can deal with tens to hundreds of organisms in parallel and thus are well suited to the better embryo availability at those stages – it compares favorably with microinjection in terms of throughput. Despite this general trend of using parallel plate electrodes only for simple biological objects, studies on larger and more complex organisms or tissues have to be mentioned. It concerns whole *Xenopus* tadpole (Eide et al. 2000), silkworm brain (Moto et al. 1999), and mouse cochlea explant (Driver and Kelley

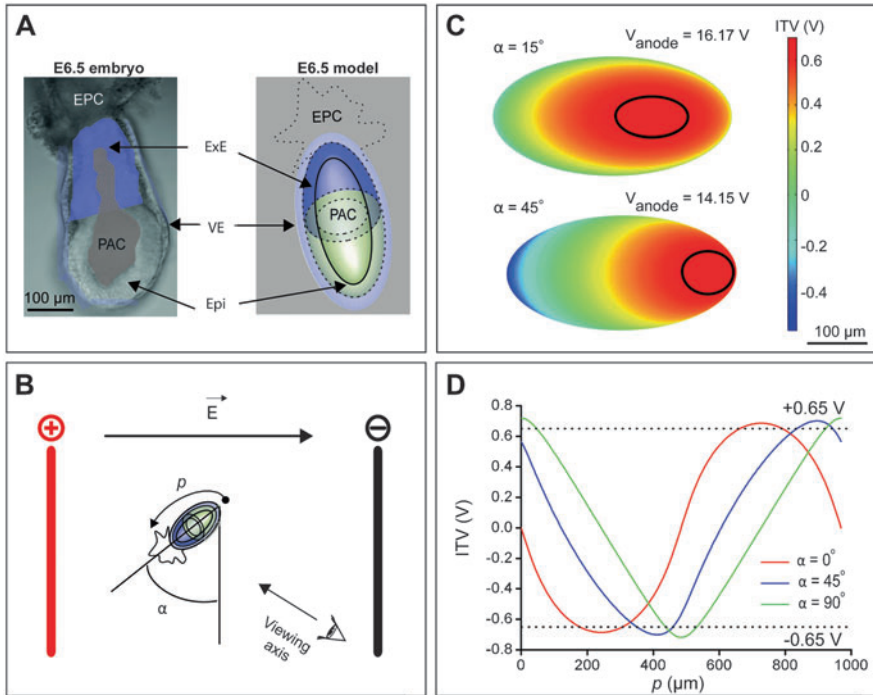


Fig. 3 Computation by FEM simulations of the ITV at the surface of an E6.5 mouse embryo electroporated between parallel plate electrodes. **(A)** Bright-field image of the conceptus and schematic representation of the corresponding numerical model. The anatomical annotations refer to the three main tissues, i.e., the epiblast (*Epi*), the extraembryonic ectoderm (*ExE*), and the visceral endoderm (*VE*), as well as to the proamniotic cavity (*PAC*) and to the ectoplacental cone (*EPC*). The embryo is approximated by two concentric prolate spheroids of respective length and width 400 and 200 μm for the buffer/*VE* interface and 300 and 100 μm for the *PAC*/*Epi*+*ExE* one – see Mazari et al. (2014) for technical details on the used electrical parameters. **(B)** Schematic top view of the 4 mm cubic electroporation cuvette with the conceptus positioned at its centered (not to scale). The embryo revolution axis forms an angle α with the two planes of the electrodes and the curvilinear coordinate along its largest horizontal cross-section is denoted p . **(C)** View of the simulated ITV on the anterior surface of the embryo, for orientations corresponding to $\alpha = 15$ and 45° . The applied voltage difference, V_{anode} , was adjusted in order to induce pore formation over exactly 6% of the total surface of the outer spheroid. The black line delimitates the area where the ITV is superior to the permeation threshold $\text{ITV}_{\text{pore}} = 0.65 \text{ V}$. **(D)** ITV as a function of p for various α , V_{anode} being tuned as above indicated

2010), as well as chick limb bud, gut, and heart explants (Harrison et al. 1998; Fukuda et al. 2000; Bobick et al. 2014). In some of these experiments, a simple orientation of the tissue could yield a fair enough targeting.

Containment of the Nucleic Acids Solution

A first strategy to restrict the size of the transfected area is to inject the nucleic acid solution in a natural body cavity with a glass micropipette mounted on a micromanipulator. The electric pulses are next applied in between parallel plate or wire electrodes, either set at fixed positions in a chamber or attached to the movable arms of tweezers. Whatever the configuration, the electric field is roughly homogeneous and poration is non-localized. However, gene expression is only modified in the lining of the cavity containing the molecules to transfect. Incidentally, with such a technique molecular biology reagents can be used in very small amount, and their concentration can be quite well controlled.

Brain vesicles are the most commonly harnessed cavities for site-specific delivery, both in vitro (Calegari et al. 2002; Takahashi et al. 2008a) and in utero (Saito 2006; De la Rossa and Jabaudon 2015) in mouse but also in chick (Momose et al. 1999), zebrafish (Teh et al. 2003; Hendricks and Jesuthasan 2007; Kera et al. 2010), and *Xenopus* (Haas et al. 2002). Again in the nervous system, one has relied on the central canal of the spinal cord in chick (Pekarik et al. 2003) and *Xenopus* (Lin et al. 2007). Other examples include, at earlier stages, the proamniotic (Soares et al. 2008), the amniotic (Mellitzer et al. 2002), and the yolk sac (Giroux et al. 2007) cavities in post-implantation mouse embryos as well as the space between the vitelline membrane and the epiblast (Cui et al. 2006, Iimura and Pourquié 2008, Hatakeyama and Shimamura 2008, Muramatsu et al. 1996, 1997 – Fig. 2a), the lumen of the neural tube (Kos et al. 2003; Krull 2004), and the somitocoels (Scaal et al. 2004) in avian embryos. Likewise, utilization has been made of the subretinal space in mouse pup (Donovan and Dyer 2006), of the rays of the caudal fin in zebrafish (Tawk et al. 2002), and of the hemocoel (Thomas 2003) and of the body cavity (Ando and Fujiwara 2013) in silkworm.

Conversely, reports can be found where the injection is performed in the bulk of a tissue, an approach often necessary when targeting the mesenchyme. Structures that have been treated this way are for instance the limb bud (Oberg et al. 2002 – Fig. 2b) and the cranial mesenchyme (Momose et al. 1999) in chick, the blastema in the regenerating limb of axolotl (Echeverri and Tanaka 2005) and newt (Kumar et al. 2007), as well as palatal (Lee et al. 2008), genital ridge (Tanaka et al. 2014), and kidney (Alie et al. 2007) explants from mouse embryos. Mesenchymal cells are reputed hard to transfect by electroporation, for reasons that may be from both biological and biophysical origins (Bobick et al. 2014). Still, the low success rate has equally been explained by the diffusion of pDNA in between the loosely attached cells of this conjunctive tissue (Krull 2004). Therefore, it has been advised to end the injection with an oil bolus that should act as a plug, preventing nucleic acids to escape (Oberg et al. 2002).

Another ingenious method for situations where no cavity is available makes use of agarose beads that have been soaked in the transgene solution and that are applied on the targeted site during the electroporation (Hatakeyama and Shimamura 2008; Simkin et al. 2009).

Generation of an Electric Field Gradient

Instead of controlling the place where the nucleic acids are applied, restraining the area over which cells are porated constitutes an alternative strategy to spatially limit gene overexpression or knockdown. More explicitly, the molecules to transfect can now be present everywhere since they will not cross the plasma membrane if the ITV is lower than the ITV_{pore} threshold.

Such localization effect can only be obtained if the electric potential varies a lot in close proximity to the targeted tissue. Laying the embryo in between much smaller electrodes that have been microfabricated on a flat substrate is an option (Murakami et al. 1994). Nevertheless, the most popular implementation of electric field focusing relies on tungsten microneedles (Fig. 4a): strong electric potential gradients are here generated around the highly curved conductors upon charging (Olofsson et al. 2003). Applications to chick (Momose et al. 1999; Brown et al. 2012) and mouse (Davidson et al. 2003; Quinlan et al. 2008) embryos have for instance been reported.

To achieve an optimum reduction of the porated area size, the metal tip must be very close to the tissue. However, chemical species are produced by electrolysis at the surface of both the anode and the cathode during pulses, which is problematic (chapters “► [Electrode Erosion and Metal Release Under Electroporation Conditions](#),” “[Electrolysis During Pulse Electric Field Treatment](#),” and “► [Combining Electrolysis and Electroporation for Tissue Ablation](#)”; Wang and Lee 2013). Indeed, metal ions are directly toxic for cells, whereas protons and hydroxide ions yield dangerous pH changes. Furthermore, gas like H_2 , O_2 , and Cl_2 are also released. Thus, bubbles may form (Cerdea et al. 2006 – Fig. 4b), which can be detrimental to the plasma membrane integrity and which alter the geometry of the electric field lines. A way to reduce harmful species production is to limit the current, by lowering the buffer conductivity for instance (chapter “► [Parameters Affecting Cell Viability Following Electroporation](#)”). Incidentally, it will also prevent excessive temperature increase due to Joule heating.

In order to bypass the lethality issues associated with metal microneedles, one can employ “liquid electrodes,” as it has been done for single cell electroporation (Olofsson et al. 2003, 2007). More precisely, the electric field is channeled by a dielectric hollow structure which opening has a size close to the one of the targeted area. Therefore, the ITV_{pore} threshold is exceeded only locally, before electric potential gradients weaken in the container welcoming the embryo or the explant (Fig. 5a). Such dielectric guides result in a focusing effect similar to the one associated with microelectrodes (Mazari et al. 2014), with the advantage that harmful species are not generated in proximity to the studied tissue but around metal electrodes located afar. Applications involving microsystems have been reported for mouse (Mazari et al. 2014; Zhao et al. 2014) and zebrafish (Bansal et al. 2009) embryos. Interestingly, the latter article demonstrates that it is possible to electroporate the surface of a blastula with various arbitrary patterns.

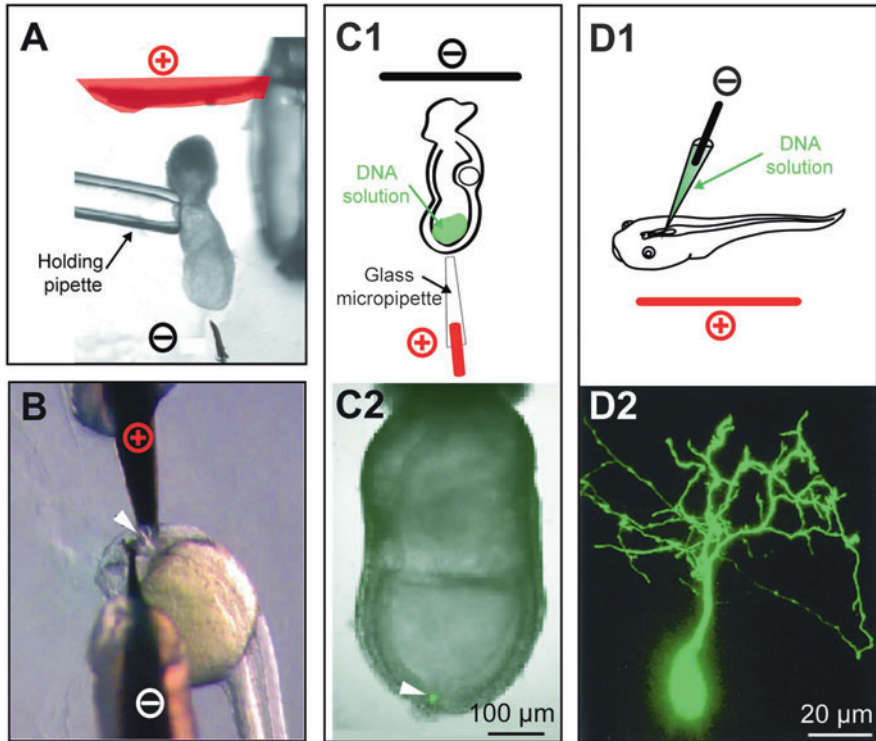


Fig. 4 Examples of strategies used to restrict the number of electroporated cells and to control their location. **(A)** Electroperoration of the distal tip of an E7 mouse embryo with a tungsten needle. A platinum plate is used as a counter-electrode, and the conceptus is fully immersed in the DNA solution (Reproduced from Quinlan et al. 2008). **(B)** Electroperoration of the midbrain of a zebrafish embryo with tungsten needle electrodes, after microinjection of the molecular biology reagent in the targeted brain vesicle (Reproduced from Cerda et al. 2006). The *white arrow head* indicates a bubble that has formed by electrolysis. **(C1–2)** Electroperoration of a few cells in the distal epiblast of an E7.5 mouse embryo (Adapted and reproduced from Huang et al. 2015). **(C1)** The amniotic cavity is microinjected with the DNA solution (in *green*), and the electric field is focused at the tip of a glass micropipette, which is 20 μm in diameter. **(C2)** Overlay of confocal and bright-field images displaying the nuclear distribution of the GFP 2 h after electroperation with the corresponding plasmid. **(D1–2)** Single neuron electroperoration in the *Xenopus* tadpole brain (Reproduced from Haas et al. 2001, Haas et al. 2002). **(D1)** A micropipette filled with the DNA solution (in *green*) is introduced into the brain of an anesthetized animal, and electrical pulses are delivered between the metal wire inserted in the pipette and the external counter-electrode. **(D2)** Confocal image of an optic tectal neuron expressing the EGFP 48 h after electroperation with the corresponding plasmid

Combination of both Molecular Localization and Electric Field Focusing

In order to more robustly restrict the spatial extent over which transfection is achieved, researchers have simultaneously enforced the two previous approaches

(sections “[Containment of the Nucleic Acids Solution](#)” and “[Generation of an Electric Field Gradient](#)”). For instance, the nucleic acid solution can be micro-injected into a cavity (Momose et al. 1999, Cerda et al. 2006, Falk et al. 2007, Quinlan et al. 2008 – Fig. 4b), or in the bulk of a tissue (Momose et al. 1999; Chernet and Levin 2012), and strong electric potential gradients generated by a microneedle electrode.

Likewise, the use of a pipette acting as a dielectric guide can be coupled with the injection in a body cavity to further improve localization (Huang et al. 2015 – Fig. 4c). Yet, the most common strategy consists in backfilling the hollow glass needle itself with the solution containing the molecule to transfect (Fig. 4d). The equipment is here similar to the one used in patch-clamp and applications mainly concern neural tissues, in *Xenopus* (Haas et al. 2001, 2002), axolotl (Echeverri and Tanaka 2003), zebrafish (Tawk et al. 2009), and chick (Hashimoto-Torii et al. 2003), for instance. Although the formation of a seal does not seem to be required, the single cell resolution is often reached. Of course with larger pipette openings more cells are transfected, as demonstrated in *Hydra* (Smith et al. 2000), chick (Atkins et al. 2000), and rat (Barker et al. 2009).

Finally, an original approach based on three electrodes has been devised to allow more flexibility in electric field lines engineering during in utero rat embryo electroporation (dal Maschio et al. 2012). After plasmid injection it then became possible to target, at the surface of brain vesicles, areas that were poorly addressed in previous studies (Fig. 5b).

Engineering Practices

Setup Conception

Computation of the ITV is valuable to interpret electroporation experiments when dealing with isolated cells. Although analytical calculations provide satisfactory results for simple geometries, finite element method (FEM) simulations are required for more complicated situations, like the one involving plated cells with irregular shapes (chapter “[► Transmembrane Voltage Induced by Applied Electric Fields](#)”). Similarly, numerical tools soon become necessary when departing from the case of the homogenous electric field generated in between parallel plate electrodes, for instance, when a metallic needle or a dielectric guide is used to yield a strong voltage gradient (Olofsson et al. 2003, 2007). For more than 15 years now, programs such as Comsol Multiphysics are thus harnessed to assist engineers in the design of instruments and microdevices dedicated to cell electroporation – see the large majority of the references reviewed in (Fox et al. 2006, Wang and Lee 2013, Geng and Lu 2013; chapter “[► Description by Electroporation in Microfluidic Devices](#)”). Surprisingly, the use of FEM simulations have little pervaded in developmental biology, even if the structural complexity of embryos would make this practice pertinent (Murakami et al. 1994; Huang et al. 2007; dal Maschio et al. 2012; Mazari et al. 2014; Zhao et al. 2014). Two examples detailed in the following will illustrate such an opportunity.

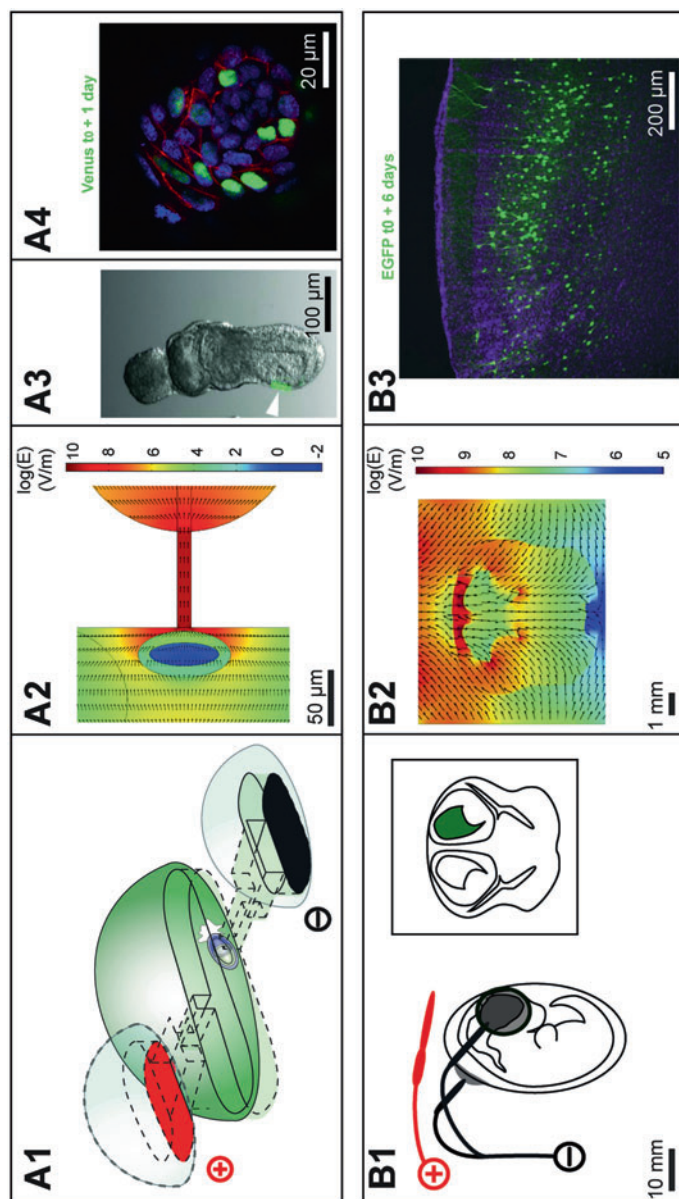


Fig. 5 Prediction of the extent of the electroporated area by FEM simulations. (A1–4) Localized transfection of the anterior visceral endoderm of an E6.5 mouse embryo thanks to a dielectric guide device (Partially adapted from Mazari et al. 2014). (A1) Schematic representation of the embryo in position, with the targeted cells in front of the 110 μm high and 60 μm large cathodic aperture. The electroporation chamber is filled with the DNA solution (in green). (A2) View of the norm of the simulated electric field (in log scale) in a cross-sectional plane 70 μm above the chamber surface. *Arrows* indicate the field direction. (A3) Confocal and bright-field images displaying the nuclear distribution of Venus 24 h after electroporation with the corresponding plasmid (anterior is to the left). (A4) Confocal images of the same embryo observed from the anterior side after counterstaining with Hoechst (in blue) and Alexa555-conjugated phalloidin

Figures 3 and 5a display studies performed on an E6.5 mouse embryo. This developing organism has roughly the shape of a hollow spheroid and is made of three tissues organized in a double-layered epithelium (Fig. 3a). Since GAP junctions electrically connect adjacent cells (Imura and Pourquié 2008; Mazari et al. 2014), it was possible to only model the interface of the tissues with the electroporation solution on the outside and with the liquid of the proamniotic cavity on the inside (Fig. 3b). In this approach an epithelium thus behaves as a kind of macroscopic cell: without surprise, cuvette electroporation of the mouse embryo yields results similar to the ones found for spheroidal cells – compare (Fig. 3d) and the data in (chapter “► Transmembrane Voltage Induced by Applied Electric Fields”). Despite its simplicity, such a numerical model has also permitted to better understand the working principle of a microsystem far more complicated than a basic cuvette with two plate electrodes (Mazari et al. 2014 – Fig. 5a). In addition, it helped to devise an upgrade of this device (Zhao et al. 2014).

Simulations have also been helpful in the conception of a triple-electrode system dedicated to site-directed in utero transfection of the rat brain (dal Maschio et al. 2012) (Fig. 5b). More precisely, electric field computation has allowed the authors to orient each of their three plates and to define the applied voltage values necessary to achieve a well-controlled electrophoretic motion of the plasmid toward a precisely defined area at the surface of given brain vesicles. The neural tissue was here modeled with macroscopic electrical parameters, without taking into account any details present at the cell scale.

Incidentally, calculations are always run in stationary mode since it provides a very good approximation for pulses that are usually tens of milliseconds long (chapters “► Critical Electric Field and Transmembrane Voltage for Lipid Pore Formation in Experiments” and “► Transmembrane Voltage Induced by Applied Electric Fields”).

Although numerical estimates relying on coarse representations of embryonic tissues agree with experimental outcomes, FEM simulations still need to be backed up by systematically acquired data to gain in popularity. For instance, measurements could be performed on simpler systems to validate the electrical properties of the basic tissular units found in developing organisms, e.g., mesenchymal tissues, single-layered and stratified epithelia. In this way, one may be able to understand why particular anatomical tissues, like the mesenchyme, are more difficult to electroporate (Itasaki et al. 1999; Oberg et al. 2002; Scaal et al. 2004; Krull 2004;

←

Fig. 5 (continued) (in red). **(B1–3)** Localized transfection of the motor cortex of an E17 rat embryo thanks to a three-electrode probe (Reproduced from dal Maschio et al. 2012). **(B1)** Schematic representation of the in utero electroporation procedure after injection of the DNA solution in the lateral ventricle (in green in the insert). **(B2)** Coronal view of the norm of the simulated electric field (in log scale). *Arrows* indicate the field direction. **(B3)** Confocal image of a brain slice displaying the cytoplasmic distribution of the EGFP 6 days after electroporation with the corresponding plasmid (the sample was counterstained with Hoechst (in magenta))

Imura and Pourquié 2008) and why complex organs, like kidney explants, have been reported to respond to electrical pulses differently (Alie et al. 2007). Thus, a deeper knowledge of the biophysics at work would certainly favor the rational design of more efficient transfection protocols (chapters “► 3D Culture Models to Assess Tissue Responses to Electroporation,” “► 3D Tissue Models to Bridge the Gap Between Cell Culture and Tissue in Assessing Electroporation,” and “► Effects of Electroporation of Mammalian Cells on Cytoskeleton and Intercellular Connections”).

Material Selection

Electroporation of embryos and embryonic tissues is mainly performed relying on trains of square voltage pulses (section “Organisms and Tissues”). The most commonly used machines are the CUY21 and the NEPA21 from NepaGene (Ishikawa, Japan), the TSS20 Ovodyne from Intracel (St Ives, UK), and the ECM830 and the ECM2001 from BTX Harvard Apparatus (Holliston, USA) – see the provider’s webpage for detailed specifications; Echeverri and Tanaka (2003), Krull (2004), and Cerda et al. (2006) for comparative analyses; and Ando and Fujiwara (2013) and Bullmann et al. (2015) for instructions on the homemade assembly of cheaper apparatuses (costing less than 200 €).

Relatively low pulse amplitudes are selected to limit cell death, whereas long durations allow nucleic acids to reach the targeted area upon electrophoresis (chapter “► Gene Delivery by Electroporation In Vitro: Mechanisms”). More precisely, a series of three to six pulses is generally applied. Their amplitude of course depends on the electrodes geometry and spacing as well as on the tissue shape and nature (section “Setup Conception”) (Krull 2004; Chernet and Levin 2012); however, it usually falls within the 10–100 V range. Concerning the length of the pulses and the dwell time between them, the respective 50 ms and 1 s values established during early studies seem today consensual (Itasaki et al. 1999); they consequently represent a good starting point for any optimization in a new biological system. Larger amplitudes and longer durations will be associated with higher poration efficiency but also with lower cell, or even embryo, viability (Muramatsu et al. 1997; Momose et al. 1999; Eide et al. 2000; Echeverri and Tanaka 2003; Teh et al. 2003; Abud et al. 2004; Hendricks and Jesuthasan 2007; Kera et al. 2010; Mazari et al. 2014; Simkin et al. 2014; chapters “► Gene Delivery by Electroporation In Vitro: Mechanisms” and “► Parameters Affecting Cell Viability Following Electroporation”). Note also that more specific adjustments may be required in the case of organs with a more complicated structure (Alie et al. 2007).

Despite the success of square-wave electroporation, some experiments are based on other electrical sequences: exponentially decaying voltage pulses are extensively used on zygotes and on embryos including only a small number of cells (Buono and Linser 1992; Kamdar et al. 1995; Leopold et al. 1996; Corbo et al. 1997; Bosch et al. 2002); rapid trains of pulses produced with neurophysiological simulators look more

appropriate when utilizing a patch-clamp pipette (Atkins et al. 2000; Haas et al. 2001; Echeverri and Tanaka 2003; Tawk et al. 2009).

Concerning the electroporation setup per se, platinum is the material of choice for electrode fabrication. Although expensive this noble metal is inert and thus resistant to corrosion. Furthermore, it is quite soft, which enables one to easily shape foils and wires in house (Haas et al. 2002; Krull 2004; Scaal et al. 2004; Quinlan et al. 2008). This latter property obviously becomes a drawback when penetration in a tissue is necessary. In this case one will favor tungsten, which is harder and which can be electrochemically sharpened to yield microneedles (Momose et al. 1999; Quinlan et al. 2008). Options cheaper than platinum include stainless steel and aluminum (Leopold et al. 1996; Thomas 2003) but these two materials are prone to fast electrochemical degradation (chapter “► [Electrode Erosion and Metal Release Under Electroporation Conditions](#)”; Wang and Lee 2013). Other noble metals can equally be considered: silver is utilized to build bulk electrode, whereas gold is only plated. Finally, standard procedures exist in microelectronics to deposit thin film of platinum or gold; therefore, those two materials are often used to apply voltage pulses in miniaturized electroporation devices (Murakami et al. 1994; Huang et al. 2007; Bansal et al. 2009; Mazari et al. 2010).

Dielectric guides usually consist in a glass micropipette in which a tungsten, silver, or platinum wire has been inserted (Haas et al. 2002; Echeverri and Tanaka 2003; Tawk et al. 2009; Huang et al. 2015). The former part of the setup can simply be pulled out from a glass capillary thanks to a microforge (Huang et al. 2015) – for more complex injection scheme, one can even rely on double-barreled microtubes (Atkins et al. 2000; Barker et al. 2009). When the structure that focused the electric field is integrated in a microsystem, as reviewed in Fox et al. (2006), Geng and Lu (2013), Wang and Lee (2013) (chapters “► [Description by Electroporation in Microfluidic Devices](#)” and “► [Nanochannel Electroporation: Delivery of Precise Amounts of Biomolecules into Living Cells](#)”), options in terms of material are more diverse. Glass is often used, alone (Zhao et al. 2014) or in association with polymers like photoresists (Mazari et al. 2014), photocurable glues (Mazari et al. 2011), plastics (Huang et al. 2007), elastomers (Falk et al. 2007; Bansal et al. 2009), and/or paraffins (Mazari et al. 2014). In fact, the choice of a given material is first related to the microfabrication procedure, itself selected in terms of laboratory know-how as well as of desired spatial resolution and planned functionality. Eventually, it is compulsory to consider the compatibility between the foreseen experiment and the properties of the material, such as its biological innocuity (Mazari et al. 2010, 2014) and its wettability (Mazari et al. 2014; Zhao et al. 2014).

To conclude this instrumentation section, it is interesting to discuss the electroporation protocol itself. Targeting a given area can be achieved by simple orientation of the tissue with respect to plate electrodes or thanks to a setup enabling electric field focusing, e.g., a microelectrode or a dielectric guide (section “[Strategies to Spatially Restrict Transfection](#)”). Whatever the selected option, two main strategies are available: in the first one the electrodes and their appendages are set in place around the embryonic tissue; in the second one the position of the biological object is adjusted within a fixed device. Naturally, some situations enforce a procedure:

tweezers terminated by paddle or needle electrodes are mandatory when surgery is involved, e.g., when performing *in ovo* (Momose et al. 1999; Krull 2004; Scaal et al. 2004) or *in utero* electroporation (Saito 2006; dal Maschio et al. 2012; De la Rossa and Jabaudon 2015); on the opposite, non-localized electroporation of isolated cells or of small cellular clusters is simply realized in batch in cuvette (Corbo et al. 1997; Bosch et al. 2002; Bobick et al. 2014). However, in many cases the choice remains open. On one hand, manipulating the electrodes allows the experimenter to easily adapt the protocol to individuals, which can be important when considering the non-negligible size and shape variability encountered in embryology – especially for higher organisms or when a lack of accessibility makes it difficult to synchronize the experimental timing with the developmental one. On the other hand, adjusting the position of the electrodes can be tricky and thus time consuming (Kos et al. 2003; Krull 2004; Scaal et al. 2004). Furthermore, relying on a well-defined experimental device may be preferable since it enables some standardization, synonym of a better reproducibility – this is especially the case when using microsystems that had been fabricated with a precision close to the micrometer (Fox et al. 2006; Geng and Lu 2013; Wang and Lee 2013; chapters “► Description by Electroporation in Microfluidic Devices” and “► Nanochannel Electroporation: Delivery of Precise Amounts of Biomolecules into Living Cells”).

Reagents Preparation

After plasmids have been produced in bacteria, they must be purified while taking into account two important recommendations: endotoxin-free kits must be employed (Scaal et al. 2004; Saito 2006; Mazari et al. 2014) and nucleic acids recovery must be performed in water (Haas et al. 2002; Krull 2004; Falk et al. 2007; Mazari et al. 2014). In particular, the use of EDTA in buffers is not recommended, albeit contradictory information may be found (Krull 2004; Huang et al. 2007; Odani et al. 2008). As far as the other nucleic acids are concerned, mRNA are produced by *in vitro* transcription, whereas siRNA and morpholinos are chemically synthesized. Hence, they come clean of harmful contaminants.

The titer in pDNA of the electroporation solution must be at least around 1 $\mu\text{g}/\mu\text{L}$ (Krull 2004). It can be increased to improve the transfection yield but the benefit will plateau around 5 $\mu\text{g}/\mu\text{L}$, i.e. $\sim 1 \mu\text{M}$, while the reagent preparation step will become more laborious (Momose et al. 1999; Haas et al. 2002; Sasagawa et al. 2002; Davidson et al. 2003, Scaal et al. 2004; Cerda et al. 2006; Voiculescu et al. 2008; Takahashi et al. 2008a; Kera et al. 2010; Tanaka et al. 2014; Simkin et al. 2014). Interestingly, coelectroporation is a very efficient strategy to introduce two different plasmids in the same cells, which can be useful when bi-cistronic constructs are not available or when some toxicity due to the pDNA size is observed (chapter “► Parameters Affecting Cell Viability Following Electroporation”). Relying on such protocol, a gene encoding for a fluorescent protein can be transfected with the nucleic acids of interest in order to precisely locate the modified cells (Calegari et al. 2002; Oberg et al. 2002; Mellitzer et al. 2002; Takahashi et al. 2008b; Odani

et al. 2008; Streit et al. 2013). This approach is also necessary when working with the CRISPR/Cas9 system, the many components of which are scattered over several plasmids (Sasaki et al. 2014; Véron et al. 2015; Tsunekawa et al. 2016). As far as mRNA is concerned, its typical concentration in the electroporation buffer is 0.5–2 $\mu\text{g}/\mu\text{L}$, i.e., $\sim 1 \mu\text{M}$ (Sasagawa et al. 2002; Cerda et al. 2006; Bansal et al. 2009; Chernet and Levin 2012). For siRNA the recommended titer varies between 0.05 and 5 $\mu\text{g}/\mu\text{L}$, i.e., 3 and 300 μM (Mellitzer et al. 2002; Grabarek et al. 2002; Pekarik et al. 2003; Soares et al. 2005, 2008; Tanaka et al. 2014), whereas for morpholinos a consensus exists with values around 0.5–1 mM (Kos et al. 2003; Cerda et al. 2006; Voiculescu et al. 2008; Tawk et al. 2009; Peng et al. 2012).

Whereas in developmental biology most of the *ex vivo* cultures are carried out in media rich in salts, growth factors, and nutriment, electroporation is usually performed in dilute buffers (e.g., phosphate buffer saline, HEPES buffer saline) (chapter “► Parameters Affecting Cell Viability Following Electroporation”). Whatever the selected components, relying on low salinity solutions enables to reduce Joule heating and thus tissue degradation. In the particular case of sea water organism, such as ascidians, mannitol is used to replace some of the dissolved ions while keeping the osmolarity constant (Corbo et al. 1997).

The nucleic acid solution may be supplemented with various adjuvants. For instance, a dye is often employed to facilitate delivery by microinjection close to the cells to be transfected. Fast green is the far most popular molecule (Haas et al. 2002; Krull 2004; Saito 2006; Huang et al. 2015; De la Rossa and Jabaudon 2015) but the use of methyl green (Momose et al. 1999), trypan blue (Pekarik et al. 2003), and phenol red (Krull 2004; Cui et al. 2006) has also sporadically been reported – interestingly, some authors have pointed out that fast green may inhibit genetic control by morpholinos (Kos et al. 2003) or be toxic to embryos (Krull 2004). Other additives may include carboxymethyl cellulose which, by making the injected mixture more viscous, prevents its spreading outside of the targeted tissue or cavity (Scaal et al. 2004; Falk et al. 2007). *Trans*-cyclohexane-1,2-diol has also been mentioned, its role being to disrupt the selectivity of the nuclear pores and thus to favor the passive diffusion of plasmids into the nucleus (De la Rossa and Jabaudon 2015).

Performances Validation

In test experiments, transfection success, both in terms of efficiency and localization, is assessed thanks to plasmids that encode readily detectable proteins. Early on, enzymes such as the β -galactosidase (Muramatsu et al. 1997, Momose et al. 1999, Itasaki et al. 1999, Swartz et al. 2001, Oberg et al. 2002 – Fig. 6a) or the luciferase (Murakami et al. 1994; Muramatsu et al. 1996; Harrison et al. 1998; Sasagawa et al. 2002) were used, the first one producing a colored product and the second one releasing photons upon reaction with its substrate. Nowadays, most technical developments are undertaken relying on constructs driving the expression of a fluorescent protein, like the GFP or the mCherry (Fig. 6b). Those markers are not only more sensitive and more practical; they also enable live imaging (Fig. 6c). The

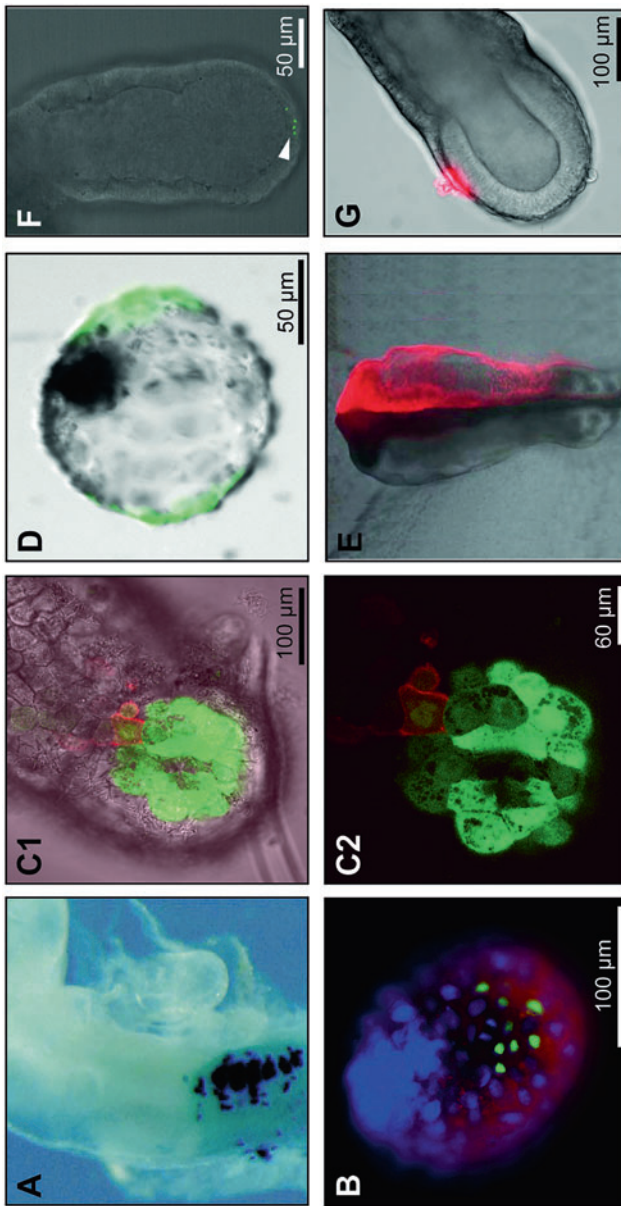


Fig. 6 Utilization of molecular markers to investigate electroporation in embryos. (A) Detection of the β -galactosidase 18–24 h after in ovo electroporation of a chick embryo at the 8–10 somites stage. The plasmid carrying the *LacZ* gene had been microinjected between the neural tube and the somites, and parallel wire electrodes were used (Reproduced from Itasaki et al. 1999). (B) Confocal image of the nuclear distribution of Venus 24 h after cuvette electroporation with the corresponding plasmid of a D10 bovine embryo. Counterstaining was performed with DAPI (in blue) and Alexa555-conjugated phalloidin (in red). (C1) Overlay of bright-field and single confocal image of visceral endoderm cells from a transgenic Hex-GFP-positive E6.5 mouse embryo electroporated at E5.75 in a dielectric microdevice with a plasmid encoding FusionRed-LifeAct. Hex-GFP (green) marks anterior visceral endoderm cells and FusionRed-LifeAct (red) is an actin reporter. (C2) Zoom on a dividing cell, extracted from the previous picture. Red fluorescence enables to image cortical actin structures, and cytoplasm is in green. (D) Incorporation of FITC-dextran in the cells of a D9 bovine embryo after cuvette electroporation. (E) Repartition of a lissamine-tagged morpholino at

onset of expression can even be determined quite precisely provided one utilizes a fast maturing protein (Shaner et al. 2004; Chudakov et al. 2010). Fluorescence starts to be detected 2–4 h after electroporation, as reported in zebrafish (Teh et al. 2003; Kera et al. 2010), *Xenopus* (Haas et al. 2002; Falk et al. 2007), chick (Oberg et al. 2002; Sauka-Spengler and Barembaum 2008), quail (Cui et al. 2006), axolotl (Echeverri and Tanaka 2003), and mouse (Abud et al. 2004).

Nevertheless, one may fail to observe any modification in gene expression upon electroporation. Several reasons may then be invoked, among which pores that do not open in the plasma membrane, nucleic acids that do not enter through them, or transfected cells that die. Each of these issues can in fact be systematically addressed with the help of appropriate fluorescent probes.

The technique to detect pore formation is the same than the one working for isolated cells (chapter “► [Fluorescent Indicators of Membrane Permeabilization Due to Electroporation](#)”). It consists in applying the voltage pulses in presence of a molecule that normally does not enter into the cytoplasm. Dextrans labeled with dyes such as fluorescein, tetra-methyl-rhodamine, or Texas Red are the most popular markers (Haas et al. 2002, Bosch et al. 2002, Grabarek et al. 2002, Barker et al. 2009, Hendricks and Jesuthasan 2007, Bansal et al. 2009, Tawk et al. 2009, Mazari et al. 2014, Zhao et al. 2014 – Fig. 6d). Their molecular weight is usually ~ 4 kDa. Interestingly, such size also prevents the molecule to diffuse from cell to cell through GAP junction, thereby allowing one to trace lineage (Stern and Fraser 2001; Bhattacharyya et al. 2008; Kretschmar and Watt 2012). Other reporters of poration include propidium iodide (Harrison et al. 1998; Eide et al. 2000; Barker et al. 2009), trypan blue (Huang et al. 2007; Bansal et al. 2009), and even quantum dot (Huang et al. 2007).

Evaluating if nucleic acids enter the targeted cells is the next step in developing an efficient transfection protocol. The neutral morpholinos are most often tagged with a fluorescent dye that provides them a charge and consequently enables their transport by electrophoresis to the tissue to be transfected. As a result they can be tracked thanks to labels like lissamine (Cerda et al. 2006; Falk et al. 2007; Sauka-Spengler and Barembaum 2008 – Fig. 6e), fluorescein (Kos et al. 2003; Falk et al. 2007; Voiculescu et al. 2008; Tawk et al. 2009), or carboxyfluorescein (Kos et al. 2003). Although it is not necessary to favor their electroporation, siRNA have also been conjugated to fluorophores, and their presence in embryos could then be monitored (Soares et al. 2005). Concerning plasmid labeling, the strategy involving non-covalent ligands of the double helix, such as TOTO-1, is very popular to investigate electroporation at the cell level (Golzio et al. 2002; chapter “► [Gene](#)



Fig. 6 (continued) staged HH10 after unilateral electroporation of neural crest and neural progenitors a chick embryo at stage HH4 (Reproduced from Sauka-Spengler and Barembaum 2008). (F) Formation of nucleic acids aggregates at the surface of an E5.5 mouse embryo after electroporation in a dielectric guide device with a plasmid that had been previously chemically conjugated to FITC. (G) Detection of dead cells using propidium iodide uptake and morphological analysis after electroporation of an E6.5 mouse embryo in a dielectric guide device

[Delivery by Electroporation In Vitro: Mechanisms](#)”). However, it has never been experimented in embryos. Instead, utilization has been made of reacting dyes able to covalently bind to pDNA (Mazari et al. 2014 – Fig. 6f).

The third issue to be studied is whether the cells that have been exposed to the voltage pulses are still healthy or not. Immediate death by plasma membrane disruption is suspected when darker areas appear (Huang et al. 2015) or when cellular morphology is abnormal (Mazari et al. 2014 – Fig. 6g). However, to secure the diagnosis, a post-electroporation staining procedure can be performed (chapter “► [Different Cell Viability Assays Following Electroporation In Vitro](#)”), which involves dyes that do not cross intact phospholipidic bilayers and that also stain genomic DNA inside the nucleus, e.g., propidium iodide (Haas et al. 2002, Barker et al. 2009, Mazari et al. 2014 – Fig. 6g), Sytox Green (Barker et al. 2009), and RedDot1 (Huang et al. 2015). More complex assays can further be realized to detect cells entering apoptosis: TUNEL reports on DNA fragmentation (Krull 2004; Falk et al. 2007; Peng et al. 2012), propidium iodide staining informs on nuclei structure (Eide et al. 2000), and immunohistochemistry is used to evidence the activation of the caspase3 signaling pathway (Brown et al. 2012). Yet, the ultimate test is functional: one has to check if the electroporated cells behave as expected, with respect to their division rate, their migration route, and their differentiation pathway for instance (Echeverri and Tanaka 2003; Mazari et al. 2014). Indeed, electroporation is known to alter both the cytoskeleton and the intercellular connections, which may result in subtle and/or delayed effects on the tissue structure and/or on its function (chapter “► [Effects of Electroporation of Mammalian Cells on Cytoskeleton and Intercellular Connections](#)”).

Conclusion

The successful implementation of electroporation in developmental biology may be attributed to the following characters: the protocols are quite straightforward to set up, time-saving, low cost, and relatively harmless for the manipulated organisms (Table 1). It took roughly 15 years of methodological research to be able to introduce nucleic acids in embryonic tissues in a save and efficient way (section “[Organisms and Tissues](#)”). Meanwhile, molecular biology tools were conceived in order to perform loss-of-function experiments more easily, consequently adding to the already existing constructs allowing gain-of-function experiments (section “[Molecular Biology Tools](#)”). As a result, electroporation is now a mature technique routinely employed to decipher the workings of the genetic networks involved in the transformation of a unicellular fertilized egg in an autonomous multicellular organism.

Although the previous assertion holds for the most popular animal models (e.g., mouse, chick, frog, zebrafish), the situation is rather different for numerous species which embryology and functional genomics are less advanced, despite their economic importance (e.g., silkworm, cow, sheep, pig, horse). This situation is paradoxical since electroporation represents an effective methodology to tackle the lack

of genetic tools. However, things should change soon thanks to the large corpus of studies now available: numerous instruments have been invented that can be inspiring to design more specific devices (sections “[Strategies to Spatially Restrict Transfection](#)” and “[Material Selection](#)”), and clear procedures have been published that describe how to validate an electroporation protocol or at least how to understand what is going wrong with it (section “[Performances Validation](#)”).

Besides those applied issues, a few challenges remain in the field of biophysics. For example, through the literature it has been reported that mesenchymal tissues are difficult to transfect (Itasaki et al. 1999; Oberg et al. 2002; Scaal et al. 2004; Krull 2004; Sakai and Trainor 2014). However, the invoked reasons have not been so far strongly backed up by experimental facts. Although some have raised concerns about the leaking of the nucleic acids solution out of the injection site, deeper causes related to the structure of the mesenchyme have been proposed. Indeed, dealing with cells dispersed into a conjunctive matrix (Itasaki et al. 1999; Krull 2004), or with a tissue far less electrically coupled than the surrounding epithelia, may be problematic (Oberg et al. 2002). Therefore, more fundamental studies are needed that would analyze results acquired on massive tissues and on small cellular systems like spheroids, cysts, and organoids (chapters “[► 3D Culture Models to Assess Tissue Responses to Electroporation](#)” and “[► 3D Tissue Models to Bridge the Gap Between Cell Culture and Tissue in Assessing Electroporation](#)”). These data would also benefit the conception of more accurate numerical models (section “[Setup Conception](#)”).

Finally, one of the last frontiers that may present opportunities for technological development is the one of resolution, both in space and in time. As a matter of fact, the physical tools that have been devised so far have reached their intrinsic limitations. The patch-clamp pipette technique is already able to transfect a single cell. Similarly, each molecular biology tool has its own response time (Table 1), which can hardly be reduced because it depends on how long it for the nucleic acids reach the concerned cellular machinery and interact with it. Thus, a paradigm shift appears necessary. For example, controlling the protein synthesis or functionality can be achieved well after electroporation relying on some external trigger. The latter signal can be molecular, like in the activation by the 4-hydroxytamoxifen of a Cre/lox-mediated inducible expression system (Matsuda and Cepko 2007) and by the doxycycline of Tet-On or Tet-Off ones (Takahashi et al. 2008b). Alternatively, light proves useful when it drives photoactivation of fluorescent proteins (Stark and Kulesa 2007; Bhattacharyya et al. 2008). Noteworthy, using photons also allows one to act deep inside organisms, in places that are normally reluctant to genetic modulation by methods requiring some kind of physical intimacy between the targeted cells and the nucleic acids (e.g., microinjection, viral infection, and electroporation). A last approach to manage both the timing and the location of expression involves the use of tissue-specific *cis*-regulatory elements; in this case the protein is only produced when cells engage into a given developmental pathway (Itasaki et al. 1999; Matsuda and Cepko 2007).

Acknowledgments This book chapter was written in the context of collaborative research projects funded by the grants “ElectroMice” (CNRS PI: Physique Chimie Biologie 2008), “Electro-TagMam” (Cnano IdF 2011), “ElectroDev” (PHC Tournesol 2014), and “RhoGTPases and collective migration” (FNRS MIS 2013).

Cross-References

- ▶ [3D Culture Models to Assess Tissue Responses to Electroporation](#)
- ▶ [3D Tissue Models to Bridge the Gap Between Cell Culture and Tissue in Assessing Electroporation](#)
- ▶ [Combining Electrolysis and Electroporation for Tissue Ablation](#)
- ▶ [Critical Electric Field and Transmembrane Voltage for Lipid Pore Formation in Experiments](#)
- ▶ [Description by Electroporation in Microfluidic Devices](#)
- ▶ [Different Cell Viability Assays Following Electroporation In Vitro](#)
- ▶ [Effects of Electroporation of Mammalian Cells on Cytoskeleton and Intercellular Connections](#)
- ▶ [Electrode Erosion and Metal Release Under Electroporation Conditions](#)
- ▶ [Electrolysis During Pulse Electric Field Treatment](#)
- ▶ [Fluorescent Indicators of Membrane Permeabilization Due to Electroporation](#)
- ▶ [Gene Delivery by Electroporation In Vitro: Mechanisms](#)
- ▶ [Nanochannel Electroporation: Delivery of Precise Amounts of Biomolecules into Living Cells](#)
- ▶ [Nucleic Acid Electrotransfer in Mammalian Cells: Mechanistic Description](#)
- ▶ [Parameters Affecting Cell Viability Following Electroporation](#)
- ▶ [Transmembrane Voltage Induced by Applied Electric Fields](#)

References

- Abud HE, Lock P, Heath JK (2004) Efficient gene transfer into the epithelial cell layer of embryonic mouse intestine using low-voltage electroporation. *Gastroenterology* 126:1779–1787
- Akamatsu W, Okano HJ, Osumi N, Inoue T, Nakamura S, Sakakibara SI, Miura M, Matsuo N, Darnell RB, Okano H (1999) Mammalian ELAV-like neuronal RNA-binding proteins HuB and HuC promote neuronal development in both the central and the peripheral nervous systems. *Proc Natl Acad Sci U S A* 96:9885–9890
- Alie TM, Vrljicak PJ, Myburgh DB, Gupta IR (2007) Microinjection and electroporation of embryonic kidney explants: an improved method. *Kidney Int* 72:121–125
- Ando T, Fujiwara H (2013) Electroporation-mediated somatic transgenesis for rapid functional analysis in insects. *Development* 140:454–458
- Atkins RL, Wang D, Burke RD (2000) Localized electroporation: a method for targeting expression of genes in avian embryos. *BioTechniques* 28:94–100
- Bansal T, Lenhart J, Kim T, Duan C, Maharbiz MM (2009) Patterned delivery and expression of gene constructs into zebrafish embryos using microfabricated interfaces. *Biomed Microdevices* 11:633–641
- Barenbaum M, Bronner-Fraser M (2007) Spalt4 mediates invagination and otic placode gene expression in cranial ectoderm. *Development* 134:3805–3814

- Barker M, Billups B, Hamann M (2009) Focal macromolecule delivery in neuronal tissue using simultaneous pressure ejection and local electroporation. *J Neurosci Methods* 177:273–284
- Bartkowska K, Paquin A, Gauthier AS, Kaplan DR, Miller FD (2007) Trk signaling regulates neural precursor cell proliferation and differentiation during cortical development. *Development* 134:4369–4380
- Bhattacharyya S, Kulesa PM, Fraser SE (2008) Vital labeling of embryonic cells using fluorescent dyes and proteins. In: Bronner-Fraser M (ed) *Avian embryology*, 2nd edn. Academic, London, pp 187–210
- Bobick BE, Alexander PG, Tuan RS (2014) High efficiency transfection of embryonic limb mesenchyme with plasmid DNA using square wave pulse electroporation and sucrose buffer. *BioTechniques* 56:85–89
- Bosch TCG, Augustin R, Gellner K, Khalturin K, Lohmann JU (2002) In vivo electroporation for genetic manipulations of whole hydra polyps. *Differentiation* 70:140–147
- Brown CY, Eom DS, Amarnath S, Agarwala S (2012) A simple technique for early in vivo electroporation of E1 chick embryos. *Dev Dyn* 241:545–552
- Bullmann T, Arendt T, Frey U, Hanashima C (2015) A transportable, inexpensive electroporator for in utero electroporation. *Develop Growth Differ* 57:369–377
- Buono RJ, Linser PJ (1992) Transient expression of RSVCAT in transgenic zebrafish made by electroporation. *Mol Mar Biol Biotechnol* 1:271–275
- Calegari F, Haubensak W, Yang D, Huttner WB, Buchholz F (2002) Tissue-specific RNA interference in postimplantation mouse embryos with endoribonuclease-prepared short interfering RNA. *Proc Natl Acad Sci U S A* 99:14236–14240
- Cerda GA, Thomas JE, Allende ML, Karlstrom RO, Palma V (2006) Electroporation of DNA, RNA, and morpholinos into zebrafish embryos. *Methods* 39:207–211
- Chabot S, Rosazza C, Golzio M, Zumbusch A, Teissié J, Rols MP (2013) Nucleic acids electro-transfer: from bench to bedside. *Curr Drug Metab* 14:300–308
- Chernet BT, Levin M (2012) A versatile protocol for mRNA electroporation of *Xenopus laevis* embryos. *Cold Spring Harb Protocol*:447–452
- Chudakov DM, Matz MV, Lukyanov S, Lukyanov KA (2010) Fluorescent proteins and their applications in imaging living cells and tissues. *Physiol Rev* 90:1103–1163
- Corbo JC, Levine M, Zeller RW (1997) Characterization of a notochord-specific enhancer from the Brachyury promoter region of the ascidian, *Ciona intestinalis*. *Development* 124:589–602
- Couly GF, Coltey PM, Le Douarin NM (1993) The triple origin of skull in higher vertebrates: a study in quail-chick chimeras. *Development* 117:409–429
- Cui C, Lansford R, Filla MB, Little CD, Chevront TJ, Rongish BJ (2006) Electroporation and EGFP labeling of gastrulating quail embryos. *Dev Dyn* 235:2802–2810
- dal Maschio M, Ghezzi D, Bony G, Alabastri A, Deidda G, Brondi M, Sato SS, Zaccaria RP, Fabrizio ED, Ratto GM, Cancedda L (2012) High-performance and site-directed in utero electroporation by a triple-electrode probe. *Nat Commun* 3:960
- Danielian PS, Muccino D, Rowitch DH, Michael SK, McMahon AP (1998) Modification of gene activity in mouse embryos in utero by a tamoxifen-inducible form of Cre recombinase. *Curr Biol* 8:1323–1326
- Davidson BP, Tsang TE, Khoo PL, Gad JM, Tam PPL (2003) Introduction of cell markers into germ layer tissues of the mouse gastrula by whole embryo electroporation. *Genesis* 35:57–62
- De la Rossa A, Jabaudon D (2015) In vivo rapid gene delivery into postmitotic neocortical neurons using iontoporation. *Nat Protoc* 10:25–32
- deCastro M, Saijoh Y, Schoenwolf JC (2006) Optimized cationic lipid-based gene delivery reagents for use in developing vertebrate embryos. *Dev Dyn* 235:2210–2219
- Donovan SL, Dyer MA (2006) Preparation and square wave electroporation of retinal explant cultures. *Nat Protoc* 1:2710–2718
- Driver EC, Kelley MW (2010) Transfection of mouse cochlear explants by electroporation. *Curr Protocol Neurosci*. Chapter 4:Unit 4.34.1–10

- Echeverri K, Tanaka EM (2003) Electroporation as a tool to study in vivo spinal cord regeneration. *Dev Dyn* 226:418–425
- Echeverri K, Tanaka EM (2005) Proximodistal patterning during limb regeneration. *Dev Biol* 279:391–401
- Eichele G, Tickle C, Alberts BM (1985) Studies on mechanism of retinoid-induced pattern duplications in the early chick limb bud: temporal and spatial aspects. *J Cell Biol* 101:1913–1920
- Eide FF, Eisenberg SR, Sanders TA (2000) Electroporation-mediated gene transfer in free-swimming embryonic *Xenopus laevis*. *FEBS Lett* 496:29–32
- Falk J, Drinjakovic J, Leung KM, Dwivedy A, Regan AG, Piper M, Holt CE (2007) Electroporation of cDNA/morpholinos to targeted areas of embryonic CNS in *Xenopus*. *BMC Dev Biol* 7:107
- Fox MB, Esveld DC, Valero A, Lutttge R, Mastwijk HC, Bartels PV, van den Berg A, Boom RM (2006) Electroporation of cells in microfluidic device: a review. *Anal Bioanal Chem* 385:474–485
- Fukuchi-Shimogori T, Grove EA (2001) Neocortex patterning by the secreted signaling molecule FGF8. *Science* 294:1071–1074
- Fukuda K, Sakamoto N, Narita T, Saitoh K, Kameda T, Iba H, Yasugi S (2000) Application of efficient and specific gene transfer systems and organ culture techniques for the elucidation of mechanisms of epithelial-mesenchymal interaction in the developing gut. *Develop Growth Differ* 42:207–211
- Geetha-Loganathan P, Nimmagadda S, Hafez I, Fu K, Cullis PR, Richman JM (2011) Development of high-concentration lipoplexes for in vivo gene function studies in vertebrate embryos. *Dev Dyn* 240:2108–2119
- Geng T, Lu C (2013) Microfluidic electroporation for cellular analysis and delivery. *Lab Chip* 13:3830–3821
- Gilbert SF (2013) *Developmental biology*, 10th edn. Sinauer, Sunderland
- Giroux SJD, Alves-Leiva C, Lécluse Y, Martin P, Albagl O, Godin I (2007) Gene transfer to pre-hematopoietic and committed hematopoietic precursors in the early mouse yolk sac: a comparative study between in situ electroporation and retroviral transduction. *BMC Dev Biol* 7:79
- Golzio M, Teissie J, Rols MP (2002) Direct visualization at the single-cell level of electrically mediated gene delivery. *Proc Natl Acad Sci U S A* 99:1292–1297
- Grabarek JB, Plusa B, Glover DM, Zernicka-Goetz M (2002) Efficient delivery of dsRNA into zona-enclosed mouse oocytes and preimplantation embryos by electroporation. *Genesis* 32:269–276
- Haas K, Sin WC, Javaherian A, Li Z, Cline HT (2001) Single-cell electroporation for gene transfer in vivo. *Neuron* 29:583–591
- Haas K, Jensen K, Sin WC, Foa L, Cline HT (2002) Targeted electroporation in *Xenopus* tadpoles in vivo—from single cells to the entire brain. *Differentiation* 70:148–154
- Harrison RL, Byrne BJ, Tung L (1998) Electroporation-mediated gene transfer in cardiac tissue. *FEBS Lett* 435:1–5
- Hashimoto-Torii K, Motoyama J, Hui CC, Kuroiwa A, Nakafuku M, Shimamura K (2003) Differential activities of sonic hedgehog mediated by Gli transcription factors define distinct neuronal subtypes in the dorsal thalamus. *Mech Dev* 120:1097–1111
- Hatakeyama J, Shimamura K (2008) Method for electroporation for the early chick embryo. *Develop Growth Differ* 5:449–452
- Hendricks M, Jesuthasan S (2007) Electroporation-based methods for in vivo, whole mount and primary culture analysis of zebrafish brain development. *Neural Dev* 2:6
- Huang KS, Lin YC, Su KC, Chen HY (2007) An electroporation microchip system for the transfection of zebrafish embryos using quantum dots and GFP genes for evaluation. *Biomed Microdevices* 9:761–768
- Huang Y, Wilkie R, Wilson V (2015) Methods for precisely localized transfer of cells or DNA into early postimplantation mouse embryos. *J Vis Exp* 106:53295

- Iba H (2000) Gene transfer into chicken embryos by retrovirus vectors. *Develop Growth Differ* 42:213–218
- Iimura T, Pourquié O (2008) Manipulation and electroporation of the avian segmental plate and somites in vitro. In: Bronner-Fraser M (ed) *Avian embryology*, 2nd edn. Academic, London, pp 257–270
- Inoue K (1992) Expression of reporter genes introduced by microinjection and electroporation in fish embryos and fry. *Mol Mar Biol Biotechnol* 1:266–270
- Itasaki N, Bel-Vialar S, Krumlauf R (1999) ‘Shocking’ developments in chick embryology: electroporation and *in ovo* gene expression. *Nat Cell Biol* 1:E203–E207
- Jaenisch R (1988) Transgenic animals. *Science* 240:1468–1474
- Kaestner L, Scholz A, Lipp P (2015) Conceptual and technical aspects of transfection and gene delivery. *Bioorg Med Chem Lett* 25:1171–1176
- Kamdar KP, Wagner TN, Finnerly V (1995) Electroporation of *Drosophila* embryos. In: Nickoloff JA (ed) *Animal cell electroporation and electrofusion protocols*. Humana Press, Totowa, pp 239–243
- Katahira T, Nakamura H (2003) Gene silencing in chick embryos with a vector-based small interfering RNA system. *Develop Growth Differ* 45:361–367
- Kera SA, Agerwala SM, Home JH (2010) The temporal resolution of in vivo electroporation in zebrafish: a method for time-resolved loss of function. *Zebrafish* 7:97–108
- Kos R, Tucker RP, Hall R, Duong TD, Erickson CA (2003) Methods for introducing morpholinos into the chicken embryo. *Dev Dyn* 226:470–477
- Kretzschmar K, Watt FM (2012) Lineage tracing. *Cell* 148:33–45
- Krull CE (2004) A primer on using *in ovo* electroporation to analyze gene function. *Dev Dyn* 229:433–439
- Kumar A, Godwin JW, Gates PB, Garza-Garcia AA, Brookes JP (2007) Molecular basis for the nerve dependence of limb regeneration in an adult vertebrate. *Science* 318:772–777
- Le Douarin N, Dieterlen-Lièvre F, Creuzet S, Teillet MA (2008) Quail–chick transplantations. In: Bronner-Fraser M (ed) *Avian embryology*, 2nd edn. Academic, London, pp 19–58
- Lee JM, Takahashi M, Mon H, Koga K, Kawaguchi Y, Kusakabe T (2005) Efficient gene transfer into silkworm larval tissues by a combination of sonoporation and lipofection. *Cell Biol Int* 29:976–979
- Lee JM, Kim JY, Cho KW, Lee MJ, Cho SW, Kwak S, Cai J, Jung HS (2008) Wnt11/Fgfr1b cross-talk modulates the fate of cells in palate development. *Dev Biol* 314:341–350
- Leopold RA, Hughes KJ, DeVault JD (1996) Using electroporation and a slot cuvette to deliver plasmid DNA to insect embryos. *Genet Anal: Biomol Eng* 12:197–200
- Lin G, Chen Y, Slack JMW (2007) Regeneration of neural crest derivatives in the *Xenopus* tadpole tail. *BMC Dev Biol* 7:56
- Matsuda T, Cepko CL (2007) Controlled expression of transgenes introduced by in vivo electroporation. *Proc Natl Acad Sci U S A* 104:1027–1032
- Mazari E, Laniel J, Dubois G, Griffon S, Marty F, Perea-Gomez A, Gosse C (2010) Mouse embryo electroporation and culture in devices made by soft lithography. In: Verpoorte S, Andersson-Svahn H, Ennéus J, Pamme N (eds) *Proceedings of the 14th international conference on miniaturized systems for chemistry and life sciences*. CBMS, San Diego, pp 312–314
- Mazari E, Mantelet M, Iranzo J, Perea-Gomez A, Gosse C (2011) Localized electroporation of mouse embryo using dielectric guides. In: *Digest of the technical papers of the 16th international conference on solid-state sensors, actuators, and microsystems*. IEEE, Piscataway, pp 1172–1175
- Mazari E, Zhao X, Migeotte I, Collignon J, Gosse C, Perea-Gomez A (2014) A microdevice to locally electroporate embryos with high efficiency and reduced cell damage. *Development* 141:1–11
- Mellitzer G, Hallonet M, Chen L, Ang SL (2002) Spatial and temporal ‘knock down’ of gene expression by electroporation of double-stranded RNA and morpholinos into early post-implantation mouse embryos. *Mech Dev* 118:57–63

- Momose T, Tonegawa A, Takeuchi J, Ogawa H, Umesono K, Yasuda K (1999) Efficient targeting of gene expression in chick embryos by microelectroporation. *Develop Growth Differ* 41:335–344
- Moto K, Salam SEA, Sakurai S, Iwami M (1999) Gene transfer into insect brain and cell-specific expression of *Bombyxin* gene. *Dev Genes Evol* 209:447–450
- Müller F, Lele Z, Varadi L, Menczel L, Orban L (1993) Efficient transient expression system based on square pulse electroporation and in vivo luciferase assay of fertilized fish eggs. *FEBS Lett* 324:27–32
- Murakami Y, Motohashi K, Yano K, Ikebukuro K, Yokoyama K, Tamiya E, Karube I (1994) Micromachined electroporation system for transgenic fish. *J Biotechnol* 34:35–42
- Muramatsu T, Mizutani Y, Okumura J (1996) Live detection of the firefly luciferase gene expression by bioluminescence in incubating chicken embryos. *Amin Sci Technol (Jpn)* 67:906–909
- Muramatsu T, Mizutani Y, Ohmori Y, Okumura J (1997) Comparison of three nonviral transfection methods for foreign gene expression in early chicken embryos *in ovo*. *Biochem Biophys Res Commun* 230:376–380
- Nakamura H (2009) Electroporation and sonoporation in developmental biology. Springer, Tokyo
- Nakamura H, Funahashi J (2013) Electroporation: past, present and future. *Develop Growth Differ* 55:15–19
- Oberg KC, Pira CU, Revelli JP, Ratz B, Aguilar-Cordova E, Eichele G (2002) Efficient ectopic gene expression targeting chick mesoderm. *Dev Dyn* 224:291–302
- Odani N, Ito K, Nakamura H (2008) Electroporation as an efficient method of gene transfer. *Develop Growth Differ* 50:443–448
- Ogura T (2002) In vivo electroporation: a new frontier for gene delivery and embryology. *Differentiation* 70:163–171
- Ohta S, Suzuki K, Tachibana K, Yamada G (2003) Microbubble-enhanced sonoporation: efficient gene transduction technique for chick embryos. *Genesis* 37:91–101
- Olofsson J, Nolkranz K, Ryttsén F, Lambie BA, Weber SG, Orwar O (2003) Single-cell electroporation. *Curr Opin Biotechnol* 14:29–34
- Olofsson J, Levin M, Strömberg A, Weber SG, Ryttsén F, Orwar O (2007) Scanning electroporation of selected areas of adherent cell cultures. *Anal Chem* 79:4410–4418
- Paganin-Gioanni A, Bellard E, Escoffre JM, Rols MP, Teissié J, Golzio M (2011) Direct visualization at the single-cell level of siRNA electrotransfer into cancer cells. *Proc Natl Acad Sci U S A* 108:10443–10447
- Pekarik V, Bourikas D, Miglino N, Joset P, Preiswerk S, Stoekli ET (2003) Screening for gene function in chicken embryo using RNAi and electroporation. *Nat Biotechnol* 21:93–96
- Peng H, Wu Y, Zhang Y (2012) Efficient delivery of DNA and morpholinos into mouse preimplantation embryos by electroporation. *PLoS One* 7:e43748
- Powers DA, Hereford L, Cole T, Chen TT, Lin CM, Kight K, Creech K, Dunham R (1992) Electroporation: a method for transferring genes into the gametes of zebrafish (*Brachydanio rerio*), channel catfish (*Ictalurus punctatus*), and common carp (*Cyprinus carpio*). *Mol Mar Biol Biotechnol* 1:301–308
- Pu H, Young AP (1990) Glucocorticoid-inducible expression of a glutamine synthetase-CAT-encoding fusion plasmid after transfection of intact chicken retinal explant cultures. *Gene* 89:259–263
- Quinlan GA, Khoo PL, Wong N, Trainor PA, Tam PPL (2008) Cell grafting and labeling in postimplantation mouse embryos. In: Sharpe P, Mason I (eds) *Molecular embryology: methods and protocols*, 2nd edn. Humana Press, New-York, pp 47–70
- Saito T (2006) In vivo electroporation in the embryonic mouse central nervous system. *Nat Protoc* 1:1552–1558
- Saito T, Nakatsuji N (2001) Efficient gene transfer into the embryonic mouse brain using in vivo electroporation. *Dev Biol* 240:237–246
- Sakai D, Trainor PA (2014) Gene transfer techniques in whole embryo cultured post-implantation mouse embryos. In: Lewandoski M (ed) *Mouse molecular embryology*. Humana Press, New-York, pp 227–234

- Sasagawa S, Takabatake T, Takabatake Y, Muramatsu T, Takeshima K (2002) Improved mRNA electroporation method for *Xenopus* neurula embryos. *Genesis* 33:81–85
- Sasaki H, Yoshida K, Hozumi A, Sasakura Y (2014) CRISPR/Cas9-mediated gene knockout in the ascidian *Ciona intestinalis*. *Develop Growth Differ* 56:499–510
- Sato M, Ohtsuka M, Watanabe S, Gurumurthy CB (2016) Nucleic acids delivery methods for genome editing in zygotes and embryos: the old, the new, and the old-new. *Biol Direct* 11:16
- Sauka-Spengler T, Barembaum M (2008) Gain- and loss-of-function approaches in the chick embryo. In: Bronner-Fraser M (ed) *Avian embryology*, 2nd edn. Academic, London, pp 237–256
- Scaal M, Gros J, Lesbros C, Marcelle C (2004) *In ovo* electroporation of avian somites. *Dev Dyn* 229:643–650
- Semple-Rowland SL, Berry J (2014) Use of lentiviral vectors to deliver and express bicistronic transgenes in developing chicken embryos. *Methods* 66:466–473
- Shaner NC, Campbell RE, Steinbach PA, Giepmans BNG, Palmer AE, Tsien RY (2004) Improved monomeric red, orange and yellow fluorescent proteins derived from *Discosoma sp* red fluorescent protein. *Nat Biotechnol* 22:1567–1572
- Sharpe P, Mason I (2008) *Molecular embryology: methods and protocols*, 2nd edn. Humana Press, New-York
- Shin MK, Levorse JM, Ingram RS, Tilghman SM (1999) The temporal requirement for endothelin receptor-B signalling during neural crest development. *Nature* 402:496–501
- Simkin JE, McKeown SJ, Newgreen DF (2009) Focal electroporation *in ovo*. *Dev Dyn* 238:3152–3155
- Simkin JE, Zhang D, Ighaniyan S, Newgreen DF (2014) Parameters affecting efficiency of *in ovo* electroporation of the avian neural tube and crest. *Dev Dyn* 243:1440–1447
- Skachkov I, Luan Y, van der Steen AFW, de Jong N, Kooiman K (2014) Targeted microbubble mediated sonoporation of endothelial cells in vivo. *IEEE Trans Ultrason Ferroelectr Freq Control* 61:1661–1667
- Slack JMW (2006) *Essential developmental biology*, 2nd edn. Blackwell, Malden
- Smith KM, Gee L, Bode HR (2000) HyAlx, an aristaless-related gene, is involved in tentacle formation in hydra. *Development* 127:4743–4752
- Soares ML, Haraguchi S, Torres-Padilla ME, Kalmar T, Carpenter L, Bell G, Morrison A, Ring CJA, Clarke NJ, Glover DM, Zernicka-Goetz M (2005) Functional studies of signaling pathways in peri-implantation development of the mouse embryo by RNAi. *BMC Dev Biol* 5:28
- Soares ML, Torres-Padilla ME, Zernicka-Goetz M (2008) Bone morphogenetic protein 4 signaling regulates development of the anterior visceral endoderm in the mouse embryo. *Develop Growth Differ* 50:615–621
- Spemann H, Mangold H (1924) Über die Induktion von Embryonalanlagen durch Implantation artfremder Organisatoren. *W Roux' Arch f Entw d Organism u mikrosk Anat* 100:599–638. Translated and reprinted as: Spemann H, Mangold H (2001) Induction of embryonic primordia by implantation of organizers from different species. *Int J Dev Biol* 45:13–38
- Stark DA, Kulesa PM (2007) An *in vivo* comparison of photoactivatable fluorescent proteins in an avian embryo model. *Dev Dyn* 236:1583–1594
- Stern CD, Fraser SE (2001) Tracing the lineage of tracing cell lineages. *Nat Cell Biol* 3:E216–E218
- Stern CD, Ireland GW, Herrick SE, Gherardi E, Gray J, Perryman M, Stoker M (1990) Epithelial scatter factor and development of the chick embryonic axis. *Development* 110:1271–1284
- Stolfi A, Gandhi S, Salek F, Christiaen L (2014) Tissue-specific genome editing in *Ciona* embryos by CRISPR/Cas9. *Development* 141:4115–4120
- Streit A, Tambalo M, Chen J, Grocott T, Anwar M, Sosinsky A, Stern CD (2013) Experimental approaches for gene regulatory network construction: the chick as a model system. *Genesis* 51:296–310
- Svingen T, Wilhelm D, Combes AN, Hosking B, Harley VR, Sinclair AH, Koopman P (2009) *In vivo* magnetofection: a novel strategy for the study of gene function in mouse organogenesis. *Dev Dyn* 238:956–964

- Swartz M, Eberhart J, Mastick GS, Krull CE (2001) Sparking new frontiers: using in vivo electroporation for genetic manipulations. *Dev Biol* 233:13–21
- Tabata H, Nakajima K (2001) Efficient in utero gene transfer system to the developing mouse brain using electroporation: visualization of neuronal migration in the developing cortex. *Neuroscience* 103:865–872
- Takahashi M, Nomura T, Osumi N (2008a) Transferring genes into cultured mammalian embryos by electroporation. *Develop Growth Differ* 50:485–497
- Takahashi Y, Watanabe T, Nakagawa S, Kawakami K, Sato Y (2008b) Transposon-mediated stable integration and tetracycline-inducible expression of electroporated transgenes in chicken embryos. In: Bronner-Fraser M (ed) *Avian embryology*, 2nd edn. Academic, London, pp 271–280
- Tanaka SS, Yamaguchi YL, Jones VJ, Tam PPL (2014) Analyzing gene function in whole mouse embryo and fetal organ in vitro. In: Lewandoski M (ed) *Mouse molecular embryology*. Humana Press, New-York, pp 367–393
- Tawk M, Tuil D, Torrente Y, Vriza S, Paulin D (2002) High-efficiency gene transfer into adult fish: a new tool to study fin regeneration. *Genesis* 32:27–31
- Tawk M, Bianco IS, Clarke JDW (2009) Focal electroporation in zebrafish embryos and larvae. In: Lieschke GJ, Oates AC, Kawakami K (eds) *Zebrafish: methods and protocols*. Humana Press, Dordrecht, pp 145–151
- Teh C, Chong SW, Korzh V (2003) DNA delivery into anterior neural tube of zebrafish embryos by electroporation. *BioTechniques* 35:950–954
- Thomas JL (2003) Electroporation, an alternative to biolistics for transfection of *Bombyx mori* embryos and larval tissues. *J Insect Sci* 3:17
- Thomas JL, Bardou J, L'hoste S, Mauchamp B, Chavancy G (2001) A helium burst biolistic device adapted to penetrate fragile insect tissues. *J Insect Sci* 1:9
- Tsunekawa Y, Terhune RK, Fujita I, Shitamukai A, Suetsugu T, Matsuzaki F (2016) Developing a de novo targeted knock-in method based on in utero electroporation into the mammalian brain. *Development* 143:3216–3222
- Véron N, Qu Z, Kipen PAS, Hirst CE, Marcelle C (2015) CRISPR mediated somatic cell genome engineering in the chicken. *Dev Biol* 407:68–74
- Voiculescu O, Papanayotou C, Stern CD (2008) Spatially and temporally controlled electroporation of early chick embryos. *Nat Protoc* 3:419–426
- Wang S, Lee LJ (2013) Micro-/nanofluidics cell electroporation. *Biomicrofluidics* 7:011301
- Zhao X, Mazari E, Suárez-Boomgaard D, Migeotte I, Perea-Gomez A, Gosse C (2014) Finite element model simulations to assist the design of microdevices dedicated to the localized electroporation of mouse embryos. *ECS Trans* 64:7–14

Conception et fabrication d'outils microfluidiques réutilisables pour étudier la dynamique de phénomènes biologiques: application à l'influx / efflux d'antibiotiques dans les bactéries et à la migration des cellules pendant le développement de la souris

Résumé en français

Au cours de cette thèse, nous avons développé des outils microfluidiques réutilisables et leur protocoles expérimentaux afin de mettre en place l'utilisation d'instrumentations miniaturisées dédiées à l'étude des objets biologiques à différentes échelles. Ce développement permet à l'émergence de stratégies innovantes ainsi que de répondre à d'importantes questions en sciences de la vie. Cette thèse est divisée en deux sous-parties : l'application dans le domaine microbiologie et l'application dans le domaine embryologie.

Part I :

La recherche sur les antibiotiques a commencé il y a plus d'un siècle. A partir du premier rapport au sujet du phénomène de l'antagonisme, à la découverte fortuite de la pénicilline, ensuite les recherches des antibiotiques dans l'habitat naturel, et enfin la synthèse/semi-synthèse artificielle des antibiotiques, des antibiotiques ont joué un grand rôle dans la médecine moderne.

Cependant, actuellement l'être-humain fait face à un problème plus sévère : à cause de l'abus des antibiotiques, de plus en plus de bactéries résistantes apparaissent, donc l'être-humain dispose de moins en moins de médicaments, mais en même temps, la recherche et le développement de nouveaux médicaments stagnent.

Autour de ce grand thème, cette première partie de thèse se focalise sur l'influx et l'efflux de la molécule d'antibiotique à travers l'enveloppe bactérienne, en combinaison avec l'application d'un nouveau dispositif microfluidique, pour offrir un autre angle de vision dans la première période où les bactéries entrent en contact avec les antibiotiques, dans une petite échelle de temps.

Les bactéries peuvent être classifiées de différentes façons, en fonction de leur

apparence, de leur type nutritionnel, de leurs besoins en oxygène pendant la croissance, de leur préférence de température ou de leur structure cellulaire. Notre étude utilise un organisme de modèle bien étudié, *Escherichia coli*, qui est bacilli et bactérie Gram-négative.

Les antibiotiques peuvent être classifiés par leurs mécanismes d'action spécifiques. Cinq cibles principales sont identifiées: la synthèse de la paroi cellulaire, l'intégrité de la membrane cellulaire, la synthèse des protéines, la synthèse des acides nucléiques et la synthèse du folate.

Quant à ce qui concerne l'interaction entre les bactéries et les antibiotiques, il faut parler de la résistance aux antibiotiques. Le mécanisme de résistance peut être généralement divisé en quatre catégories : l'inactivation de l'antibiotique par enzyme, l'altération du site de cible, les changements de la perméabilité de la membrane et l'expulsion active de l'antibiotique par les bactéries. Les deux derniers forment une paire de mécanismes de multiples résistance, et c'est aussi le point focal du travail actuel : influx / efflux.

Dans les recherches sur l'influx / efflux rapportées, on voit en général la méthode à trois échelles : études sur le comportement du groupe ; études sur le comportement de cellules individuelles, et études sur le comportement des protéines du canal individuel. Dans chaque échelle, deux genres de systèmes sont trouvés, le système naturel ou la construction artificielle. Ces études utilisent diverses technologies de détection, e.g. la microscopie de fluorescence, la spectrométrie de masse, la mesure électrophysiologique. Récemment, les outils microfluidiques sont intégrés pour traiter ces petits objets.

Notre recherche est menée dans le cadre de l'IMI (INNOVATIVE MEDICINES INITIATIVE) en collaboration avec Soleil synchrotron et UMR-MD1 à Marseille. Cette recherche vise à utiliser les antibiotiques naturellement fluorescents, fluoroquinolones, par l'imagerie sous irradiation UV, à observer l'accumulation de l'antibiotique dans le corps des bactéries en fonction du temps. Selon de différentes espèces mutantes, de différents antibiotiques, voire même de différents adjuvants ajoutés, ce niveau d'accumulation doit varier. Ceci est une technique sans marquage permettant la détection en temps réel aux études du système réel biologique, il offre de certaines significations cliniques.

Étant donné que la méthode employée par le passé a des défauts, elle ne peut être

appelée que « méthode statique ». Par exemple, il n'y a aucun moyen de changer le liquide environnemental extérieur, il n'y a aucun moyen d'obtenir des informations de fond. Nous avons donc décidé de mettre en œuvre un moyen plus flexible en introduisant l'outil microfluidique.

Il s'agit de se focaliser sur une petite gamme de bactéries immobilisées et isolées. Dans les recherches rapportées, nous avons résumé que trois catégories de méthodes peuvent être trouvées par rapport à l'application du dispositif microfluidique à l'échelle de cellule unique : électromagnétiques (diélectrophorèse ou pinces optiques), adhésions chimiques ou physiques (revêtement de surface ou matrice de gel), et des pièges stériques (chambre microfluidique, vanne annulaire élastomère ou membrane semi-perméable). En même temps, notre dispositif microfluidique doit pouvoir répondre aux demandes : une immobilisation complète des bactéries, une isolation des bactéries jusqu'à single-cell pour permettre l'imagerie parallèle, une nécessité d'entrée et de sortie du fluide, et une préférence d'être réutilisable.

Après avoir testé la diélectrophorèse et la vanne bouton élastomère sans succès, nous avons décidé de concevoir un dispositif qui peut remplir les quatre demandes ci-dessus. Il est basé sur la méthode statique précédente, une des deux lamelles a été réduite, un timbre de PDMS a été assemblé de la manière réversible avec le substrat, et des pousse-seringues vont réaliser de l'input et l'élimination du liquide.

Ensuite, à travers une analyse grossière de « circuit résistif » et une simulation numérique précise, le comportement de fluide dans le dispositif est clarifié : dans le « canal d'approvisionnement » le fluide est renouvelé par advection pour offrir une source stable alors que dans le « canal de bactérie », en raison de la résistance hydrodynamique très importante, le transfert de masse est conduit principalement par diffusion. ROI (region of interest) est sélectionnée dans la zone de 15~35 μm à la frontière de « couvercle de la chambre d'observation », donc le changement de l'environnement liquide est plus rapide que la vitesse à laquelle les bactéries absorbent les molécules de l'antibiotique de l'environnement. C'est une méthode qui peut refléter l'interaction véritable entre les bactéries et les molécules antibiotiques.

Le focus du travail suivant est concentré essentiellement sur 2 points : 1. Pour les

bactéries de différentes mutations, est-ce que elles présentent de différents niveaux d'accumulation par rapport aux même médicaments ? 2. Pour les mêmes bactéries, à l'utilisation de différents adjuvants, est-ce qu'elles présentent de différentes réponses ? Cela guidera le développement des futurs antibiotiques. Nous démontrons également les possibilités de ce dispositif en terme de plate-forme d'observation pour la culture des bactéries.

Part II:

Dans cette 2^{ème} partie de thèse, nous avons pour but d'étudier un processus de vie d'un organisme de modèle qui est un embryon de souris de stade précoce de 5.5 jours : son endoderme viscéral distal déplace vers un côté de l'embryon pour définir le futur endoderme viscéral antérieur et donc l'axe et le plan du corps. Pour révéler ce processus, la technique de marquage-traçage est utilisée.

La transfection est une technique spécialisée pour la délivrance de gènes exogènes dans les cellules. Avec le développement de la recherche sur les fonctions des gènes et des protéines, elle est devenue une méthode de laboratoire de base. Les protocoles de transfection peuvent être classés en trois types : physique (e.g. sonoporation ou électroporation), chimique (e.g. lipofection) et biologique (e.g. infection lentivirale ou infection rétrovirale). Parmi lesquels, l'électroporation est une des méthodes physiques, efficace et non toxique. L'électroporation utilise l'effet de chocs électriques pour déstabiliser la membrane cellulaire pendant de courtes périodes, permettant ainsi la pénétration de molécules ou de principes actifs peu perméables. Ce phénomène peut être réversible si les paramètres électriques sont bien contrôlés. A travers ces trous, des ADN ou d'autres macromolécules déjà présents dans la solution peuvent translocater dans les cellules.

L'ancienne doctorante a développé la conception d'un dispositif basé sur « guide diélectrique ». Grâce à cette conception, d'une part la possibilité de contact direct entre l'embryon et les électrodes est évitée ; d'autre part, la focalisation des lignes de champ électrique est mise en place afin de réaliser une électroporation ciblée précise. Par EM5 et EM6, les deux versions de dispositifs à usage unique, le design du guide diélectrique a été validé. EM5 a utilisé la méthode de « lithographie molle » pour la moitié supérieure de la structure, puis elle est collée avec un substrat en verre ordinaire pour fermer le canal; EM6 a

utilisé de la métallisation, une résine négative de photolithographie, et un collage thermique pour former la structure du canal. Cependant, en raison de la mauvaise bio-compatibilité des matériaux et la complexité de technologies, ces deux versions ne sont pas applicables à la propagation dans la communauté biologique. Par conséquent, nous voulons que ces dispositifs soient pratiques à utiliser pour que les biologistes puissent se dispenser de la dépendance d'une salle blanche.

Pour la réutilisabilité, deux options s'offrent à nous : premièrement, la micro puce par moulage thermoplastique comme les « petri dish » à usage unique : ils sont jetables, et peuvent être produits en masse. Deuxièmement, la micro puce répétitivement nettoyable et recyclable, comme un bécher en verre. Étant donné deux prémisses importantes, nous avons finalement choisi le développement et la fabrication en verre : d'abord, la conception de la nature particulière du dispositif et la diversité des tailles des embryons de souris exigent que les dimensions du dispositif soient flexibles ; et le second, ce dispositif nécessite que la surface de dispositif soit hydrophile.

Dans mon travail, nous nous sommes efforcés de développer des puces réutilisables en verre qui sont nommées EM7. La version EM7-01 était basée sur la gravure humide pour la structure de substrat, le microsablage pour le couvercle et la colle photo sensible aux UV pour l'assemblage. EM7-02 a rendu l'usinage du verre de couvercle plus précis en introduisant l'ablation au laser. Cependant, l'assemblage reposait toujours sur la colle photo sensible aux UV et l'alignement entre ces deux couches était toujours un problème. Dans EM7-11, l'étape d'alignement a eu lieu pendant l'ablation au laser en réservant les marques d'alignement pour augmenter la précision et non plus pendant l'assemblage comme précédemment. En outre, l'assemblage a été complété par simple collage d'un substrat neuf par HSQ. En parallèle, EM7-21, une puce réutilisable monolithique était faite par externalisation, par une entreprise experte en « selective laser-induced etching ».

Ce dispositif a été envoyé à l'Université Libre de Bruxelles pour participer aux essais biologiques. Combiné avec les paramètres électriques fournis à partir des simulations numériques, nos collaborateurs ont mené avec succès plusieurs électroporations et observé des expressions de différentes protéines correspondantes aux plasmides électroporés dans des embryons.

En développant ce dispositif, nous proposons une stratégie d'électroporation à haute précision, haute reproductibilité, et faible toxicité. En plus de la méthode marquage-traçage, il peut, bien sûr, être appliqué sur la modification de la fonction cellulaire localement. Grâce au choix des matériaux et technologies, ce dispositif est réutilisable et facile à propager dans les laboratoires de biologie.

Université Paris-Saclay

Espace Technologique / Immeuble Discovery

Route de l'Orme aux Merisiers RD 128 / 91190 Saint-Aubin, France



Titre : Conception et fabrication d'outils microfluidiques réutilisables pour étudier la dynamique de phénomènes biologiques: application à l'influx / efflux d'antibiotiques dans les bactéries et à la migration des cellules pendant le développement de la souris

Mots clés : microfluidique, imagerie de fluorescence, multirésistance, embryologie, microfabrication

Nous voulons mettre en évidence et analyser la réponse de systèmes biologiques à l'introduction de perturbations spatio-temporelles. Plus précisément, afin de développer des stratégies innovantes pour l'étude des systèmes biologiques, nous proposons d'utiliser des outils microfluidiques. Nous concevons des microsystèmes adaptés qui permettent d'influencer localement sur les comportements biologiques, ceci afin qu'un expérimentateur macroscopique puisse contrôler l'environnement externe d'objets biologiques dont l'échelle est microscopique.

Cette stratégie d'ingénierie est générique et multidisciplinaire. Au cours de cette thèse, elle a été mise en œuvre dans le cadre de deux projets collaboratifs, d'une part à l'échelle de la bactérie *E. coli*, et d'autre part à celle de l'embryon de souris à un stade post-implantation précoce. Les objets d'étude choisis sont caractéristiques à bien des égards des champs biologiques concernés : taille, représentativité, complexité. Nous avons mis nos compétences de spécialistes en conception et en fabrication de dispositifs fluidiques au service de la ligne DISCO du synchrotron SOLEIL et de l'équipe d'embryologie de la souris de l'IRIBHM. Le cœur de mon travail a été de concevoir et fabriquer des outils microfluidiques recyclables qui peuvent être utilisés de façon simple dans des laboratoires de biologie générique ne possédant pas de salle blanche. Au cours de cette thèse, nous avons développé non seulement des microdispositifs réutilisables mais aussi des protocoles expérimentaux adaptés à l'utilisation de ces instruments miniaturisés.

Plus précisément, le projet de microbiologie à SOLEIL avait pour objet l'étude de l'influx et l'efflux de molécules antibiotiques dans des bactéries. Pour ce faire, nous avons développé un dispositif réutilisable pour immobiliser les microorganismes et changer leur environnement chimique pendant l'imagerie en microscopie d'épifluorescence dans l'UV. Cette étude s'effectue en utilisant deux partenaires typiques : la bactérie *E. coli* et un médicament de la famille des fluoroquinolones. Le projet d'embryologie a reposé sur l'électroporation localisée d'acides nucléiques des embryons de souris et le suivi des migrations cellulaires.

Title: Conception and fabrication of reusable microfluidic tools to study the dynamics of biological phenomena: application to antibiotic influx/efflux in bacteria and to cell migration during mouse development

Key words: microfluidics, fluorescence microscopy, multidrug resistance, embryology, microfabrication

We want to analyze the response of biological systems to the introduction of spatio-temporal modulations. More specifically, in order to develop innovative strategies for the study of biological systems, we propose to use microfluidic tools. We design dedicated microsystems that can locally influence biological behaviors, so that a macroscopic experimenter can control the external environment of biological objects which scale is microscopic.

This engineering strategy is generic and multidisciplinary. In this thesis, it has been implemented in two collaborative projects, on one hand, at the scale of the *E. coli* bacterium and on the other hand at the scale of the mouse embryo at an early stage post-implantation. These objects are selected since they are, in many aspects, characteristic of the concerned biological fields: size, representativeness, complexity. We provided our expertise in fluidic device design and manufacturing to the DISCO beamline of the SOLEIL synchrotron and to the IRIBHM mouse embryology team. The key point of my work has been to produce recyclable microfluidic tools that can be used simply in generic biological laboratories that do not possess clean room. In this thesis, we have developed not only reusable microdevices but also experimental protocols adapted to the use of these miniaturized instruments.

More precisely, the microbiology project at SOLEIL focused on the influx and the efflux of antibiotic molecules in bacteria. We have developed a reusable device for immobilizing those microorganisms and changing their chemical environment during UV imaging on an epifluorescence microscopy. This study was carried out using two typical partners: the *E. coli* bacterium and a drug from the fluoroquinolone family. The embryology project relied on the localized electroporation of nucleic acids into mouse embryos and the monitoring of cell migrations.